In vivo imaging of long-term changes in the
Drosophila neuromuscular system

PhD Thesis

in partial fulfillment of the requirements

for the degree Dr. rer. nat.

in the Neuroscience Program

at the Georg August University Göttingen,

Faculty of Biology

submitted by

Tobias Manuel Rasse

born in

Ludwigshafen am Rhein

2004

I hereby declare that I have written the PhD thesis:

**"*In vivo* imaging of long-term changes in the
    Drosophila neuromuscular system"**

independently and with no other sources and aids than quoted.

Göttingen, October, 2004

…………………………………………..
                    Tobias Manuel Rasse

TABEL OF CONTENTS

6. APPENDIX

List of Figures

List of Tables

<u>Acknowledgements</u>

1 Summary

So far synaptogenesis could hardly be studied in its native settings. In this thesis, an assay, which allows the study of synapse formation and maturation *in vivo* was established in a genetically ideally addressable model system, the fruit fly *Drosophila melanogaster*. Transgenic expression of GFP-labeled glutamate receptors was used to directly observe glutamate receptor dynamics at neuromuscular synapses of intact *Drosophila* larvae during the functional and structural strengthening of this synaptic circuit. It could be shown that small functional synapses form at sites distant from established synapses to then grow to a mature size. Thereby, the growth of the postsynaptic density (PSD) is directly driven by the entry of glutamate receptors containing the subunit DGluRIIA. These receptors enter from diffuse extrasynaptic pools as shown by *in vivo* photo-labeling. Thus, *de novo* formation and subsequent growth of synapses but not the split of pre-existing synapses mediates strengthening of glutamatergic circuits *in vivo*. Once matured, PSDs of *Drosophila* neuromuscular synapses seem to be remarkably stable entities that show little receptor entry and no detectable exit of receptors. To complement *in vivo* imaging of synapse formation, a screen allowing the genome-wide GFP-labeling of proteins expressed from their endogenous genetic loci was initiated. To optimize the screening strategy, automated sorting of GFP-positive *Drosophila* embryos was combined with the usage of a novel transposable-element. How assembly of pre- and postsynaptic structures is coordinated *in vivo* is largely unknown. Here, the first *Drosophila* protein localized to the cytomatrix of active zones (*Drosophila* Cast) was identified. This served as an entry point for genetic analysis of the presynaptic active zone and allows the co-visualization of pre- and postsynaptic assembly *in vivo*.

2 Introduction

2.1 Synapses

2.1.1 Function of Synapses

Synapses are specialized junctions through which cells of the nervous system signal to one another and to non neuronal cells such as glands or muscles. Synapses form the circuits that interconnect the central nervous system. In the human brain about 10^{15} synaptic contacts interconnect the 10^{10}-10^{11} nerve cells. These specialized sites of asymmetric cell-cell contact are designed to mediate rapid and efficient transmission of signals from the presynaptic bouton of one neuron to the plasma membrane of the postsynaptic cell. This transmission forms the basis for the biological computations that underlie perception and thought.
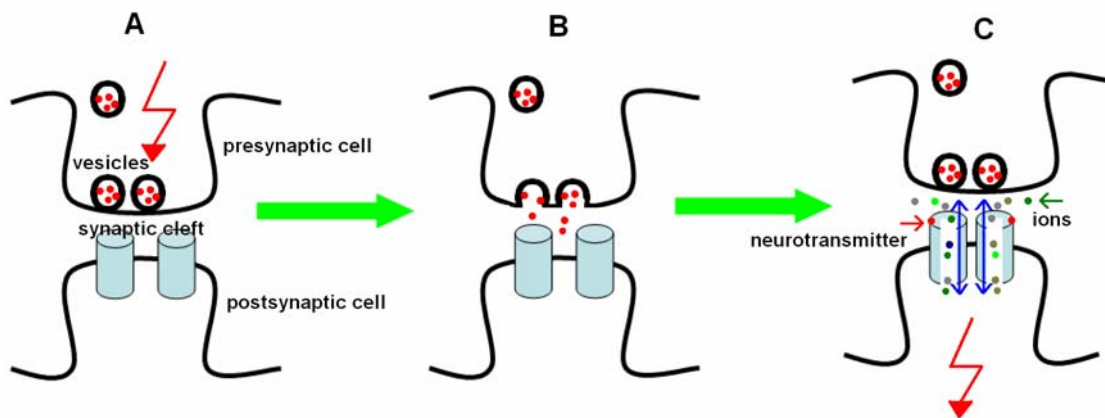
Fig. 1 Synapses allow communication between two nerve cells (see text)

The transmission is mediated by the presynaptic rapid release of neurotransmitter triggered by the arrival of a nerve impulse also called action potential. The action potential produces an influx of calcium ions, which causes vesicles already docked at the presynaptic membrane to fuse and release their neurotransmitter into the synaptic cleft (Fig. 1 A,B). Classical neurotransmitters include glutamate, acetylcholine and γ-amino-butyric acid.

Glutamate is the most important and prevalent excitatory neurotransmitter in the central nervous system of vertebrates. The following work will focus on glutamatergic synapses, since these synapses are thought to be the key elements in central nervous system information processing. Glutamate receptors on the postsynaptic side of the synaptic cleft bind the neurotransmitter released by the vesicle fusion (Fig. 1 C). These glutamate receptors can be subdivided into ionotropic and metabotropic receptors. Fast responses are transmitted via the ligand-gated ionotropic glutamate receptors, which change their conformation upon binding of the neurotransmitter. Metabotropic glutamate receptors activate a coupled G-protein that, in most cases, directly binds to a separate ion channel, causing a change in conductance. This conformational change allows ions to cross the membrane, which causes a change in the membrane potential (Fig. 1 C). For a better understanding of the mechanisms mediating the neurotransmission both the structure and function of the pre- and postsynaptic compartment will be discussed in more detail in chapter 2.1.2 and 2.1.3.

2.1.2 Function and structure of the presynaptic compartment of glutamatergic synapses

The presynaptic bouton can be subdivided into several compartments. In the active zone * (AZ), the area where the vesicle fusion takes place, the presynaptic AZ membrane is precisely aligned with the postsynaptic membrane, where the postsynaptic neurotransmitter reception apparatus is localized. In the AZ docked vesicles fuse rapidly with the presynaptic AZ membrane a process triggered by the influx of Ca^{2+} ions via voltage gated ion channels in response to action potentials. The precise regulation of this multistep process is believed to be central to nervous system operation. It demands a specialized cytoarchitecture called cytoskeletal matrix assembled at the active zone (CAZ).

The CAZ is supposed to define the neurotransmitter release site by anchoring and localizing presynaptic membrane proteins and so organizing the endo- and exocytotic machinery. Within the CAZ, a network of microfilaments and associated proteins have been implicated in functional and spatial organization of individual steps of the synaptic vesicle (SV) cycle, including the docking of vesicles (for review see (Garner et al., 2000)).

---

* The term active zone is often used to describe the part of the presynaptic membrane, where vesicle fusion takes place. In this thesis this structure will be referred to as active zone membrane. The term active zone is also frequently used to describe both the active zone membrane together with the portion of the presynaptic bouton in which vesicles are clustered on a specialized cytoarchitecture called cytoskeletal matrix assembled at the active zone (CAZ). In this thesis the term active zone will therefore be used to refer to the entire structure, which can be subdivided into AZ membrane and CAZ.
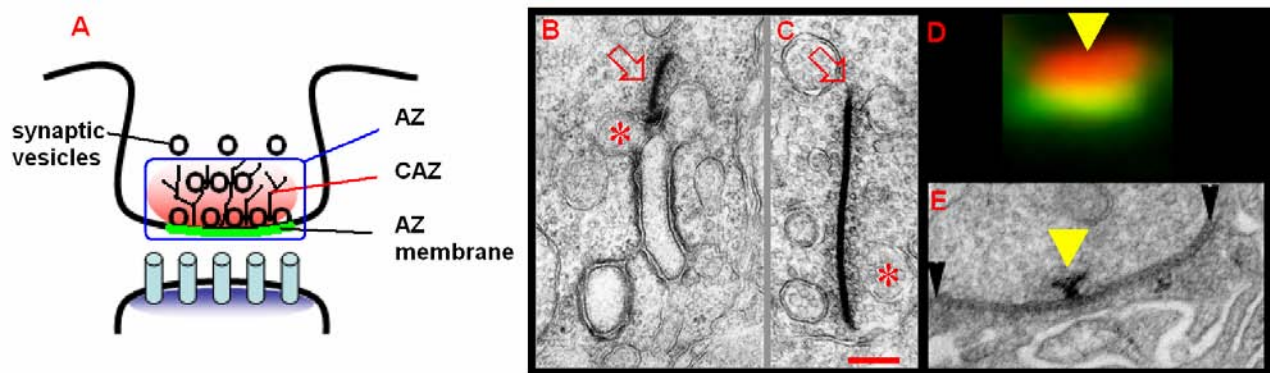
Fig. 2 Organization of the presynaptic compartments of glutamatergic synapses in vertebrates and *Drosophila*

A) Schematic drawing of a presynaptic bouton. Synaptic vesicles are clustered at the AZ. **B-E)** Visualization of the AZ in different preparations using electron (B,C,E) or light microscopy (D). **B,C)** Synapses from the outer plexiform layer of mouse *retina*. Presynaptic terminals (rod spherules and cone pedicles) are invaginated by fine neuritis of bipolar and horizontal cells. No postsynaptic densities are formed but terminals contain dense lamella called the synaptic ribbon perpendicular to the presynaptic membrane. Synaptic vesicles are clustered around the ribbon (arrows) and they are also present in processes of horizontal cells (asterisks). Scale bar 300 nm (B,C were kindly provided by Josef Spacek, Synapse Web, Medical College of Georgia, http://synapses.mcg.edu/) **D)** *Drosophila* wild type larvae stained with monoclonal antibody nc82 (red) that marks the active zones (arrowhead) and with the *Drosophila* glutamate receptor subunit DGluRIIC (green). **E)** The so-called T-bars or dense bodies (arrowhead) present at *Drosophila* neuromuscular junctions seem to be part of the CAZ. Synaptic vesicles are clustered around the T-bar (E taken from (Sigrist et al., 2002)).

Synapses are ultrastructurally characterized by pre- and postsynaptic membrane thickenings (see chapter 2.1.3) and, on the presynaptic side, by synaptic vesicle accumulation (Fig. 2 A,B,C,E). Parts of the AZ can be visualized in synaptic preparations, like the vertebrate retina (Fig. 2 B,C) and the *Drosophila* neuromuscular junction (NMJ) (Fig. 2 E), using electron microscopy. In *Drosophila* the monoclonal antibody (MAB) nc82 (chapter 4.3.1) was found to be a useful light microscopic tool to label the AZ (Fig. 2 D,
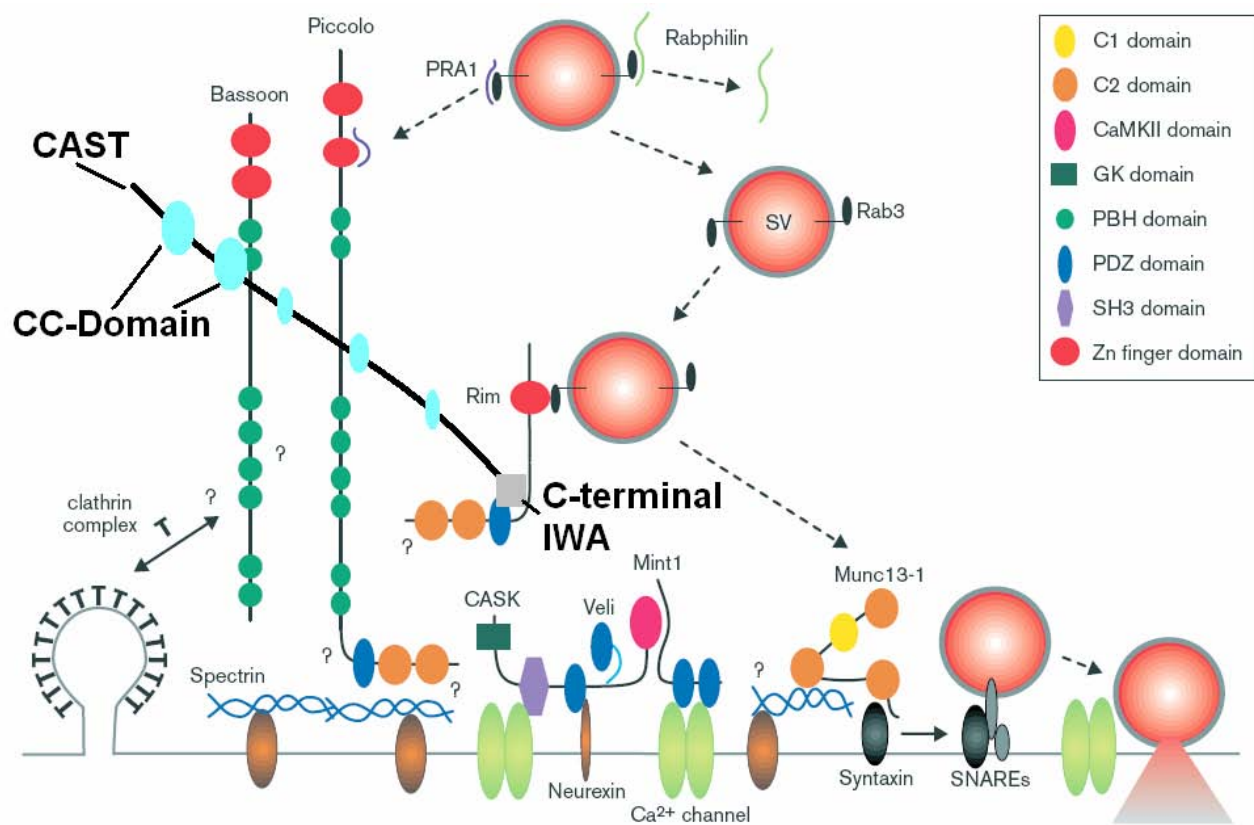
Fig. 3 Schematic representation of the molecular composition of the active zone (adapted from (Garner et al., 2000))

In vertebrates, several molecular components of the AZ have been identified. In addition to the general cytoskeletal proteins actin and spectrin the large protein Bassoon (420 kDa) (tom Dieck et al., 1998; Shapira et al., 2003) is specifically found at the CAZ. This protein has been shown to be involved in structural active zone formation and/or maintenance in glutamatergic synapses (tom Dieck et al., 1998). However, Bassoon does not seem to be essential for AZ assembly at all glutamatergic synapses. Furthermore, Bassoon does not appear to be important for synapse formation, but instead to play an essential role in regulated neurotransmitter release from a subset of glutamatergic synapses (Altrock et al., 2003). Loss of Bassoon causes a reduction in normal synaptic transmission, which can be attributed to the inactivation of a significant number of glutamatergic synapses (Altrock et al., 2003). At these synapses the clustered vesicles are unable to fuse (Altrock et al., 2003). Photoreceptor ribbons lacking Bassoon are no longer anchored to the presynaptic active zones and synaptic transmission is impaired at these synapses (Dick et al., 2003). Besides Bassoon, the protein Piccolo, (Fenster et al., 2000) containing several putative protein-protein interaction domains, is assumed to help

to organize several components of the active zone, including Rab3-interacting molecule (RIM1), Munc-13, and the CAZ-associated structural protein (CAST). While most proteins found to be relevant for structure and/or function of the vertebrate nervous system are conserved in invertebrates, no homologs of Bassoon or Piccolo have been detected in the *Drosophila* genome.

This thesis will describe the identification and characterization of DCast, which turned out to be the first CAZ protein found to be conserved between mammals and flies. This protein with homology to the vertebrate CAST/ERC localizes at the presynaptic active zone. The high degree of conservation indicates that *Drosophila* Cast (DCast) could potentially be part of the core complex establishing the AZ. Rat *CAST1* belongs to a family of genes important for both neuronal and non-neuronal membrane traffic. Only the neuronal isoforms CAST1 and CAST2α can bind to RIM via the IWA motif. While CAST1 (=ERC2) seems to be exclusively localized to active zones (Ohtsuka et al., 2002), CAST2α (=ERC1b) seems to be present in both a cytosolic and an insoluble active zone form (Wang et al., 2002).

2.1.3 Function and structure of the postsynaptic compartment of glutamatergic synapses

The postsynaptic densitity (Fig. 4 A) is a postsynaptic membrane thickening which lies opposite of the presynaptic active zone (see chapter 2.1.2). It contains the proteins that are important for transmission on the postsynaptic side. Using electron microscopy it can be visualized by a dark electron dense staining (Fig. 4 B,D). On the light microscopic level immunostainings against neurotransmitter receptors can be used to visualize the PSD (Fig. 4c).
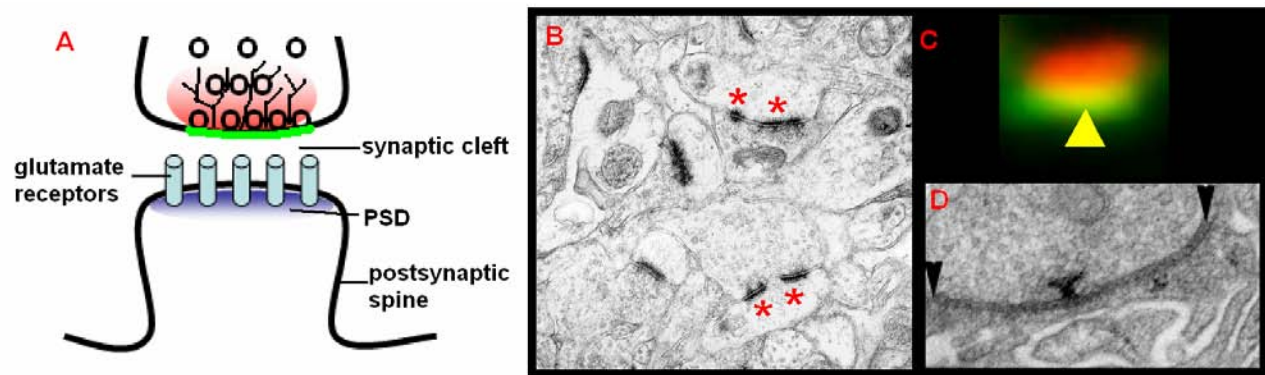
Fig. 4 Postsynaptic organization of glutamatergic synapses in vertebrates and *Drosophila*.
A) Schematic drawing of a postsynaptic spine. The PSD is shown in blue **B-D)** Visualization of the PSD in different preparations using electron (B,D) or light microscopy (C). **B)** the darkly stained postsynaptic densities of synapses are in contrast with all other much lighter structures. Densities appearing to be doubled (asterisks) are in fact, when three dimensionally reconstructed, parts of one perforated density. Scale 1µm (mouse, neocortex) (B was kindly provided by Josef Spacek, Synapse Web, Medical College of Georgia, http://synapses.mcg.edu/) **C)** *Drosophila* wild type larvae stained by the monoclonal antibody nc82 (red) which marks the active zone and the *Drosophila* glutamate receptor subunit DGluRIIC (green), which labels the PSD (arrowhead) **D)** The postsynaptic density at the *Drosophila* neuromuscular synapses. The PSD is the electron dense staining between the two arrowheads on the postsynaptic membrane of this synapses (D taken from (Sigrist et al., 2002)).

The most important class of ion channels in the postsynapse are ionotropic glutamate receptors. They are composed of subunits, probably four in total, that are likely to be arranged as a dimer of dimers (Sun et al., 2002). Each subunit contains three transmembrane domains plus a loop region, and an intracellular C-tail, important for receptor assembly and anchorage in synapses. Ionotropic glutamate receptors can be subdivided into N-methyl-D-aspartate (NMDA) receptors and AMPA / Kainate type (non-NMDA receptors) glutamate receptors.
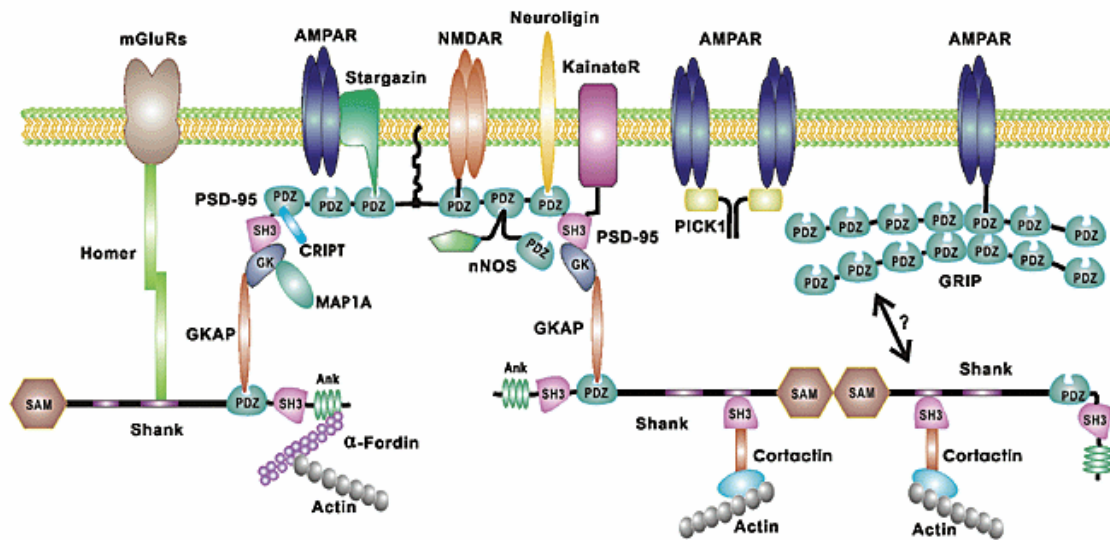
Fig. 5 Molecular composition of the PSD in mammals Glutamate receptor signaling complex organization in PSDs. Clustering of NMDA receptors is mediated by direct binding of the cytoplasmic tail of its NR2 subunits to the first two PDZ domains of PSD-95. The PDZ domains of PSD-95 can also interact with the C-terminus of the cell-adhesion protein neuroligin and AMPA receptor targeting protein stargazin. Kainate receptors interact with the SH3 domain of PSD-95. PSD-95 is attached to the postsynaptic membrane via the N-terminal palmitate group (wiggly line). The AMPA receptors also bind to two additional PDZ proteins GRIP/ABP and PICK1 via PDZ domain-mediated protein interactions. These glutamate receptors are further organized by Shank situated at the deeper side of the synapse. The GK domain of PSD-95 binds to GKAP, and the C-terminal tail of GKAP directly binds to the PDZ domain of Shank. Shank also couples the metabolic glutamate receptors via a bridging protein Homer. Shank may also directly interact with the GRIP/AMPAR complex. Like many other scaffold proteins, Shank can multimerize via its SAM domain. Finally, Shank is directly linked to the cytoskeleton via two actin-binding proteins cortactin and α-fordin (taken from (Zhang and Wang, 2003))

The functional properties of non-NMDA receptor channels are subunit dependent (Geiger et al., 1995) and in heteromeric non-NMDA receptors the kinetics, single-channel conductance, Ca^{2+}-permeability and rectification may be determined by one type of subunit. These receptors are integrated in a large complex of interacting proteins at the PSD. One of the best-studied complexes within the PSD is that associated with NMDA receptors which includes molecules such as SAP90/PSD95, α-actinin and CaMKII, neuroligin, the microtubule-binding protein CRIPT, the guanylate kinase domain-binding proteins GKAP/SAPAPs, and other proteins such as ProSAP/Shank, Homer and cortactin (Scannevin and Huganir, 2000; Sheng, 2001; Sheng and Sala, 2001).

2.1.4 Formation of new synaptic contacts

While there is a basic understanding of the molecular organization of the AZ and the PSD relatively little is known about the cellular processes by which AZs and PSDs are assembled (Ziv and Garner, 2001; Goda and Davis, 2003; McGee and Bredt, 2003). Communication between pre- and postsynaptic sites during synapse formation is thought to be a complex process involving a variety of cell surface receptors, their ligands and cell adhesion molecules (for review see (Gundelfinger and tom Dieck, 2000; Yamagata et al., 2003; Shen, 2004)). Spatial and temporal correlation between pre- and postsynaptic maturation is the first step toward understanding the interaction between these structures.
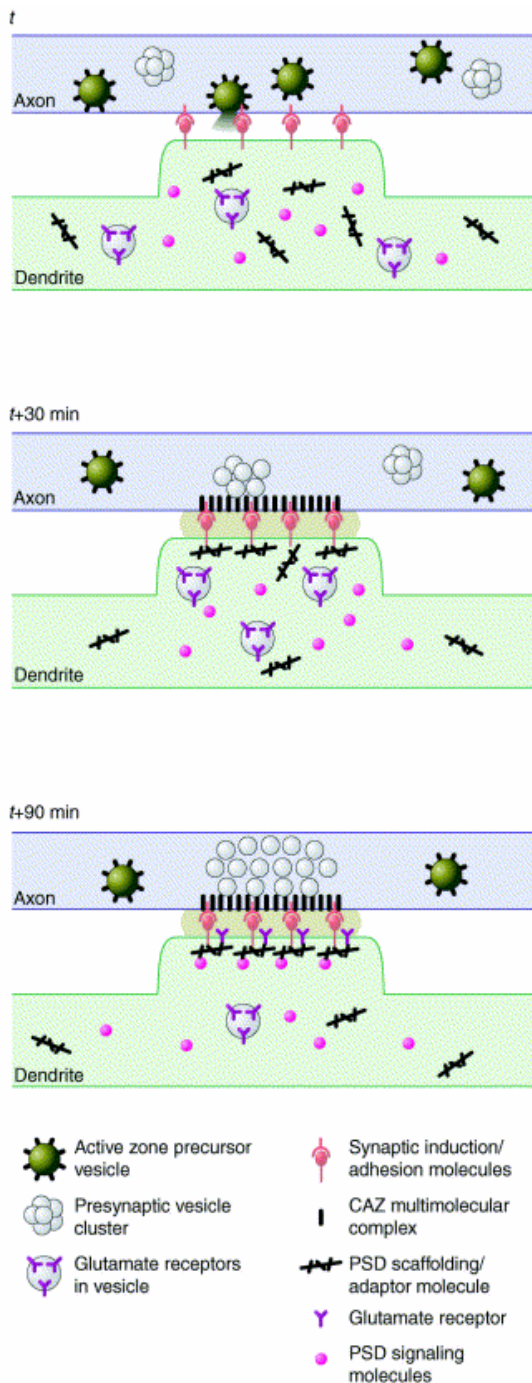
Fig. 6 Synaptic differentiation by insertion of pre-assembled precursor vesicles versus sequential *in situ* recruitment of synaptic components. In this simplified 'time-lapse sequence', presynaptic differentiation is shown to occur by the insertion of precursor vesicles containing full complements of CAZ complexes, which leads to the formation of functional active zones in a "quantal mode". Postsynaptic differentiation is shown to occur by the sequential recruitment of PSD scaffolding molecules followed by glutamate receptors and PSD signaling molecules. The differentiation processes are presumed to be initiated by interactions between the external aspects of axonal and dendritic membrane molecules. The time points represent the approximate time course of these processes in minutes starting from the point of first axodendritic contact. Taken from (Ziv and Garner, 2001)

19

Results obtained *in vitro* including retrospective immunohistochemistry so far suggest that presynaptic development precedes postsynaptic assembly. New AZs can be functional within 30-60 min of initial axodendritic contact (for review, see (Ziv and Garner, 2001)). Thereby several units of CAZ material are transported to nascent presynaptic sites in preformed precursors vesicles (Roos and Kelly, 2000). The fusion of 1-4 of such vesicles with the presynaptic plasmamembrane may be sufficient to form an AZ (Zhai et al., 2001; Shapira et al., 2003; Bresler et al., 2004). Examples for such AZ precursors are SV packets shown to be transported and recruited to new presynaptic sites together with other presynaptic molecules, including voltage-dependent calcium channels, synapsin, and amphiphysin (Ahmari et al., 2000) and 80 nm axonal dense-core vesicles named Piccolo-Bassoon transport vesicles (PTVs). PTVs contain the CAZ matrix components Basson, Piccolo and CAST as well as RIM/UNC10, Munc13/UNC-13 and Munc18/UNC-18 (Zhai et al., 2001; Shapira et al., 2003). This suggests that the building material for presynaptic AZs is pre-assembled somatically and that it can be deposited upon contact with postsynaptic partners. Considering that presynaptic sites are usually formed at remote axonal sites, far from the somatic and dendritic biosynthetic center (translational aggregates are usually found only in dendrites and the soma, but not in the axon), the pre-packing of AZ components in small modular units seems appropriate.

Bresler and co-workers used a GFP-fusion to Basson to address the role of these transport vesicles *in vitro*. Discrete Basson-GFP punctae move rapidly along the axon. To form an AZ several of these come to rest at a previously non synaptic site (Bresler et al., 2004). The time measured from the first detection of stationary Basson-GFP at a future synaptic site to the acquisition of a capacity for activity-evoked endocytosis and exocytosis ranged from 15 to 45 min (Bresler et al., 2004), which is in agreement with previous studies based on retrospective immunohistochemistry (Friedman et al., 2000; Zhai et al., 2001). Retrospective immunochemistry further showed that it takes about one hour for the major postsynaptic proteins PSD-95, GluR1 and NMDAR1 to accumulate at the sites of styryl dye staining after the initial appearance of vesicle recycling (Friedman et al., 2000). How the mechanisms for postsynaptic assembly work in detail is even less clear than for the presynaptic compartment. Postsynaptic compartments are usually dendritic and therefore rather close to the somatic and dendritic biosynthetic centers, which probably

reduces the need for elaborate delivery mechanisms. Some studies showed discrete and mobile SAP90/PSD-95 particles, leading to suggestions that these might constitute modular PSD units (Marrs et al., 2001; Prange and Murphy, 2001). Washbourne and colleagues (Washbourne et al., 2002) furthermore described the delivery of modular NMDAR1 and GluR1 transport vesicles to synapses in young hippocampal neurons. In older neurons (Bresler et al., 2004), however, no similar transport vesicles could be observed for NMDAR1 nor were they detectable for other NMDAR subunits (Guillaud et al., 2003). This argues against the hypothesis that generally precursor vesicles - similar to those described for the AZ - transport glutamate receptors to synapses. Moreover, the recruitment of SAP90/PSD-95, PSD-Zip45/Homer 1c, NMDR1, ProSAP1 and ProSAP2 to new synaptic sites was reported to occur in a gradual manner and not from discernible precursor particles (Bresler et al., 2001; Marrs et al., 2001; Okabe et al., 2001; Okabe et al., 2001; Bresler et al., 2004). Hereby the recruitment kinetics of SAP90/PSD-95, NMDR1, ProSAP1, ProSAP2 are remarkably similar (Bresler et al., 2001; Bresler et al., 2004). This behavior could be explained by a two step process. Thereby PSDs components might form multimolecular complexes in the dendritic membrane prior to being trapped or cross-linked in PSDs. Alternatively the recruitment of each molecule could be dependent on the prior recruitment of the molecule to which it binds. If the recruitment rates of downstream molecules were relatively high, the slow recruitment of upstream molecules could control the formation of PSDs.

2.2 Synaptic changes during long-term strengthening and information storage

2.2.1 Long-term potentiation

Information is acquired, stored, and retrieved by the brain. Thereby it is unlikely that a single neuron encodes a specific memory; rather whole ensembles of neurons participate in maintaining a representation that serves as memory. Changes in interactions between neurons are thought to be the basis of memory, which implies a need for use-

dependent changes in synaptic function. These changes in interactions could be established by "neuronal growth" as proposed by Cajal in 1893 (Cajal S., 1893). At the same time Tanzi argued that changes in existing connections might underlie information storage in the brain (Tanzi, 1893). In 1949 both ideas were combined by Hebb who postulated that alterations in synaptic strength, as well as formation of new synapses, are responsible for memory storage (Hebb, 1949). Clinical data from Milner showed in 1966 that lesions in the hippocampus produce retrograde amnesia (Milner, 1966), which was followed by the first experimental induction of long-term potentiation (LTP) in the mammalian hippocampus in 1973 by Bliss and Lomo (Bliss and Lomo, 1973). They used brief tetanic stimulation to induce synaptic plasticity, which lasted for hours. Since then much emphasis has been put on studying LTP in central glutamatergic synapses of the hippocampus, which are thought to be the information processing centers of our brains. A first step towards a molecular understanding of LTP at these synapses was taken in 1984, when Lynch and Baudry proposed that LTP involves an increase in the number of synaptic glutamate receptors (Lynch and Baudry, 1984).

2.2.2 Molecular dynamics of the PSD at existing synaptic contacts

Following up that idea of Lynch and Baudry it could be shown by electrophysiological and molecular biology approaches that NMDA and AMPA receptors can be recruited to postsynaptic membranes independently of each other, via both constitutive and activity-dependent pathways (Carroll et al., 1999; Luscher et al., 1999; Shi et al., 1999; Grosshans et al., 2002; Malenka, 2002). In fact, even the various subunits of the same receptor type (e.g. AMPA-receptor subunits GluR1 and GluR2) differ in the dynamics of their insertion into the postsynaptic membrane and in their dependence on synaptic activity for insertion (Passafaro et al., 2003). AMPA receptors are hetero-oligomeric complexes consisting of different subunits (Seeburg, 1993). In the mouse hippocampus, an important mammalian model system for plasticity studies, subunits GluR1-GluR4 are expressed (Hollmann and Heinemann, 1994). Investigations indicate that alterations of AMPA receptor-mediated transmission apparently play a central role in the induction and stabilization of long-term potentiation (Linden and Connor, 1992; Bliss and Collingridge, 1993; Nicoll and Malenka, 1995). Interestingly, different combinations of

AMPA receptor subunits form different populations of AMPA complexes which in turn mediate distinct functions during synaptic plasticity. GluR1/GluR2 receptors are thought to be transported from intracellular compartments to synaptic zones (Shi et al., 2001), which could be a key mechanism in converting silent into active synapses during LTP. However, GluR1/GluR2 receptor complexes are continuously replaced by GluR2/GluR3 receptor complexes, which stabilize previously activated zones (Shi et al., 2001).

The cellular machinery transporting vesicular pools of AMPA receptors is still largely uncharacterized. Recently, the glutamate receptor interacting protein (GRIP) was suggested to specifically interact with AMPA receptors, and also to associate with the cargo-binding domain of the conventional kinesin molecule (Setou et al., 2002). The synaptic transport of different AMPA receptor complexes also exhibits mechanistic differences (Sheng and Lee, 2001). Proteins with PDZ-domains (e.g. the GRIP) are likely responsible for such subunit-specific regulation of either the transport and/or the synaptic presentation of receptor subunits. Glutamate receptors can also be synthesized locally. There is evidence that increased synaptic activity triggers the local synthesis of the ionotropic glutamate receptor subunit DGluRIIA (Sigrist et al., 2000), which in turn promotes the formation of additional active sites at the *Drosophila* NMJ (Sigrist et al., 2002). In fact, most recently work in rodent neuronal culture has suggested the occurrence of local synthesis of AMPA receptors in dendritic compartments (Ju et al., 2004).

2.2.3 Structural synaptic changes during long-term strengthening processes

Although altered gene expression, the synthesis of new proteins, and synaptic growth have been found to be critical for the formation of LTP, little is known about the cellular mechanisms that initiate and maintain structural changes (for review see (Bailey and Kandel, 1993; Bliss et al., 2003)). Furthermore, there is a lack of clear evidence demonstrating which structural changes are required to establish LTP. Do the alterations in synaptic strength that underlie LTP result from structural changes of pre-existing synapses - for example potentiation of existing synapses, the conversion of non-functional

(silent) to functional synapses, or splitting of existing connections? Or is the growth of new synapses required to establish LTP? Or are both processes required?

First indications came from a long-term sensitization *in vitro* model of the gill-withdrawal reflex in the marine mollusk *Aplysia californica*. There was 18 h after stimulation a significant increase in functional synapses detected (Kim et al., 2003). About two third of these new synapses were added after stimulation, while one third of the newly active synapses had previously been silent synapses (Kim et al., 2003). This activation of non-functional synapses, which occurred 3-6 h after stimulation might contribute to the early phase of LTP, while the addition of new synapses (occurring 12-18 h after stimulation) might be important for the late phase of LTP (Kim et al., 2003).

How might functional changes at existing synapses be mediated? Aside from changes in the molecular composition of AZ and PSD "morphological changes" at the level of the individual existing synapse might be important. *In vivo* imaging revealed that postsynaptic spines are very mobile. Changes in spine neck length (Yuste and Bonhoeffer, 2001) and changes in size or width of the synaptic cleft (Liu et al., 1999) are likely to alter synaptic efficacy. One role of spines is likely to isolate inputs biochemically and endow them with an independent calcium regulation. Since diffusion through the spine neck scales with its length (Svoboda et al., 1996), changes in the length thereby alter the compartmentalization of calcium important for input specific synaptic plasticity (Malenka et al., 1988; Engert and Bonhoeffer, 1997). Especially the enlargement of spine heads has been shown to occur in response to synaptic potentiation (Matsuzaki et al., 2004). Thereby spine enlargement was induced with little time delay (Matsuzaki et al., 2004), as it has been reported for the early phase LTP (Gustafsson and Wigstrom, 1990). This suggests that spine enlargement might be important for the early onset of LTP.

In contrast, new filopodia or spines require at least 20 min to emerge from dendrites after the induction of LTP. This is consistent with the observation that the formation of new synapses was delayed compared to the activation of existing synapses in *Aplysia* (Kim et al., 2003). Therefore, the rapid onset of LTP (Engert and Bonhoeffer, 1999; Maletic-Savatic et al., 1999) can not be explained by the formation of new synapses. New formation of synapses might rather contribute to a later phase of LTP. Once grown, enlarged synaptic spines are stable for months in the intact mouse cerebral cortex (Trachtenberg et al., 2002). Notably, in this model modification of existing connections and the establishment of new connections are two separate processes. chapter 2.2.4 will discuss a model in which these two processes are interconnected.

2.2.4 Changes at synapses during LTP: Is strengthening mediated by splitting of existing contacts?

Mainly based on comparative electron microscopy it was proposed that PSDs split during LTP. Although controversially discussed, this hypothesis is very attractive, since input specificity would be maintained during synaptic strengthening.
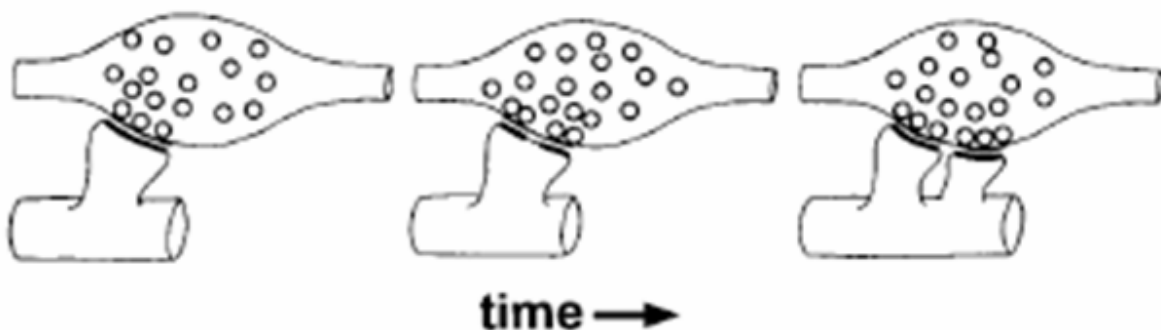
Fig. 7 Input-specific growth of new spines. In mature neural networks, modifications to the network are often viewed as adjustments in synaptic efficacy. One way in which this is accomplished is by the addition of redundant connections. In response to the activation of one synapse (left) an additional active zone appears, generating a perforated synapse (center). This spine may then split into two mature functional spines (right), strengthening the synaptic connectivity of specific synaptic partners (taken from (Jontes and Smith, 2000)).

According to this model first morphological changes can be observed 30 minutes after induction of LTP: spines become larger (Fifkova and Van Harreveld, 1977; Desmond and Levy, 1986) and there is a concomitant increase in synaptic area (Desmond and Levy, 1988). Subsequently synapses, which were already large, break apart (Fig. 7 center) forming perforated synapses (Peters and Kaiserman-Abramof, 1969; Toni et al., 1999). This is followed by the bifurcation of spines and ultimately by closely associated pairs of spines emanating from one dendrite and touching the same presynaptic element (Fig. 7 right) (Toni et al., 1999). The hypothesis that PSDs split during LTP was recently challenged by electron microscopic (EM) reconstructions of Harris and co-workers. They argue that pairs of spines converging on one presynaptic bouton (interpreted as evidence for synapse splitting (Luscher et al., 2000; Hering and Sheng, 2001; Yuste and Bonhoeffer, 2001)), can in fact not arise from synapse splitting, providing electron microscopic data that mature dendrites and axons pass through the gaps between the pair of spines (Fiala et al., 2002). *In vivo* imaging data addressing the question how new synapses are added within a functional circuitry will be presented in chapter 4.2.

2.3 Glutamatergic synapses in *Drosophila*

2.3.1 *Drosophila* neuromuscular synapses as a model system to study synaptic function and development

For various reasons, the *Drosophila* neuromuscular junction (NMJ) is an attractive model system to study fundamental questions concerning neuronal development and activity-dependent plasticity. *Drosophila* has short generation time and allows to establish, test and to efficiently apply different transgenic and knock out strategies. In its neuromuscular system, all motoneurons are identified and the exact target muscle they innervate is known. Most molecules involved in synaptic transmission are conserved between flies and vertebrates. The possibility to screen very efficiently for mutants in neuronal outgrowth and target recognition as well as in learning and memory has allowed identifying many genes involved in different aspects of neuronal development. Even subtle alterations in synaptic efficacy can reliably be identified since electrophysiological techniques are established for both the embryonic and the larval NMJ.

2.3.2 Organization and development of *Drosophila* NMJ synapses

The larval musculature together with its innervations is composed of a segmentally repeated set of 30 muscle cells each innervated by identified motoneurons (Goodman et al., 1986). The neuromuscular junction is organized into a series of boutons, which can be added during development and plasticity.
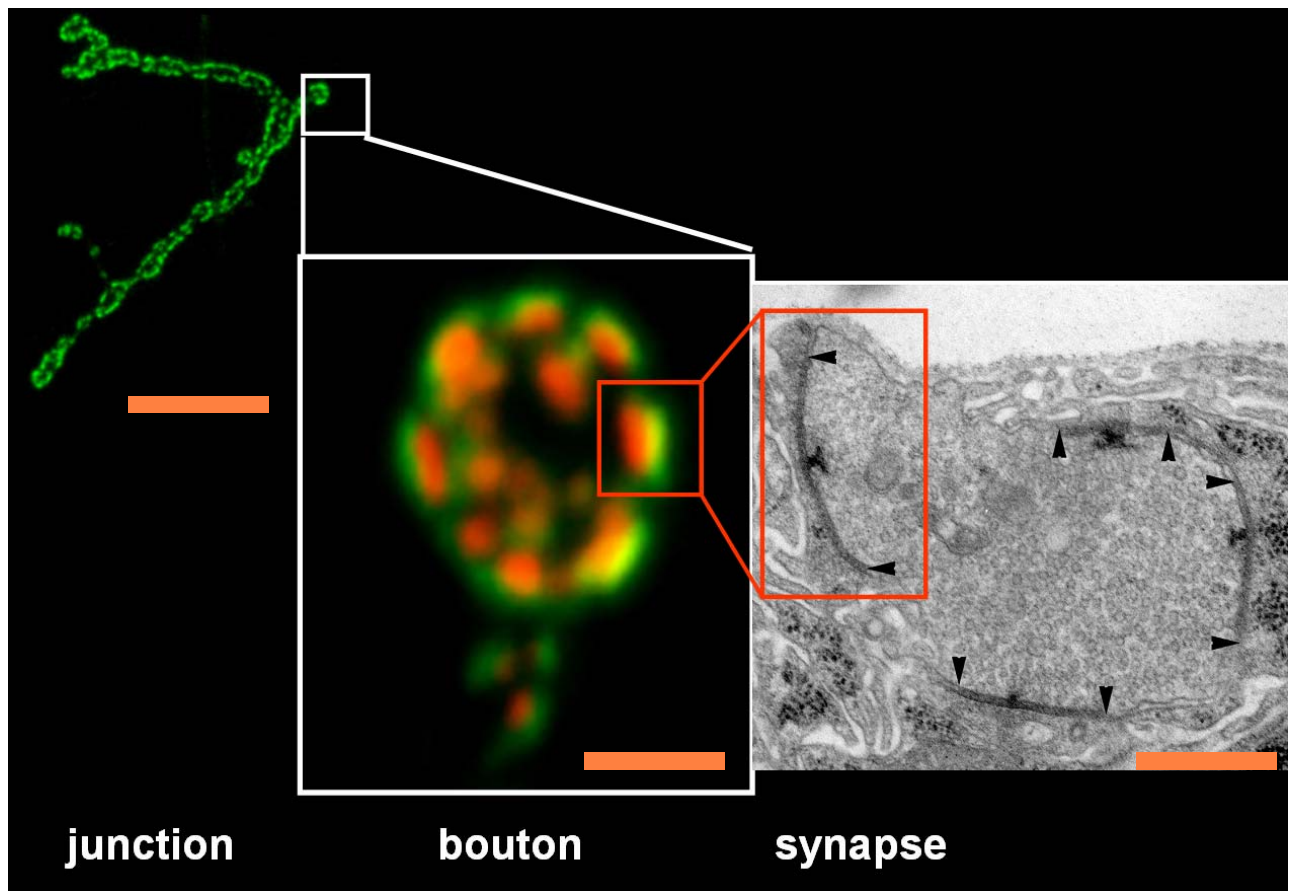
Fig. 8 Organization of *Drosophila* neuromuscular junctions. The NMJ in mature *Drosophila* larvae is composed from several boutons, each of them containing several individual synapses as visualized by nc82 (red, marks cytomatrix of active zone) and *Drosophila* glutamate receptor subunit DGluRIIC (green). The same structure is shown using electron microscopy. The PSDs are visualized as electron dense material between the arrowheads. The presynaptic bouton is filled with small, clear synaptic vesicles containing glutamate. Scale bars (from left to right) 20 µm, 1 µm and 300 nm (EM micrograph taken from (Sigrist et al., 2002)).

Each bouton (Fig. 8 central panel) contains several synapses identified as pairs of a postsynaptic density with corresponding specializations on the presynaptic site (the active zone is marked by the expression of the nc82 epitope and presynaptic Ca^{2+} channels (Kawasaki et al., 2004)).

This thesis will focus on type 1 boutons of the NMJ. These boutons contain small, clear synaptic vesicles (Atwood et al., 1993). Adjacent to the PSD, the postsynaptic muscle membrane folds in a typical manner. This structure, referred to as the subsynaptic

reticulum, surrounds the presynaptic terminal with multiple layers of elaborately folded muscle membrane. Many proteins shown to be relevant for the proper function of the neuromuscular junction like the N-CaM homolog Fasciclin II (Davis et al., 1996; Schuster et al., 1996, 1996) and the PSD95 homolog discs large (Budnik et al., 1996), have been shown to localize to the subsynaptic reticulum.

2.3.3 Non-NMDA type glutamate receptors are expressed at *Drosophila* NMJ synapses

The glutamate receptors expressed at the *Drosophila* neuromuscular junction are structurally and functionally similar to mammalian AMPA-/Kainate-type receptors. So far three different glutamate receptor subunits have been described at the neuromuscular junction. The *Drosophila* glutamate receptor subunit IIA (DGluRIIA) (Schuster et al., 1991) and IIB (DGluRIIB) (Petersen et al., 1997) share 44 % overall amino acid identity with each other. Animals double mutant for *dglurIIA* and the related *dglurIIB* subunit are embryonic lethal, while they can be rescued to adult vitality by transgenic expression of either DGluRIIA or DGluRIIB (Petersen et al., 1997; DiAntonio et al., 1999). Thus, either a DGluRIIA or a DGluRIIB subunit seems to be required to form functional ion channels at the NMJ. *Drosophila* glutamate receptor subunit IIC (DGluRIIC) is essential for neurotransmission and for synaptic localization of DGluRIIA or DGluRIIB, likely by acting as obligate binding partner of either DGluRIIA or DGluRIIB (Marrus et al., 2004). Like their vertebrate relatives *Drosophila* receptors desensitize within milliseconds in the presence of glutamate. The kinetics of glutamate binding and channel gating hereby are similar to those of vertebrate non-NMDA-type receptors (Heckmann and Dudel, 1997).

2.3.4 Activity-dependent plasticity of *Drosophila* neuromuscular junctions induced by genetic means

Analysis of synaptic plasticity at the *Drosophila* NMJ has allowed the identification of several mutants which suppress or stimulate outgrowth of the NMJ. The cell adhesion molecule Fascicilin II has been shown to mediate growth and activity dependent changes at the neuromuscular junction (Davis et al., 1996; Schuster et al., 1996, 1996). Genetic reduction of Fascicilin II by 50% yields significantly larger NMJs (Davis et al., 1996; Schuster et al., 1996, 1996). Thus reduction of cell adhesion seems to be an important prerequisite for additional outgrowth in response to increased presynaptic activity (Davis et al., 1996; Schuster et al., 1996, 1996). Such increase in presynaptic activity can be achived using a double mutant combination of both the ether a go-go (eag) and Shaker (Sh) potassium channel in which the frequency of presynaptic action potentials is strongly enhanced (Zhong et al., 1992). This "increase in activity" in turn provokes an increase of cAMP levels and finally enhanced morphological outgrowth of the junction. Increased morphological outgrowth of *eag, Sh* mutants is cAMP dependent, and the learning mutant dunce (Dudai et al., 1976) shows a very similar phenotype (Zhong et al., 1992). The dunce mutation affects the cAMP specific phosphodiesterase, which leads to elevated cAMP level (Kauvar, 1982). Junctional outgrowth can be suppressed (Zhong et al., 1992) in double mutants of dunce and rutabaga (Dudai and Zvi, 1984; Livingstone et al., 1984; Dudai and Zvi, 1985; Livingstone, 1985) with the latter mutation reducing cAMP synthesis. The outgrowth phenotype of *Sh* and *dunce* single mutants was further enhanced in double mutants (Zhong et al., 1992). In addition to these morphological changes mediated by the cAMP cascade, changes in glutamate receptor subunit composition have been shown to be able to provoke long-term changes of synaptic performance (Petersen et al., 1997; DiAntonio et al., 1999; Sigrist et al., 2002). Ultrastructural reconstruction of NMJ boutons has demonstrated the formation of additional synaptic sites in situations of increased DGluRIIA expression (Sigrist et al., 2002). The genetic analysis of plasticity mutants at the NMJ has thus already provided insights into molecular mechanisms controlling the formation of synapses in this model system. However, due to the chronic defects caused by mutations a time-resolved analysis of these mechanisms and their functional relationships is difficult.

2.3.5 Experience-dependent plasticity of *Drosophila* neuromuscular junctions

Recently, experience-dependent plasticity independent of genetic manipulation could be demonstrated at the NMJ. To this end, the locomotor activity (and therefore the extent of synaptic transmission) of *Drosophila* larvae was experimentally controlled in an acute and chronic manner (Sigrist et al., 2003; Zhong and Wu, 2004). When larval locomototion was increased either by chronically rearing a larval culture at 29°C instead of 18°C or 25°C, or by acutely transferring larvae from a culture vial onto agar-plates, a significant potentiation of synaptic transmission was detected within 2 hours (Sigrist et al., 2003). Enhanced locomotor activity was also associated with a significant increase in the number of subsynaptic translation aggregates (Sigrist et al., 2003). DGluRIIA, mRNA of which is present at the neuromuscular junction, has been suggested to be a target of local translation activity (Sigrist et al., 2000). In these experiments, an increased occurrence of subsynaptic translation aggregates was shown to be associated with the significant increase of DGluRIIA synaptic immunoreactivity (Sigrist et al., 2000). After 4 hours, postsynaptic DGluRIIA glutamate receptor subunits started to transiently accumulate in ring-shaped areas around synapses. Upon chronic locomotor stimulation at 29°C they condensed into typical postsynaptic patches (Sigrist et al., 2003). These NMJs showed a reduced perisynaptic expression of the cell adhesion molecule Fasciclin II, an increased number of boutons per NMJ and significantly more synapses (Sigrist et al., 2003). When combined with synapse live imaging, this experience dependent plasticity might be an important tool for *in vivo* study of activity-driven synapse formation.

2.3.6 Addressing the cellular and molecular basis of synaptic long-term changes at the *Drosophila* NMJ

As the muscles grow from embryo to mid third instar larvae their surface increases more than 100 fold which leads to a drop of input resistance (Jan and Jan, 1976; Broadie and Bate, 1993). Accordingly the synaptic current collectively mediated by the set of synapses within a junction increases more than two orders of magnitude during larval development (Broadie and Bate, 1993; Sigrist et al., 2003). Here, synapse formation was

studied within this time window. A principal question is, in how far these results can be compared to long-term potentiation (LTP) of existing circuitry. Long-term potentiation of synaptic systems means a long lasting increase of synaptic strength in response to a stimulus. In other words, a synaptic system challenged towards higher transmission strength reacts to that stimulus by structural and/or functional changes of its synaptic circuitry. This is in turn very similar to the increase in synaptic strength observed at the neuromuscular junction during development where the system provides additional synapses in order to maintain sufficient depolarization of a postsynaptic muscle cell which dramatically increases its size. Lessons learned "in development" might thus well be helpful in understanding the cellular basis of long-term potentiation and in turn learning and memory processes. This idea is consistent with a hypothesis of Cajal, saying that growth processes involved in the development of the nervous system persist into the adult where they subserve learning and memory (Cajal S., 1911). While this idea recently gained increased popularity (Kandel and O'Dell, 1992) it still needs to be further assayed in studies testing whether the same process is required for both neuronal development and synaptic plasticity. Due to the existence of alternative mechanisms, which mediate learning, this experiment is not easy to perform. Even when the system is severely disturbed as in the α-CamKII knockout mice (Silva et al., 1992; Silva et al., 1992; Silva et al., 1992; Tonegawa et al., 1995) there is still some learning present. Nonetheless, especially the similarities between learning and development in *Aplysia*, as described for the role of serotonergic axosomatic contacts, the activation of transcription factors, the necessity of an appropriate postsynaptic target, the role of cAMP as a second messenger and the common role of cell adhesion molecules, support the idea that learning and development share many common processes (Marcus et al., 1994). Results obtained from *in vivo* imaging of synapse formation and plasticity at the *Drosophila* NMJ might thus contribute substantially to our understanding of the fundamental cellular mechanisms important for establishing synaptic long-term changes.

2.4 High-throughput screen for the systematic identification and labeling of synaptic proteins in *Drosophila*

A key to understanding synapses formation and reorganization would be to follow the dynamic changes of many synaptic proteins in native cells and tissues. While a large number of proteins are known to be present at vertebrate synapses, the number of proteins known to localize to either presynaptic active zones or PSDs of *Drosophila* NMJ synapses is very limited. So far, the only proteins described to have such a specific localization are the glutamate receptor subunits DGluRIIA (Schuster et al., 1991), DGluRIIB (Petersen et al., 1997) and DGluRIIC (Marrus et al., 2004) as well as the *Drosophila* homologue of p21-activated kinase pak kinase (Harden et al., 1996) and Rho-type guanine nucleotide exchange factor DPix (Parnas et al., 2001) as well as the presynaptic calcium channel cacophony (Kawasaki et al., 2004). While one aim of this thesis was to directly GFP-tag some of the mentioned proteins, it was clear that this set of proteins might only be a small fraction of all proteins important for the function and structure of *Drosophila* NMJ synapses. Therefore, it was decided to also take an inverse genetic approach in order to identify more components specifically expressed at neuromuscular junctions. Although antibodies that specifically recognize a protein provide a great amount of information, they can be only used in fixed preparations. GFP-fusion proteins, however, allow the dynamic study of the fusion product's behavior living cells and tissues.

Morin and co-workers (Morin et al., 2001) first described the so called exon-trap strategy which allows the efficient random generation of on locus GFP-fusions on a genome-wide scale. In an exon-trap screen, randomized insertional mutagenesis is combined with the use of a GFP encoding exon lacking initiation and stop codon. This exon is placed in a P-element based vector in which the GFP is flanked by functional splice sites derived from the *Drosophila* myosin heavy chain II gene. During randomized genomic integration, such a cassette can become integrated into an intron. Upon subsequent splicing, an mRNA is generated that contains GFP sequences but no other vector sequences.
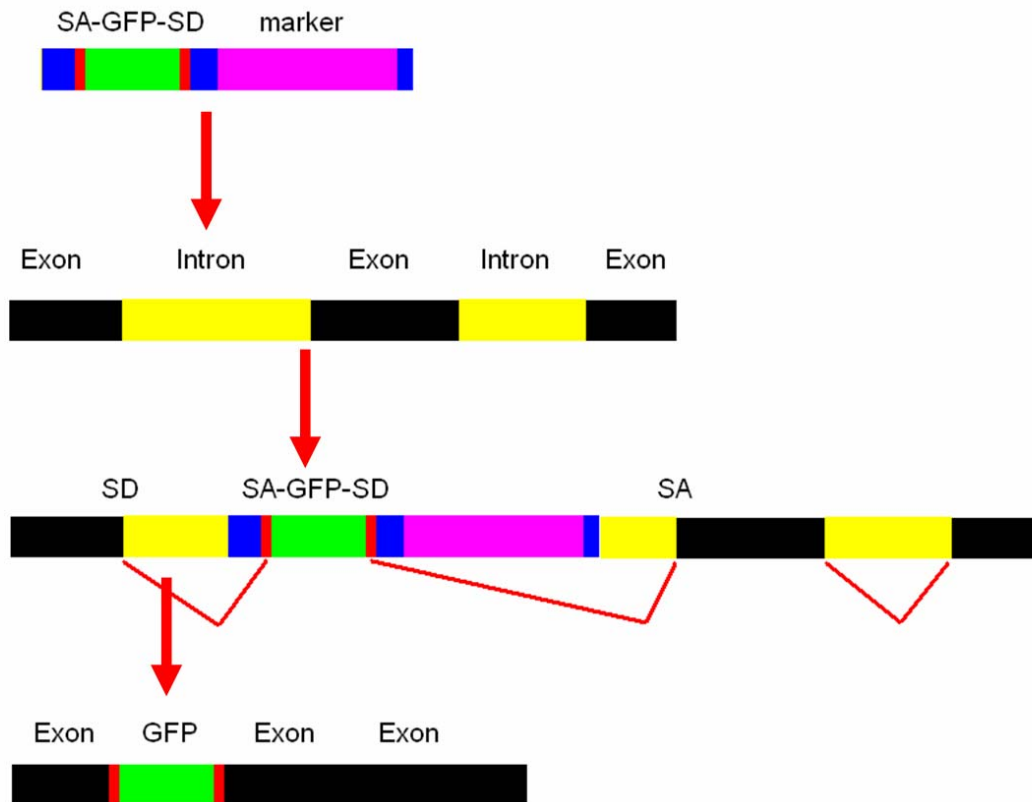
Fig. 9 Principle of exon-trap screen. When an exon-trap vector gets integrated into a genomic intron, subsequent splicing leads to the expression of a genomically encoded and expressed GFP-fusion protein

In detail, this is achieved by splicing out all sequences 5' and 3' of the GFP cassette. At the 5' end of GFP splicing occurs between the GFP splice acceptor site (SA) and the splice donor (SD) site of the upstream exon of the protein in which the vector has integrated. At the same time the SD site 3' of GFP splices with the SA site of the downstream exon (Fig. 9). Thereby it is possible to remove all vector and marker sequences and to create a fusion protein, in which GFP is inserted as an artifical additional exon. Based on the random character of this screen only a small number of transpositions will give rise to a chimeric fusion protein. One sixth of the integration events will be in the right orientation and frame. Of these insertions those will be selected, which lie in an intron of a protein that tolerates GFP insertion and is expressed at a sufficiently high level at the timepoint of screening. Thus Morin and co-workers reported that about 1 in 1600 transpositions will lead to a productive, i.e. GFP positive chimeric fusion protein (Morin et al., 2001). Fortunately, these events can be easily identified based on the GFP

expression. The GFP-tagged proteins usually appear to be targeted normally (Morin et al., 2001). Furthermore, once a protein with a subcellular localization of interest has been identified, mutants can be easily introduced by imprecise excision of the GFP-encoding transposon.

2.5 Technical improvements of exon-trap screening by the use of a *novel* transposable element

So called P-Elements are the standard transformation vector used for *Drosophila* germ line transformation. Unfortunately, P-elements as used by Morin and coworkers have a high tendency to integrate into the 5' regulatory sequences of endogenous genes (which cannot lead to productive events in exon-trap-screening). Therefore in this thesis an alternative transformation vector ("*piggyBac*") showing a broader selection of insertion sites (Berghammer et al., 1999; Cary et al., 1989; Horn and Wimmer, 2000) was adapted for GFP-exon-trap screening. The *piggyBac* transposon belongs to a group of TTAA-specific, short repeat elements that share similar structures and properties of movement. Other members of this family include the *tagalong* elements, the *Spodoptera frugiperda* derived elements IFP1.6 (Beames and Summers, 1988) and the transposon-like insertion within the *EcoR*I-J,N region of the *Autographa californica* nuclear polyhedrosis virus (Oellig et al., 1987). The *piggyBac* element was originally identified as an insertion within both *Autographa californica* and *Galleria mellonella* nuclear polyhedrosis virus genomes following *in vitro* passage of the viruses in the insect cell line *Trichoplusia ni*, TN-368. While *piggyBac* (formerly IFP2) was isolated in an insect cell line other elements of the TTAA-class appear to be common among other animals as well. These elements show a strong preference for TTAA target sites, whether inserting within the viral FP-locus (Cary et al., 1989; Wang et al., 1989) or at other regions of the viral genome (Wang et al., 1989; Fraser et al., 1995). While the importance of these elements for genetic manipulation has been appreciated only recently, experimental evidence is accumulating, which suggests that they will be extremely useful tools to generate transgenic animals, particularly insects in the orders Diptera, Lepidoptera, and Coleoptera.

piggyBac encodes its own transposase which operates using a precise cut-and-paste mechanism. During insertion the target TTAA tetranucleotide sequences are duplicated. Upon excision the duplicated sequences are again reformed to a single target site, leaving no footprint behind (Cary et al., 1989; Fraser et al., 1995; Elick et al., 1996; Fraser et al., 1996).This is in contrast to P-elements, which excise either precisely or imprecisely (leaving parts of the element behind, or taking along some target sequence). The *piggyBac* transposable element is a 2472 bp short inverted terminal repeat element composed of a 2374 bp transposase-encoding internal repeat flanked by a asymmetric terminal repeat (TR). The 5' TR consists of a 19 bp internal repeat sequence separated from the 13 bp terminal repeat sequence by 3 bp, while the 3' terminal repeat has a 31 bp spacer separating the internal and terminal repeat sequences (Cary et al., 1989; Fraser et al., 1995; Elick et al., 1996). Besides being capable of mediating germ-line transformation in *Drosophila* (Berghammer et al., 1999; Handler and Harrell, 1999; Horn et al., 2000; Horn and Wimmer, 2000) *piggyBac* meanwhile is also the standard vector for germline transformation in non-drosopholid insect species. Species which have been successfully germline transformed include *Ceratitis capitata* (Handler et al., 1998), *Tribolium castaneum* (Berghammer et al., 1999), *Bactrocera dorsalis* (Handler and McCombs, 2000), *Bombyx mori* (Tamura et al., 2000), *Aedes aegypti* (Lobo et al., 2002), *Anastrepha suspense* (Handler and Harrell, 2001), *Anopheles gambiae* (Grossman et al., 2001), *Anopheles albimanus* (Perera et al., 2002), *Anopheles stephensi* (Nolan et al., 2002), *Musca domestica* (Hediger et al., 2001), *Lucilia cuprina* (Heinrich et al., 2002), the planarian *Girardia tigrina* (Gonzalez-Estevez et al., 2003) and the screwworm Cochliomyia homivorax (Allen et al., 2004).

2.6 Objectives

So far no coherent picture has been established of how new glutamatergic synapses form in their native settings. This thesis sought to establish assays that allow for directly studying identified sets of glutamatergic synapses in intact *Drosophila* over time. These results should help us to further understand the cellular and molecular basis of long-term changes in both functional strength and architecture of synaptic connections. Such assays should help addressing for the first time *in vivo*, whether new glutamatergic synapses form exclusively *de novo* or as previously suggested by splitting events. To this end, *in vivo* photo-labeling procedures had to be established and glutamate receptor dynamics had to be monitored during synapse formation. To allow *in vivo* analysis of presynaptic assembly relative to postsynaptic assembly, proteins localized into presynaptic active zones of *Drosophila* were to be identified. Finally, to obtain a more complete picture of the proteins and mechanisms controlling the formation of new synapses, a genome-wide genetic screen resulting in a systematic identification of synaptic proteins expressed as GFP fusions from their endogenous locus was to be initiated.

3. Material and methods

3.1 Molecular biology

3.1.1 Materials used in molecular biology

All molecular biology was performed according to standard procedures (Sambrook, 1989). All enzymes for molecular biology were except explicitly otherwise stated obtained from Roche, Mannheim, Germany. This includes T4 Ligase (used for all ligations), Phosphatase alkine shrimp (used for all dephosphorilations), as well as all restriction enzymes. The restriction enzymes *Pme*I, *Asc*I and *Dpn*I were obtained from New England Biolabs, Frankfurt am Main, Germany. For all PCRs, which lead to the construction of transgenic constructs Vent Polymerase (New England Biolabs, Frankfurt am Main, Germany) was used. For all other PCRs (except otherwise stated) Amplitaq Polymerase (Applied Biosystems, Foster City, CA, USA) was used.

3.1.2 Annealing of oligos

To anneal oligos 20 µL of each oligo (dilluted to 100 pmol/µl) were mixed with 5 µL water and and 5 µl of annealing buffer (100 mM $MgCl_2$, 250 mM Tris pH=8,0). This solution was put (in a 1,5 ml eppendorf cup) into 1 L of boiling water. The water was allowed to cool down to room temperature (usually over night). Once cooled down 1 µl of a 1:10 dillution of the oligo solution was after used for ligations. The oligos were already ordered with a 5'-Phosphate modification (MWG-Biotech AG, München, Germany).

3.1.3 Construction of fluorescently labeled DGluRIIA

Summary:

To express fluorescently tagged DGluRIIA, an *Eco*RI/*Xba*I genomic fragment from BACR35L07 entailing 1,2 kb sequence upstream of the start codon was used. The fluorescent tags (GFP, mRFP and photo-activatable GFP) were inserted in the intracellular C-terminus of DGluRIIA after amino acid (AA) S893. To construct DPak^{GFP} the myc-tag in UAS-pak-myc (Ang et al., 2003) was replaced by EGFP. All constructs were confirmed by double-strand sequencing and transgenic flies were produced using standard procedures.

Construction of pUAST IIA-Genomic-GFP:

To construct pKS-*Eco*RI-*Xho*I-IIA-Genomic BACR35L07 was digested with *Eco*RI and *Xho*I and the 5579 bp fragment was ligated into pBluescript II KS+ (Stratagene) cut with *Eco*RI and *Xho*I.

To construct pSL-*Bam*HI/*Nco*I-IIA-Genomic pKS-*Eco*RI/*Xho*I IIA-Genomic was cut with *Bam*HI and *Nco*I and ligated into pSLfa1180fa (Horn et al., 2000) cut with *Bam*HI and *Nco*I.

To construct pSL-*Bam*HI/*Nco*I-IIA-Genomic-GFP EGFP was amplified from p-EGFP-1 (Clontech) with TR 393 (5'-GGC GCG CCG AGC AAG GGC GAG GAG CTG TTC ACC GG-3') and TR394 (5'-CGG GCG CGC CGC CCT TGT ACA GCT CGT CCA TGC CGA GA-3') and ligated blunt into pSL-*Bam*HI/*Nco*I-IIA-Genomic which had been amplified with TR 391 (5'-GGC AGA TGT GTA TAA GAG ACA GAT CCG GTT CCA GAC GCA GCT CCA AG-3') and TR 392 (5'-AGA TGT GTA TAA GAG ACA GGA ACC GGA TGA TCG CCT GGA CGA CG -3').

To construct pSL-*Eco*RI-*Xho*I-IIA-Genomic pKS-*Eco*RI-*Xho*I-IIA-Genomic was digested with *Eco*RI and *Xho*I and ligated into pSLfa1180fa (Horn et al., 2000) cut with *Eco*RI and *Xho*I.

After verification by sequencing pSL-*Bam*HI/*Nco*I-IIA-Genomic-GFP was digested with *Nco*I and *Bam*HI and ligated into pSL-*Eco*RI-*Xho*I-IIA-Genomic cut with *Nco*I and *Bam*HI to construct pSL-*Eco*RI-*Xho*I-IIA-Genomic-GFP.

To construct pUAST-IIA-Genomic-GFP pSL-*Eco*RI-*Xho*I-IIA-Genomic-GFP was digested with *Eco*RI and *Xho*I and ligated into pUAST trangenesis vector (Brand and Perrimon, 1993) cut with *Eco*RI and *Xho*I.

Construction of pUAST IIA-Genomic-C1-mRFP1:

To construct pTR+ pSLfa1180fa (Horn et al., 2000) was digested *Bam*HI and XbaI and ligated into pBluscriptII KS+ (Stratagene) cut with *Bam*HI and XbaI.

To construct pTR-*Bgl*II/*Xho*I-IIA-Genomic-GFP pSL-*Eco*RI-*Xho*I-IIA-Genomic-GFP was digested *Bgl*II and *Xho*I and ligated into pTR+ cut with *Bgl*II and *Xho*I.

To construct pTR-*Bgl*II/*Xho*I-IIA-Genomic-mRFP1 mRFP1 was amplified from pRSETb mRFP1 (gift from Roger Y. Tsien, Howard Hughes Medical Insitute, USA) with TR 307 (5'-GGT CGG CGC GCC GCC CTT GTA CAG CTC GTC CAT GCC G-3') and TR308 (5'-GTC AGG CGC GCC GAG CAA GGG CGA GGA GCT GTT CAC C-3') cut with *Asc*I and ligated into pTR-*Bgl*II/*Xho*I-IIA-Genomic-GFP cut with *Asc*I.

After verification by sequencing pTR-*Bgl*II/*Xho*I-IIA-Genomic-mRFPI was digested with *Bgl*II and *Xho*I and ligated into pUast-*Eco*RI-*Xho*I-IIA-Genomic-GFP cut with *Bgl*II and *Xho*I to construct pUast-*Eco*RI-*Xho*I-IIA-Genomic-mRFP1.

3.1.4 Construction of fluorescently labeled DGluRIIC

<u>Plasmids of general use:</u>

To construct pSL GFP Asc1 EGFP was amplified from pEGFP-1 (Clontech, Palo Alto, USA) with TR 308 (5'- GTC AGG CGC GCC GAG CAA GGG CGA GGA GCT GTT CAC C-3') and TR307 (5'- GTC AGG CGC GCC GAG CAA GGG CGA GGA GCT GTT CAC C-3') cut with *Asc*I and ligated into pSL1180fa cut *Asc*I.

To construct TgPT0(Cyan)delta kan TGPT0 was digested with *Srf*I and religated.
To construct TgPT1(GFP)delta kan TGPT1 was digested with *Srf*I and religated.

To construct pSL Cyan Trans Cyan was amplified from TgPT0(Cyan)delta kan with TR 297 (5'- GCA CCG CTA GCC ACA TCT GGC GCG CCG AGC AAG GGC -3') and TR305 (5'- GCTCAGATCTTATACACATCTGCCCGGGCGC -3') cut with *Nhe*1 and *Bgl*2 and ligated into pSL1180fa cut with *Nhe*I and *Bgl*II.

To construct pSL EGFP Trans GFP was amplified from TgPT1(GFP)delta kan with TR286 (5'- GAC GGC TAG CCT TAT ACA CAT CTG GCG CGC CAG CA -3') and TR288 (5'- GCC GAG ATC TCT TAT ACA CAT CTG CCC GGG C -3') cut with *Nhe*I and *Bgl*II and ligated into pSL1180fa cut with *Nhe*I and *Bgl*II.

<u>DGluRIIC^{GFP}:</u>

To construct pSL IIC AB CDNA a part of the DGluRIIC cDNA (RE65796) was amplified with the primers TR306 (5'- GTG AAG ATC TGC GGC CGC CAT GGA ATC GCC AGC CCG TGT GCT -3') and TR274 (5'- CGC ATC TAG AAC CTC GGG ATC CGG ATT GCA CGG ATG -3') cut *Bgl*II and *Xba*I and ligated into pSL1180fa.

To construct pSL IIC C CDNA part of the DGluRIIC cDNA (RE65796) were amplified with the primers ST275 (5'- GGG CTG GCA AGC CAC GTT TGG TG -3') and TR302 (5'- GGT

ATT CCC GGA CTA GGA AGC TCC CCC TGA TCA CGA TCG TCG C -3')cut with Xba1 and *Nhe*I and ligated into pSL1180fa cut with *Xba*I and *Nhe*I.

To construct pSL IIC CDNA pSL IIC AB CDNA was digested Not1 and Xba1 ligated into pSL IIC C CDNA cut with *Not*I and *Xba*I

To construct pTR IIC 259 A CDNA part of IIC CDNA were amplified from pSL IIC CDNA with the primers TR306 (5'- GTG AAG ATC TGC GGC CGC CAT GGA ATC GCC AGC CCG TGT GCT -3') and TR283 (5'- GAC TGC TAG CGT AAA CGA TGT TGT CCC TTT GGG TG -3') cut with *Bgl*II and *Nhe*I and ligated into pTR cut with *Bgl*II and *Nhe*I.

To construct pSL IIC 259 B CDNA part of IIC CDNA were amplified from pSL IIC CDNA with the primers TR284 (5'- GAC TAG ATC TAT CGT TTA CGA AAG CAG CGA TCC GC -3') and TR304 (5'- GCC ACA GTC AAC CAG CCA GTA TTG TG -3') cut with *Bgl*II and *Xba*I and ligated into pSL1180fa cut with *Bgl*II and *Xba*I.

To construct pTR IIC 259 B GFP CDNA the 0,8 kb *Bgl*II/*Not*I Fragment of pSL IIC 259 B CDNA and the 0,8 kb *Nhe*I/*Bgl*II Fragment of pSL EGFP Trans were ligated into pTR IIC 259 A CDNA cut with *Nhe*I and *Not*I.

To construct pSL IIC GFP 259 CDNA the 2,5 kb *Not*I/*Xba*I Fragment of pTR IIC 259 B GFP CDNA was ligated into pSL IIC CDNA cut with *Not*I and *Xba*I.

To construct pUAST IIC GFP 259 CDNA the 3,6 kb *Not*I/*Spe*I Fragment of pSL IIC GFP 259 CDNA was ligated into pUAST cut with *Not*I and *Xba*I.

3.1.5 Construction of fluorescently labeled DPak

To construct pKS-EGFP-Linker EGFP was amplified from p-EGFP-1 (Clontech, Palo Alto, USA) with CM604 (5'-CCC AAG CTT ATG GTG AGC AAG GGC GAG G-3') and CM605 (5'-CCG ATA TCT TAC TTG TAC AGC TCG TCC ATG-3'), cut with *Hind*III and *Eco*RV

and was subsequently ligated into pBluscriptII KS+ (Stratagene) cut with *Hind*III and *Eco*RV.

To construct pKS-pak-EGFP pak was amplified from UAS-pak-myc (Ang et al., 2003) with CM616 (5'-CCG CTC GAG ATG TCC AGC GAG GAA GAC AAA CCG-3') and CM617 (5'-CCC AAG CTT GTT GCC CTT GGT AGC CTC CTT TG-3'), cut with *Xho*I and *Hind*III and was subsequently ligated into pKS-EGFP-Linker cut with *Xho*I and *Hind*III.

To construct pUAST-pak-EGFP pak-EGFP was amplified from pKS-pak-EGFP with CM826 (5'-CGG AAT TCA TGT CCA GCG AGG AAG ACA AAC CG-3') and CM827 (5'-CGG AAT TCT TAC TTG TAC AGC TCG TCC ATG-3'), cut with *Eco*RI and was subsequently ligated into pUAST cut with *Eco*RI.

All constructs were confirmed by double-strand sequencing.

3.1.6 Construction of fluorescently labeled DCast

Summary of cloning strategy:

In a multiple step cloning strategy the N-term of DCast was isolated via RT PCR from adult head mRNA and joined with the known partial cDNA clone AT09405 to construct a full length cDNA. Alternatively an *Asc*I site was inserted into the N-Term. This *Asc*I site was used to introduce different fluorophores (GFP, mRFP).

Subcloning of N-term of DCast:

To construct pCR2 Cast N -Term Clone 1.2 the N-Term of DCast was amplified from random primed adult head cDNA using the primers TR674 (5'- ATG GGC AGT CCA TAC TAC CGC GAC ATG-3') and TR626 (5'- CCA TCT CCT CCT TGA TCT TTT CCA C -3') using Takara Taq Polymerase (RP 002 M, Takara Bio Inc., Shiga, Japan). The PCR product was cut with and subcloned into precut pCR 2.1 (part in the TA cloning kit (K 2040-01, Invitrogen)).

Construction of full length DCast:

To construct pKS N-term Cast2 wt the plasmid pCR2 Cast N -Term Clone 1.2 was digested *Nsi*I and *Hind*III. The 2,9 kb insert was ligated into pKS+ Bluscript2 cut with *Pst*I and *Hind*III.

To construct pKS Cast2 wt the DCast cDNA AT09405 was digested *Bgl*II. The 3 kb insert was ligated into pKS N-term Cast2 wt cut with *Bgl*II.

To construct pUAST XL+ an artificial MCS (containing the following restriction sites: *Pme*I, *Spe*I, *Nae*I, *Fse*I, *Pac*I, *Asc*I, *Swa*I) was introduced into the *Eco*RI site in pUAST. To this aim pUAST was digested with *Eco*RI, dephosphorilated and ligated to the annealed oligos TR914 (5'-AAT TCG TTT AAA CTA GTG GCC GGC CTT AAT TAA GGC GCG CCA TTT AAA TG-3') and TR 915 (5'-AAT TCA TTT AAA TGG CGC GCC TTA ATT AAG GCC GGC CAC TAG TTT AAA CG-3'). After sequencing the clones with the orientation 5'-*Pme*I-..-*Swa*I-3' were named pUAST XL+, while clones with the orientation 5'-*Swa*I-..-*Pme*I-3' were named pUAST XL-. It would have made no difference to use either pUAST XL+ or pUAST XL- for the last cloning step pUAST Cast2 GFP. Therefore it was cloned in one of the resulting pUAST XL vectors (Mini1). After sequencing it turned out that this Mini carried a tandem MCS in -/+ orientation (5'-*Swa*I-..-*Pme*I-*Pme*I-..*Swa*I-3') and was therefore named pUAST XL-/+. This vector was never used again except for the next cloning step and the simultaneous construction of pUAST Cast2 GFP.

To construct pUAST Cast2 wt the plasmid pKS Cast2 wt was digested with *Spe*I and *Asp*718. The insert was ligated into pUAST XL-/+ cut with *Spe*I and *Asp*718.

Construction of Cast[GFP]:

To construct pCR2 Cast N-Term Clone 1.2 delta *Bam*HI the plasmid pCR2 Cast-N-Term Clone 1.2 was cut with *Kpn*I and *Spe*I, blunted and religated.

To construct pCR2 N-Term *Asc*I Cast2 vorstufe the entire plasmid pCR2 Cast-N-Term Clone 1.2 was amplified via circular PCR using the Primer 831 (5'-GAC TGG CGC GCC CGG CAG TCC ATA CTA CCG CGA CAT GG-3') and 832 (5'- GTC TGG CGC GCC CAT TGC TGA AAT TCA CAC ACA CAG AGA -3'). After the PCR residual template was removed via a *Dpn*I digest. Next the PCR product was cut with *Asc*I and religated.

To construct pCR2 N-Term *Asc*I Cast2 the plasmid vorstufe pCR2 N-Term *Asc*I Cast2 was digested with *Bam*HI and *Nsi*I. The 0,2 kb fragment was ligated into Cast N-Term Clone 1.2 delta *Bam*HI.

To construct pKS N-Term *Asc*I Cast2 the plasmid pCR2 N-Term *Asc*I Cast2 was cut with *Hind*III and *Nsi*I. The 2,9 kb fragment was ligated into pKS+ Bluscript2 cut with PstI and *Hind*III.

To construct pKS Cast2 *Asc*I the cDNA clone entailing the C-Term of DCast (AT09405) was cut with *Bgl*II. The 3,6 kb fragment was ligated into pKS N-Term *Asc*I Cast2 cut with *Bgl*II.

To construct pKS Cast2 GFP the construct pSL-*Eco*RI-*Xho*I-IIA-Genomic-GFP was digested with *Asc*I. The resulting GFP flanked by two *Asc*I sites then inserted into pKS Cast2 *Asc*I digested with *Asc*I.

To construct pUAST Cast2 GFP the plasmid pKS Cast2 GFP was digested with *Spe*I and *Asp*718. The insert was ligated into pUAST XL-/+ cut with *Spe*I and *Asp*718.

Construction of Cast^{mRFP}:

To construct pUAST Cast2 FP-Site the plasmid pKS Cast2 GFP was digested with *Spe*I and *Asp*718. The insert was ligated into pUAST XL+ cut with *Spe*I and *Asp*718.

To construct pUAST Cast2 mRFP the plasmid pTR-*Bgl*II-*Xho*I-IIA-Genomic-mRFP1 (construction details see chapter 2.1.5) was digested with *Asc*I. The 700 bp mRFP fragment was inserted into pUAST Cast2 FP-Site cut with *Asc*I.

3.1.7 Exon-trap screen: Reading frames

For all constructs the same splice acceptor (SA) GFP splice donor (SD) cassette was used as in the screen of Morin and co-workers (Morin et al., 2001). The SA fragment derived from the intron 18 exon 19 junction of the *Drosophila* myosin heavy chain (MHC) gene. The intron part is given in small letters, while the exon part is shown in capital letters. For the three reading frames pP-GA (ccg cag ATC CAC CAT CAT CAC CAC CAT GGC GCG TCG), pP-GB (ccg cag ATC CCA CCA TCA TCA CCA CCA TGG CGC GTC G) and pP-GC (ccg cag ATC CAC ACC ATC ATC ACC ACC ATG GCG CGT CG) the reading frame correction is underlined, while the reading frame is indicated by the spaces between the nucleotide triplets.

3.1.8 Exon-trap screen: Construction of *piggyBac* vectors

Overview of constructs:
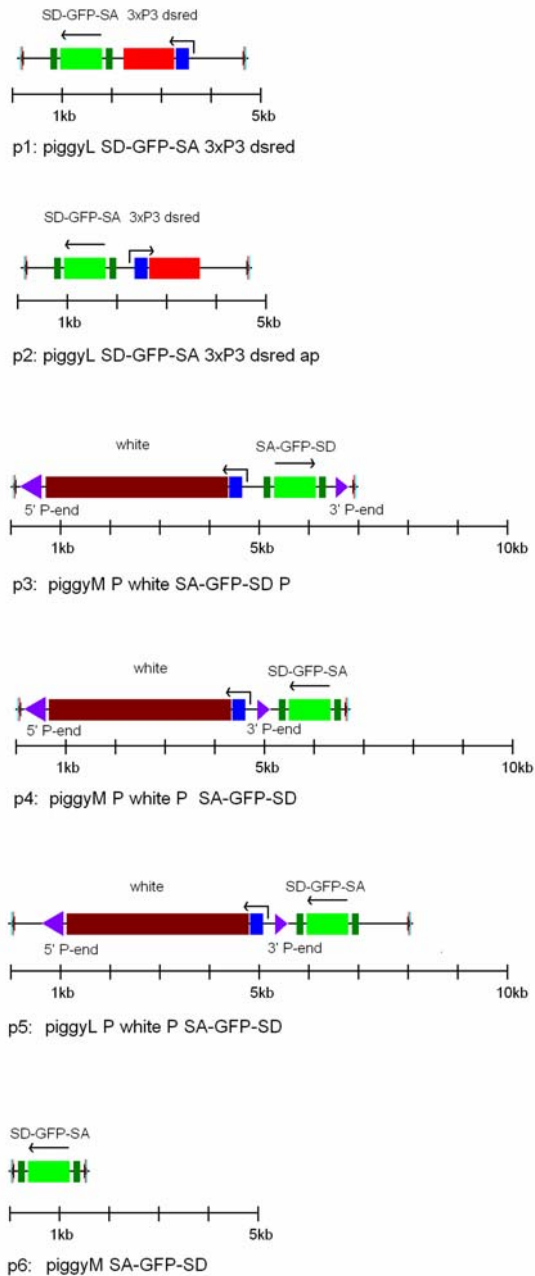
Fig. 10 Overview of all *piggyBac* constructs. For details concerning construction see text

Cloning of cassettes of central importance for the *piggyBac* vector generation:

To construct pSL 3x P3 ds-red the 3x-ds-red cassette was amplified from pSL 3xP3 ds-red af (gift of Ernst Wimmer, University of Göttingen, Germany) with S182 (5'GAG TGC TAG CAG AGC TCG CCC GGG GAT CTA ATT CAA TT-3') and S180 (5'-GAC TAG ATC TCG AGA TCG GCC GGC CTA GGC GCG C-3') cut with *Nhe*I and *Bgl*II and ligated into pSL1180fa cut with *Nhe*I and *Bgl*II.

To construct pSL SD-GFP-SA (A) the SD-GFP-SA cassette was amplified from pP-GA with the primers S179 (5'-GCA CGG ATC CTT TAT TTT TAA TAA TTT GCG AGT ACG-3') and S181 (5'- CCG AAT TCT AGT ATG TAT GTA AGT TAA GAT CTC AGC-3') cut with *Bam*HI and *Bgl*II and cloned into pSL1180fa cut with *Bgl*II *Bam*HI. The functionality of both *Bam*HI and *Bgl*II site were verified.

To construct pSL SD-GFP-SA (B) the SD-GFP-SA cassette was amplified from pP-GB with the primers S179 (5'-GCA CGG ATC CTT TAT TTT TAA TAA TTT GCG AGT ACG-3') and S181 (5'- CCG AAT TCT AGT ATG TAT GTA AGT TAA GAT CTC AGC-3') cut with *Bam*HI and *Bgl*II and cloned into pSL1180fa cut with *Bgl*II *Bam*HI. The functionality of both *Bam*HI and *Bgl*II site were verified.

To construct pSL SD-GFP-SA (C) the SD-GFP-SA cassette was amplified from pP-GC with the primers S179 (5'-GCA CGG ATC CTT TAT TTT TAA TAA TTT GCG AGT ACG-3') and S181 (5'- CCG AAT TCT AGT ATG TAT GTA AGT TAA GAT CTC AGC-3') cut with *Bam*HI and *Bgl*II and cloned into pSL1180fa cut with *Bgl*II and *Bam*HI. The functionality of both *Bam*HI and *Bgl*II site were verified.

To construct pTR+ SD-GFP-SA (A) the SD-GFP-SA cassette was amplified from pP-GA with the primer S179 (5'-GCA CGG ATC CTT TAT TTT TAA TAA TTT GCG AGT ACG-3') and S181 neu (5'- GCT GAG ATC TTA ACT TAC ATA CAT ACT AGA ATT CGG -3') cut with *Bam*HI and *Bgl*II and ligated into pTR+ cut with *Bam*HI and *Bgl*II.

To construct pTR+ SD-GFP-SA (B) the SD-GFP-SA cassette was amplified from pP-GB with the primer S179 (5'-GCA CGG ATC CTT TAT TTT TAA TAA TTT GCG AGT ACG-3') and S181 neu (5'- GCT GAG ATC TTA ACT TAC ATA CAT ACT AGA ATT CGG -3')cut with *Bam*HI and *Bgl*II and ligated into pTR+ cut with *Bam*HI and *Bgl*II.

To construct pTR+ SD-GFP-SA (C) the SD-GFP-SA cassette was amplified from pP-GC with the primer S179 (5'-GCA CGG ATC CTT TAT TTT TAA TAA TTT GCG AGT ACG-3') and S181 neu (5'- GCT GAG ATC TTA ACT TAC ATA CAT ACT AGA ATT CGG -3') cut with *Bam*HI and *Bgl*II and ligated into pTR+ cut with *Bam*HI and *Bgl*II.

To construct pTR+ white delta *Bam*HI vorstufe the white cassette was amplified from pUAST delta *Bam*HI with the primer TR 505 (5'- GAC AGG TAC CGC TAG CTC GTC GAT AGC CGA AGC TTA CCG AA -3') and TR 506 (5'- CTT CAG ATC TAA GCT CAC GAT GAG AAT GGC CAG AC -3') cut with *Bgl*II and *Asp*718 and ligated into pTR+ cut with *Bgl*II and *Asp*718.

Cloning of the backbones piggy mini (piggyM) and piggy large (piggyL):

To construct piggy mini vorstufe a circular PCR was performed with the primer TR503 (5'-CCG TTA ACA GAT CTT AAA AGT TTT GTT ACT TTA TAG AAG -3') and TR 504 (5'-CGC GCC GCT AGC ATA TCT ATA ACA AGA AAA TAT ATA TA -3')and pE3.12 as template. The product was digested with *Dpn*I to remove residual template, then phosphorilated and ligated to itself.

To construct piggy mini the construct piggy mini vorstufe was cut with *Eco*RV *Nsi*I and the 0,7kb Fragment containing the piggy mini MCS was ligated into pE3.12 cut with *Eco*RV and *Nsi*I.

To construct piggyL the construct pE3.12 was digested with *Bgl*II and *Hpa*I and dephosphorilated and ligated with an artificial multiple cloning site (MCS) consisting of the annealed oligos TR963 (5'- GAT CCG CTA GCG GCG CGC CAG ATC TGT T-3') and TR964 (5'- AAC AGA TCT GGC GCG CCG CTA GCG -3').

<u>Cloning of p1: piggyL SD-GFP-SA 3x P3 ds-red (X)</u>

To construct piggy L SD-GFP-SA (A) the plasmid pSL SD-GFP-SA A was digested with *Bam*HI and *Hpa*I. The SD-GFP-SA cassette was cloned into pE3.12 cut with *Bgl*II and *Hpa*I.

To construct piggy L SD-GFP-SA (B) the plasmid pSL SD-GFP-SA B was digested with *Bam*HI and *Hpa*1. The SD-GFP-SA cassette was cloned into pE3.12 cut with *Bgl*II and *Hpa*I.

To construct piggyL SD-GFP-SA (C) the plasmid pSL SD-GFP-SA C was digested with *Bam*HI and *Hpa*I. The SD-GFP-SA cassette was cloned into pE3.12 cut with *Bgl*II and *Hpa*I.

To construct piggyL SD-GFP SA 3x P3 ds-red (A). The plasmid pSL 3x P3 ds-red was digested with *Bgl*II and *Nhe*I. The 3x P3 ds-red cassette was cloned into piggyL SD-GFP-SA (A) cut with *Bgl*II and *Nhe*I.

To construct piggyL SD-GFP SA 3x P3 ds-red (B). The plasmid pSL 3x P3 ds-red was digested with *Bgl*II and *Nhe*I. The 3x P3 ds-red cassette was cloned into piggy L SD-GFP-SA (B) cut with *Bgl*II and *Nhe*I.

To construct piggyL SD-GFP-SA 3x P3 ds-red (C). The plasmid pSL 3x P3 ds-red was digested with *Bgl*II and *Nhe*I. The 3x P3 ds-red cassette was cloned into piggyL SD-GFP-SA (C) cut with *Bgl*II and *Nhe*I.

Cloning of p2: piggyL SD-GFP-SA 3x P3 ds-red ap (A):

To construct piggyL SD-GFP-SA 3x P3 ds-red ap (A) the plasmid pSL 3x P3 ds-red was digested with *Nde*I and *Eco*RI. The 1,3 kb insert was blunted and cut again with *Nhe*I. Then it was ligated into pSL SD-GFP-SA (A) was digested with *Nhe*I and *Hpa*I.

Cloning of p3: piggyM P white SA-GFP-SD P (X):

To construct piggyM P white SA-GFP-SD P (A) the pP-GA cassette was amplified from pP-GA with the primer US100 (5'-GTA CGC TAG CGT CTG GCC CAT GAT GAA ATA ACA TAA GG-3') and US101 (5'-GTA CAG ATC TGG CCA GAC CAT GAT GAA ATA ACA TAA GG-3') cut with about *Bgl*II and *Nhe*I and ligated into piggy mini cut with *Bgl*II *Nhe*I.

To construct piggyM P white SA-GFP-SD P (B) the pP-GB cassette was amplified from pP-GB with the primer US100 (5'-GTA CGC TAG CGT CTG GCC CAT GAT GAA ATA ACA TAA GG-3') and US101 (5'-GTA CAG ATC TGG CCA GAC CAT GAT GAA ATA ACA TAA GG-3') cut with *Bgl*II and *Nhe*I and ligated into piggy mini cut with *Bgl*II and *Nhe*I.

To construct piggyM P white SA-GFP-SD P (C) the pP-GC cassette was amplified from pP-GC with the primer US100 (5'-GTA CGC TAG CGT CTG GCC CAT GAT GAA ATA ACA TAA GG-3') and US101 (5'-GTA CAG ATC TGG CCA GAC CAT GAT GAA ATA ACA TAA GG-3') cut with *Bgl*II and *Nhe*I and ligated into piggy mini cut with *Bgl*II and *Nhe*I.

Cloning of p4: piggyM P white P SA-GFP-SD (X):

To construct pTR+ white delta *Bam*HI the construct pUAST delta *Bam*HI was cut with *Hind*III. The 6 kb Fragment was ligated into pTR+ white delta *Bam*HI vorstufe cut with *Hind*III.
To construct pUAST delta *Bam*HI the construct pUAST was cut with *Bam*HI and religated

after removing the 1,3 kb Fragment via gel purification.

To construct pTR+ P white P SA-GFP-SD (A) the construct pTR+ white delta *Bam*HI was cut with *Kpn*I and *Bgl*II. The fragment containing the with gene was ligated into pTR+ SA-GFP-SD (A) cut with *Kpn*I and *Bam*HI.

To construct pTR+ P white P SA-GFP-SD (B) the construct pTR+ white delta *Bam*HI was cut with *Kpn*I and *Bgl*II. The fragment containing the with gene was ligated into pTR+ SA-GFP-SD (B) cut with *Kpn*I and *Bam*HI.

To construct pTR+ P white P SA-GFP-SD (C) the construct pTR+ white delta *Bam*HI was cut with *Kpn*I and *Bgl*II. The fragment containing the white gene was ligated into pTR+ SA-GFP-SD (C) cut with *Kpn*I and *Bam*HI.

To construct piggyM P white P SA-GFP-SD (A) the construct pTR+ SA-GFP-SD w+P (A) was cut with *Bgl*II and *Nhe*I and the P white P SA-GFP-SD (A) cassette was ligated into piggy mini cut with *Bgl*II and *Nhe*I.

To construct piggyM P white P SA-GFP-SD (B) the construct pTR+ SA-GFP-SD w+P (B) was cut with *Bgl*II and *Nhe*I and the P white P SA-GFP-SD (B) cassette was ligated into piggy mini cut with *Bgl*II and *Nhe*I.

To construct piggyM P white P SA-GFP-SD (C) the construct pTR+ SA-GFP-SD w+P (C) was cut with *Bgl*II and *Nhe*I and the P white P SA-GFP-SD (C) cassette was ligated into piggy mini cut with *Bgl*II and *Nhe*I.

Cloning of p5: piggyL P white P SA-GFP-SD (X)

To construct piggyL P white P SA-GFP-SD (A) the construct pTR+ P white P SA-GFP-SD (A) was cut with *Bgl*II and *Nhe*I. The P white P SA-GFP-SD cassette was ligated into piggyL MCS cut with *Bgl*II and *Nhe*I.

To construct piggyL P white P SA-GFP-SD (B) the construct P white P SA-GFP-SD (B)

was cut with *Bgl*II and *Nhe*I. The P white P SA-GFP-SD cassette was ligated into piggyL MCS cut with *Bgl*II and *Nhe*I.

To construct piggyL P white P SA-GFP-SD (C) the construct P white P SA-GFP-SD (C) was cut with *Bgl*II and *Nhe*I. The P white P SA-GFP-SD cassette was ligated into piggyL MCS cut with *Bgl*II and *Nhe*I.

3.1.9 Sequencing of exon-trap lines

The sequencing of lines obtained in the exon-trap screen was done as previously described (Horn et al., 2003).

3.2 Fly Genetics

3.2.1 *Drosophila* culture and germline transformation

Fly strains were reared under standard laboratory conditions (Sigrist et al., 2003). *Drosophila* germlines transformation was performed as previously described (Horn et al., 2000; The_FlyBase_Consortium_2003, 2003).Transgenic animal were exept otherwise stated established in w- flies (Castiglioni, 1951). DGluRIIA^{GFP} was injected in double mutant background w-;*Df(2L)cl^{h4}*/GlaBc;+/+ (DiAntonio et al., 1999)

3.2.1 Exon-trap screen

To create jumpstarter pHerm{3xP3-ECFP,α-tub-*piggyBac*K10}/CyO (Horn et al., 2003) males were crossed to virgins of either homozygous mutator constructs (p1-p5) or to heterozygous mutator constructs balaced over MKRS (The_FlyBase_Consortium_2003, 2003). The non CyO, non MKRS jumpstarter were outcrossed against w- virgins (Castiglioni, 1951).

3.2.2 DGluRIIA^FP

DGluRIIA^GFP, DGluRIIA^mRFP, DGluRIIA^GFP-PA and DGluRIIA were expressed from a genomic transgene. DGluRIIA^GFP and DGluRIIA were tested for rescue activity in the *dglurIIA&IIB* double mutant background (*Df(2L)cl^h4/dglurIIA&B^SP22*) (DiAntonio et al., 1999). Both constructs rescued in mendelian ratio.

3.2.3 DPak^GFP

Transgenic DPak^GFP expression was induced at 16 °C using G14-Gal4 as driver. DPak^GFP males were therefore crossed to w-;G14-Gal4/CyO-GFP;+/+ virgins (Aberle et al., 2002).

3.2.4 DCast^GFP

Transgenic DCast^GFP expression was induced at 16 °C using OK6-Gal4 as driver. DCast^GFP males were crossed to w-;OK6-Gal4/ OK6-Gal4;+/+ virgins (Aberle et al., 2002).

3.2.5 DGluRIIC^GFP

Transgenic DGluRIIC^GFP expression was induced at 25 °C using G14-Gal4 as driver. DGluRIIC^GFP males were crossed to w-;G14-Gal4/CyO-GFP;+/+ virgins (Aberle et al., 2002).

3.3 *In situ* hybridization

All *in situ* hybridizations were performed following the BDGP standard protocol (www.fruitfly.org). In detail the 5' region of the *Cast* transcript was amplified from random primed adult head cDNA using the primers TR674 (5'- ATG GGC AGT CCA TAC TAC CGC GAC ATG-3') and TR687 (5'- CCC GGC ACT CTA GAT CCT TGA T-3') using Takara Taq Polymerase (RP 002 M, Takara Bio Inc., Shiga, Japan). The PCR product which corresponds to the first 700 nt of CG12933 was cut and subcloned into precut pCR 2.1 (part in the TA cloning kit (K 2040-01, Invitrogen)). After identifying a clone with the

right orientation the vector was cut with *Spe*I to make the *in situ* probe with T7 (5'- AAT ACG ACT CAC TAT AG -3'). The antisense probe for the 3' region was made with T7 after cutting AT09405 with *Bam*HI. The sense control probe for the 3' region was made with SP6 (5'- GAT TTA GGT GAC ACT ATA G -3') after cutting AT09405 with *Sma*I.

3.4 Preparation of *Drosophila* first instar larvae for automated sorting

To prepare *Drosophila* first instar larvae for automated sorting 24 - 29h old embryo collections (25 °C) were washed and put on new plates containing a patch of fresh yeast. 4 h later all larvae, which had gone to the yeast were isolated and washed again. As larvae have a strong tendency to move to the yeast, this method was an efficient way to separate living larvae from embryos, dead larvae, and empty eggshells (all of which have high autofluorescence, as well as a high tendency to plug the sorter). There was a recovery of 50-80% of the theoretically possible number of larvae. These 28 - 33h old first instar larvae were sorted in sheath fluid (Select Sheath, Union Biometrica, Somerville, MA, USA).

3.5 Electrophysiology and styryl dye labeling

Intracellular recordings were made at 22 °C from muscle fiber 6 of abdominal segments 2 and 3, of late third instar larvae. The larvae were dissected in ice-cold, calcium-free haemolymph-like saline (HL-3) according to Stewart et al. (1994). Composition of the HL-3 solution was (in mM): NaCl 70, KCl 5, $MgCl_2$ 20, $NaHCO_3$ 10, trehalose 5, sucrose 115, HEPES 5, pH adjusted to 7.2. Larval fillets were rinsed with 2ml of HL-3 saline containing 1 mM Ca^{2+}, before being transferred to the recording chamber where two-electrode voltage clamp (TEVC) recordings were performed in 1 mM extra cellular Ca^{2+}. The larval NMJ was visualized with a fixed-stage upright microscope (Olympus, 40x water immersion lens). Whole muscle recordings of both miniature and evoked postsynaptic currents were recorded in TEVC mode (AxoClamp 2B, Axon Instruments) using sharp microelectrodes (borosilicate glass with filament, 1,5 mm outer diameter) with resistances of 15-35 MΩ and filled with 3M KCL. All cells selected for analysis had resting potentials between -55 and -

70 mV and the input resistance was ≥ 4 MΩ. For stimulation, the cut end of the segmental nerve was pulled into a fire-polished suction electrode and brief (300 µs) depolarizing pulses were passed at 0.2 Hz (npi stimulus generator and isolation unit). To ensure the stable recruitment of both innervating motoneurons, the amplitude of the pulse was determined by increasing the stimulation strength to 1.5 times the amplitude needed to reach the threshold of double motoneuron recruitment. The clamp was tuned such that it responded to a voltage step from -60 to -70 mV with settling times of 1 ms for mEJCs and 500-750 µs for eEJCs, this gave voltage errors of maximally 4 mV for eEJCs of approx. -100 nA. Both eEJCs (voltage clamp at -60 mV) and mEJCs (voltage clamp at -80 mV) were low-pass filtered at 1 kHz. For each cell, 20 eEJCs and 90 s of mEJCs recordings were used for subsequent analysis (pClamp9, Axon Instruments). Concerning the receptor photo-bleaching experiment, responses to 30 consecutive stimuli, delivered at 1 Hz were averaged (Robert Kittel / Stephan Sigrist, personal communication).

FM5-95 uptake was essentially done as described (Kuromi and Kidokoro, 2002). In short: terminals at muscle 4 were labeled by replacing normal saline with normal saline containing 20 µM FM5-95 (T-23360, Molecular Probes, Eugene, USA) followed by stimulating the innervating nerve at 30 Hz for 5 min. After stimulation, preparations were washed three times with Ca^{2+}-free saline. Destaining was done by applying high K^+ saline for 5 min (Andreas Schmid / Stephan Sigrist, personal communication).

3.6 Immunofluorescence staining

3.6.1 Antibodies

The rabbit-α-DGluRIIC antiserum was raised against the two peptide sequences (PRRSLDKSLDRTPKS+C and C+SGSNNAGRGEKEARV), affinity purified and used at a dilution of 1:200. The other antibodies were used at the following concentrations: mouse-α-nc82 (1:100) (gift of E. Buchner, University of Würzburg, Germany), rabbit-α-PAK (1:2000) (gift of N. Harden, The Hospital for Sick Children, Toronto, Canada), mouse-α-FasII (1:50) (ID4, Developmental Studies Hybridoma Bank, University of Iowa, USA),

rabbit-α-GFP (1:500) (A-11122, Molecular Probes, Eugene, USA), mouse-α-DGluRIIA (1:100) (concentrated 8B4D2, Developmental Studies Hybridoma Bank, University of Iowa, USA).

3.6.2 Staining protocol

Second or third instar larvae were immobilized, opened dorsally to remove the inner organs and immunostained as previously described (Schuster et al., 1996) with the following exception. All stainings in which the mouse-α-DGluRIIA antibody was used were fixed for 5 min using cold methanol (-20°C). The further immunostaining steps were again performed as previously described (Schuster et al., 1996).

3.7 Image Acquisition

In vivo imaging was performed on a Leica DM IRE2 microscope equipped with a Leica TCS SP2 AOBS scanhead. The GFP signal was detected at a gain of 720 and with the detection window set to 495 - 538 nm. The mRFP signal was detected at a gain of 800 and with the detection window set to 567 – 627 nm. FM5-95 labels were scanned on a Leica DM LFSA equipped with a Leica TCS SP2 scanhead, using the TD 488/543/633 as principal beamsplitter for immunostainings and the GFP-channel for FM5-95 labeling and the DD 458/514 to visualize FM5-95. The *in vivo* imaging, as well as all immunostainings were scanned using a Leica HCX PL Apo CS 63x 1.32 NA OIL UV objective, and the FM5-95 labeling was imaged using the Leica HCX APO L 40x 0,8 NA W objective. The other settings were as follows: *in vivo* imaging voxel size: 98nm*98nm*244nm. The timeseries shown in Fig. 17 were performed at 16 °C, where development is slowed down by a factor of 3 compared to 25°C (Economos and Lints, 1984). This allowed to work early in the morning and at evenings when the shared microscope was available on a regular basis. All other experiments were, except otherwise stated, performed at 25 °C. Settings for fluorescence recovery after photo-bleaching (FRAP) experiments and photo-activation experiments: Pinhole 1,5 Airy Units, voxel size: 98nm*98nm*488nm, all immunostainings pinhole 1 Airy Unit: voxel size 49nm*49nm*145nm; styryl dye labeling: Pinhole1,5 Airy Units for GFP and 1 Airy Unit for FM5-95 voxel size: 98nm*98nm*246nm.

4. Results:

4.1 Developing protocols and genetic tools for *in vivo* imaging with single synapse resolution in *Drosophila*

4.1.1 Motivation for *in vivo* imaging

The observation of relevant processes directly in their native settings is of crucial importance for a deeper understanding of long-term synaptic changes (Niell and Smith, 2004). In seminal experiments, fluorescently tagged toxins, which bind postsynaptic acetylcholine receptors, have been used to observe synapse formation at mammalian neuromuscular junctions (Purves and Lichtman, 1987). However, in terms of size, ultrastructure and experience-dependent plasticity mammalian neuromuscular junctions are fundamentally different from glutamatergic synapses, the key elements in central nervous system (CNS) information processing. In contrast, glutamatergic *Drosophila* neuromuscular synapses are similar to glutamatergic CNS synapses in ultrastructural terms and combine several other advantages that make them an attractive study model (see chapter 2.3.1). In principle the transparent larvae are ideal for imaging. However, a stable and non-toxic anesthetization of larvae which is a prerequisite for following identified synapses over time had not been established. Thus, in order to directly visualize synapse formation both a suitable imaging protocol for *Drosophila* larvae and genetic tools had to be established, which were amongst the main aims of this thesis.

4.1.2 Anesthetization of intact *Drosophila* larvae

Because *Drosophila* larvae move strongly, live imaging of individual identified synapses critically demands stable anesthetization. So far, a single study describing the *in vivo* imaging of *Drosophila* larvae (Zito et al., 1999) was published. Here Zito and co-workers used a construct, which labels the subsynaptic reticulum (SSR), thereby describing the development of the bouton structure at an identified neuromuscular junction over the time-course of days. Yet their imaging protocol was not applicable for the imaging

of individual synapses over time since the degree of anaesthetization was not high enough to allow high resolution imagining. Moreover, when using ether anethetization the survival rate was less than 20%. In result, only 3 pictures of an identified larva were shown at most. Since ether anesthetization harms the animal, unwanted side effects also can not be excluded. Therefore, different anesthetics and application procedures were systematically tested. Among the anesthetics tested, only the vaporous application of isoflurane and desflurane seemed to be suitable. Both substances anesthetized the animals completely abolishing any internal movements. Comparing desflurane to isoflurane, the slightly faster onset (about 2 min compared to 4 min) and the faster recovery (about 1 min compared to 5 min) favored the use of desflurane over isoflurane. Control experiments using 10 consecutive anesthetizations, separated by 5 min recovery intervals, revealed neither any developmental delay nor increased mortality in anesthetized larvae compared to non-anesthetized but otherwise identically treated sibling larvae. In all following experiments desflurane was used for anaesthetization.

To visualize single synaptic sites (in the range of 100-500 nm) no internal movements within a 5 min time interval can be tolerated. The main determinants relevant for resolution in confocal imaging are voxel size and signal to noise ratio. The signal to noise ratio can be improved by averaging. Usually 2 to 4 times line averaging was used, which increases the time needed for image acquisition by a factor of 2 or 4 respectively. Apart from the fluorophor used, the limit of averaging and thereby of the signal to noise ratio is set by the duration and degree of anesthetization. When properly applied, desflurane suppressed the heartbeat completely. This effect is fully reversibly. Another important issue is the survival rate of the anesthetized animals. Repeated complete anesthetization of larvae, should allow imaging of individual synapses at high resolution without any negative influence on larval development and survival. The application of a desflurane air mixture via a custom built vaporizer achieved this goal.
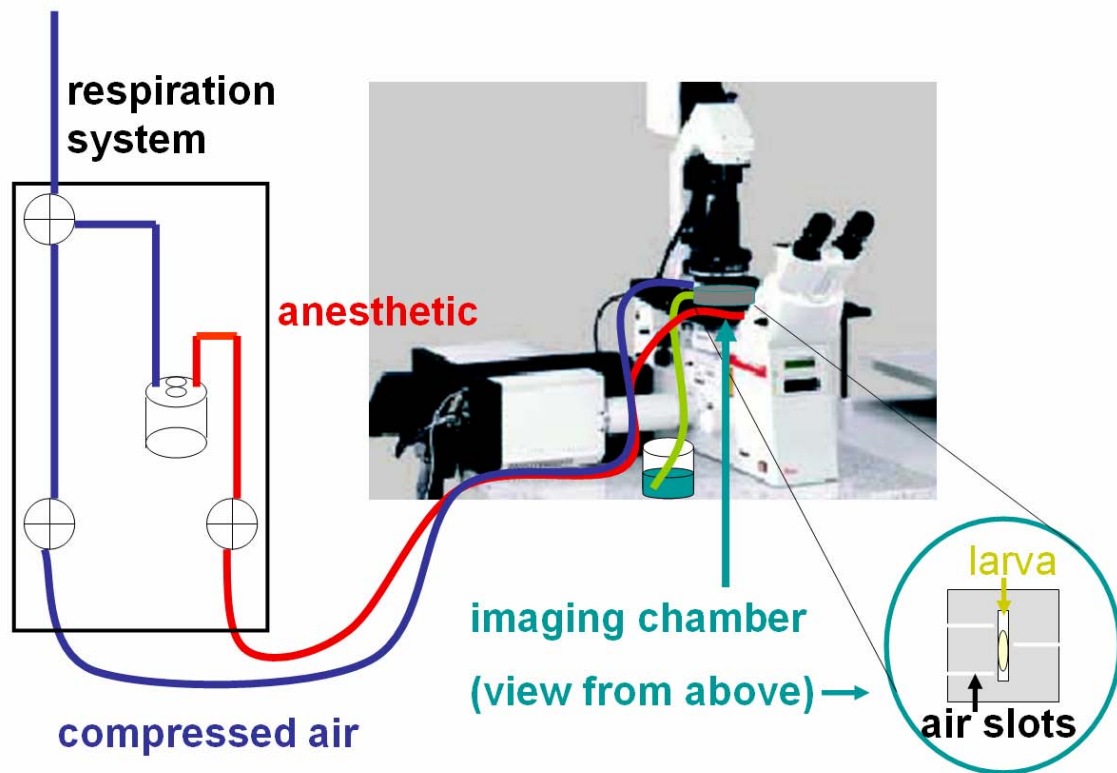
Fig. 11 Setup used to anesthetize intact living *Drosophila* larvae for *in vivo* imaging. Air and anesthetic were applied to the larva via 3 "air-slots", which led from each side of the slit (in which the larva was placed) towards the edge of the plastic slide. The plastic slide itself was placed in an imaging chamber, which was connected to the respiration system. The custom made 2 channel respiration system (see text) contained a simple custom made vaporizer.

To follow the outgrowth of synapses the following protocol proved to be optimal: Second to third instar larvae were mounted between two 0,12 mm microscope coverslips, which were held apart by a plastic slide. The larva was placed in a slit in the center of the plastic slide (Fig. 11). Width and length of the slit, as well as the height of the plastic slide were adjusted to the size of the larva to prevent turning of the larva and to allow only minimal movement of the larva in the direction of the slit. The lower coverslip was covered with a thin film of Voltalef H10A Oil (Lehmann & Voss, Hamburg, Germany). Air and anesthetic were applied to the larva via three "air-slots" (Fig. 11) of 200 µm width and 40 µm height, which led from each side of the slit (in which the larva was placed) towards the edge of the plastic slide. The plastic slide itself was placed in an imaging chamber, which was connected to the respiration system. The custom made 2 channel respiration system consisted of one channel for compressed air (6 psi) and one channel

for anesthetic, which contained a simple custom made vaporizer. The vaporizer consisted of a 0,5 L bottle that was connected to compressed air via an input and to the imaging chamber via an outlet (Fig. 11). Prior to the experiment the bottle was filled with 50-100 ml of the anesthetic. During the experiment both input air pressure to the vaporizer and temperature of the bottle could be controlled, thus giving rise to a defined partial pressure of anesthetic at the outlet side. The larvae were anesthetized by the application of 15% (v/v) of desflurane (Suprane, Baxter, Unterschleissheim, Germany) for 2 min via the anesthetic channel. Larvae were woken up by the application of air for 2 min via the air channel of the respiration system.

4.1.3 Comparison of 2-Photon and conventional confocal microscopy for *in vivo* imaging

Laser scanning microscopy allows the visualization of single synapses both in 2-Photon and in "1-Photon" excitation mode. In the following the principal advantages of both modes will be compared. Initial experiments were performed using 2-Photon microscopy. The main advantages of 2-Photon microscopy are less out of focus photo-bleaching and the inherent confocality that allows the collection of scattered emitted photons. This is of great importance, when structures deep in scattering tissues are to be imaged (Denk et al., 1990; Theer et al., 2003). Pilot experiments were performed, in which the outgrowth of the neuromuscular junction was studied using an artificial hybrid protein composed of the CD8-transmembrane domain fused to GFP^{S65T} and the intracellular C-term of the shaker ion channel (Zito et al., 1999). This construct labels the subsynaptic reticulum of the *Drosophila* NMJ and thus allows for tracing the outgrowth of new synaptic boutons.
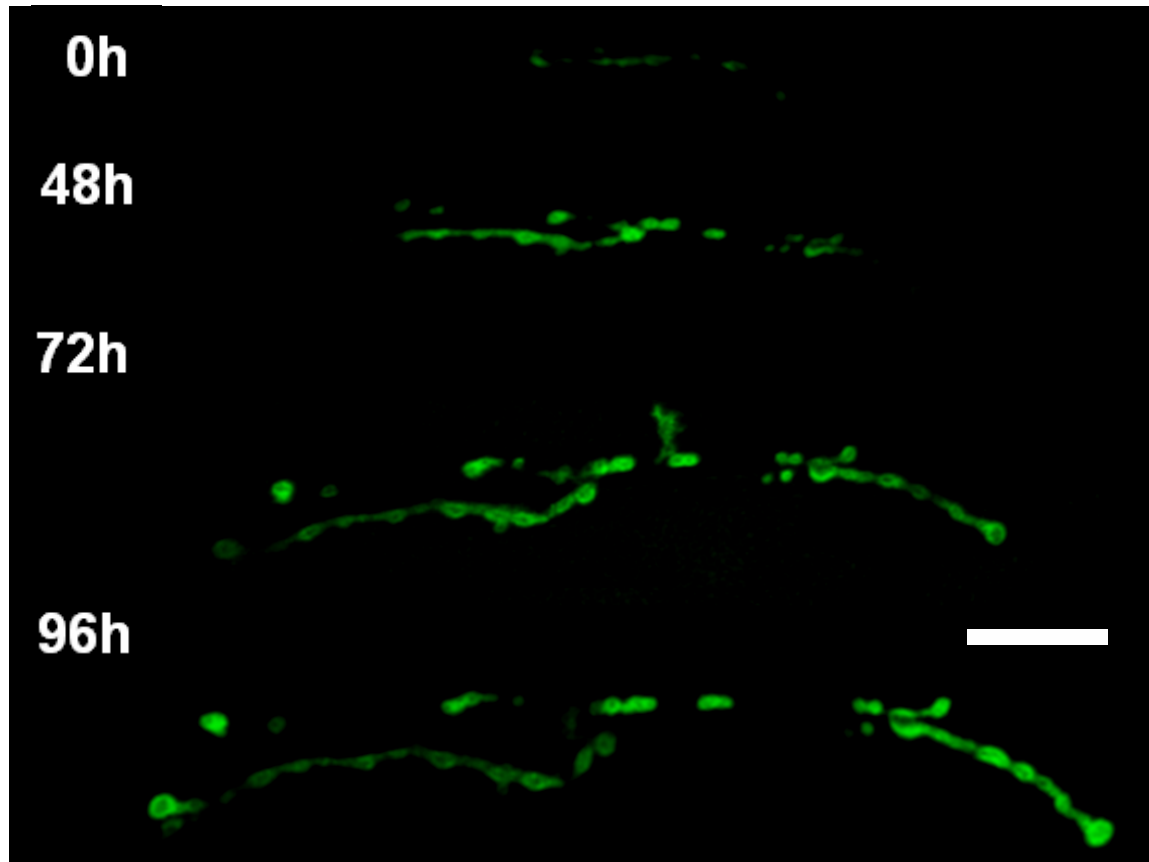
Fig. 12 *In vivo* imaging the development of individual neuromuscular synapses. Time series of Mhc driven CD8-GFP-Sh expressing in larva developing at 25°C. Time after the start of observation is indicated. Images were obtained using 2-Photon microscopy at 820 nm. Scale bar 20 µm.

Using 2-Photon microscopy it was possible to image any NMJ in *Drosophila* larvae. Neuromuscular junction 6/7 was used for the time series shown in Figure 12. NMJ 6/7 is the junction usually used for electrophysiology, since it is easily accessible in an opened preparation and well characterized. At the same time NMJ 6/7 is among the least accessible junctions when imaging in the intact animal, since it has maximal distance to the epidermis. Using 2-Photon microscopy NMJ 6/7 could nevertheless be imaged at high quality. Care had to be taken not to focus the 2-Photon laser on the nearby fatbody, which causes damage to the animal due to the high infrared adsorption typical for this tissue. It thus was addressed, whether using conventional single photon laser scan microscopy would be more practical for imaging junctions located close to the cuticle. For these junctions (NMJ 26 and 27) the imaging quality obtained by using conventional laser scan

63

confocal microscopy is higher than by using 2-Photon microscopy. Particularly, the xy-resolution is higher when using the conventional laser scan confocal microscopy. Moreover the AOBS Leica confocal microscope used for this study allows the simultaneous detection of several fluorophores, which proved to be important for tracing different proteins and for fluorescence recovery after photo-bleaching (FRAP) experiments.

4.1.4 Microscope settings used for *in vivo* imaging of identified synapses in live intact *Drosophila* larvae

To allow repeated imaging of individual synapses, laserpower, pinhole, and photo-multiplier (PMT) gain had to be adjusted to the specific requirements of the experiment. Care was taken not to photo-bleach the animal to such a degree that further images would be affected or that bleaching artifacts within the z-stack would arise. Hereby, the *in vivo* imaging was performed on a Leica DM IRE2 microscope equipped with a Leica TCS SP2 AOBS scanhead. Laser power, pinhole, gain and offset were adjusted such that all pixel values were in the range of 1 to 254 using the dynamic range of the PMTs in the optimal way while avoiding over- or undersaturation. This was achieved by varying the laser power for the 561 nm laser between 10-50% and the 488 nm laser line in the range of 5 to 20% (as defined in the software, while the laser power switch was turned to approximately 75% power (3 o'clock position of the switch)). In FRAP and photo-activation experiments special care had to be taken to avoid any artifacts introduced by photo-bleaching. Therefore, it was decided to open the pinhole to 1.54 airy unit for all experiments in which DGluRIIA^{mRFP} was imaged, while the pinhole was set to 1 airy unit for all other experiments. Setting the pinhole to 1.54 airy units allowed reducing the laser power, while keeping the PMT gain constant. The slightly reduced optical sectioning caused no further problems during image processing. For more details on microscope settings see Material and Methods 3.7.

4.1.5 Quantitative analysis of imaging data

Visualizing the assembly of postsynaptic densities (PSDs) during *in vivo* synapse formation was a focus of this thesis. To quantify the growth of individual imaged PSDs, an assay had to be established, which allowed for semi-automatic processing in a non-biased way. This method should include background substraction, quantification of the PSD size, measurement of the total fluorescent intensity of PSDs (being a correlate of the number of fluorescent receptors) and the calculation of fluorophor ratios in FRAP experiments. Therefore, the 4-dimensional or 5-dimensional (for FRAP series) raw data had to be processed in several steps. No commercial software was able to automatically perform all the tasks. Consequently, a new image processing protocol was established, mainly based on the ImageJ 1.32b (Wayne Rasband, NIH USA, http://rsb.info.nih.gov/ij/download.html) software. It was not feasible to automate the entire image processing. Hence, segmentation and identification of synapses throughout the time series was done semi-manually. In detail a binary segmentation mask was projected on a sum projected z-stack to segment individual synapses. To do so, the sum projected 32-bit z-stack was defined as Image1 in the *Image Calculator* function *Min.* A binary mask, in which synapses had the value 65025 and non-synaptic areas the value 0 was defined as Image2. The mask itself was obtained by thresholding a median filtered (radius: 1 pixel), background corrected, maximum projected z-stack. While most synapses were segmented automatically, some had to be segmented manually. This was due to the fact that the fluorescence intensity between two large bright synapses in close proximity was often higher than the intensity in the center of a small, dim, (nascent) synapse. Since reliable tracing of these small synapses is important the threshold was selected such, that it would not remove these small synapses. In result, large bright synapses in close proximity were often separated insufficiently. This could be solved by applying further segmentation algorithms to test, whether the fluorescent intensity in the middle of an object was brightest (as expected and observed for individual synapses) or whether the fluorescent intensity in the middle of an object was significantly lower than observed for two peaks of intensity located outside the center of the object (as expected for two synapses in close proximity). In the second case it could be tested whether the valley between this peak is significantly low (60% of peak intensity or lower) to be used to segment the object further

(with a combination of segmentation procedures related to top head thresholding and watershed segmentation algorithms). These ideas will be implemented in future image analysis procedures. Doing the second segmentation step manually has the advantage that 3-dimensional (3-D) information can easily be used to reliably trace synapses. A few synapses, which could not be segmented properly (due to technical reasons) were excluded from further analysis. Individual synapses, which were not separated by the automatic protocol, were manually segmented using criteria as described for proposed automatic separation of synapses in close proximity. In the segmented image synapses were analyzed with the *Analyze Particles* function using the following settings: *Set threshold* of the image to 1 - 65025, and *Set Measurements* parameters to *Limit to Threshold, Area, Standard Deviation, Mean Gray Value*. Using this procedure the original pixel values were written back into the mask, which contained the information, which pixel belongs to which synapse. This method was advantageous, since writing back the original pixel values makes this protocol less susceptible to artifacts introduced by image acquisition and processing. If for example in one image the threshold was set slightly lower than in another image, then the synapses might appear bigger, when just counting pixels that belong to one synapse. Since the original pixel value was written back in the synapse, pixel values can be added up. After subtracting the mean background intensity the mean pixel value can be multiplied with the number of pixels in that synapse, which gives a reliable estimate for the number of glutamate receptors present in that synapse. Even if the threshold was chosen so low that the synapse was twice as big as in reality, this did not change the calculated receptor number of that particular synapse to any great extent, since the extra synaptic pixels added to that synapse by the software have pixel values, which do not differ much from the background (which is anyway subsequently subtracted). Furthermore, comparing data on increase of synapse area (pixels that belong to a certain synapse) and receptor number (synapse area multiplied by normalized mean fluorescent intensity of that synapse) revealed that the thresholding was reproducible enough so that even small changes in synaptic area could be attributed to growth rather than to image processing artifacts.

4.1.6 Genetic tools to visualize postsynaptic densities *in vivo*

To study synaptogenesis in the intact larvae tools had to be established that label the PSD and the presynaptic active zone *in vivo*. Thus GFP-label glutamate receptors were constructed in order to visualize the PSD. However, those first attempts to GFP-tag *Drosophila* glutamate receptors failed. The tagged receptors no longer localized to PSDs but were retained in the endoplasmatic reticulum or the Golgi apparatus (Qin Gang / Stephan Sigrist and Aaron DiAntonio, personal communication). In contrast to vertebrate glutamate receptors (Luo et al., 2002), *Drosophila* glutamate receptors neither tolerate GFP-tagging after the signal peptide nor at the absolute C-term. Hence, another approach was taken to label PSDs. The fusion of the C-term of the shaker ion channel to the artificial fusion protein CD8-GFP leads to the correct targeting of GFP to the subsynaptic reticulum. Furthermore, the C-term of glutamate receptors is known to be important for targeting and synaptic anchorage of the ion channel (Dong et al., 1997; Srivastava et al., 1998; Srivastava and Ziff, 1999). Therefore, the C-terms of three different *Drosophila* glutamate receptor subunits (DGluRIIA, DGlurIIB, DGluRIIC) were fused to CD8-GFP and expressed as transgenes. However, none of these constructs mediated PSD localization. This indicates that the C-terms are not sufficient to mediate synaptic localization. In consequence a second attempt to GFP-tag *Drosophila* glutamate receptors was initiated.
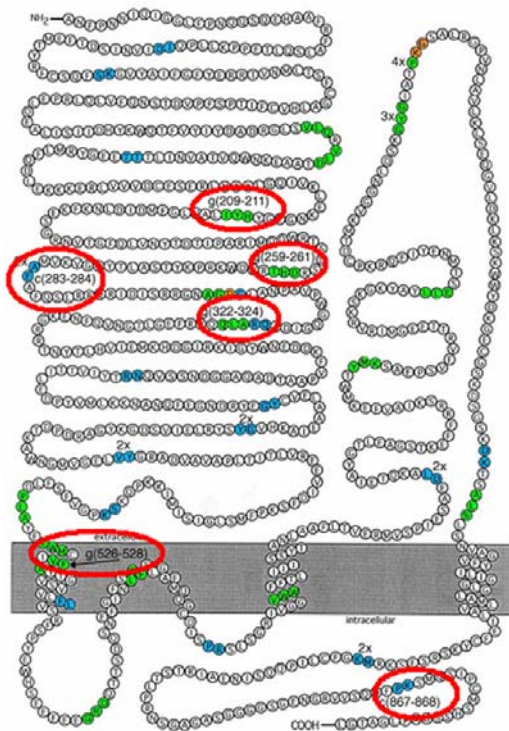
Fig. 13 Random screen for positions that are permissive for functional GFP insertion in the rat glutamate receptor R1. Figure adapted from (Sheridan et al., 2002)

A systematic evaluation of permissive locations for insertion of GFP within GluR1 was speeded up by the use of randomly generated libraries of GFP-fusion proteins (Sheridan et al., 2002). Sheridan and colleagues characterized several sites within the rat glutamate receptor R1 that tolerate GFP insertion as marked by red ellipses in Figure 13. Three of these sites were selected (AA 259-261; AA 283-284; AA 867-868) in the *Drosophila* homologs DGluRIIC and DGluRIIA and subsequently tested for functionality by transgenic expression.

Tabel 1 Transgenic expression of GFP-fused *Drosophila* glutamate receptors. Further analysis focused on the analysis of the cDNA construct of DGluRIIC with GFP inserted after AA 261 (insertion site in Rat GluR1) (DGluRIIC[GFP]) and the analysis of DGluRIIA[GFP] (genomic construct with GFP inserted after AA 868 in Rat GluR1)

Receptor	Type	Insertion in GluR1 after AA	Rescue	Expression / Localization
DGluRIIC	Genomic	261		no detectable expression
DGluRIIC	Genomic	284		no detectable expression
DGluRIIC	**cDNA**	**261**		**strong PSD label**
DGluRIIC	cDNA	284		diffuse expression
DGluRIIC	cDNA	868		strong PSD label
DGluRIIA	Genomic	261	YES	weak PSD label
DGluRIIA	Genomic	284	NO	no detectable expression
DGluRIIA	**Genomic**	**868**	**YES**	**strong PSD label**

A clear PSD label was observed in two transgenenic constructs: in a cDNA construct of DGluRIIC with GFP inserted (DGluRIIC[GFP]) after amino acid 261 (insertion site in Rat GluR1) and in DGluRIIA[GFP] (genomic construct with GFP inserted after amino acid 868 in Rat GluR1). Further characterization focused on these two transgenic constructs. Both of them proved to be ideal for live imaging of PSDs. For DGluRIIA specific mutants are available (Petersen et al., 1997; DiAntonio et al., 1999). Thus, it was possible to address the functionality of GFP-labeled DGluRIIA receptor subunits *in vivo* (see chapter 3.1.6).
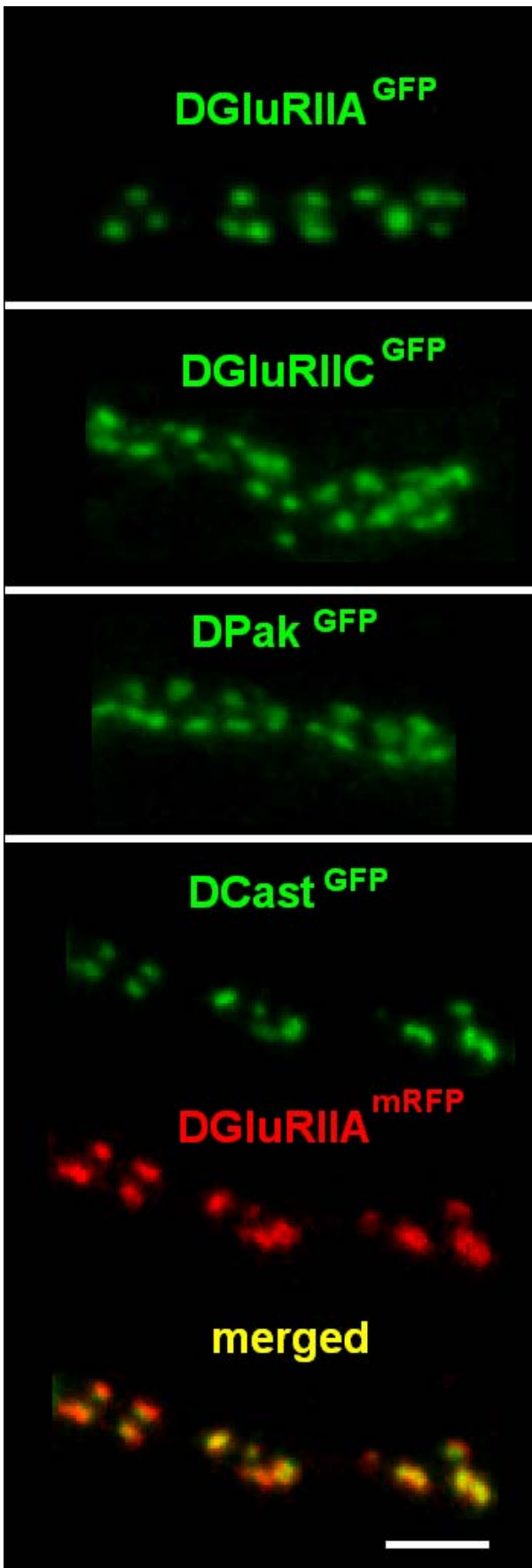
The transgenic expression of DGluRIIA[GFP] is driven by its own endogenous promoter. This ensures a physiological expression level, which is important for further analysis. Therefore DGluRIIA was further characterized (see chapter 4.1.7 and 4.3.2) and used as a principle tool for subsequent analysis (see chapter 4.2 and 4.4 and 4.5). It appeared relevant to have a PSD label which would be independent of glutamate receptors as well. To this end, the p21-activated kinase (DPak), another PSD localizing protein, was GFP-tagged. Moreover, the *Drosophila* homolog of the vertebrate CAZ component CAST (DCast) was identified as part of this thesis (chapter 3.3). Consequently, DCast[GFP] was produced and turned out to be a suitable marker for labeling the presynaptic active zone of live *Drosophila*. DGluRIIA[mRFP], DGluRIIA tagged with monomeric red fluorescent protein (mRFP) (Campbell et al., 2002), was produced to allow for coimaging with DCast[GFP].

Fig. 14 Fluorescently tagged synaptic proteins used in this thesis. When expressed transgenically, DGluRIIA[GFP], DGluRIIC[GFP], DPak[GFP] and DGluRIIA[mRFP] localize to the PSD. DCast[GFP] labels AZ (see text). Scale bar 2 µm.

4.1.7 The properties of DGluRIIA^{GFP} are indistinguishable from the wild type receptor DGluRIIA

After inserting EGFP into the middle of the intracellular C-term (chapter 3.1.3 and 4.1.6) of the *Drosophila* glutamate receptor subunit IIA, the functionality of the receptor had to be further investigated. The following experiments showed that the cellular and physiological features of transgenically expressed DGluRIIA^{GFP} and wild type DGluRIIA are indistinguishable and that the PSDs identified by DGluRIIA^{GFP} expression are the postsynaptic elements of functional synaptic sites (chapter 3.2.1).
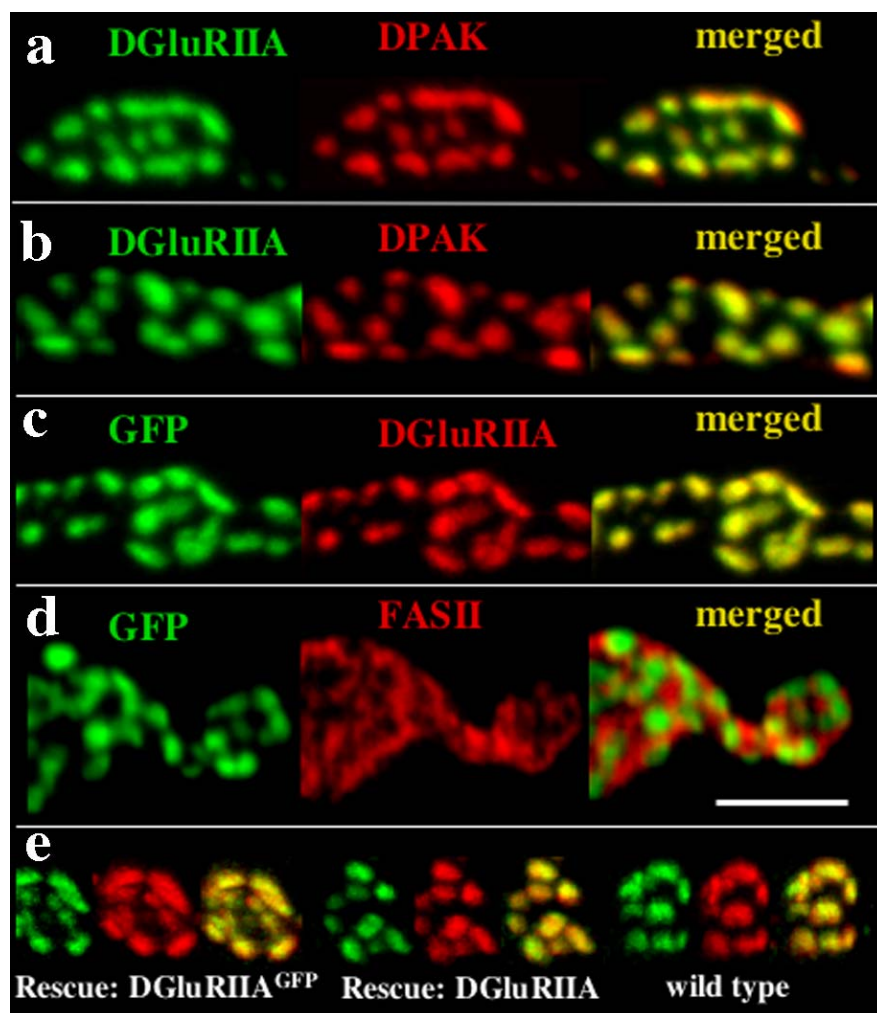
Fig. 15 DGluRIIA^{GFP} expression at neuromuscular synapses of *Drosophila* **A)** wild type neuromuscular PSDs in *Drosophila* larvae stained for DGluRIIA (green) and DPak (red). **B-D)** larva expressing DGluRIIA^{GFP} (see text) stained for DGluRIIA (B, green), GFP (C-D, green), DPak (B, red), DGluRIIA (C, red) or Fasciclin II (D, red). Right panels in A-D: merged images. **E)** larvae rescued by DGluRIIA^{GFP} or untagged DGluRIIA expression (see text), stained for DGluRIIA (green) and DGluRIIC (red), right panel: wild type control. Scale bar for A-E: 5 µm

Endogenous DGluRIIA colocalizes in immunostainings with DPak in individual patches of a few hundred nanometers (Fig. 15 A), which correspond to the postsynaptic density region (PSD), as previously shown by electron microscopy (Petersen et al., 1997; Sone et al., 2000). Transgenically expressed DGluRIIA^{GFP} also localizes properly in individual PSDs, as shown by its colocalization with DPak (Fig. 15 B) and endogenous DGluRIIA (Fig. 15 C). In addition, DGluRIIA^{GFP} patches are surrounded (Fig. 15 D) by the typical perisynaptic expression of Fasciclin II (Sone et al., 2000). Animals double mutant for *dglurIIA* and the related *dglurIIB* subunit are embryonic lethal, but can be rescued to adult vitality by transgenic DGluRIIA expression (Petersen et al., 1997; DiAntonio et al., 1999). Furthermore, in *dglurIIA&IIB* double mutant individuals, transgenic expression levels of DGluRIIA^{GFP} and DGluRIIA are indistinguishable (Fig. 15 E, green), and both constructs give rise to adult flies in mendelian ratio (not shown). In rescued animals, both DGluRIIA and DGluRIIA^{GFP} perfectly colocalize with DGluRIIC, the subunit essential for NMJ neurotransmission, likely by acting as an obligate binding partner in forming functional channels. This indicates that DGluRIIA^{GFP} becomes part of functional ion channels to a normal extent.
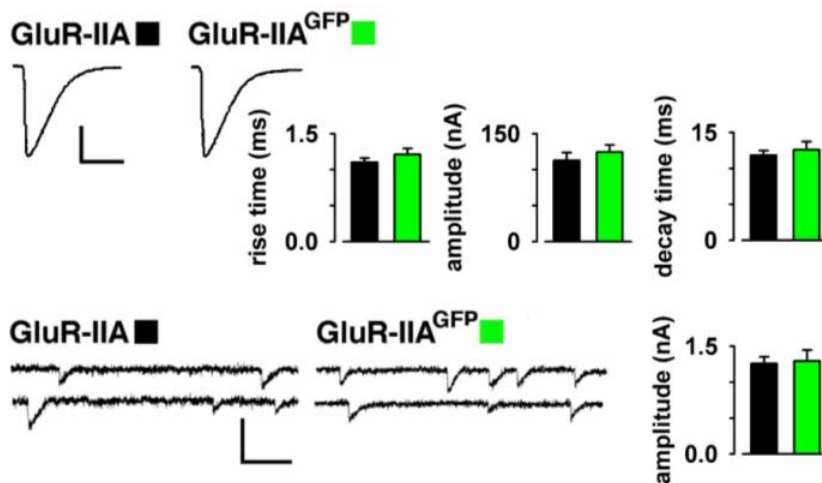
Fig. 16 DGluRIIA^{GFP} is fully functional (data kindly provided by Robert Kittel / Stephan Sigrist, personal communication). Spontaneous and nerve evoked synaptic currents from muscle 6 of *dglur-IIA&IIB* deficient animals rescued with untagged DGluRIIA or DGluRIIAGFP. Shown are representative traces from two-electrode voltage clamp recordings of both nerve evoked junctional currents (scale bars: 20 nA and 50 ms) with bar graphs plus standard errors for mean rise time, amplitude, and decay time constant and spontaneous junctional currents (scale bars: 20 nA and 50 ms) with bar graphs for mean amplitude. N = 9 experiments with each genotype (p > 0.05 for all parameters).

There are no significant differences between evoked (Fig. 16, upper panel) and spontaneous (Fig. 16, lower panel) junctional currents between DGluRIIA^{GFP} and DGluRIIA rescued larvae (Fig. 16) (Robert Kittel / Stephan Sigrist, personal communication). Collectively these results demonstrate that the cellular and physiological features of DGluRIIA^{GFP} and wild type DGluRIIA are indistinguishable. DGluRIIA^{GFP} could therefore be used as a tool to visualize synapses and receptor mobility. For the following experiments, one transgenic copy of DGluRIIA^{GFP} was expressed together with one endogenous gene copy of DGluRIIA. It was furthermore verified that PSDs labeled by DGluRIIA^{GFP} expression are the postsynaptic parts of functional synapses (see chapter 4.3.2).

4.2 *In vivo* imaging of individual postsynaptic densities during synaspse formation

4.2.1 Quantitative analysis of PSD growth during synapse formation

Chapter 4.1 described the establishment of an assay which allows studying individual synapses during synapse formation in a synaptic circuit of intact *Drosophila,* which undergoes strengthening. After verifying that essentially all PSDs* labeled by DGluRIIA^{GFP} expression are part of functional synapses PSD dynamics were analyzed over time in intact larvae. Thereby, the larvae moved freely on food-containing apple agar plates in-between imaging sessions. A individual neuromuscular junction of early third instar larvae was typically imaged every 12h for 2-3 days at 16°C.

_____

* Studies addressing the issue of PSD remodeling so far used electron microscopy as principal technology. Since this work uses mainly *in vivo* imaging no PSDs as described by electron microscopy were visualized, but the postsynaptic patches in which receptors localize. As shown in Figure 15 B these PSDs colocalize perfectly with the PSD marker DPak. Both structures, receptor field and PSD, are essentially identical. It was therefore decided to use the more common term PSD from here on, when referring to the postsynaptic patches in which receptors localize.
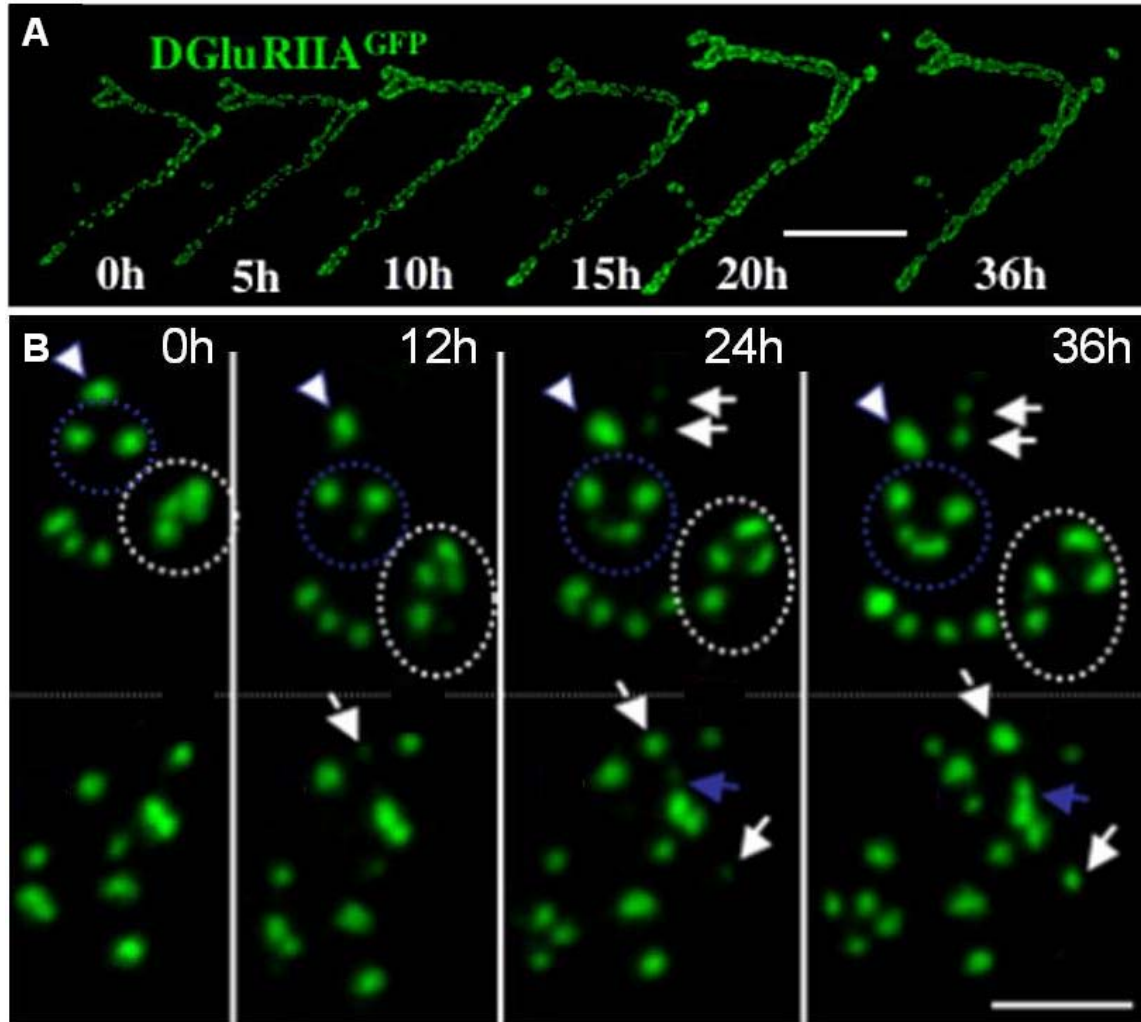
Fig. 17 *In vivo* imaging of PSD formation during the development of individual neuromuscular synapses

A-B) Confocal time series of a DGluRIIA^GFP expressing larva. Time after the start of observation is indicated.

A) *In vivo* imaging of an NMJ in lower magnification, scale bar 15 μm.

B) Time series of dynamic changes at identified populations of PSDs shown in higher magnification. Newly appearing PSDs are marked by arrows, a PSD present at the start of observation (t=0 h) by arrow heads. Blue circles label an area where PSDs grow dense, white circles label an area where PSDs increase distance over time (see text). White arrows label PSDs which form distant from pre-existing PSDs. The blue arrow shows an example of two PSDs, which are so close together after outgrowth, that they can no longer be separated by confocal microscopy. Scale bar 4 μm.

Consistent with a previous report (Zito et al., 1999; Goda and Davis, 2003), it was found that the gross morphology of an individual junction is relatively stable whereas its size increases as development continues (Fig. 17 A, Fig. 17 B). Figure 17 B shows the PSDs

of a part of the junction in high magnification. We first recognized that the PSDs which were established at the beginning of a live series (Fig. 17 B, arrow) generally showed only little change during the time series. Thus, individual PSDs can be stable for at least days in intact *Drosophila*. These PSDs also served as "landmarks", between which the outgrowth of new PSDs was observed. These new PSDs form predominantly distant from pre-existing PSDs suggesting that they form independent from neighboring PSDs (Fig. 17 B, white arrows). In the following, this mode of PSD formation will be referred to as *de novo* mode. In a few instances the formation of new PSDs in close proximity to pre-existing PSDs was observed (Fig. 17 B, white circle). Here, it was to be clarified, whether these PSDs also formed *de novo*, or whether they derived from a PSD, which broke apart giving rise to two new PSDs. In the following such a potential mode of PSD formation will be referred to as splitting mode. Chapters 4.2.2-4.2.4 will address the mode of PSD formation in more detail. Here, first the outgrowth of clearly identified PSDs was quantitatively evaluated. During the *in vivo* imaging substantial formation of additional synapses was observed. Starting with a total of about 309 PSDs 165 new PSDs were formed within 36h.
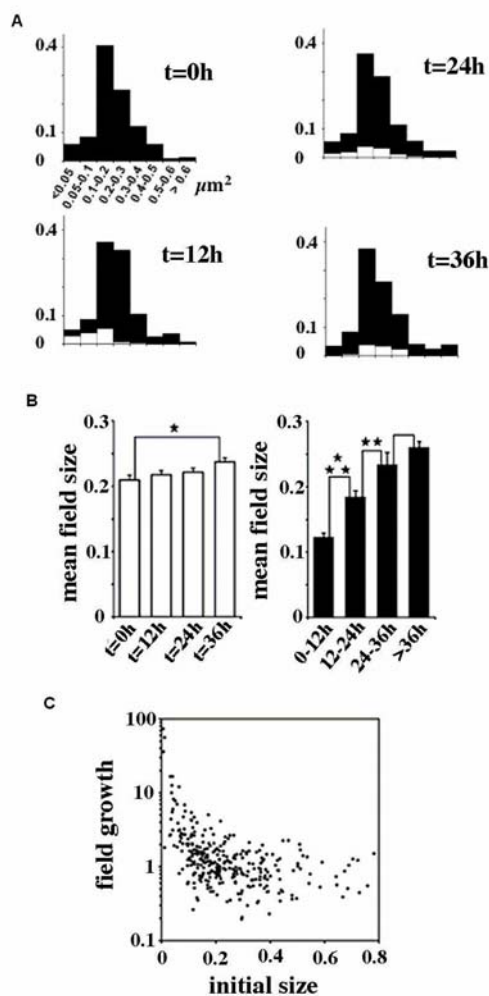
Fig. 18 Quantification of *in vivo* imaging data on PSD formation

A-C) Quantification of PSD dynamics from 5 pooled imaging series. **A)** Size distribution of PSDs at individual imaging time points in histogram plot showing binned PSD sizes (in μm^2). The overall size distribution of PSDs is relatively stable over time. PSDs, which were first observed at the 12 h imaging time point, are shown as white parts within black bars. New PSDs are small when first observed but later approach average PSD size distribution (t=24 and 36h). **B)** White bars: average PSD size calculated for different imaging time points. Average PSD size increases moderately over time. When PSDs were pooled according to their age (black bars), a strong increase in average PSD size can be observed during the first 24h. Standard error bars are shown. **C)** Relative growth of individual PSDs within 36h ($size_{t=36h}/size_{t=0h}$) plotted semi-logarithmically

The overall PSD size distribution was rather stable over time (Fig. 18 A) and the mean PSD size increased only very moderately (from 0,21 µm^2 to 0,24 µm^2 in 36h, p<0,001, see white bars Fig. 18 B). However, new PSDs, which represent the majority of all small PSDs present at any given time point, grow rapidly (shown in Fig. 18 A in white, for t=12h). Following the development of such an age-matched population (later time points see Fig. 18 A) it could be shown that, on average newly formed PSDs reach half maximal size (0,12 µm^2) within 6h and 0,18 µm^2 within 18h of their first observation (age class 0h-12h and age class 12h-24h, see black bars in Fig. 18 B). In contrast, 24h-36h old PSDs are only slightly and non-significantly smaller (0,23 µm^2 to 0,26 µm^2, p=0,23, see black bars in Fig. 18 B) than PSDs older than 36h (black bars 18 B). Thus, after about 36h at 16°C PSDs seem to have reached their mature size. This observation is confirmed when focusing on individual PSDs. Here, most small PSDs (<0,15 µm^2) grow strongly while large, mature PSDs (>0,4 µm^2) change less, showing small decreases and increases to a similar degree (Fig. 18 C). It should be noted that these experiments were done at 16°C. Development of *Drosophila* larvae is 3 times faster at 25°C compared to 16°C (Economos and Lints, 1984).

4.2.2 Morphological imaging suggests that new PSDs form *de novo*, not from splitting events

Synapse formation allows for an increase in synaptic transmission, e.g. during later stages of long-term potentiation and adaptive behavior, including learning and memory. Substantial evidence suggests that PSDs are key structures in this context (Ziff, 1997; Gundelfinger and tom Dieck, 2000; Kennedy, 2000). As discussed in detail in chapter 2.2.4 it has been proposed for more than two decades that growth, perforation and subsequent splitting of individual PSDs may be essential structural intermediates of synapse formation during synaptic potentiation (Nieto-Sampedro et al., 1982; Carlin and Siekevitz, 1983). Although this hypothesis is attractive, it remains, despite a large number of careful studies, controversial because so far it was impossible to track individual PSDs during synaptic potentiation *in vivo* (Toni et al., 1999; Lüscher et al., 2000; Yuste and Bonhoeffer, 2001; Fiala et al., 2002). Analyzing the 165 new synapses, which formed

within 36h (see chapter 4.2.1) demonstrated that most of them formed at sites clearly distant from pre-existing PSDs.

Fig. 19 Calculation to which degree unequal split could be differentiated from *de novo* formation of new PSDs close to pre-existing PSDs. **A-D)** Here the point spread function of the microscope used in this thesis was applied to hypothetical intermediates of PSD formation. The left panel always shows different hypothetical intermediates of unequal splitting. The right panel always shows hypothetical intermediates
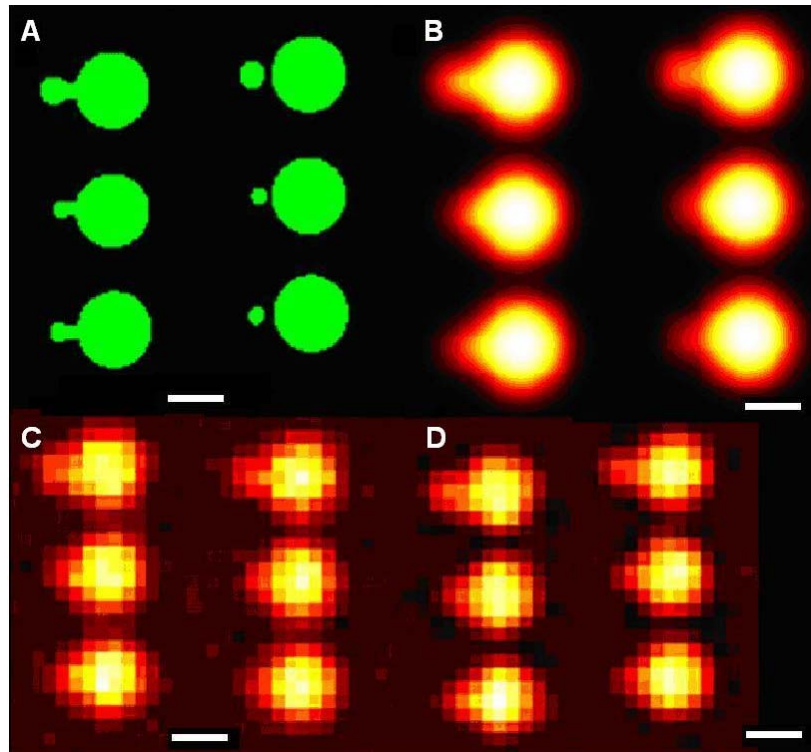
during *de novo* formation of new PSDs in close proximity to existing PSDs. This calculation illustrates why any *de novo* formation of new PSDs within the radius of 200 nm of pre-existing PSDs can hardly be clearly identified as such. Scale bar (A-D) is 500 nm. **A)** Hypothetical intermediates of unequal split (left panel) and *de novo* formation (right) of PSDs. This theoretical image was the source image for the calculations shown in B-D. **B)** B shows the theoretical image shown in A after applying the point spread function of the microscope. For this calculation a pixel size of 2x2 nm was used. In B it is already difficult to differentiate unequal split intermediates (left panel) and *de novo* formation of a new PSDs in close proximity to an existing PSD (right panel). **C)** C theoretical image shown in A after applying the point spread function in the microscope and simulating noise. The results of the calculations are shown in the pixel size used for *in vivo* imaging (98x98 nm). Here it is clearly not possible to differentiate unequal split intermediates (left panel) and *de novo* formation of a new PSDs in close proximity to an existing PSD (right panel) **D)**. While noise is reduced, the image quality of the simulated image C would not increase substantially after deconvolution.

In a few instances, however, situations were observed, which at first glance mimicked potential splitting processes (Fig. 17 B, white circle). A closer inspection of such examples, however, always indicated that these PSDs are in fact separate units forming in close proximity (<200 nm) to each other. Since they cannot be separated using conventional confocal microscopy (Fig. 19) they can only be identified as clearly separate PSDs after they have increased the distance to one another by growth of the presynaptic

bouton they are located on (Fig. 17 B, white circle). Consistently, new PSDs that formed often in very close to established PSDs (Fig. 17 B, blue arrow) were observed. As they grow, these PSDs sometimes reach a density at which individual PSDs can no longer be clearly separated (Fig. 17 B, blue circle). The fact that PSDs forming in close proximity can not be differentiated using light microscopy was further supported by an observation made when tracing the origin of new receptors (Fig. 20 D). Thereby fluorescence recovery after photo-bleaching experiments allow differentiating "old" from "new" receptors. During these experiments "PSDs" were observed, which had a uniform DGluRIIA^{GFP} staining, suggesting that they represent only one individual PSD (Fig. 20 D, left panel, arrowhead). The FRAP of a second fluorescently labeled receptor subunit indicated however that new receptors were only inserted in the lower half of this "PSD" (Fig. 20 D, central panel, arrowhead). This indicates that there was no receptor exchange between the lower and upper half of this structure. This structure might therefore actually represent two distinct PSDs forming in such close proximity that they can no longer be separated using light microscopy. In the following they might increase distance to one another by the growth of the presynaptic bouton they are located on. Therefore they might be visualized as two distinct PSDs in a subsequent image, falsely suggesting the split of PSDs (see similar example in Fig. 17 B, white circle). Thus, the imaging analysis so far suggests that in *Drosophila* PSDs form independently from pre-existing PSDs as small precursors, which grow until they reach their mature size.

4.2.3 FRAP of synaptic receptor population shows that the outgrowth of new PSDs is supported by "new receptors"

The data presented so far implied that new PSDs form *de novo*. However, PSD splitting could happen fast and therefore have escaped detection. The origin of the molecular components, which accumulate in newly forming PSDs was thus traced using FRAP experiments. The synaptic turnover of a label, suitable for tracing the origin of PSD components, must be in a similar time domain as new formation or growth of PSDs. DGluRIIA^{GFP} met this criterion as discussed in chapter 4.5.1. To verify that bleaching does not affect receptor function the following experiment was performed. Animals double

mutant for *dglurIIA* and the related *dglurIIB* subunit are embryonic lethal, but can be rescued to adult vitality by transgenic DGluRIIA expression (Petersen et al., 1997; DiAntonio et al., 1999). There are no significant differences in evoked junctional currents between DGluRIIA[GFP] and wild type DGluRIIA rescued larvae (chapter 4.1.7) (Robert Kittel / Stephan Sigrist, personal communication). In these double mutant animals, in which all glutamate receptors present in the muscle should contain a GFP-tagged DGluRIIA subunit, evoked junctional currents were indistinguishable before and after completely bleaching all GFP signal (Robert Kittel / Stephan Sigrist, personal communication) (Fig. 20 A). Thus it was concluded that bleaching of the GFP does not affect receptor function.

In the following FRAP of DGluRIIA could thus be used to differentiate *de novo* formation from split-like partitioning modes of PSD formation. Thus, transgenic animals co-expressing GluR-IIA[GFP] and GluR-IIA[mRFP] were generated. 24h after specifically bleaching DGluRIIA[mRFP] in these animals, FRAP of GluR-IIA[mRFP] was clearly heterogenous between PSDs (Fig. 20 B). Stable PSDs showed very little or no receptor entry regardless of whether they were large (Fig. 20 C, white arrow heads) or rather small (Fig. 20 C, blue arrow head). Pre-existing PSDs which grew during the time series (Fig. 20 C, yellow arrowhead), however, showed considerable glutamate receptor entry (FRAP of DGluRIIA[mRFP]).
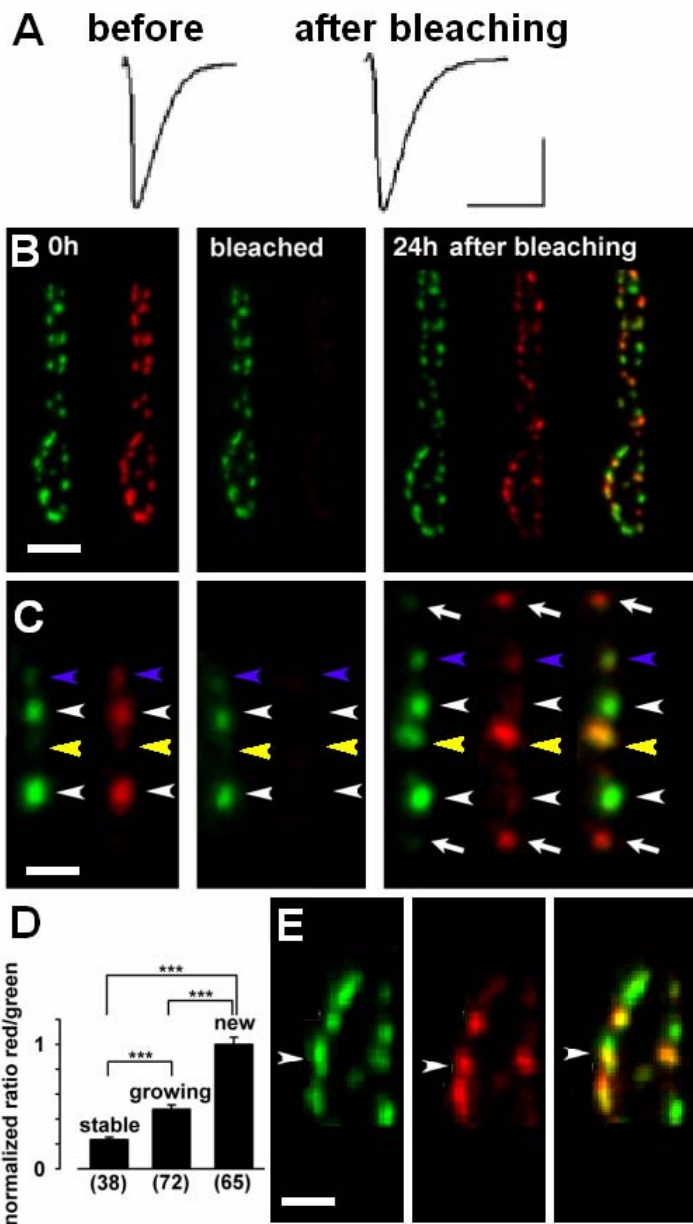
Fig. 20 Visualization of glutamate receptor entry and exit during *in vivo* PSD formation A) Nerve evoked synaptic currents from muscle 6 of a DGluRIIA^{GFP} expressing larvae, recorded in two-electrode voltage clamp mode, prior to and after bleaching DGluRIIA^{GFP}. Scale bar: 20 nA, 50 ms (Robert Kittel / Stephan Sigrist, personal communication) **B-C)** Receptor entry into PSDs was visualized using FRAP and co-expression of DGluRIIA^{GFP} (green) and DGluRIIA^{mRFP} (red). DGluRIIA^{GFP} and DGluRIIA^{mRFP} were imaged prior to and after selectively bleaching DGluRIIA^{mRFP}. **B)** Scale bar 4 μm **C)** The higher magnifications show that recovery of DGluRIIA^{mRFP} is restricted to PSDs, which are either new (white arrows) or which grew substantially during the experiment (yellow arrow head). PSDs, which grew little (white and blue arrow heads) show weak DGluRIIA^{mRFP} FRAP. Scale bar 1 μm. **D)** The normalized ratio of DGluRIIA^{mRFP} and DGluRIIA^{GFP} signal 24 h after bleaching shows that stable or mature PSDs and growing PSDs (size increase > 1.5 fold) receive less new (unbleached) DGluRIIA^{mRFP} than new PSDs (*** indicates $p < 0.001$). This is consistent with the hypothesis that new PSDs form *de novo*, but do not split. **E)** Receptor entry into PSDs was visualized using FRAP and co-expression of DGluRIIA^{GFP} (green) and DGluRIIA^{mRFP} (red). DGluRIIA^{GFP} and DGluRIIA^{mRFP} were imaged 24 h after selectively bleaching DGluRIIA^{mRFP}. Based on the DGluRIIA^{GFP} expression (green) the arrowhead seems to point a single PSD. The DGluRIIA^{mRFP} expression further shows that new receptors were only inserted in the lower half of this "PSD". This indicates that there is no receptor exchange between the lower and upper half of the structure. This structure might therefore actually represent two distinct PSDs in such close proximity that they can no longer be separated using light microscopy. In the following the two PSDs might increase their distance to one another (by the growth of the presynaptic bouton they are located on). Therefore they might be visualized as two distinc PSDs in a subsequent image, falsely suggesting the split of PSDs. (the issue of "pseudo-splits" is addressed in chapter 4.2.2). Scale bar 1 μm.

In all experiments of this type (n>40) newly formed PSDs showed even more FRAP of DGluRIIA^{mRFP} (Fig. 20 D, arrows). This suggests that new PSDs receive "new" receptors from outside the bleached area and not from neighboring PSDs, which is not consistent with splitting (see chapter 4.2.2). This impression is further supported by the more quantitative analysis in Fig. 20 D, which shows the ratio of the DGluRIIA^{mRFP} signal relative to the DGluRIIA^{GFP} signal for stable, growing and new PSDs. The much higher red/green ratio of new PSDs compared to growing and stable PSDs is a strong argument for the hypothesis that new PSDs form exclusively *de novo* and do not form by splitting or fragmentation of established PSDs.

4.2.4 Photo-activation of synaptic receptor population shows that the outgrowth of new PSDs is supported by new receptors
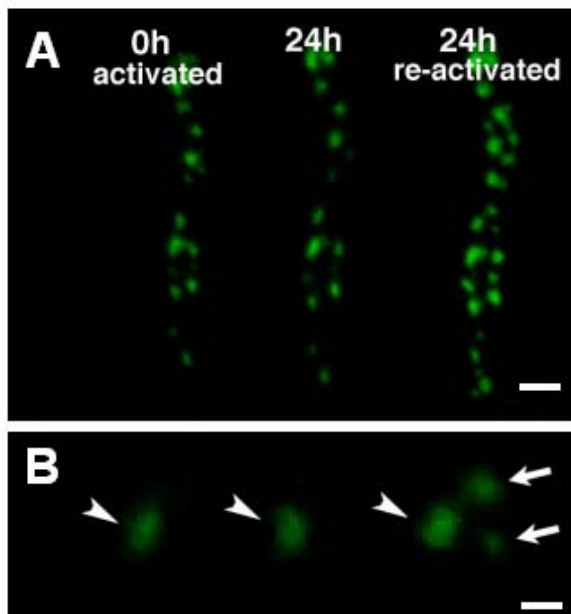
The direct tracing of a labeled receptor population is an alternative approach to address the mode by which glutamatergic PSDs form *in vivo*. To do so, photo-activatable GFP (Patterson and Lippincott-Schwartz, 2002) was inserted into DGluRIIA (DGluRIIA^{GFP-PA}) and transgenically expressed.

Fig. 21 Direct visualization of glutamate receptor entry and exit during *in vivo* PSD formation using photo-activation. **A-B)** Confocal time series of a DGluRIIA^{GFP-PA} expressing junction imaged prior to and after a second photo-activation. **A)** Scale bar 2 µm **B)** Higher magnifications of A are shown. Receptor label does not spread into new PSDs (central panel), which are visible only after the second photo-activation (right panel). The white arrowhead points at a mature or stable PSD and the arrows point at 2 newly formed PSDs nearby. Scale bar 0,5 µm.

GFP was activated at t=0 h in parts of a junction with a spot of UV-light and traced in confocal time series experiments. Again no evidence for PSD splitting was obtained (Fig. 21 A,B). PSDs present at the beginning of an experiment kept their glutamate receptors (Fig. 21 A,B, arrowhead). Only after a second round of photo-activation at the

end of the experiment new PSDs became visible (Fig. 21 B, arrows). Thus, it was again observed that the glutamate receptors for new PSDs are not derived from neighboring synapses but from more distant pools. PSDs seem therefore to form truly *de novo* and grow until they reach their mature size. Using such experimental strategies additional questions "Where are the receptors inserted in these new synapses derived from?" (chapter 4.5.1) and "How is the outgrowth of the pre- and postsynaptic compartment regulated?" (see chapter 4.4) were addressed in this thesis.

4.3 Characterization of synaptic active zones in *Drosophila*

4.3.1 Characterizing the cytomatrix at the active zone at *Drosophila* NMJ synapses

By definition, synapses display particular specializations at both the pre- and postsynaptic site. The active zone is the region of the presynaptic plasma membrane where synaptic vesicles dock, fuse, and release their neurotransmitters (Shapira et al., 2003). While markers for synaptic vesicles like synaptobrevin and synaptotagmin (Littleton et al., 1993; Broadie, 1995, 1996) stain the whole cortex of the presynaptic bouton, a molecule localizing specifically to AZs in *Drosophila* was yet to be identified.
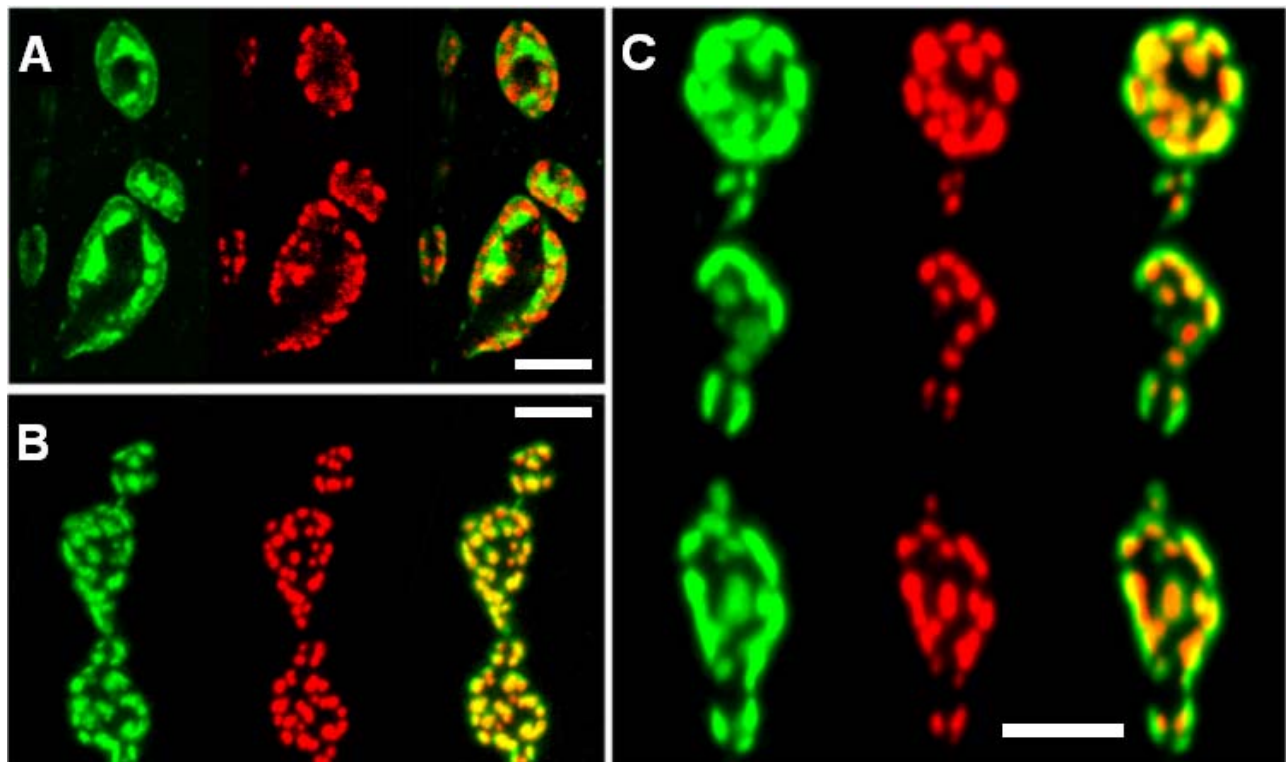
Fig. 22 Nc82 labels a component of the presynaptic active zone at neuromuscular synapses of *Drosophila* A-C) Neuromuscular synaptic boutons in wild type *Drosophila* larvae immunostained with MAB nc82 (red) and with antisera against dynamin (green, **A**), DGluRIIC (green, **B**) or DPak (green, **C**). Right panels in A-C: merged images. Scale bar A-C 5 µm.

Interestingly, the monoclonal antibody (MAB) nc82 selectively labels discrete small spots (Fig. 22, A, red) in the presynaptic bouton, which are are surrounded by dynamin (Fig. 22, A, green). Dynamin GTPase is known to be involved in synaptic vesicle endocytosis. It is localized to the so-called peri-active zone, a region important for cell adhesion and endocytosis, which surrounds the active zones. MAB nc82 shows a complementary distribution to dynamin suggesting that MAB nc82 labels active zones. To further test this hypothesis MAB nc82 was used in co-labelings against the glutamate receptor subunit DGluRIIC (Marrus et al., 2004) (Fig. 22 B) and DPak (Harden et al., 1996) (Fig 22 C), which were used to directly label the postsynaptic density region (PSD) at individual synaptic sites (Fig. 22 B,C, green). The MAB nc82 label always lies directly opposite the postsynaptic densities (on the presynaptic site) and is aligned with the center of PSDs (Fig. 22 B, C). Again, this shows that the nc82-labeled spots represent the area of the presynaptic active zone.

Next, the molecular nature of its antigen was to be clarified (chapter 4.3.3 - chapter 4.3.5) in order to be able to GFP-tag the corresponding protein. This GFP-tagged protein was then to be used as marker for *in vivo* imaging of the AZ (chapter 4.4 and chapter 4.5.2).

4.3.2 DGluRIIA^GFP labels functional synapses

Prior to co-imaging PSDs and AZs, the PSDs labeled by DGluRIIA^GFP were further characterized. It could be shown that even small PSDs are associated with presynaptic pools of recycling vesicles (Andreas Schmid / Stephan Sigrist, personal communication, see Fig. 23, A,B) as visualized by the internalization of the styryl dye FM5–95 upon high frequency stimulation (Kuromi and Kidokoro, 2002; Wucherpfennig et al., 2003).
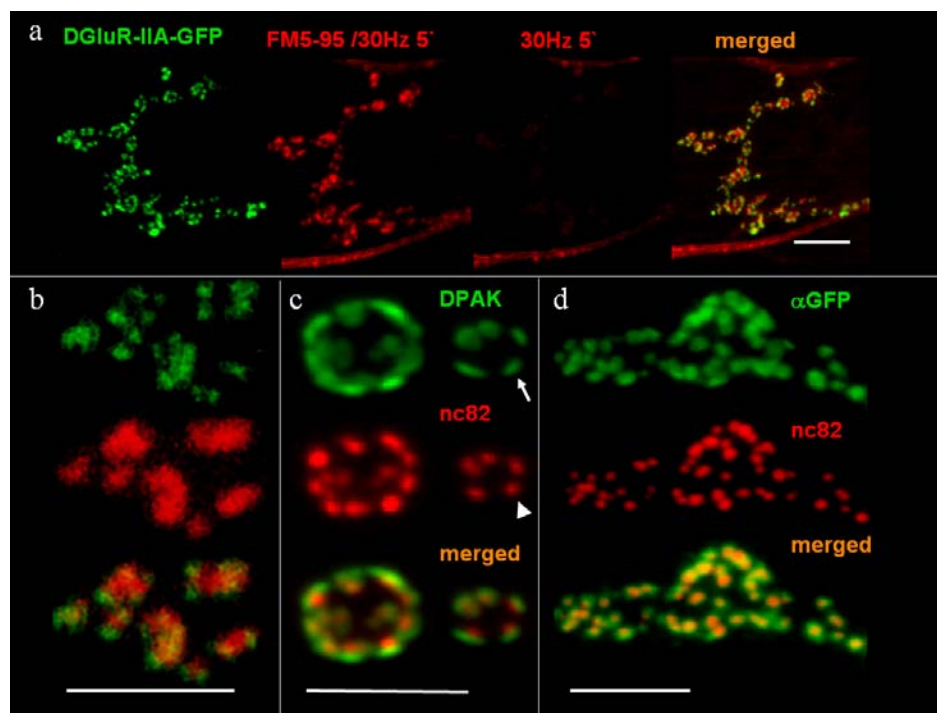
Fig. 23 DGluRIIA^GFP labels PSDs which are part of functional synapses
A) Confocal images of FM5-95 labeling (30Hz stimulation for 3 min) on a DGluRIIA^GFP expressing larvae, **B)** shows higher magnification. FM5-95 labeling after stimulation was destained after an additional stimulation round (30 Hz, 3x3min) in the absence of FM5-95. Scale bar e**:** 10 μm, scale bar b: 5 μm (A,B Andreas Schmid / Stephan Sigrist, personal communication) **C-D)** α-DPak (green) and α-nc82 (red) staining (**C**) and α-GFP (green) and α-nc82 (red) staining (**D**) in DGluRIIA^GFP expressing larvae, lower panels: merged images. Scale bars: 5 μm.

In chapter 4.3.1 the MAB nc82 was shown to label AZs (Heimbeck et al., 1999; Wucherpfennig et al., 2003). Consistently, the nc82 signal overlaps with the immunolabel for the *Drosophila* voltage-gated Ca^{2+}-channel Cacophony (not shown), which also localizes to AZs of *Drosophila* neuromuscular synapses (Kawasaki et al., 2004). Individual AZs are represented by a dot-like staining (Fig. 23 C, arrowhead) which lies opposite and is aligned with the middle of PSDs (Fig. 23 C, arrow). This indicates its presynaptic localization. In fact, essentially all PSDs are associated with presynaptic AZs and *vice versa* (Fig. 23 C,D). Thus, the PSDs identified by DGluRIIA[GFP] expression are the postsynaptic elements of functional synaptic sites. These synapses seem to be functional early on, since small synapses (Fig. 23 A-D) already display all properties of established synapses (presynaptic vesicle recycling (Fig. 23 B), colocalization with PSD marker DPak (Fig. 15 B) and active zone marker nc82 (Fig. 23 D)). To study the coordinated outgrowth of pre- and postsynaptic organizations the molecular nature of the antigen recognized by the MAB nc82 was analyzed in collaboration with the Laboratory of Erich Buchner (University of Würzburg).

4.3.3 MAB nc82 identifies a protein of about 200 KDa*

* The data described in chapter 4.3.3 were produced by the Laboratory of Erich Buchner. In chapter 4.3.3 their results will be briefly summarized to coherently describe the characterizing of the molecular nature of the antigen recognized by the MAB nc82. Apart from the results described in chapter 4.3.3 other supporting evidence obtained in the Laboratory of Erich Buchner will be presented and acknowledged as such.

In short, Western blots of homogenized *Drosophila* heads could show that MAB nc82 recognizes two proteins of about 190 and 180 kDa apparent size (data not shown, see attached manuscript 2 / chapter 6.4). In order to identify the protein responsible for this reactivity, *Drosophila* head homogenates were subjected to 2-D gel electrophoresis and Western blotting. After probing with MAB nc82 two signals of the expected molecular weight were detected. They were found near pH = 5.6 and could be matched in Coomassie stained gels with two spots, which were excised and subjected to MALDI-TOF

mass spectroscopy (Toplab GmbH, Martinsried, Germany). Comparing of the peptide fragments with the *Drosophila* protein database reliably identified the two spots as isoforms of a protein which can be conceptually translated from the cDNA clone AT09405, corresponding to the predicted gene locus CG30337 (Berkeley *Drosophila* Genome Project; Flybase Consortium, 2003).

It was directly tested whether the cDNA AT09405 encoded protein contained the MAB nc82 epitope. In fact, the protein expressed from the cDNA in *E. coli* is recognized by MAB nc82 (data not shown). However, the calculated molecular weight of this protein is only 127.4 kDa, while the by MAB nc82 identified spots migrate in near 190 and 180 kDa SDS gels. Northern blots of head poly-A$^+$-RNA produced a strong signal at about 11 kb and a weak signal at about 2.3 kb (data not shown, see attached manuscript 2 / chapter 6.4). The 3' end of the AT09405 cDNA seems to contain the correct stop, followed by a poly-adenylation signal and a terminal poly-A-tail. The 5' end of the mRNA sequence was obviously truncated.

4.3.4 MAB nc82 identifies the *Drosophila* CAST homolog

BLAST homology searches of the computed *Drosophila* proteome with various vertebrate active zone proteins revealed that the predicted gene CG12933, which is located 22 kb upstream of CG30337, shows significant similarity to CAST/ERC, a protein associated with the cytomatrix at the active zone (Ohtsuka et al., 2002; Wang et al., 2002). This led to the speculation that the two open reading frames CG30337 and CG12933 might actually belong to the same gene. This idea was tested by RT PCR using mRNA from third instar larvae. Sequencing the specific products demonstrated that the mRNA encoding the MAB nc82 antigen incorporates the predicted genes CG12933, CG30336, CG30337 as well as a short exon between CG30336 and CG30337 (Fig. 24).
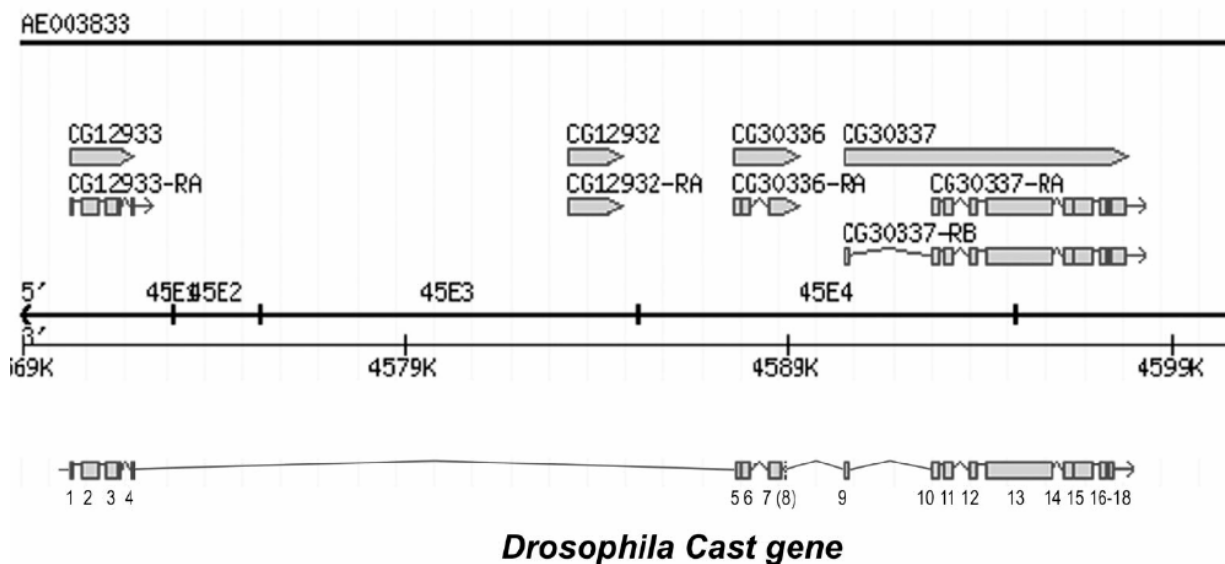
Fig. 24 The *Drosophila Cast* gene

The *Drosophila Cast* gene consists of 18 exons derived from three loci (CG12933, CG30336 and CG30337), which were previously annotated as independent genes

The cDNA isolates obtained from adults were largely identical to the cDNA isolates obtained from larvae, which were used for GFP-tagging of DCast (chapter 4.4). In some adult mRNAs the small exon 8 (33 bp) appears to be inserted by alternative splicing, replacing the amino acids VL at amino acid position 560-1 (position 652-3 in alignment Fig. 25) with the 11 amino acids (MQLEEQTTLHK) in the encoded protein (Dhananjay Wagh / Erich Buchner, personal communication).
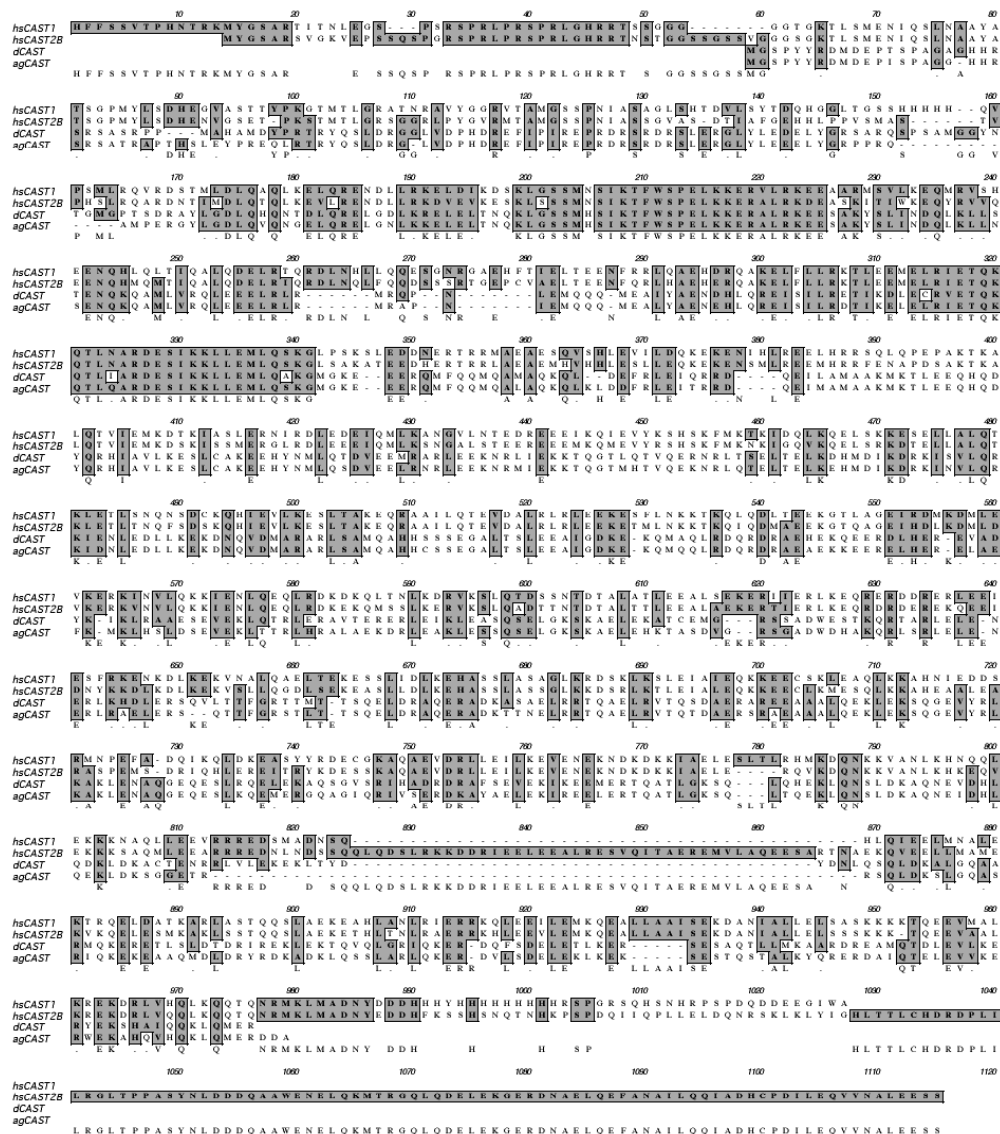
Fig. 25 Alignment of two insect and two human Casts

Two human CAST family members, the human KIAA0378 (hsCAST1) and the human Rab6-IP-2δ (hsCAST2B) were aligned with the N-terminal half of two insect Casts: the *Drosophila melanogaster* Cast (DCast) and the *Anopheles gambiae* Cast (agCast)

Due to the significant homology of the N-term of the encoded protein (Fig. 25) and its specific localization at the active zone it was proposed that the identified gene encodes the *Drosophila* homolog of the mammalian CAST/ERC.

Fig. 26 Alignment of *Drosophila* Cast and *Anopheles* Cast

While the homology between insect and vertebrate CASTs is restricted to the N-terminal half of the Cast protein, there is a high homology between *Drosophila* Cast and *Anopheles* Cast both in the N-terminal and the C-terminal region of the protein.

The genomic organization found in *Drosophila* was compared to that of the highly diverged dipteran insect species, *Anopheles gambiae.* The predicted genes CG30336 and CG30337 correspond to the predicted *Anopheles* protein ENSANGP00000014221, while

CG12933 corresponds to the neighboring protein ENSANGP00000002918. Both predicted proteins were connected. The thereby assembled *Anopheles* protein closely matches DCast (Fig. 5). Further comparison of the predicted *Anopheles* protein (agCast) (Fig. 26), of DCast and the genomic region in *Anopheles* allowed the prediction of two more exons, which were missing in the predicted protein ENSANGP00000014221. A fourth predicted gene (CG12932) is located between CG12933 and CG30336 in *Drosophila*, and thus could in principle represent a large alternatively spliced exon of the *Cast* gene (Fig. 24). Furthermore, the *Anopheles* CG12932 homolog lies in a very similar relative genomic position (3R: 52 788 996 : 52 789 985, (Holt et al., 2002)) when compared to the genomic organization of *Drosophila melanogaster*. However, all attempts to connect CG12932 to the *Cast* gene by RT PCR failed. Thus, CG12932 seems not to be part of the Dcast transcription unit. As discussed in detail in chapter 3.1.6 our RT PCR product and the cDNA AT09405 were fused. The new cDNA contains the complete predicted open reading frame of *DCast.* This sequence has been deposited in the database GENEMBL (accession number pending).

Next the supposedly complete protein sequence of *Drosophila* Cast was analyzed in more detail. The N-terminal part of the protein reveals high homology with all mammalian CAST proteins and the *Anopheles* homolog. The conservation is highest in regions corresponding to the first two coiled-coil domains of CAST (Fig. 25, for the domain structure of CAST see (Ohtsuka et al., 2002)). Both the *Drosophila* as well as the *Anopheles Cast* genes contain a large C-terminal region (Fig. 26), which is not present in mammalian CASTs and for which no homologous proteins apart from insect CASTs could be found. The high level of conservation between *Drosophila* and *Anopheles* within this domain, however, indicates that this domain is likely to be functionally important for insect Cast function.

Analysis of the amino acid sequence of *Drosophila* Cast predicts a possible nuclear localization (not supported by immunohistochemistry), numerous possible phosphorylation sites, no transmembrane domains, two leucine zipper domains, and a glutamine-rich C-term. However, no PDZ interaction motif for RIM interaction as found in several mammalian CAST forms as well as in a *C. elegans* homolog seems to be present in the

insect Cast forms. In addition, significant sequence similarities to myosin heavy chain, plectin, and restin are found, mainly due to coiled-coil regions and leucine zipper domains of the proteins.

4.3.5 *Drosophila* Cast is specifically expressed in differentiating neurons

In order to identify the cells expressing the *Drosophila Cast* gene, *in situ* hybridization on *Drosophila* embryos was performed. For this, *Cast*-specific antisense RNA probes derived from both the C-terminal part (AT09405) as well as from the N-terminal part (CG12933, see chapter 3.3) of this complex locus were used, while corresponding sense probes served as specificity controls.
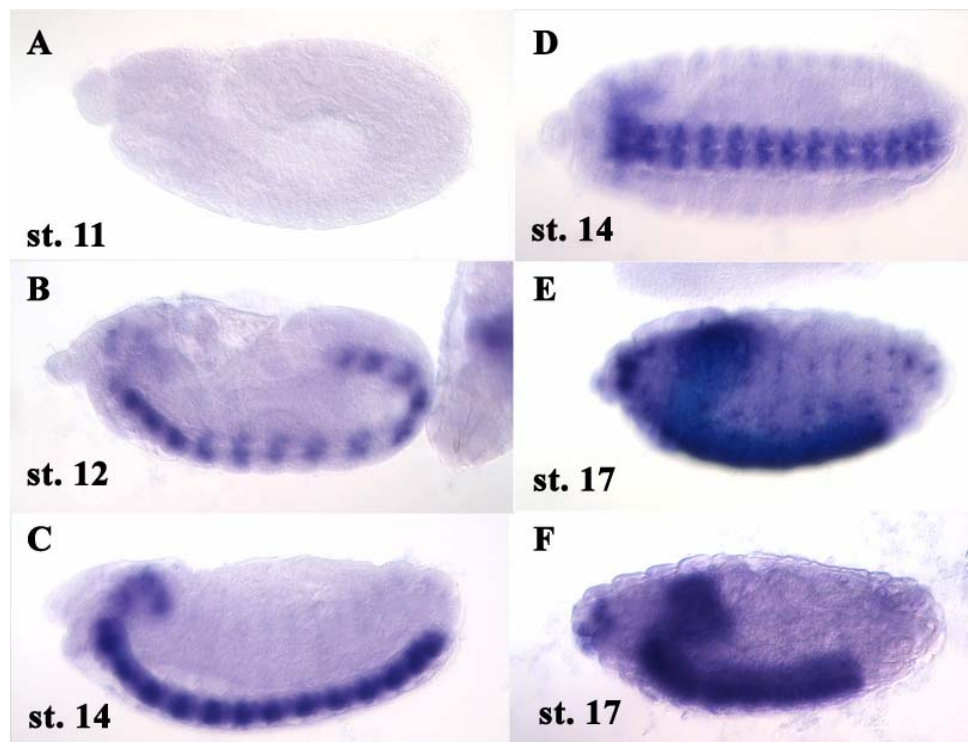
Fig. 27 *Drosophila* Cast expression in the embryo
In situ hybridization of *Drosophila* embryos.
A-E, the C-terminal part of the *Cast* cDNA was used to generate the anti-sense probe, **F**, the N-terminal part of the *Cast* cDNA was used to generate the anti-sense probe (see chapter 3.3).
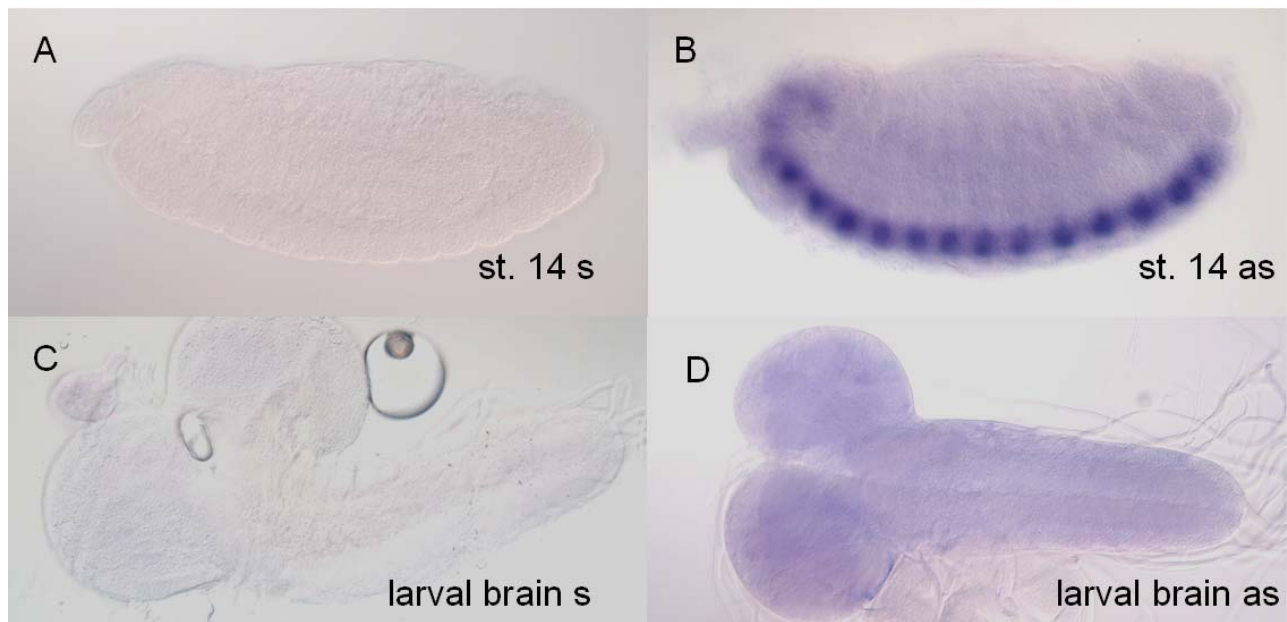
Fig. 28 *Drosophila Cast* is specifically expressed in the postmitotic neurons

In situ hybridization of *Drosophila* embryos, The N-terminal part of the *Cast* cDNA was used to generate a negative control (sense probe) (**A,** stage 14 embryo, **C,** larval brain). The corresponding anti-sense probe shows a specific staining (**B,** stage 14 embryo, **D,** larval brain).

Both in embryos and in larval brain the sense probe was negative (Fig. 28 A,C). Using CAST antisense probes, a strong specific label, indicating *Cast* mRNA expression, was detected from stage 12 on (compare Fig. 27 A and B). *In situ* labelings with C-terminal (Fig. 27 A-E) and N-terminal probe (Fig. 27 F) were identical, with both CNS (Fig. 27 B-F, stage14-stage17) and peripheral nervous system (PNS) neurons (Fig. 27 E,F, stage 17) show strong specific labels. This expression persisted in the larval stage, where specific expression in the brain was detected (Fig. 28 D). No expression in non-neuronal tissues like e.g. muscle was observed (Fig. 27 B-F). The onset of *Cast* expression corresponds to the onset of neuronal differentiation including the formation of the axon (Broadie and Bate, 1993). Thus, the spatio-temporal expression profile of *Cast* mRNA is fully consistent with DCast being a component specifically localized at the active zones of presumably all presynaptic terminals.

4.4 *In vivo* co-imaging active zones and postsynaptic outgrowth

Communication between pre- and postsynaptic sites during synapse formation is a complex process, which could be hardly addressed *in vivo*. Spatial and temporal correlation between pre- and postsynaptic maturation is the first step toward understanding the interaction between these structures during synaptogenesis. The identification of the antigen recognized by MAB nc82 was a molecular entry point to study AZ assembly *per se*, and the coordination of this process together with PSD formation. In immunofluorescence stainings of *Drosophila* larvae against DGluRIIA and DCast it was observed that large PSDs tend to have large corresponding presynaptic AZs, while smaller PSDs tend to have smaller corresponding AZs (Fig. 29). *In vivo* imaging of transgenic larvae (chapter 3.2.2 and chapter 3.2.4) co-expressing DCast^{GFP} and DGluRIIA^{GFP} should directly address the temporal sequence of AZ versus PSD assembly and the possibility of a coordinated maturation of AZ and PSD. First, immunohistrochemistry should give an indication of the temporal sequence of pre- versus postsynaptic assembly. If the AZ assembles first, nc82 dots without postsynaptic counterparts are expected to be found. Should the PSD assemble first, small PSDs without nc82 label are expected to be found. In the case of AZ and PSD forming simultaneously every AZ should have a corresponding PSD. Figure 29 shows an example of such a staining.
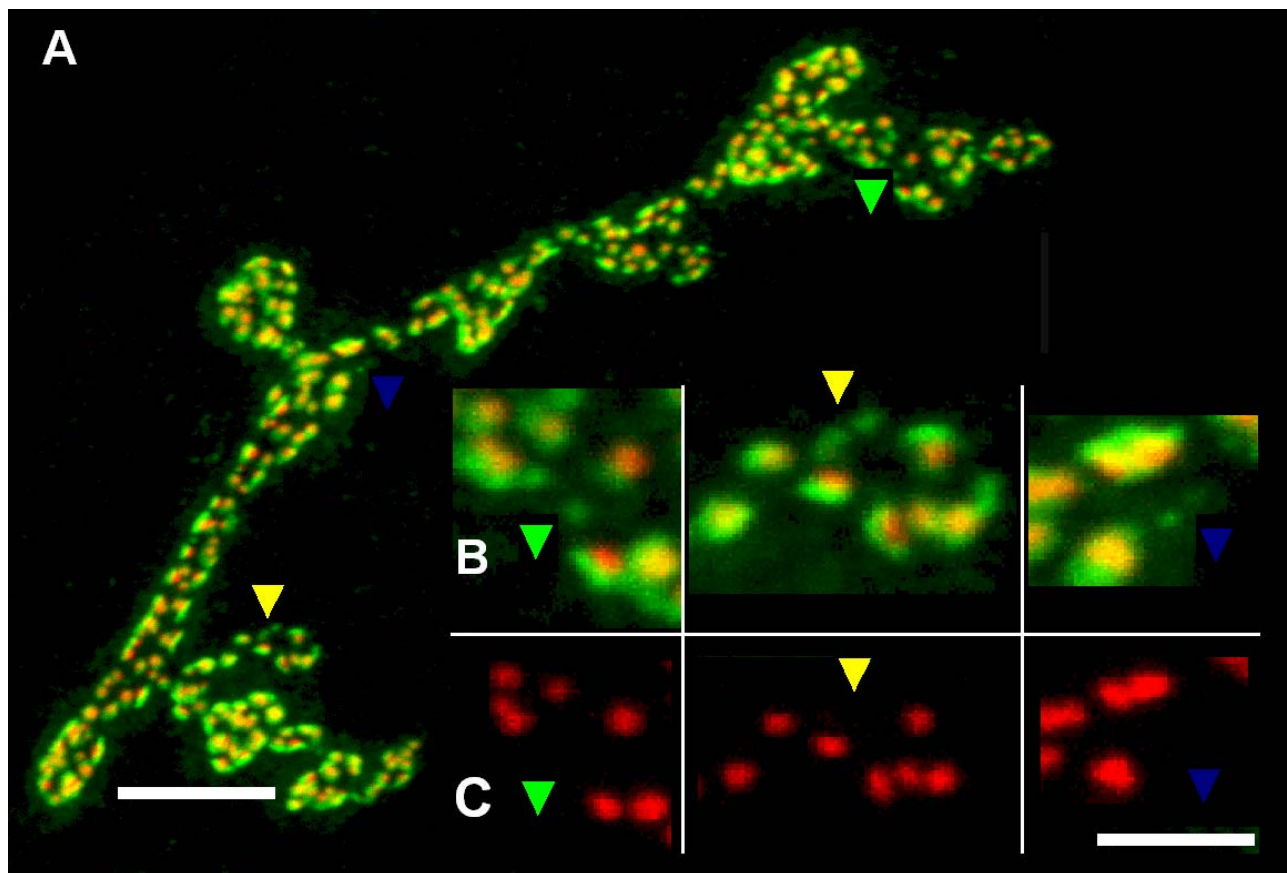
Fig. 29 Immunohistochemistry gives first indications concerning the temporal sequence of active zone and PSD assembly

A-C) Confocal images of DGluRIIC (green) and nc82 (red) staining at the NMJ of third instar wild type larvae. Arrowheads point at PSDs without a corresponding AZ label. **A)** Scale bar: 15 µm. **B)** magnification of A, **C)** nc82 staining as shown in B, without corresponding DGluRIIC staining. Scale bar (B,C) 3 µm.

The large majority (>95%) of all PSDs have a complementary presynaptic AZ staining (Fig. 3.3.8d). However, a small but consistent fraction of PSDs (Fig. 29 arrowheads) have no corresponding AZ label. This might indicate that a functional PSD can assemble prior to the assembly of the AZ. To directly visualize this process, co-imaging of DGluRIIA^{mRFP} and DCast^{GFP} was performed. Here again the large majority of all PSDs were found to have presynaptic AZ staining. When analyzing the first preliminary data some examples of both DCast^{GFP} signal without corresponding DGluRIIA^{mRFP} label and DGluRIIA^{mRFP} signals without corresponding DCast^{GFP} label were found. The latter examples were more frequent.
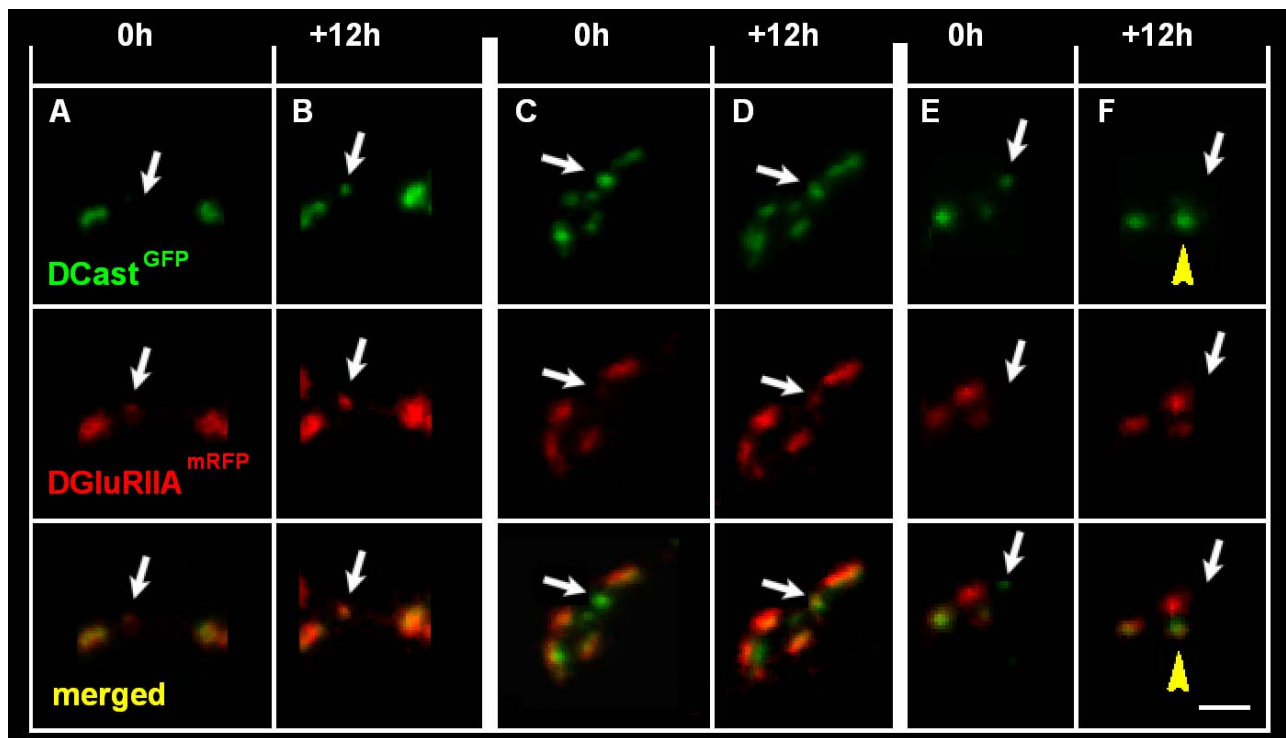
Fig. 30 *In vivo* imaging gives first indications concerning the temporal sequence of active zone and PSD assembly

A-F) Confocal time series of DCast^{GFP} (green) and DGluRIIA^{mRFP} (red) co-expressing third instar larvae. Scale bar: 1 µm. **A)** An example for a position where a DGluRIIA^{mRFP} label without a corresponding DCast^{GFP} label was detected (arrow). **B)** 12h later both a DCast^{GFP} and a DGluRIIA^{mRFP} label were found at this position, indicating the formation of a synapse (arrow) **C)** Example for a position where a DCast^{GFP} label without a corresponding DGluRIIA^{mRFP} label was detected (arrow). **D)** 12h later both a DCast^{GFP} and a DGluRIIA^{mRFP} label were found at this position, indicating the formation of a synapse (arrow) **E)** Example for a position where a DCast^{GFP} label without a corresponding DGluRIIA^{mRFP} label was detected (arrow). **F)** 12h later neither a DCast^{GFP} nor a DGluRIIA^{mRFP} label were found at this position, indicating that no synapse was formed at this position. While the DCast^{GFP} signal at the original position (arrow) was lost, a neighboring AZ increased significantly in intensity (arrowhead). Thus, it can be speculated that this DCast^{GFP} label actually represents transport clusters similar to the active zone precursor vesicles containing Piccolo and Bassoon as described in vertebrates (Shapira et al., 2003). This transport cluster might have fused with the neighboring AZ (arrowhead).

Usually a PSD with a corresponding AZ was present at positions where PSDs without corresponding DCast^{GFP} label were found 12h earlier (Fig 30 A,B arrow). At positions where a DCast^{GFP} signal without a corresponding PSD was observed, subsequent analysis revealed either the formation of synapses (Fig 30 C,D arrow) or a complete absence of both DCast^{GFP} and DGluRIIA^{mRFP} signals (Fig 30 E,F arrow). While

in the example shown in Figure 30 E the DCast^{GFP} signal at the original position (Fig 30 E,F arrow) was lost a neighboring AZ gained significantly in intensity (Fig 30 E,F arrowhead). Thus, it can be speculated that DCast^{GFP} signals without corresponding PSDs might in some instances actually represent transport clusters similar to the active zone precursor vesicles containing Piccolo and Bassoon as described in vertebrates (Shapira et al., 2003). Clustering of receptors might lead to the formation of the PSDs and ultimately to the establishment of the presynaptic AZ. To exclude artifacts introduced by the different folding times of mRFP and GFP new lines are currently being established in which DCast is labeled by mRFP and DGluRIIA is labeled by GFP. Next, a staining of the presynaptic membrane with CD8-Venus should help to estimate the distance of the DCast staining to the membrane. The distance of the DCast particles from the presynaptic membrane should help to identify whether they are transport particles or whether they represent AZs. Imaging with shorter time intervals than currently used should further help to clarify this issue as well.

4.5 Molecular dynamics during synaptogenesis

4.5.1 Molecular dynamics of PSD components

Measuring local protein turnover is a powerful tool for understanding the molecular basis of long-term changes within a biological system. While two synapses might have the same number of molecules of a certain protein, a newly gained high rate of incorporation in one of the two synapses might indicate, that long-term changes are currently taking place at this particular synapse. Application of drugs might substantially alter local protein turnover, while no changes in the steady state level might be observable. Here synaptic turnover of proteins will be used to trace the origin of the receptors integrated in new, growing PSDs.

As discussed in chapters 4.2.3 and 4.2.4 both FRAP experiments and photo-activation experiments consistently showed that the receptors, which become integrated into growing synapses do not derive from neighboring synapses but instead must be either newly synthesized or derived from extrasynaptic pools. It could further be shown that the growth of a given PSD directly correlates with the entry of glutamate receptor DGluRIIA at this site (Fig. 31).
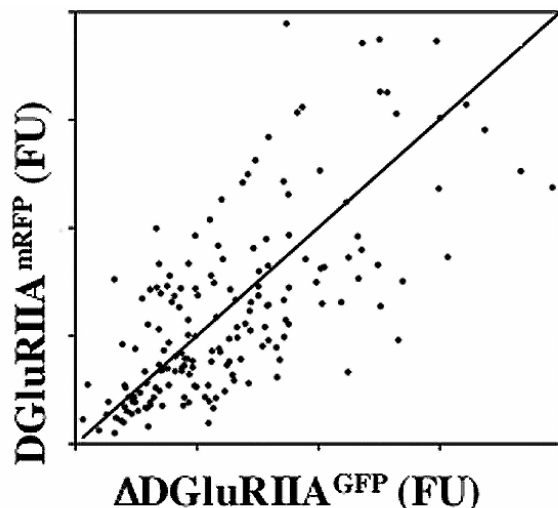
Fig. 31 Correlation of PSD growth and receptor entry
Receptor entry (DGluRIIA^{mRFP} recovery after FRAP) at individual PSDs versus change in DGluRIIA^{GFP} signal (representing PSD growth over 24h). R^2 of linear fit is 0.59, FU: arbitrary fluorescence units.

Consistently, large stable PSDs showed very low or no receptor entry (Fig. 20, white arrowheads). Additional FRAP experiments were performed in order to clarify where the glutamate receptors supporting the growth of newly forming PSDs are derived from. To this end the size of the bleached area was systematically varied on consecutive segments of one larva (Fig. 32 A,B).
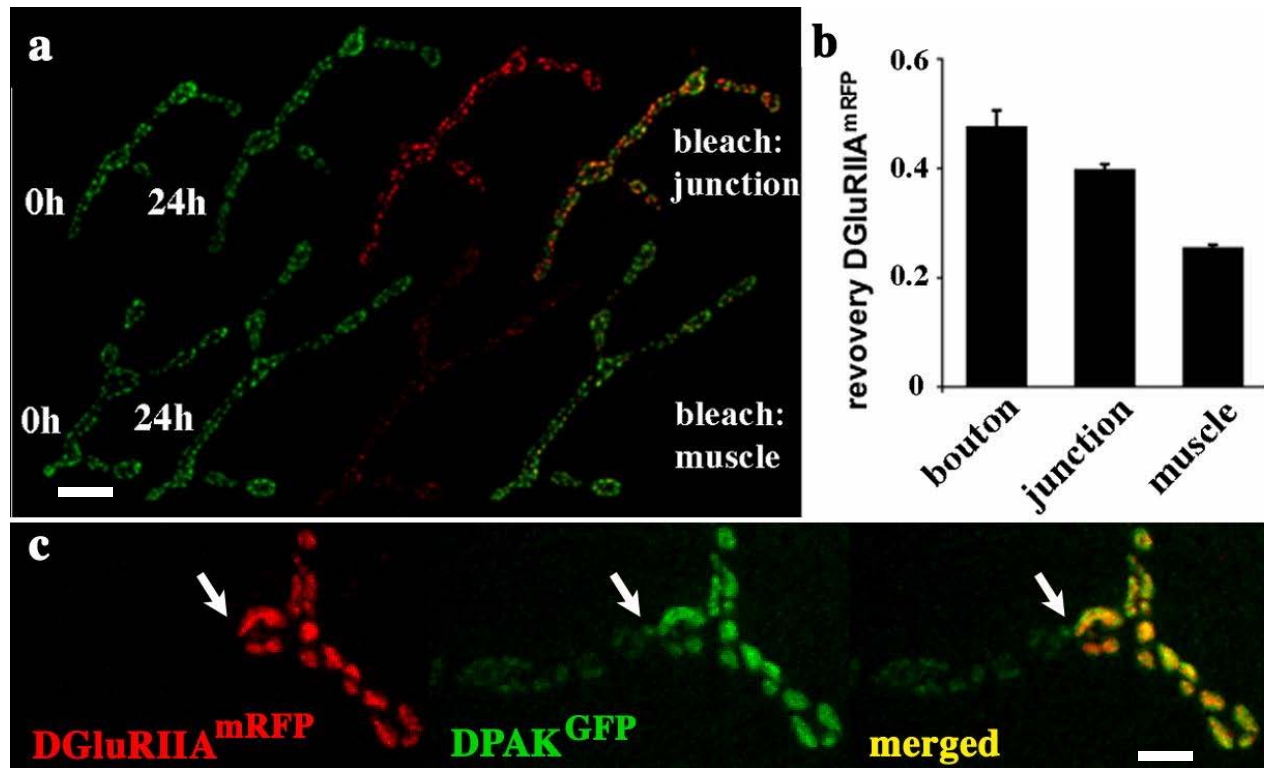
Fig. 32 *In vivo* **visualization of receptor entry and exit at individual PSDs**

A) From left to right: DGluRIIA[GFP] (green) at t=0 h, DGluRIIA[GFP] (green), DGluRIIA[mRFP] (red) and merged signal (yellow) 24 h after bleaching the DGluRIIA[mRFP] label. Bleaching the entire muscle (lower panel) allows only low DGluRIIA[mRFP] recovery at 24 h when compared to bleaching the junction (upper panel). Note that junctional outgrowth and PSD formation are not affected by whole-muscle bleaching. Scale bar 15 µm. **B)** Quantification of bleach-area dependence of FRAP. Recovery of the DGluRIIA[mRFP] signal decreases when the bleached area covers increasing parts of the postsynaptic muscle cell. Standard errors are indicated. **C)** *In vivo* FRAP: Confocal time series of a DGluRIIA[mRFP] (red) and PAK[GFP] (green) expressing junction. The area below the red line was bleached. 20 min later FRAP of PAK[GFP] is visible while no DGluRIIA[mRFP] FRAP is visible. Scale bar 1 µm.

After bleaching the whole muscle, some DGluRIIA[mRFP] signal reappeared after 24h (Fig. 32 A, lower panel and B), indicating that newly synthesized receptors contribute to

PSD growth as previously suggested (Sigrist et al., 2000). When smaller areas were bleached, significantly more unbleached DGluRIIA^{mRFP} entered within 24 h compared to bleaching the whole muscle (Fig. 32 A, compare upper and lower panel, quantification see B). Since the exact position of PSDs within the bleached area has no influence on the recovery of the fluorescent signal (not shown) it was concluded that stores of glutamate receptors in close proximity do not significantly contribute to PSD growth. This is consistent with the lack of any discernable accumulations of DGluRIIA outside the PSDs. The results rather imply that receptors are recruited into newly forming PSDs from pools dispersed over the muscle membrane. Broadie and Bate had already (using electrophysiology) described the existence of such extrasynaptic receptors in the muscle membrane (Broadie and Bate, 1993).

What are the molecular mechanisms controlling the local synaptic turnover or stabilization of glutamate receptors? As discussed in chapter 4.2.3 and 4.2.4 DGluRIIA^{GFP} has a low synaptic turnover. Therefore it was possible to use fluorescently tagged DGluRIIA as a tool to trace the origin of PSDs (chapter 4.2.3 and 4.2.4). Here the molecular mechanisms determining the synaptic residence time of molecules were addressed. Is the low synaptic turnover of DGluRIIA^{GFP} glutamate receptors specific or is the molecular composition of the postsynaptic density generally "static" (showing low synaptic turnover) in this neuromuscular system? To address this question, FRAP experiments were performed on DPak^{GFP}, another PSD localizing protein (Fig. 15 A). After photo-bleaching, the recovery time of DPak^{GFP} was about 20 times faster than that of DGluRIIA (Fig. 32 C). This suggests that DGluRIIA is specifically stabilized once integrated in PSDs, while the molecular composition of the PSD is highly dynamic *per se*. Do only glutamate channels containing the DGluRIIA subunit have a low synaptic turnover within this dynamic system, or are glutamate receptors inherently stably integrated into PSDs? Or is the low synaptic turn over an effect caused by the insertion of GFP into the C-term of DGluRIIA? In first experiments addressing these questions the turnover of DGluRIIA^{mRFP} was directly compared to the turnover of DGluRIIC^{GFP}. All data concerning receptor subunit composition so far suggests that the muscular glutamate receptors consist of 3 obligatory, essential subunits (DGluRIIC, DGluRIID, DGluRIIE) and either a

DGluRIIA or a DGluRIIB subunit (Qin Gang / Stephan Sigrist, personal communication, see attached manuscript 3 / chapter 6.5).
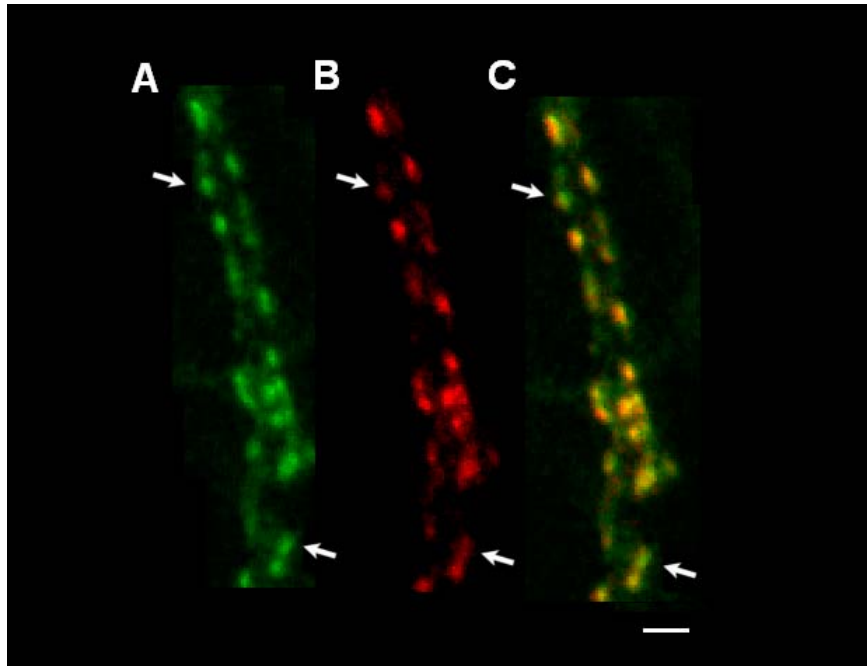
Fig. 33 Comparison of receptor entry and exit between DGluRIIC and DGluRIIA

A-C) FRAP recovery of DGluRIIC[GFP] and DGluRIIA[mRFP] 24 h after photo-bleaching both fluorophores. The recovery of both fluorophores was restricted to new and growing PSDs, while many PSDs present before bleaching (not shown) show little or no FRAP. A few PSDs, which show a high DGluRIIC[GFP] (A) label and a low DGluRIIA[mRFP] (B) label were observed 12h after bleaching (arrows). Most likely this label reflects PSDs consisting of mainly receptors with a DGluRIIB, DGluRIIC, DGluRIID, DGluRIIE stoichometry. PSDs with a DGluRIIA[mRFP] label were always DGluRIIC[GFP] positive (all other examples, compare also merged image (C), which is consistent with the idea of DGluRIIC being an essential subunit (Marrus et al., 2004). The recovery of DGluRIIC[GFP] was, like the recovery of DGluRIIA[mRFP], restricted to a few PSDs, while many PSDs show little or no FRAP. Scale bar 2 µm.

As shown in Fig. 33 PSDs, which show a particularly strong DGluRIIC[GFP] label and little DGluRIIA[mRFP] were observed 12h after bleaching (arrows). Most likely this label reflects PSDs consiting of mainly receptors with a DGluRIIB, DGluRIIC, DGluRIID, DGluRIIE stoichometry. PSDs with a DGluRIIA[mRFP] label were always DGluRIIC[GFP] positive, which is consistent with the idea of DGluRIIC being a subunit essential for forming glutamate receptors in this synaptic model (Marrus et al., 2004). The recovery of DGluRIIC[GFP] was, as the recovery of DGluRIIA[mRFP], restricted to a few PSDs, while many PSDs show little or no FRAP. This indicates that the turnover of DGluRIIC[GFP] is in a similar time domain like the turnover of DGluRIIA[GFP]. With DGluRIIC being a essential subunit (present in all muscular glutamate receptors) (Marrus et al., 2004) these results reflect the turnover of all glutamate receptors present in the muscle. Thus in the moment it

seems as if all glutamate receptors once integrated into PSDs might have only little turnover.

4.5.2 Molecular dynamics of the active zone

The quantification of PSD turnover revealed that the set of receptors present at the PSDs is remarkably stable. Is the same also true for proteins localized at the presynaptic AZ? To address this question simultaneous FRAP experiments were performed in which both DGluRIIA^{mRFP} and DCast^{GFP} were photo-bleached. 3 hours after bleaching essentially no FRAP can be observed for DGluRIIA^{mRFP}, while there is substantial recovery of the DCast^{GFP} signal.
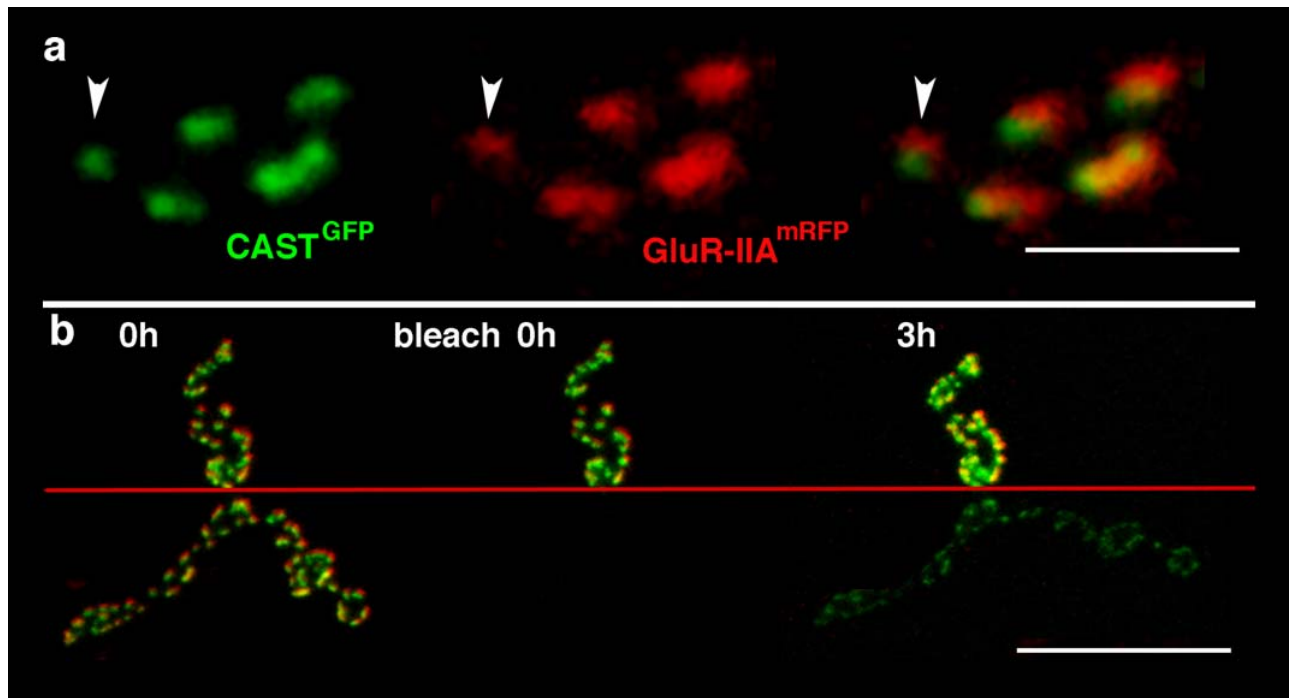
Fig. 34 Estimating synaptic protein turnover at both the pre- and the postsynaptic site
A) Examples of PSDs (visualized by DGluRIIA^{mRFP}) and AZs label (visualized by DCast^{GFP}) shown at high magnification. Scale bar 2 µm **B)** FRAP of DGluRIIA^{mRFP} and DCast^{GFP}. The lower part of the junction (below red line) was photo-bleached at t=0 h (central panel). 3 h later (right panel) substantial recovery of DCast^{GFP} was observed, while there is essentially no recovery of the DGluRIIA^{mRFP} signal. Scale bar 20 µm.

These results indicate that the AZ might be more dynamic than previously thought. Potentially there are also two distinct pools of DCast, one stably localized to the AZ and

one with a high turnover. To address this question DCast^{mRFP} is currently being produced, which allows addressing these question in FRAP experiments similar to those described in chapter 4.2.3.

4.6 Screening for proteins localized to the neuromuscular junction

4.6.1 Genetic screens for on locus GFP-fusions

The preliminary *in vivo* imaging data on DCast^{GFP} suggested that there is a correlation between the localization of DCast to the AZ and the localization of DGluRIIA to the PSD (chapter 4.4). Once a synapse is established, a much higher turnover of DCast^{GFP} compared to the postsynaptic glutamate receptors was observed (chapter 4.5.2). While it is very tempting to generalize these results and to make claims concerning AZ and PSD assembly one has to be aware that these results just represent the behavior of one pair of proteins. To fully understand the temporal sequence of AZ versus PSD assembly first the individual components of either AZ or PSD need to be identified. So far, the number of proteins known to localize specifically to active zones or PSDs at the *Drosophila* NMJ is very limited (see chapter 2.4). Therefore a screen was started that should help isolate additional proteins, which localize to neuromuscular synapses. Morin and co-workers defined a screen paradigm in which they used a P-element based cassette that contained the GFP-coding region flanked by known splice sites to efficiently screen for GFP-fusions. Upon intergration in introns there is a certain probability that the GFP-cassette is interpreted as additional exon (Morin et al., 2001). Based on the random character of this so-called exon-trap screen about 1 in 1600 transpositions events will lead to a productive, e.g. GFP positive chimeric fusion protein (Morin et al., 2001) (for principles of exon-trap screening see chapter 2.4).

4.6.2 Large scale larval screen for proteins localized at the NMJ

The screen of Morin and co-workers was based on P-elements as transgenic vectors. Two disadvantages of P-elements are their tendency to integrate in 5' untranslated regions of genes and to preferentially target a small subset of genes that map to so-called hotspots (Thibault et al., 2004). Prior to starting a large-scale screen the vectors were therefore redesigned. It was decided to base the screen on the transposable element *piggyBac,* since reports showed that *piggyBac* has (along with other advantages reviewed in chapter 2.5) less genomic hotspots compared to the *Drosophila* P-elements used by Morin and co-workers (Cary et al., 1989; Berghammer et al., 1999; Horn and Wimmer, 2000; Horn et al., 2003). Therefore, it was expected to get a spectrum of targeted genes different from that predicted for P-elements, and to yield higher insertion rates into intronic sequences. As a transformation marker either the white gene or the 3xP3 ds-red marker were used (Sheng et al., 1997; Horn and Wimmer, 2000). The 3xP3 ds-red marker contains the fluorophore ds-red under the control of the artificial 3xP3 promoter. The 3xP3 promoter, consisting of three Pax-6 homodimer binding sites, drives expression mainly in the eye (Horn et al., 2000). This marker was originally designed for the use in non-drosopholid insect species (in which the white marker can not be used) and has several advantages compared to white. First of all, it is with only 1,3 kb large much smaller than the mini-white gene (4-5 kb). This is important, since transposition frequency is known to decrease with insert size. Furthermore, the larger the insert in an intron, the more likely it is that problems with splicing of the message occur. And finally, 3xP3 ds-red is easily identifiable in larvae and can be detected in adults even in the presence of the white gene.

Thus 3xP3 ds-red was used as marker a for the first generation of *piggyBac* exon-trap constructs, comprised of p1 (piggyL SD-GFP-SA 3xP3 ds-red) and p2 (piggyL SD-GFP-SA 3xP3 ds-red ap). Figure 10 shows a map of all constructs used in the two screens described in chapters 4.6.2 and 4.6.3. The constructs p1 and p2 are almost identical. For both the "SD-GFP-SA 3xP3 ds-red cassette" was cloned into *piggyBac* (=pE3.12, see chapter 2.1.2), at the same time removing 0,8 kb of the former transposase reading frame. For both constructs the GFP cassette is oriented anti-parallel to the former transposase reading frame. In p2 but not in p1 this is also the case for the marker. After obtaining transgenic flies a manual pilot screen was performed to test whether the lines produce GFP- fusions after transposition.

While it is very laborious to screen 40000 larvae by hand, a larval sorter can perform this task in less than an hour. In principle the larval sorter works like in a cell sorter. Fluorescence-activated cell sorting (FACS) is widely used to isolate subpopulations of cells based on antigen display, nucleic acid content, and gene expression. During FACS analysis, cells are observed in laminar flow, which is then dispersed into droplets of solution of such a size that only one cell is contained within a droplet. Cells are usually sorted by electrostatic deflection of the droplet, displacing it away from the laminar flow of solution. While this method has also been applied for *Drosophila* embryos (Furlong et al., 2001) the sorter used for this work separated embryos by displacing the solution via a constant air flow into the waste container. Once a positive embryo is detected this airflow is briefly interrupted, thereby collecting the embryo or the larva. To begin with, the parameters for selection had to be optimized. The system works via a software interface as shown in Figure 35.
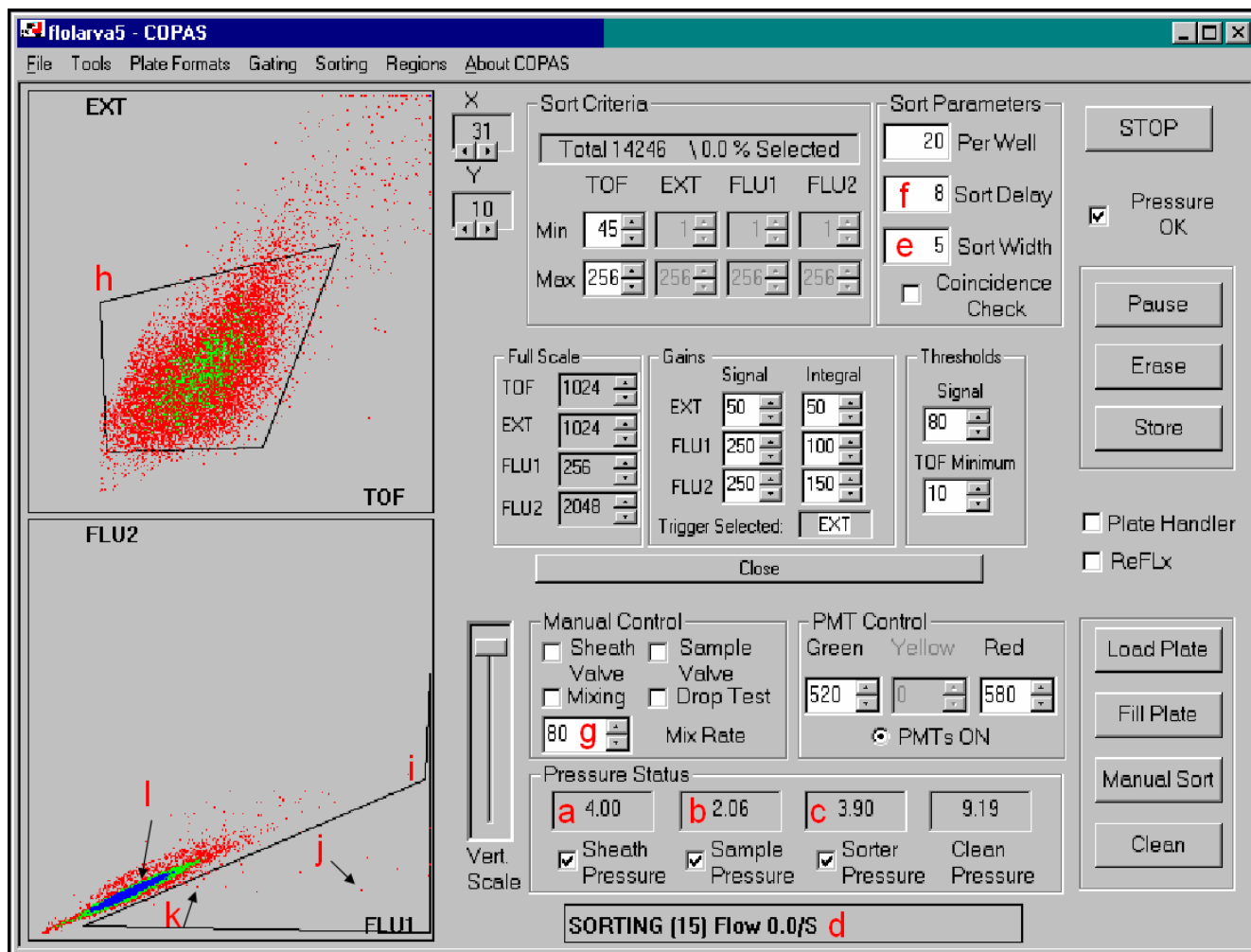
Fig. 35 Software interface used for automated embryo sorting. For detailed description of parameters defining flow of sample and selection criteria see text.

All parameters can be subdivided into parameters either defining flow or selection criteria. The flow parameters ensure that the larvae pass the detector at the right speed. If the flow rate is too slow, the sorting takes too long. If the flow rate is too fast, the sorter might either be blocked or multiple embryos might pass the detector in the same time interval. Then all these embryos are discarded, which might cause the loss of a positive embryo. Optimal results were obtained at the following pressures: sheath 4 psi, sample 2 psi, sorter 4 psi (Fig. 35 A-C). Next the larvae were diluted such, that 20 larvae were detected per second (Fig. 35 D). Statistically every 50 ms one larva passes through the sorter. Therefore, the chances to have two events within 5 ms (the sort with, (Fig. 35 E))

are low. When a second event is detected within that interval, both embryos will be discarded. This is thought to minimize false positives. A further reduction of the chance of false positives is achieved by coincidence check. Here the interval, in which the detection of no more than one event is allowed, will be enlarged to "sort width" plus "sort delay". This option was deactivated, since it was more important to avoid false negatives than false positives. The sort delay (Fig. 35 F) defines how many milliseconds after detection of a positive event the air pressure will be interrupted. The air pressure usually displaces the solution into the waste container. Interruption of the pressure leads to the collection of the animal. Sort width (Fig. 35 E) controls for how long the airflow is interrupted. If these settings are not properly matched with the flow of the solution (as defined by the pressures and the viscosity of the carrier medium) the wrong events will be sorted. A mixrate of 80 (Fig. 35 G) ensured that the density of particles was roughly constant throughout the sort. The remaining parameters were set as summarized in table 2.

Table 2 Optimized sorting parameters for automated sorting of GFP positive larvae

Full Scale:	Gains Signal:	Gains Integral:	Thresholds:	PMT Control:	Sort Criteria:
TOF: 1024	EXT: 50	EXT: 50	Signal: 80	Green: 520	TOF Min: 45
EXT: 1024	FLU1: 250	FLU1: 100	TOF Min: 10	Red: 580	TOF Max: 256
FLU1: 256	FLU2: 250	FLU2: 150			
FIU2: 2048					

While these settings are fixed standard parameters for sorting first instar larvae, the parameters defining, which larvae are positive have to be adjusted for every sort. The sorter evaluates 4 parameters of the object. The first parameter is the time of flight (TOF). The TOF is a measure of the size of the object, indicating how long it takes for the object to pass the detector. The second parameter is the extinction coefficient (EXT) determining how much the object scatters light. The combination of EXT and TOF allows the user to define the dimensions of the object of interest (e.g. larvae). Thereby air bubbles, empty eggshells, embryos and larvae can be separated. To this end, a region of interest (ROI) is

drawn into the detection window (Fig. 35 H). Only particles with an EXT/TOF combination within this window will be further analyzed by the sorter. The next two parameters are green fluorescence (FLU1) and red fluorescence (FLU2) (Flu2 = autofluorescence control). All particles with a high green fluorescence compared to red fluorescence are likely to be truly GFP positive. The exact ROI (Fig. 35 I) had to be optimized in a brief test sort. Sorting rates between 1:400 and 1:3000 turned out to be in the right range. If the ROI is chosen too restrictive only larvae with strong GFP expression (e.g. whole brain, muscle, gut) will be sorted (Fig. 35 J), while potentially interesting weak GFP expression patterns (e.g. few neurons, very specific synapse label) might be missed (Fig. 35 K). Choosing the ROI too permissive, i.e. too close to the main population (Fig. 35 L), results in the selection of too many false positive larvae. Since it was known that the larvae expressing GFP-tagged glutamate receptors, which represent a pattern of interest (see chapter 4.1.6), have a comparably low overall expression strength it was decided to choose the ROI rather permissive and to tolerate a higher rate of false positive larvae.

Of 916011 sorted larvae 2586 were sorted positive (1:350). Of these, 322 were positive after a manual rescreen at the third instar larval stage. Therefore 1:2190 sorted larvae both survived and were positive after rescreening. Of those 322 positive lines 118 lines (due to their expression pattern) were chosen for further characterization. These include 13 lines with expression at the neuromuscular junction, 14 lines showing expression at the muscle attachment sites, 22 lines with interesting patterns in the brain, 70 lines showing expression in the ovary and 17 other lines selected for various reasons. The Sigrist Laboratory was particularly interested in lines showing a specific GFP label at the NMJ. A list of all lines with specific GFP expression at the NMJ is shown in table 3.

Table 3 GFP exon-trap screening: 7 different genetic loci that show expression at the neuromuscular junction could be confirmed by sequencing

Line	Locus	Function / Homology
1	Gelded (CG31605/EMMPRIN)	metalloprotease inducer, cell adhesion
2	Neuromusculin	cell adhesion, axon guidance
3	CG5830	homology to LIM interactor-interacting factor
5	CG9338	no homologies
6	Trol/Perlecan	Immunoglobuling domains, extracellular matrix
7	Mmp2	matrix metalloproteinase
13	Shaggy	Ser/Thr kinase; transduction of wg signaling

Within the list of NMJ localizing lines, several interesting molecules have been identified. Wingless-signaling mediated by the Shaggy-kinase constitutes a prime pathway essential for synapse development (Franco et al., 2004) at the neuromuscular junction. Immunoglobulin-domain proteins with synaptic expression (like NCAM or its *Drosophila* ortholog Fasciclin II) (Mathew et al., 2003) have been broadly implicated in the control of synapse development and plasticity. Among the 13 lines two immunoglobulin-type cell adhesion molecules (Neuromusculin, Gelded) (Reed et al., 2004) that accumulate at neuromuscular synapses were identified. Sara Mertel (Laboratory of Stephan Sigrist, ENI-G, Göttingen) and Florence Besse (Laboratory of Dr. Anne Ephrussi, EMBL, Heidelberg), who participated in the screening are momentary concentrating on a further genetic analysis of Gelded. In the following this larval screen be referred to as the Heidelberg screen, since it was performed in collaboration with the Laboratory of Dr. Anne Ephrussi at the EMBL in Heidelberg.

4.6.3 Optimizing a vector for a genome-wide screen for proteins localized at synapses

After the successful larval screen (Heidelberg screen) it was decided to perform a genome-wide screen in a big consortium of laboratories. The sorting of the embryos for the genome-wide screen is performed in collaboration with Dr. Christian Klämbt at the University of Münster. Therefore, it will be referred to as the Münster screen. The aim of this co-operation is to produce 10000 GFP positive lines within the next two years. Extrapolating the discovery rate of NMJ localizing lines predicts that more than 100 lines with expression at the NMJ should be obtained.

Part of this thesis was the construction of a new set of vectors to be used for the screen of this consortium was. It is not feasible to balance and to keep 10000 lines. Therefore, it is planned to keep heterozygous stocks over several generations, just by flipping the vials. Heterozygous white expressing flies have an advantage in propagation compared to flies, which lost the insert (and the white marker, and are therefore blind again). All laboratories will evaluate the stocks within 4 weeks of their production, interesting ones will be sequenced. After removing clones of identical insertions all interesting, unique stocks will be balanced and kept. This workflow requires a selection marker, which gives the flies carying the insert an advantage compared to flies, which have lost the insert. Therefore, white was used as marker and not 3xP3 as used for the Heidelberg screen. Moreover, the *piggyBac* backbone itself was modified. In the Heidelberg Screen (vector p1 and p2) the "marker (3xP3-dsred) GFP-cassette" replaced a 0,8 kb deletion in the *piggyBac* transposase open reading frame (maps of all constructs are shown in Fig. 10). By serial deletion Fraser and others determined the minimal *piggyBac* sequences required for transposition *in vivo* (Malcom Fraser, personal communication). Based on their results it was decided to place the GFP-marker cassette in *piggyBac* vectors that contain only these minimal *piggyBac* ends. This should increase the transposition efficacy, since it is known that the transposition efficacy is higher, when the insert is smaller (Malcom Fraser, personal communication).

One main advantage of *piggyBac* is that it excises only precisely, thus leaving no potential "second site hit" back (Cary et al., 1989; Fraser et al., 1995; Elick et al., 1996; Fraser et al., 1996). Nonetheless, it would be very valuable to be able to do imprecise excisions (as usually done with P-elements) to create mutants in the genes of interest. Combining the advantages of P-elements and *piggyBac*, P-ends were placed in the *piggyBac* vector (compare Fig. 10). Thus the screen is a *piggyBac* screen, which has many advantages over P-element based screens (compare chapter 2.5). Once a functional GFP-fusion is identified the stock can be crossed to P-transposase. Thereby mutants can be easily obtained. The P-ends were either placed flanking the entire GFP-marker cassette (p3: piggyM P white SA-GFP-SD P) or only flanking the selection marker (p4: piggyM P white P SA-GFP-SD P see Fig. 10). Placing the P-ends to only flank the selection marker allows sorting for imprecise excisions.

The fact that transgenics lines of these two constructs were easily obtained (Christian Klämbt, personal communication) proved that the *piggyBac* ends must be functional *in vivo*. Nonetheless, the remobilization of these constructs using transgenically expressed *piggyBac* transposase worked only very poorly (Christian Klämbt, personal communication). One possibility was that the P-ends and the *piggyBac* ends are too close together, causing problems with *piggyBac* remobilization. To rule out this problem the GFP-marker cassette used to construct p4 was put into the *piggyBac* backbone called piggyL (piggy large). Vectors based on this backbone (p1 and p2) were successfully used in the Heidelberg screen, and remobilized well. The new construct was named piggyL P white P SA-GFP-SD (p5) (Fig. 10). Transgenic animals were easily obtained. These constructs remobilized well in the eye. Nonetheless, germ line transposition was often ineffective. (Christian Klämbt, personal communication). Finally one strain could be isolated, which showed an even better mobilization rate than p2, the construct used for the Heidelberg screen (Christian Klämbt, personal communication). The Münster screen focused on mainly late embryo stages (12-26h, 25°C) (Christian Klämbt, personal communication), while the Heidelberg screen sorted mainly 22-36 h (25°C) old first instar larvae. In the Heidelberg screen both the handling of first instar larvae, as well as the number of positively sorted animals, were significantly better (five times more positive larvae) compared to sorting embryos. Partially this can also been attributed to the fact that

in Heidelberg a lot of time was spent on optimizing conditions for larvae, which were of prime interest. In Münster mainly embryos are sorted for the consortium. Therefore an embryo sorter is used in Münster (Copas Express, Union Biometrica, Somerville, MA, USA), while in Heidelberg the more flexible COPAS Select (Union Biometrica, Somerville, MA, USA) sorter was used. The sort rate of 1:2000 (Christian Klämbt, personal communication) for embryos (using p5 compared to a ratio of 1:5000 in p2 animals) is good. It remains to be clarified to what degree these numbers reflect true positive events. In Heidelberg roughly 1:10000 embryos were positive upon manual resorting (using p2), while in first instar sorts 1:2000 sorted larvae were true positives. If most embryos sorted in Münster prove of to be positive upon resorting, this would indicate that the embryo sort protocol was substantially improved and could be a suitable alternative to sorting first instar larvae. If the number of true positives is less than 50% of the sorted embryos, sorting of first instar larvae should be considered as an alternative. Collectively this data shows that the established construct should allow meeting the goal of establishing 10000 GFP positive lines, which will contribute substantially to the characterization of the both pre- and postsynaptic compartment.

5. Discussion

5.1 Establishing a new assay to study molecular dynamics during synapse formation *in vivo*

Glutamate receptors mediating excitatory transmission in our brains are recognized as key elements in the context of activity-dependent synaptic plasticity (Shi et al., 2001; Sheng and Kim, 2002). Over the last years, convincing evidence for rapid changes in density and/or function of postsynaptic glutamate receptors has accumulated. (Dodt et al., 1999; Gundelfinger et al., 2003; Sheng and Hyoung Lee, 2003; Tardin et al., 2003; Ashby et al., 2004; Bresler et al., 2004; Matsuzaki et al., 2004). However, the understanding of how glutamate receptor dynamics are organized on longer time scales is still meager. To gain a deeper understanding of such processes, it appears necessary to observe the molecular dynamics of glutamate receptor proteins in their native settings (Niell and Smith, 2004), as elegantly performed for acetylcholine receptors in rodents (Purves and Lichtman, 1987; Akaaboune et al., 2002). It would be most valuable to do this in the mammalian brain during learning tasks. Advances in two photon microscopy (Denk et al., 1990; Theer et al., 2003) make it possible to image several hundreds of μm deep in the brains of anesthetized mice or rats (Helmchen et al., 1999; Svoboda et al., 1999; Grutzendler et al., 2002; Trachtenberg et al., 2002). A miniaturized microscope, which can be installed on a rat's head even provided recently the first images from freely behaving rats (Helmchen et al., 2001; Helmchen and Denk, 2002). Nonetheless, imaging in the mouse brain is technically demanding, and mouse genetics is very slow compared to *Drosophila* genetics. Thus, so far *in vivo* imaging of individual PSDs has never been achieved.

Drosophila is characterized by efficient genetic tools allowing the deletion of genes or the introduction of new transgenes very rapidly. While in principle the transparent *Drosophila* larva is ideal for imaging, the anesthetization of the larva has never been properly established.

The synapses to be studied have a diameter in the range of 100 nm to 600 nm and are closely spaced (100-500 nm). These diameters are close to the optical resolution limit of the microscope, as given by the excitation wavelength and the numerical aperture (NA) of the objective (using an 63x OIL 1,32 NA objective). These small structures are furthermore located on the body wall muscles, which, beside the heartbeat, are themselves the main source of internal movements. Therefore, it was challenging to establish an appropriate imaging protocol. During image acquisition a complete and reversible anesthetization (including heartbeat), was to be achieved. As this protocol had to satisfy highest standards, it was easy to modify it and to make it suitable for other purposes which were typically less demanding. In fact, the *in vivo* imaging technique could already be successfully adapted for other groups, which use it for *in vivo* imaging of tracheal development, fatbody imaging and cell-division imaging in imaginal discs. Thus, this work paves the way for *in vivo* studies in developing *Drosophila* larvae addressing a variety of biological questions, not necessarily limited to neurobiological questions. In future it will be interesting to combine this technique with fluorescence resonance energy transfer measurements to study protein interactions *in vivo*. The combination of *in vivo* imaging with the "mosaic analysis with a repressible cell marker" system (Luo and Zong, 2001) will allow studying activation or inactivation of gene products in individually fluorescently labeled cells.

5.2 PSDs of glutamatergic synapses form truly *de novo* at the *Drosophila* NMJ

Based on electron micrographs it was proposed more than two decades ago, that growth, perforation and subsequent splitting of individual PSDs may be essential intermediates during synaptic potentiation (Nieto-Sampedro et al., 1982; Carlin and Siekevitz, 1983). This hypothesis is very attractive, since input specificity would be maintained. Nonetheless, the theory of PSDs splitting remained controversial despite a large number of careful studies, mainly because it had been so far impossible to track individual PSDs during synaptic potentiation (Toni et al., 1999; Lüscher et al., 2000; Yuste and Bonhoeffer, 2001; Fiala et al., 2002).
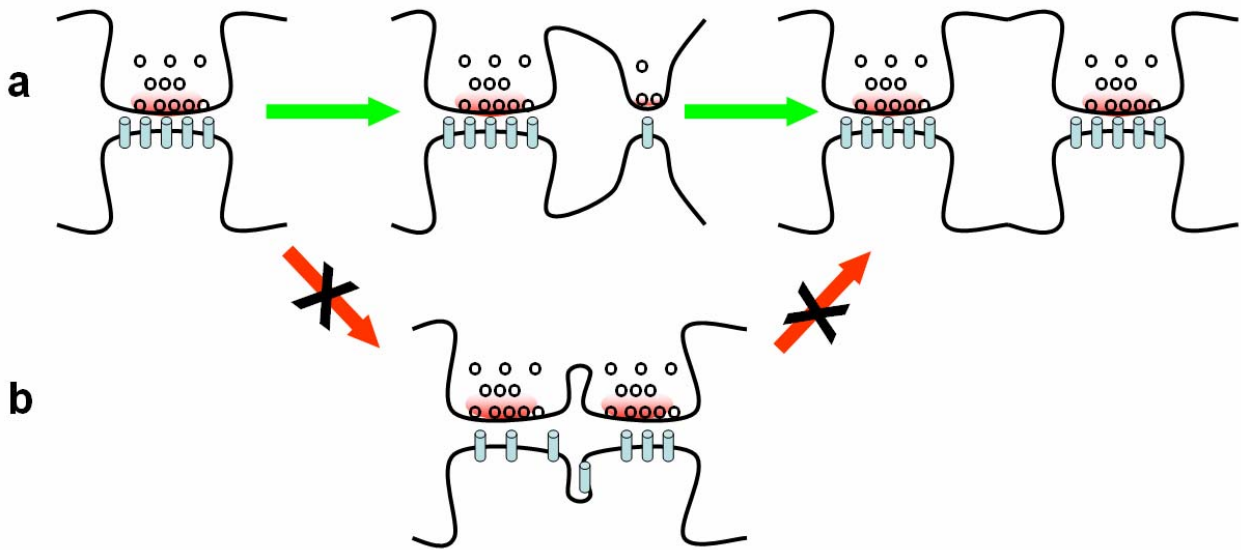
Fig. 36 Mechanisms mediating activity dependent new formation of synapses. It was shown that new synapses form (as illustrated in **A)**) distant from existing sites and do not receive glutamate receptors from neighboring mature synapses (true *de novo* formation). This is in contrast to the idea (illustrated in **B)**) that the splitting of postsynaptic densities mediates the formation of new synapse during synaptic potentiation

Based on statistical studies using electron microscopy it was believed that splitting of PSDs is a multistep process (Fig. 36 B, detailed description see chapter 2.2.4). The supposed temporal sequence is as follows: First spines become larger (Fifkova and Van Harreveld, 1977; Desmond and Levy, 1986) and there is a concomitant increase in synaptic area (Desmond and Levy, 1988). Large PSDs break apart, forming perforated PSDs (Peters and Kaiserman-Abramof, 1969; Toni et al., 1999), which is followed by the bifurcation of spines and ultimately by closely associated pairs of spines emanating from one dendrite and touching the same presynaptic element (Toni et al., 1999). At the *Drosophila* NMJ the large majority of all PSDs is formed clearly distant from pre-existing PSDs, suggesting that they formed *de novo* - independent from neighboring PSDs (Fig 17 B, arrowheads). However, a few situations were observed (Fig. 17 B, white circle), which mimicked the hypothesized CNS splitting processes at first glance (Luscher et al., 2000; Hering and Sheng, 2001; Yuste and Bonhoeffer, 2001). A closer inspection of such PSD clusters, always indicated that these PSDs were in fact separate units forming in close proximity (<200 nm) to each other. This idea was supported by the fact that also the

113

reverse process was observed (Fig. 17 B, blue arrow). Moreover, pairs of PSDs were observed that were clearly distinct as shown by their molecular composition (as visualized by FRAP of DGluRIIA^{mRFP}). These PSD pairs sometimes had a uniform DGluRIIA^{GFP} label, falsely suggesting the existence of only one, but not two distinct PSDs (Fig. 20 D). Later these two PSDs might increase the distance to one another by the growth of the presynaptic bouton they are located on. Therefore, they might be visualized as two distinct PSDs in a subsequent image, falsely suggesting the split of PSDs. It was assumed that examples of such "pseudo-splitting" process, which were rarely observed (Fig. 17 B, white circle), were just "imaging artifacts" caused by the limited resolution of light microscopy. Next a simulation was performed, which showed that new formation of PSDs in close proximity to existing PSDs can be differentiated from split-like partitioning of PSDs as of a distance of 200 nm (Fig. 19). Thus, another approach had to be taken to prove that PSDs form exclusively *de novo*. FRAP and photo-activation experiments allow the tracing of receptors inserted into newly forming PSDs. It could be shown that the receptors inserted into new PSDs are derived from outside of the bleached/photo-activated area (Fig. 20 C and Fig 21 A,B). Therefore, they can not be derived from neighboring synapses, as expected for the case PSD splitting. Thus, these experiments clearly indicated that PSDs form – at least in this preparation - independently from pre-existing PSDs as small precursors, which grow until they reach their mature size. This is fully consistent with EM reconstructions of Harris and co-workers arguing that the same-dendrite multiple synapse boutons (which are widely interpreted as evidence for synapse splitting (Luscher et al., 2000; Hering and Sheng, 2001; Yuste and Bonhoeffer, 2001) can in fact not arise from synapse splitting, since it was observed that mature dendrites and axons pass through the gaps between spines, which synapse on them (Fiala et al., 2002). In the thesis presented it was furthermore shown that these new PSDs form truly *de novo,* meaning that they do not receive glutamate receptors from neighboring PSDs.

5.3 Outgrowth of small PSDs might be responsible for strengthening of the NMJ

Collectively, the presented data proposes the following model, which explains how glutamate receptor dynamics are organized during the strengthening of a glutamatergic synaptic system. As discussed in chapter 2.3.6, the synaptic current collectively mediated by the set of synapses within a junction increases more than two orders of magnitude during larval development (Broadie and Bate, 1993; Sigrist et al., 2003). This is necessary in order to sufficiently excite the postsynaptic muscle cell, which also grows continuously in this period (Schuster et al., 1996; Gramates and Budnik, 1999). When challenged towards higher transmission strength, the system will react by forming additional synapses. This is accomplished by the *de novo* formation of synapses and not by splitting of existing synapses. While these new synapses are initially only about a few percent of the size of mature synapses they are already functional and display all properties of established synapses (presynaptic vesicle recycling, colocalization with active zone marker nc82 and the PSD marker DPak, see Fig. 23 B,D and Fig. 15 B). These small immature synapses could thus already be responsive to instructive activity patterns. The newly growing synapses (but not the mature PSDs) might be the ones responsible for strengthening the synaptic system over time. This model has interesting parallels to recent studies, which report that large synaptic spines are stable for months in the intact mouse cerebral cortex (Trachtenberg et al., 2002), while small spines can be converted into large spines upon potentiation (Matsuzaki et al., 2004). It is tempting to speculate that small PSDs are memory units, which can be potentiated to produce large mature synapses, which are in turn physical traces of memory. Although mature PSDs loose the ability to be further potentiated, they can reliably store information without interference due to readout of information or potentiation of small synapses nearby. Perforated synapses thought to be associated with LTP (Toni et al., 1999) might serve the same purpose as synapses in *Drosophila* showing multiple T-bars and the similar multiple active zone synapses described in crayfish, which were shown to have high release probability (Cooper et al., 1995; Cooper et al., 1996). These tree structures might be the highest potentiated, most reliable form of memory units. They might serve as information storage units required for

reliable readout of memory at high-frequencies, rather than as a way to create new synapses, which would also have an impact on the information stored in these synapses. This is consistent with data showing that the increased occurrence of closely related pairs of spines (spines emanating from one dendrite touching the same presynaptic element) under LTP (Toni et al., 1999) is caused by rapid independent outgrowth of growth cones (Fiala et al., 2002) and not by splitting of perforated synapses.

The idea of mature spines being stable traces of memory is supported by data on *in vivo* spine stability reporting that spines in the primary visual cortex of about 4,2 month old mice have a half-life time of more than 13 months (Grutzendler et al., 2002). This implies that synapses could persist throughout a mouse's lifetime. Nonetheless, it has to be noted that these results are still under debate, primarily since a similar study in the barrel cortex of 5 to 10 week-old mice revealed that even the stable pool of spines (representing about 60% of spines) had a limited lifetime of around 3 months (Trachtenberg et al., 2002). This discrepancy can only partially be explained by the different brain regions used and by the age difference, leaving the question open, of how long lived spines really are. If spines are short-lived this would challenge our understanding of long-term memory, while high spine stability would be fully consistent with the idea that the spines may provide a substrate for long-term memory. At the same time, it is not likely that data from slice cultures could contribute in any meaningful way to that discussion. Aside from problems in cultivating slices over extended time periods, culture artifacts are even more worrisome. Dendritic spines disappear for example during chilling (while preparing the slice), but proliferate excessively upon rewarming of the mature hippocampus (Kirov et al., 2004). This leads to a 40%-50% increase in spine and synapse number in mature hippocampal slices compared to the perfusion fixed hippocampus (Kirov et al., 1999), which raises serious questions about the degree (if at all) to which data concerning spine stability can be compared to *in vivo* and *in vitro* preparations.

5.4 Extrasynaptic glutamate receptors get selectively stabilized in growing PSDs

Returning to the concept of spines/PSDs being the substrate for long-term memory, it needs to be clarified how the transitions from new to mature and from mature to complex spines/PSDs are controlled. It seems likely that the transition from an immature to a mature PSD is mediated by stabilizing synaptic glutamate receptors. Consistently, it had been shown that large spine heads are characterized by having many AMPA receptors (Nusser et al., 1998). The synaptic system seems to support the outgrowth of synapses by providing a diffuse pool of glutamate receptors, which are selectively stabilized in or inserted into growing synapses. In contrast, mature PSDs show very little (if any) receptor insertion or removal. The overall recycling in these synapses is very small, if present at all. To rule out imaging artifacts, these results were confirmed by two independent methods, photo-activation and fluorescence recovery after photo bleaching. Both measurements lead, within the accuracy of the measurement, to the same results. Mature synapses showed little, if any synaptic turnover of glutamate receptors. It is not possible to use these methods to prove that there is no synaptic turnover at all. Calculations however showed that, if there were any turnover it must be less than 10% within 12h (based on the FRAP experiments). Independent calculations based on the photo-activation experiments showed that the recycling of synaptic glutamate receptors must be less than 20%. This indicates that in terms of their glutamate receptors mature PSDs of the *Drosophila* NMJ have a remarkably stable molecular identity.

In the neuromuscular system the molecular composition of the postsynaptic density is not static *per se.* FRAP of GFP-labeled *Drosophila* p21-activated kinase, another PSD localizing protein is about 20 times faster than FRAP of DGluRIIA. This suggests that DGluRIIA somehow gets stabilized, once integrated into PSDs, while the molecular composition of the PSD is *per se* highly dynamic (Fig. 32 C). Simultaneous FRAP experiments on the C-terminally tagged DGluRIIA[GFP] and the N-terminally tagged DGluRIIC[GFP] could further prove that the low synaptic turnover is really an inherent characteristic of all glutamate receptors in the muscle. DGluRIIC is an essential subunit

thought to be present in all glutamate receptors present in the muscle (Marrus et al., 2004). Therefore, the synaptic turnover of all types of glutamate receptors is reflected in the synaptic turnover of DGluRIIC^{GFP}, which is similar to that of DGluRIIA. Thereby it is important to mention, that DGluRIIC was N-terminally tagged with GFP. The C-term of glutamate receptors is known to be important for targeting and anchorage (Dong et al., 1997; Srivastava et al., 1998; Srivastava and Ziff, 1999). Since DGluRIIC was N-terminally tagged any alterations of receptor turnover caused by effects of the insertion of GFP into the C-term could be excluded (Fig. 33).

Where are the receptors supporting the outgrowth of new synapses derived from? It could be shown - by bleaching the entire muscle - that newly synthesized receptors contribute to PSD growth (Fig. 32a) as previously suggested (Sigrist et al., 2000). Significantly more unbleached DGluRIIA^{mRFP} entered within 24h, when bleaching only smaller areas compared to bleaching the whole muscle (Fig. 32 A,B). Moreover, the exact position of PSDs (not shown) within the bleached area has no influence on the recovery of the fluorescent signal. Collectively these data lead to the following conclusions: Stores of glutamate receptors in close proximity do not significantly contribute to PSD growth. This is consistent with the lack of any discernable accumulations of DGluRIIA outside the PSDs, which is in contrast to data describing glutamate transport vesicles in day 3-4 neurons (Washbourne et al., 2002). In older neurons (Bresler et al., 2004) however, no similar transport vesicles could be observed, nor were they detectable for other NMDAR subunits (Guillaud et al., 2003). Therefore, glutamate transport vesicles might be used during early stages of neuronal development, while the establishment or strengthening of specific PSDs within an established circuitry might be supported by diffuse pools of glutamate receptors. Electrophysiology has actually shown the existence of diffuse, extrasynaptic pools of glutamate receptors in the membrane of *Drosophila* muscles (Broadie and Bate, 1993). Such receptors might be recruited into newly forming PSDs. Thereby laterally diffusing receptors might become "trapped" in PSDs, as recently demonstrated by tracking individual glutamate receptor complexes in cultured mammalian neurons. Likewise these glutamate receptors float freely in the membrane. This enables them to diffuse in and out of synapses where they only have a low residence time (Borgdorff and Choquet, 2002; Tardin et al., 2003).
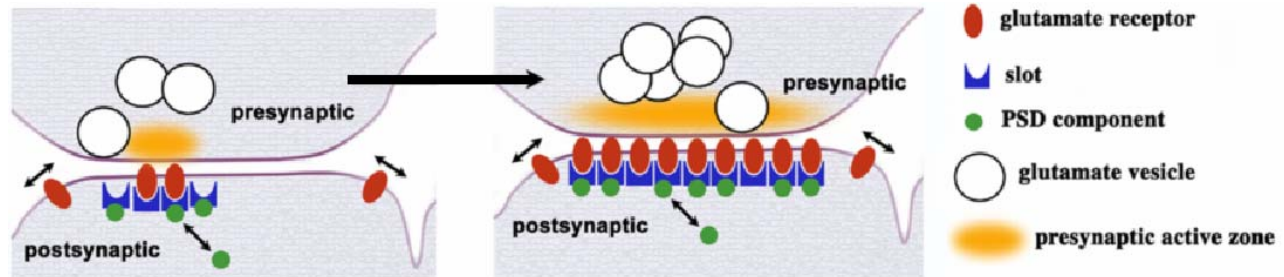
Fig. 37 Model explaining how glutamate receptor dynamics could be organized during PSD formation. The model suggests that small PSDs grow by stabilizing receptors which enter from a diffuse pool of glutamate receptors into the PSD. Thereby "synaptic tags" might differentiate "accepting" i.e. growing from "non-accepting" i.e. mature PSDs.

This pool of unbound receptors might be fundamentally different from a second pool of tightly bound receptors showing essentially no turnover. The model suggests that "synaptic tags" differentiate "accepting" (i.e. growing) from "non-accepting" (i.e. mature) PSDs (Fig. 37). These tags must be accessible to entering receptors and might be identical to the "slots" which finally immobilize receptors. At growing PSDs, the availability of both slots and glutamate receptors could be rate limiting for growth. The latter possibility is supported by the previous finding that a genetically triggered increase in the expression of the glutamate receptor DGluRIIA stimulates synapses formation and provokes an additional functional strengthening of the junction (Sigrist et al., 2002). At the *Drosophila* neuromuscular junction mature PSDs usually keep their glutamate receptors and thus retain their strength, consistent with the fact that the synaptic system has to continuously increase its overall strength (Davis and Goodman, 1998). The rarely observed shrinkage potentially reflects competition between synapses (not shown). Focusing future work on such local factors as neighbor relationships and local disparities in presynaptic release will hopefully help to decipher the molecular and cellular rules controlling learning and memory in an even more detailed manner.

5.5 Identification of the *Drosophila* homolog of the CAST/ERC protein

Over the last years, some insight into assembly and molecular composition of the cytomatrix found at vertebrate presynaptic active zones has been gained (Landis et al., 1988; Hirokawa et al., 1989; Garner et al., 2000; Dresbach et al., 2001; Phillips et al., 2001; Rosenmund et al., 2003). While there is a wealth of information on the ultra-structure of insect synapses (Atwood et al., 1993; Jia et al., 1993; Atwood and Cooper, 1996), the molecular composition of their synaptic active zones is completely unknown. This work shows that the *Drosophila* homolog of the proteins encoded by the ELKS/Rab6-IP2/CAST (ERC) gene family localizes at the presynaptic active zones of presumably all neuronal terminals. While markers for synaptic vesicles like synaptobrevin and synaptotagmin stain large proportions of the presynaptic bouton (Littleton et al., 1993; Broadie, 1995, 1996) DCast specifically labels the AZ (Fig. 22). It thereby provides an entry point to study active zone formation and function in *Drosophila*. The open reading frame of the identified cDNA corresponds in size to the protein recognized by MAB nc82. Vertebrate CAST is part of a structural meshwork formed by cytoskeletal elements like actin and spectrin and large active zone specific proteins like Piccolo and Bassoon. Both Piccolo and Bassoon contain several putative protein-protein interaction domains, which are assumed to help organize several components of the active zone. The third coiled-coil domain of Bassoon contains a motif that is highly homologous to the corresponding region of Piccolo and has been shown to compete with Piccolo to bind the second coiled-coil domain of CAST1/ERC2 (Takao-Rikitsu et al., 2004). This binding of CAST1/ERC2 to Bassoon seems to be of functional relevance. When a glutathione S-transferase (GST) fusion of the Bassoon binding site to CAST1/ERC2 was injected into neurons the excitatory postsynaptic potential amplitude could be reduced by 30% within 70 min in cultured superior cervical ganglion neurons. This suggests that the binding of CAST/ERC and Bassoon is involved in neurotransmitter release (Takao-Rikitsu et al., 2004). CAST1/ERC2 itself has furthermore been shown to bind RIM1 via the C-terminal PDZ motif IWA (Ohtsuka et al., 2002). RIM1 is a target of the RAB3A small G protein, which in turn is implicated in vesicle docking. RIM1 interacts with Munc13-1 (Augustin et al., 1999; Betz et al., 2001) implicated in vesicle priming. Together with vesicular this complex might thus control the recruitment of vesicles and their subsequent fusion with the presynaptic

membrane. However, so far no coherent picture has emerged of how Ca^{2+} dependent release is controlled at active zones in a spatially restricted manner.

In mammals CAST isoforms apparently have both neuronal and non-neuronal roles. *Drosophila* Cast seems to correspond to the neuronal CAST isoforms, while the non-neuronal functions might be vertebrate specific. Besides the protein described here the only published molecule known to localize exclusively to *Drosophila* presynaptic active zones is the Ca^{2+} channel Cacophony, which seems to be responsible for providing the calcium trigger for evoked neurotransmitter release (Kawasaki et al., 2004). This work indicates, however, that the molecular structure of the presynaptic active zone might be more conserved between vertebrate and insect synapses than previously thought, due to the lack of obvious Piccolo and Bassoon homologs in insects. Therefore, it is to be expected that studying active zone formation and function in *Drosophila* will be a valuable addition to similar studies in vertebrates, especially considering the powerful genetic tools available for *Drosophila*. In particular, it will be interesting to address the function of the CAST/ERC protein family by genetic knock-out and knock-down experiments and to study the roles of the different domains present in the *Drosophila* Cast isoforms in detail.

5.6 Assembly and molecular dynamics of the active zone

The identification of DCast provided a molecular entry point to study the development of the AZ during synapse formation. As discussed in chapter 2.1.4 the communication between pre- and postsynaptic sites during synapse formation is a complex process involving a variety of cell surface receptors, their ligands and cell adhesion molecules (for review see (Gundelfinger and tom Dieck, 2000; Yamagata et al., 2003; Shen, 2004)). Addressing the spatial and temporal correlation between pre- and postsynaptic maturation is the first step toward understanding the interaction between these structures. *In vitro* data together with retrospective immunohistochemsitry so far suggest that in vertebrates the formation of the AZ is followed by the clustering of synaptic vesicles and the assembly of the PSD (for review see chapter 2.1.4 and (Umeda and Okabe, 2001; Ziv and Garner, 2001; McGee and Bredt, 2003)). Preliminary *in vivo* imaging data addressing the temporal sequence of AZ and PSD assembly was presented

in this thesis. Both immunohistochemistry (Fig. 29) and *in vivo* imaging suggested (Fig. 30) that DGluRIIA can localize to PSDs before DCast localizes to the AZ (Fig. 30 A,B). However, also DCast[GFP] label without a corresponding DGluRIIA label was observed (Fig. 30 C,E). Subsequent analysis of these examples revealed either the formation of synapses (Fig 30 C,D arrow) or a complete absence of both DCast[GFP] and DGluRIIA[mRFP] signals (Fig 30 E,F arrow). It is likely that the DCast[GFP] label can visualize both AZs and transport clusters similar to the dense core vesicles containing Piccolo and Bassoon described in vertebrates (Shapira et al., 2003). The idea that DCast[GFP] transport particles were observed was supported by the observation of examples, in which the DCast[GFP] signal at the original position (Fig 30 E,F arrow) was lost, while a neighboring AZ gained significant in intensity (Fig 30 E,F arrowhead). To further clarify the issue of temporal sequence of AZ versus PSD assembly several steps have to be taken (Fig. 30). To exclude artifacts introduced by the different folding times of mRFP and GFP new lines are currently being established in which DCast is labeled by mRFP and DGluRIIA is labeled by GFP.

With DCast currently being the only marker for the cytomatrix at the *Drosophila* AZ it is not clear whether the AZ can assemble later than the PSD, or whether simply the localization of DCast to the AZ, and not the assembly of the AZ, follows PSD assembly in the observed examples. Next, the synaptic turnover of AZ and PSDs proteins was addressed. DCast shows significantly more synaptic turnover at existing AZ, than DGluRIIA does at the corresponding PSDs (Fig. 34 B). Again the question, whether this higher synaptic turnover is DCast specific, or whether it reflects the behaviour of the AZ *per se* needs to be addressed. Likewise, the function of DCast is to be clarified. Moreover, it needs to be addressed, to which degree "mature type" vesicle recycling takes place at nascent synapses negative for DCast. So far styryl dye labeling suggested that PSDs labeled by DGluRIIA always show presynaptic vesicle recycling (Fig. 23 A,B and Andreas Schmid / Stephan Sigrist, personal communication). This might indicate that vesicle-recycling functions at least partially in the absence of a properly organized, mature AZ. Such idea is supported by the description of synaptic-like vesicles in growth cone filopodia of *in vitro* primary cultures of postnatal day 3-5 rat visual cortical neurons (Sabo and McAllister, 2003). These vesicles contain a number of synaptic vesicle proteins including

the vesicular glutamate receptor transporter VGlut1, and fuse in with the presynaptic membrane in response to focal stimulation (Sabo and McAllister, 2003). Therefore these vesicles were proposed to be important for focal priming of postsynaptic sites and eventually synaptogenesis (Sabo and McAllister, 2003). The temporal sequence of synapse assembly at the larval NMJ synapses might thus start with vesicle recycling followed by the organization of the PSD and the localization of DCast to the AZ. To address the temporal sequence of pre- and postsynaptic assembly in more detail further components of the AZ need to be characterized and studied.

5.7 Screen to identify GFP-tagged synaptic proteins on a genome-wide scale

The presented thesis established a very robust model system to study the assembly of synapses in much detail. Both temporal sequences of recruitment of specific proteins, and synaptic turnover can be addressed on the level of individual synapses. While it is very tempting to generalize the behavior of one PSD or AZ component in order to draw conclusions about the behavior of "the PSD" or "the AZ" precaution is necessary and relevant controls need to be done. To fully understand how "the PSD" or "the AZ" changes in a certain assay, the molecular composition of the PSD or AZ need to be clarified first. To this end a large scale genetic screen to identify GFP-tagged synaptic proteins was initiated.

Of 13 500 predicted genes in the fly genome only a comparably small number has been studied in detail concerning its subcellular localization and function. While a larger number of proteins is known to localize to the neuromuscular junction (for review see *Drosophila* protocols) only 6 proteins have been shown to be specifically enriched at either the presynaptic active zone (cacophony) (Kawasaki et al., 2004) or in the PSD (DGluRIIA, DGluRIIB, DGluRIIC, DPak, DPix) (Schuster et al., 1991; Harden et al., 1996; Petersen et al., 1997; Parnas et al., 2001; Marrus et al., 2004). This work lays the foundation to identify a large portion of the so far unidentified NMJ localizing proteins within the next few years. Among the 332 proteins that were identified in a pilot screen, 13 localized

specifically to the neuromuscular junction. Of these lines 11 turned out to be independent insertions. This is a low rate of redundancy (84% independent insertions).

To achieve this high rate of independent insertion care has to be taken, to avoid clonal events caused by transpositions in sperm stem cells, giving rise to many sperm. To avoid that these sperm, carrying the same new insertion, give rise to many redundant GFP expressing offspring, it is best to have a high male to female ratio. The number of different genes hit is further lowered by so-called hotspots, local hops or a strong bias towards insertion into large introns. The 11 independent insertions represented targeted only 8 different genes. Based on this data a chance of 60% for hitting different genes was estimated.

How then can this data be extrapolated to a genome-wide screen? In pilot screens about 50-80 lines per week were produced, and characterized by the screen consortium. Thus it is realistic to produce 10000 in about 3 years. Which coverage of the genome is to be expected? The problem of saturation and genomic hotspots was addressed before in a statistical analysis of P-element mutagenesis (Spradling et al., 1999). Hotspots are genomic regions with high insertion probability. While in P-elements these hotspots account for only about 3% of all genes, they account for 39% of all hits (Spradling et al., 1999). All other genes could be further subdivided into warmspot genes (accounting for 15% of genes and 31% of all hits) and cold spot genes (accounting for 83% of genes and 30% of all hits). Here, this data was used (Fig. 38) to predict how fast saturation is reached when screening with P-elements.
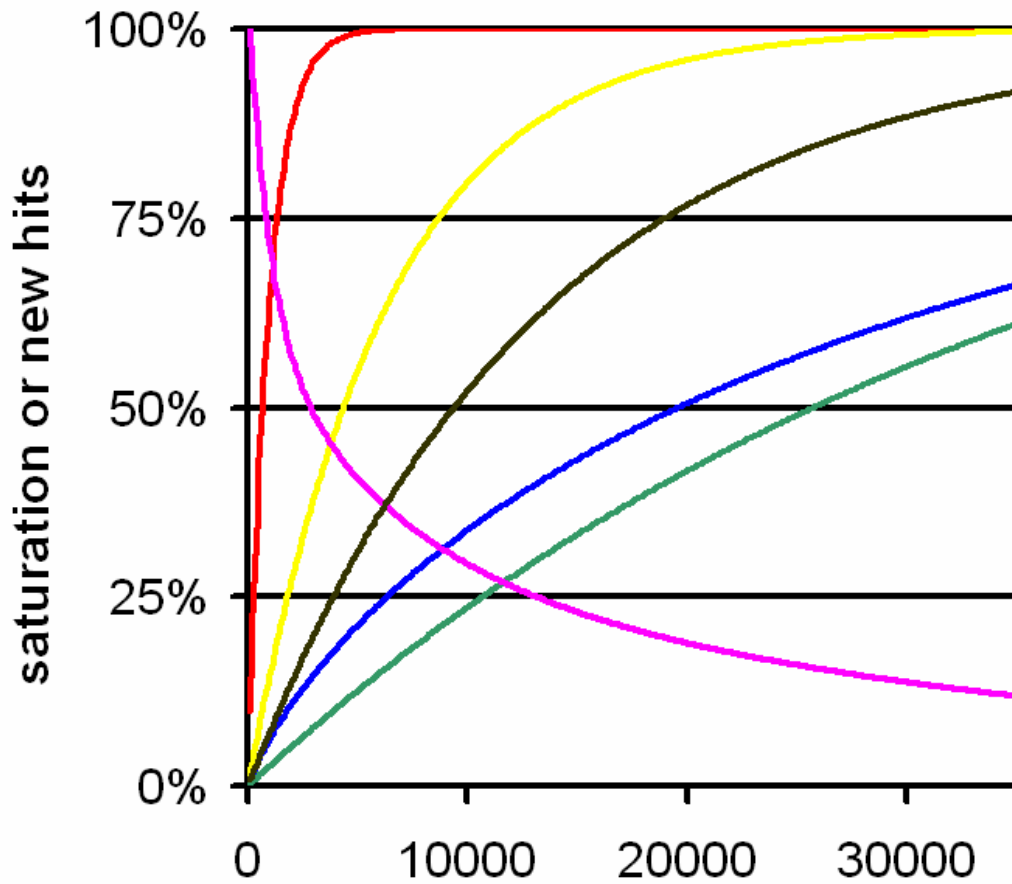
Fig. 38 Saturating mutagenesis using P-elements. P-elements are known to have a certain bias towards specific locations on the chromosome. Based on this bias genes can be grouped into hotspot (red line), warmspot (yellow line) and coldspot (green line) genes. This behavior leads to the rapid decrease in the number of new genes hit (purple line), while saturation of the genome (blue line) is reached slower than expected for ideal random insertion (black line)

Due to the high chance of being hit hotspot and warmspot genes reach saturation very rapidly (Fig. 38, red and yellow line). The possibility of them being hit does not decline when these genes are saturated for insertions. Thus most hits in these genes are redundant and the chance to hit a gene, which was not previously hit, declines (Fig. 38, purple line). At the same time the saturation in coldspot genes (Fig. 38, green line) increases much slower. Therefore saturation (Fig. 38, blue line) of the genome is much less efficient than as expected when assuming ideal random behavior (Fig. 38, black line). Using this model it is possible to predict the saturation of the genome at a given number of hits. Doing so, a 34% coverage of the *Drosophila* genome would be expected, when

producing 10000 hits in genes using P-elements. If the insertion would be ideal, without any bias, 52% coverage would be expected. Using another definition of hotspot (50 kb interval containing 30 or more inserts) 26 *piggyBac* hotspots were identified, while 23 hotspots were found with XP-elements (subtype of P-elements) with less than half the number of insertions (Thibault et al., 2004). Thus, it can be concluded that the combination of screening with P-elements and *piggyBac* (and possibly with yet another type of transposable element) is the most reasonable approach to saturate a fly genome for any kind of insertional mutagenesis available today. Thibault and co-workers further report that with the same number of transposons *piggyBac* tagged 67% more genes than XP. Based on this data, it seems safe to assume that a higher saturation rate (than the 34% predicted for P-elements) is to be expected when producing 10000 hits with *piggyBac*.

The fact that insertions in introns are selected might result in a further bias of the screen. Morin and co-workers report that 50% of all protein trap events are found in genes with introns larger than 2,5 kb, whereas few insertions were found in introns shorter than 200 bp (Morin et al., 2001). The typical intron size is smaller than 200 bp in *Drosophila* (Deutsch and Long, 1999). While saturation might be reached quickly for genes containing large introns, genes containing only small introns are much less likely to be hit. This could cause a saturation problem similar to that described for hot, warm and cold spot genes. Therefore a model was used to address, to what degree the efficacy of the screen is lowered by the intron size distribution as described in *Drosophila*. A *Drosophila* gene contains on average 2,5 introns with a total length of 606 bp (Deutsch and Long, 1999). To simplify the calculation it was assumed that 80% of all genes have 3 introns of a size of 80 bp each, that 10% of all genes consist of two introns each 2000 bp and that 10% of all genes have no intron at all. This leads to an average number of 2,6 introns per gene with a total intron length of 592 bp (which represents the real situation quite well (Deutsch and Long, 1999)). What are the chances for those genes to be tagged with GFP? The 180 Mb *Drosophila* genome contains 13500 predicted genes. In the model the 1350 large intron genes have a total intron length of 5,4 Mb, while the 10800 small intron genes have a total intron length of 2,6 Mb. Assuming ideal jumping, 3% of all jumps should insert in a large intron gene, while 1,45% should insert in an small intron gene. Assuming that all

insertions, which are in the right frame and right orientation (1:6) give rise to a GFP event, 0,5% (hits in large introns) and 0,24% (hits in small introns) should give rise to a productive GFP insert. Taking into account the average transposition frequency of 14% (Morin et al., 2001) it would be expected that 0,07% (hits in large introns) plus 0,0336% (hits in large introns) of all screened embryos are GFP positive. Thus about 1 positive embryo would be expected among 1000 screened embryos. This theoretical calculation fits the data reported by Morin and co-workers, who found about 1 in 1600 embryos to be positive (Morin et al., 2001). P-elements are known to have a bias towards inserting in the 5' UTR of genes (Thibault et al., 2004). These insertions can not give rise to GFP-fusions. This fact likely contributes to the small discrepancy between real (1:1600) and theoretical hits (1:1000). What implications do these calculations have for a genome-wide screen? To produce 10000 lines 10 million embryos need to be screened at a transposition frequency of 16%. Calculating a sort time of 16,5 h per week, and a sort rate of 30000 animals per hour the screen would take only 20 weeks. At the same time much higher transposition frequencies of 60%-80% were reported for *piggyBac* (Thibault et al., 2004). What coverage of genes can be expected?
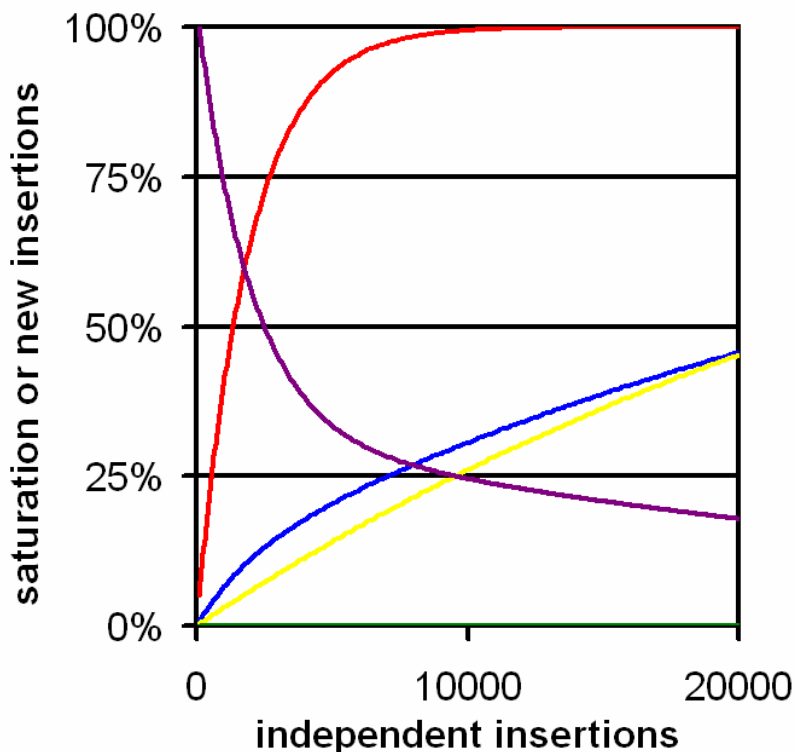
Fig. 39 Saturation of the genome in an exon-trap screen. The much higher chance to hit "large intron" genes (red line) leads to a much faster saturation of these genes compared to genes with small introns (yellow line). The chance of hitting a new gene is shown in purple.

Assuming 80% independent hits (84% independent hits were present in the larval screen chapter 4.6.1) and ideal uniform transposition probability over the *Drosophila* genome these 8000 insertions should lead to the GFP-tagging of 98% of all "large-intron" genes (Fig. 39, red line) and of 21% of all "small-intron" genes (Fig. 39, yellow line). With no hits in genes without introns this leads to 27% coverage (Fig. 39, blue line) of the *Drosophila* genome (3645 genes tagged). Already at this stage problems with redundancy are to be expected. Line number 10000 will only have a 22% chance of GFP-tagging a gene (Fig. 39, purple line), which was not previously hit (80% for not being an independent event and a 27% chance to hit a new gene, in the case of an independent hit). Unfortunately, there is not much data available to test that model. Even assuming ideal, random screening the chances of hitting small introns are low. In reality this chance might be even lower than predicted. The chance of successful splicing might be higher in a large intron. In contrast the insertion of several kb in an intron of an original size of 80 bp might be problematic. This concern is also supported by the limited data available. In the 36 lines characterized by Morin and co-workers in respect to intron size distribution 11 inserts are in introns larger than 4 kb, 20 are in the category 4-1 kb, 3 in the category 1 kb-200 bp and 2 in the category <200 bp. This shows that the tendency towards inserting in large introns is higher than theoretically expected (Morin et al., 2001). The numbers are still too small to give an accurate estimate for *piggyBac*. Of the 11 independent NMJ lines 6 inserts were in exons >4 kb, 4 in the category 4-1 kb and 1 in the category 1 kb-200 bp. This data gives first indications that also using *piggyBac* the tendency towards inserting in large introns is higher than theoretically expected. It is not clear to what degree the efficacy of the screen will be lowered by this bias. The same is true for the problem of hotspots. Although there are reports that *piggyBac* produces substantially less hotspots than P-elements, some loss attributable to hotspots needs to be included in the calculation. Therefore it is realistic to expect to reach 15-20% coverage of the genome and not 27%. 17% coverage corresponds to 2300 different genes GFP-tagged. This is to be achieved within the next two years. Among these 2300 genes 90 genes are expected to localize at the neuromuscular junction, which is a significant step forward in identifying the set of proteins responsible for setting up and regulating that model synapse.

It should be noted that a lot of insertions which were treated as redundant in this model and therefore do not turn up in the final figures, might nonetheless be interesting. After inserting GFP in one position, a protein might still be completely functional. Some insertions in the same protein might lead to a partial or complete loss of function, others might even lead to dominant negative effects. The insertion site might further determine whether all or only some of the splice variants of a protein are affected. On the other hand it is obvious that it will be difficult to ever achieve a saturation of 50% with this kind of screen. Therefore, it is suggested to change the screening procedure, if the screen is to be continued after reaching 10000 lines.

5.8 Future strategies for the systematic identification of GFP-tagged synaptic proteins on a genome-wide scale

As discussed in chapter 5.7 a substantial proportion of genes with no or only a few small introns is unlikely to be identified in an exon-trap screen. One tempting way of identifing these genes is to target exons instead of introns. While the concept of an exon-fusion screen in contrast to an exon-trap screen was never tested in *Drosophila*, a similar approach has been successfully used *in vitro* to GFP-tag different molecules in a random fashion (Sheridan et al., 2002).
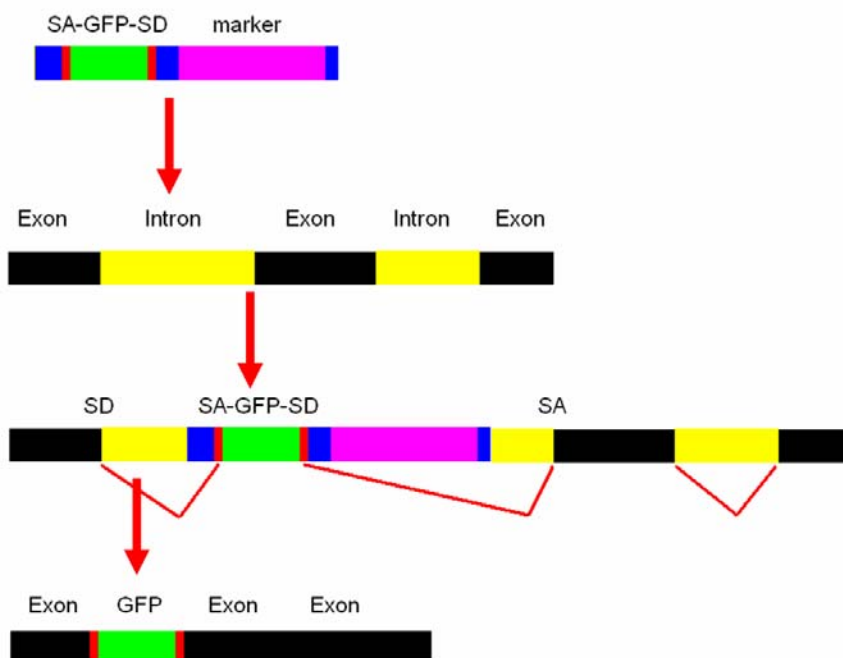
Fig. 40 Schematic drawing of an exon-trap screen. The transgenic vector gets integrated into an intron subsequent splicing leads to the production of a fusion protein

As already briefly discussed in chapter 2.4 residual vector (Fig. 40, blue box, central panel) and marker sequences (Fig. 40, pink box, central panel) need to be removed in an exon-trap as well as in an exon-fusion screen. The spliced mRNA (Fig. 40, lower panel) should ideally encode only protein (Fig. 40, black box) and GFP (Fig. 40, green box) sequences. This is accomplished by splicing out all unnecessary sequences 5' and 3' of the GFP cassette. In an exon-trap screen this is achieved as follows. The 5' end splicing occurs between the splice acceptor site (SA) 5' of GFP and the splice donor (SD) site of the upstream exon (of the protein in which the vector has integrated). At the same time the SD site 3' of GFP splices with the SA site of the downstream exon (Fig. 40, central panel). Thereby it is possible to remove all vector and marker sequences. This is not possible in an exon-fusion screen. Here the ends of the transposable element will be part of the final protein. In a *in vitro* system, for example, a Tn5 transposon was used to insert GFP in a glutamate receptor (see chapter 4.1.6). The ends of the transposon form short (7 AA) linkers between the GFP and the protein of interest (Sheridan et al., 2002). While in this case the marker (kanamycin resistance) was removed by subsequent digestion of the DNA, this is not possible in an *in vivo* exon-fusion screen. *In vivo* it is possible to screen without any marker, since positive events can be scored based on GFP expression. Alternatively the marker can be removed *in vivo* by flanking it with SD and SA sites (Fig. 41, upper panel). The GFP fusion protein is then produced as follows: All of the vector sequence 5' of the GFP (terminal ends of transposable element) serves a linker (Fig. 41, lower panel, blue box 5' of GFP) between the tagged protein (Fig. 41, lower panel, black boxes) and the GFP (Fig. 41, lower panel, green box). The marker (Fig. 41, central panel, pink box) itself gets spliced out by the flanking SD and SA sites (Fig. 41, red boxes). Only some basepairs 3' of the SA site (Fig. 41, lower panel, blue box) remain in the final protein as linker between the GFP and the protein.
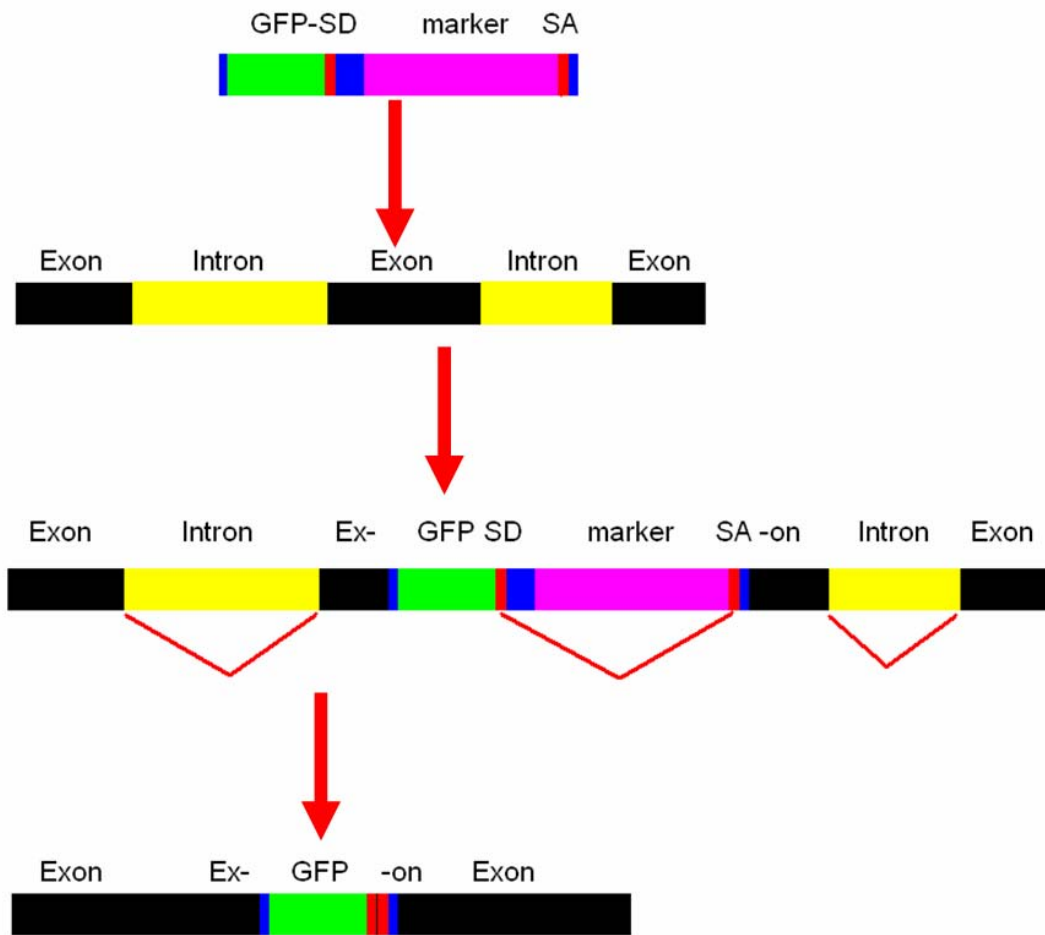
Fig. 41 Schematic drawing of an exon-fusion screen. The transgenic vector is integrated into an exon and subsequent splicing leads to the production of a fusion protein

For such a strategy it would be the most advantageous to use a vector which is well characterized and has small terminal repeats, which do not harbor stop codons. The minos (Franz and Savakis, 1991) transposable element, as well as *piggyBac* and P-elements might be suitable for that purpose. P-elements and minos might be particularly useful, since they are known to have very small minimal sequences required for transposition (Spradling and Rubin, 1982; Mullins et al., 1989) and (Graeme Davis, personal communication). Changing the strategy in that way might substantially facilitate reaching a high degree of saturation. Additionally to these forward genetic approaches also reverse genetics of a preselected class of genes might help to identify and GFP-tag synaptic proteins. Biochemical PSD characterization and cDNA isolation (Langnaese et al., 1996; Yoshimura et al., 2004) showed that about 500 proteins are enriched in synaptic

spines. After identifying the corresponding *Drosophila* homologs 100-200 candidates could be GFP-tagged. Yeast-two-hybrid screens against proteins known to have synaptic localization might provide further candidates. The corresponding constructs can be produced via long-range PCR on cDNA clones. The PCR products can be directly inserted in a precut pUAST transgenic vector, already containing an N- or C-terminal GFP. The localization of these proteins could then be scored *in vivo*. Transgenic injections are very efficient in *Drosophila*. About 1000-1500 embryos can be injected per day. On average one transgenic animal is isolated per 30 injected embryos. Injecting 100 embryos for each candidate should allow the injection of 10 candidates per day. The combination of exon-trap screening, exon-fusion screening and direct GFP-tagging of candidates might lead to the identification of the most proteins present at the *Drosophila* neuromuscular junction within the next few years.

To facilitate the genome-wide exon-trap screen it was decided to perform this screen in a big consortium of laboratories. In the larval screen only 13 out of 322 GFP positive lines were of immediate interest for the two participating laboratories of Dr. Stephan Sigrist and Dr. Anne Ephrussi. Within the "Deutsche Forschungsgemeinschaft Schwerpunkt Polarity" a consortium of laboratories joined together, which are interested in different tissues and developmental processes in the embryo, the larva or the adult. These laboratories include the laboratories of Dr. Suzanne Eaton, Dr. Anne Ephrussi, Dr. Christian Dahmann, Dr. Marcos Gonzales-Gaitan, Dr. Christian Klämbt, Dr. Eli Knust, Dr. Arno Müller, Dr. Andreas Wodarz and Dr. Stephan Sigrist. The aim of this cooperation is to produce 10000 GFP-positive lines within the next two years.

6. Appendix

6.1 Table of abbreviations

3-D	3-dimensional
AA	amino acid
AZ	active zone
AMP	adenosine 5'-monophosphate
AMPA	alpha-amino-3-hydroxy-5-methyl-4-isoxazolepropionic acid, AMPA receptors are a subclass of glutamate receptors
AOBS	acousto-optical beam splitter
bp	base pair
Ca^{2+}	$calcium^{2+}$-ion
CamKII	calmodulin-dependent protein kinase II
cAMP	cyclic AMP
Cast	cytomatrix at the active zone associated structural protein (insect homologs)
CAST	cytomatrix at the active zone associated structural protein (vertebrate protein)
CAZ	cytoskeletal matrix assembled at the active zone
CD8	transmembrane domain of the lymphocyte transmembrane protein CD8 alpha
cDNA	complementary deoxyribonucleic acid
CNS	central nervous system
DCast	cytomatrix at the active zone associated structural protein (*Drosophila* homolog)
DNA	deoxyribonucleic dcid
DGluRIIA	*Drosophila* glutamate receptor subunit IIA

DGluRIIA^{GFP}	GFP tagged variant of the *Drosophila* glutamate receptor subunit IIA
DGluRIIB	*Drosophila* glutamate receptor subunit IIB
DGluRIIC	*Drosophila* glutamate receptor subunit IIC
DGluRIIC^{GFP}	GFP tagged variant of the *Drosophila* glutamate receptor subunit IIC
ds-red	dsred; red fluorescent protein that was originally isolated from the sea anemone-relative, *Discosoma sp.*
DPak	*Drosophila* p21-activated kinase pak
eag	ether a go-go
EM	depending on context: electron microscopic or electron microscopy
ERC	synonym for CAST
EXT	extinction coefficient, parameter detected during automated embryo sorting
FACS	fluorescence-activated cell sorting
FRAP	fluorescence recovery after photo-bleaching
FLU1	green fluorescence, parameter detected during automated embryo sorting
FLU2	red fluorescence/ autofluorescence control, parameter detected during automated embryo sorting
GFP	green fluorescent protein; if not otherwise stated GFP refers to the commercial, human codon optimized, version EGFP (Clontech, Palo Alto, USA)
GFP^{S65T}	green fluorescent protein with the amino acid substitution S65T. same spectral properties like the commercial EGFP
G-Protein	guaninnucleotide-binding protein
GST	S-transferase (used as affinity tag for biochemistry)
GRIP	glutamate receptor interacting protein

IWA	last three amino acids of CAST (isoleucine, tryptophan, alanine). These amino acids are important for the interaction of RIM and CAST
kb	kilo base pair
LTP	long-term potentiation
MAB	monoclonal antibody
mRFP1	monomeric red fluorescent protein
nc82	identifier of a monoclonal antibody, which labels active zones in *Drosophila*
NMJ	neuromuscular junction
NMDA	N-methyl-D-aspartate, NMDA receptors are a subclass of glutamate receptors
non-NMDA	used in this thesis for AMPA / Kainate type glutamate receptors
p1	piggyL SD-GFP-SA 3xP3 ds-red, vector used for exon-trap screen, map see Figure 10
p2	piggyL SD-GFP-SA 3xP3 ds-red ap, vector used for exon-trap screen, map see Figure 10
p3	piggyM P white SA-GFP-SD P, vector used for exon-trap screen, map see Figure 10
p4	piggyM P white P SA-GFP-SD P, vector used for exon-trap screen, map see Figure 10
p5	piggyL P white P SA-GFP-SD, vector used for exon-trap screen, map see Figure 10
PCR	polymerase chain reaction
P-end	the terminal region of the transposable element P, which is important for transposition
PICK1	protein interacting with protein kinase C
PDZ	PSD-95, *Drosophila* discs large protein, and Zona occludens protein 1 (domain)

PMT	photo-multiplier (tube)
PSD	postsynaptic density
PSD-95	PSD localizing protein 95
PTV	Piccolo-Bassoon transport vesicle
RIM	Rab-3 interacting molecule
RNA	ribonucleic acid
ROI	region of interest
RT PCR	reverse transcription polymerase chain reaction
SDS	sodium dodecylsulphate
Sh	Shaker
SSR	subsynaptic reticulum
SV	synaptic vesicle
T-bar	dense body, electron dense T-shaped structure at the presysnaptic active zone membrane in *Drosophila*
TOF	time of flight, parameter detected during automated embryo Sorting
UV	ultra-violet

6.2 References

Aberle H, Haghighi AP, Fetter RD, McCabe BD, Magalhaes TR, Goodman CS (2002) wishful thinking encodes a BMP type II receptor that regulates synaptic growth in Drosophila. Neuron 33:545-558.

Ahmari SE, Buchanan J, Smith SJ (2000) Assembly of presynaptic active zones from cytoplasmic transport packets. Nat Neurosci 3:445-451.

Akaaboune M, Grady RM, Turney S, Sanes JR, Lichtman JW (2002) Neurotransmitter receptor dynamics studied in vivo by reversible photo-unbinding of fluorescent ligands. Neuron 34:865-876.

Allen ML, Handler AM, Berkebile DR, Skoda SR (2004) piggyBac transformation of the New World screwworm, Cochliomyia hominivorax, produces multiple distinct mutant strains. Med Vet Entomol 18:1-9.

Altrock WD, tom Dieck S, Sokolov M, Meyer AC, Sigler A, Brakebusch C, Fassler R, Richter K, Boeckers TM, Potschka H, Brandt C, Loscher W, Grimberg D, Dresbach T, Hempelmann A, Hassan H, Balschun D, Frey JU, Brandstatter JH, Garner CC, Rosenmund C, Gundelfinger ED (2003) Functional inactivation of a fraction of excitatory synapses in mice deficient for the active zone protein bassoon. Neuron 37:787-800.

Ang LH, Kim J, Stepensky V, Hing H (2003) Dock and Pak regulate olfactory axon pathfinding in Drosophila. Development 130:1307-1316.

Ashby MC, De La Rue SA, Ralph GS, Uney J, Collingridge GL, Henley JM (2004) Removal of AMPA receptors (AMPARs) from synapses is preceded by transient endocytosis of extrasynaptic AMPARs. J Neurosci 24:5172-5176.

Atwood HL, Govind CK, Wu CF (1993) Differential ultrastructure of synaptic terminals on ventral longitudinal abdominal muscles in Drosophila larvae. J Neurobiol 24:1008-1024.

Augustin I, Rosenmund C, Sudhof TC, Brose N (1999) Munc13-1 is essential for fusion competence of glutamatergic synaptic vesicles. Nature 400:457-461.

Bailey CH, Kandel ER (1993) Structural changes accompanying memory storage. Annu Rev Physiol 55:397-426.

Beames B, Summers MD (1988) Comparisons of host cell DNA insertions and altered transcription at the site of insertions in few polyhedra bacilovirus mutants. Virology 162:206-220.

Berghammer AJ, Klingler M, Wimmer EA (1999) A universal marker for transgenic insects. Nature 402:370-371.

Betz A, Thakur P, Junge HJ, Ashery U, Rhee JS, Scheuss V, Rosenmund C, Rettig J, Brose N (2001) Functional interaction of the active zone proteins Munc13-1 and RIM1 in synaptic vesicle priming. Neuron 30:183-196.

Bliss TV, Lomo T (1973) Long-lasting potentiation of synaptic transmission in the dentate area of the anaesthetized rabbit following stimulation of the perforant path. J Physiol 232:331-356.

Bliss TV, Collingridge GL (1993) A synaptic model of memory: long-term potentiation in the hippocampus. Nature 361:31-39.

Bliss TV, Collingridge GL, Morris RG (2003) Introduction. Long-term potentiation and structure of the issue. Philos Trans R Soc Lond B Biol Sci 358:607-611.

Borgdorff AJ, Choquet D (2002) Regulation of AMPA receptor lateral movements. Nature 417:649-653.

Brand AH, Perrimon N (1993) Targeted gene expression as a means of altering cell fates and generating dominant phenotypes. Development 118:401-415.

Bresler T, Ramati Y, Zamorano PL, Zhai R, Garner CC, Ziv NE (2001) The dynamics of SAP90/PSD-95 recruitment to new synaptic junctions. Mol Cell Neurosci 18:149-167.

Bresler T, Shapira M, Boeckers T, Dresbach T, Futter M, Garner CC, Rosenblum K, Gundelfinger ED, Ziv NE (2004) Postsynaptic density assembly is fundamentally different from presynaptic active zone assembly. J Neurosci 24:1507-1520.

Broadie K, Bate M (1993) Activity-dependent development of the neuromuscular synapse during Drosophila embryogenesis. Neuron 11:607-619.

Broadie KS (1995) Genetic dissection of the molecular mechanisms of transmitter vesicle release during synaptic transmission. J Physiol Paris 89:59-70.

Broadie KS (1996) Regulation of the synaptic vesicle cycle in Drosophila. Biochem Soc Trans 24:639-645.

Broadie KS, Bate M (1993) Development of the embryonic neuromuscular synapse of Drosophila melanogaster. J Neurosci 13:144-166.

Budnik V, Koh YH, Guan B, Hartmann B, Hough C, Woods D, Gorczyca M (1996) Regulation of synapse structure and function by the Drosophila tumor suppressor gene dlg. Neuron 17:627-640.

Cajal S. Ry (1893) Neue Darstellung vom histologischen Bau des Zentralnervensystem. Arch Anat Entwick:319-428.

Cajal S. Ry (1911) Histologie du systeme nerveux de l'homme et des vertebres. Paris: A. Moloine.

Campbell RE, Tour O, Palmer AE, Steinbach PA, Baird GS, Zacharias DA, Tsien RY (2002) A monomeric red fluorescent protein. Proc Natl Acad Sci U S A 99:7877-7882.

Carlin RK, Siekevitz P (1983) Plasticity in the central nervous system: do synapses divide? Proc Natl Acad Sci U S A 80:3517-3521.

Carroll RC, Beattie EC, Xia H, Luscher C, Altschuler Y, Nicoll RA, Malenka RC, von Zastrow M (1999) Dynamin-dependent endocytosis of ionotropic glutamate receptors. Proc Natl Acad Sci U S A 96:14112-14117.

Cary LC, Goebel M, Corsaro BG, Wang HG, Rosen E, Fraser MJ (1989) Transposon mutagenesis of baculoviruses: analysis of Trichoplusia ni transposon IFP2 insertions within the FP-locus of nuclear polyhedrosis viruses. Virology 172:156-169.

Castiglioni MC (1951) [Distribution of pigments in the eye of alleles of white and their compounds in Drosophila melanogaster.]. Sci Genet 4:57-60.

Cooper RL, Marin L, Atwood HL (1995) Synaptic differentiation of a single motor neuron: conjoint definition of transmitter release, presynaptic calcium signals, and ultrastructure. J Neurosci 15:4209-4222.

Cooper RL, Harrington CC, Marin L, Atwood HL (1996) Quantal release at visualized terminals of a crayfish motor axon: intraterminal and regional differences. J Comp Neurol 375:583-600.

Davis GW, Goodman CS (1998) Synapse-specific control of synaptic efficacy at the terminals of a single neuron. Nature 392:82-86.

Davis GW, Schuster CM, Goodman CS (1996) Genetic dissection of structural and functional components of synaptic plasticity. III. CREB is necessary for presynaptic functional plasticity. Neuron 17:669-679.

Denk W, Strickler JH, Webb WW (1990) Two-photon laser scanning fluorescence microscopy. Science 248:73-76.

Desmond NL, Levy WB (1986) Changes in the postsynaptic density with long-term potentiation in the dentate gyrus. J Comp Neurol 253:476-482.

Desmond NL, Levy WB (1988) Synaptic interface surface area increases with long-term potentiation in the hippocampal dentate gyrus. Brain Res 453:308-314.

Deutsch M, Long M (1999) Intron-exon structures of eukaryotic model organisms. Nucleic Acids Res 27:3219-3228.

DiAntonio A, Petersen SA, Heckmann M, Goodman CS (1999) Glutamate receptor expression regulates quantal size and quantal content at the Drosophila neuromuscular junction. J Neurosci 19:3023-3032.

Dick O, tom Dieck S, Altrock WD, Ammermuller J, Weiler R, Garner CC, Gundelfinger ED, Brandstatter JH (2003) The presynaptic active zone protein bassoon is essential for photoreceptor ribbon synapse formation in the retina. Neuron 37:775-786.

Dodt H, Eder M, Frick A, Zieglgänsberger W (1999) Precisely localized LTD in the neocortex revealed by infrared-guided laser stimulation. Science 286:110-113.

Dong H, O'Brien RJ, Fung ET, Lanahan AA, Worley PF, Huganir RL (1997) GRIP: a synaptic PDZ domain-containing protein that interacts with AMPA receptors. Nature 386:279-284.

Dudai Y, Zvi S (1984) Adenylate cyclase in the Drosophila memory mutant rutabaga displays an altered Ca2+ sensitivity. Neurosci Lett 47:119-124.

Dudai Y, Zvi S (1985) Multiple defects in the activity of adenylate cyclase from the Drosophila memory mutant rutabaga. J Neurochem 45:355-364.

Dudai Y, Jan YN, Byers D, Quinn WG, Benzer S (1976) dunce, a mutant of Drosophila deficient in learning. Proc Natl Acad Sci U S A 73:1684-1688.

Economos AC, Lints FA (1984) Growth rate and life span in Drosophila. I. Methods and mechanisms of variation of growth rate. Mech Ageing Dev 27:1-13.

Elick TA, Bauser CA, Fraser MJ (1996) Excision of the piggyBac transposable element in vitro is a precise event that is enhanced by the expression of its encoded transposase. Genetica 98:33-41.

Engert F, Bonhoeffer T (1997) Synapse specificity of long-term potentiation breaks down at short distances. Nature 388:279-284.

Engert F, Bonhoeffer T (1999) Dendritic spine changes associated with hippocampal long-term synaptic plasticity. Nature 399:66-70.

Fenster SD, Chung WJ, Zhai R, Cases-Langhoff C, Voss B, Garner AM, Kaempf U, Kindler S, Gundelfinger ED, Garner CC (2000) Piccolo, a presynaptic zinc finger protein structurally related to bassoon. Neuron 25:203-214.

Fiala JC, Allwardt B, Harris KM (2002) Dendritic spines do not split during hippocampal LTP or maturation. Nat Neurosci 5:297-298.

Fifkova E, Van Harreveld A (1977) Long-lasting morphological changes in dendritic spines of dentate granular cells following stimulation of the entorhinal area. J Neurocytol 6:211-230.

Franco B, Bogdanik L, Bobinnec Y, Debec A, Bockaert J, Parmentier ML, Grau Y (2004) Shaggy, the homolog of glycogen synthase kinase 3, controls neuromuscular junction growth in Drosophila. J Neurosci 24:6573-6577.

Franz G, Savakis C (1991) Minos, a new transposable element from Drosophila hydei, is a member of the Tc1-like family of transposons. Nucleic Acids Res 19:6646.

Fraser MJ, Cary L, Boonvisudhi K, Wang HG (1995) Assay for movement of Lepidopteran transposon IFP2 in insect cells using a baculovirus genome as a target DNA. Virology 211:397-407.

Fraser MJ, Ciszczon T, Elick T, Bauser C (1996) Precise excision of TTAA-specific lepidopteran transposons piggyBac (IFP2) and tagalong (TFP3) from the baculovirus genome in cell lines from two species of Lepidoptera. Insect Mol Biol 5:141-151.

Friedman HV, Bresler T, Garner CC, Ziv NE (2000) Assembly of new individual excitatory synapses: time course and temporal order of synaptic molecule recruitment. Neuron 27:57-69.

Furlong EE, Profitt D, Scott MP (2001) Automated sorting of live transgenic embryos. Nat Biotechnol 19:153-156.

Garner CC, Kindler S, Gundelfinger ED (2000) Molecular determinants of presynaptic active zones. Curr Opin Neurobiol 10:321-327.

Goda Y, Davis GW (2003) Mechanisms of synapse assembly and disassembly. Neuron 40:243-264.

Gonzalez-Estevez C, Momose T, Gehring WJ, Salo E (2003) Transgenic planarian lines obtained by electroporation using transposon-derived vectors and an eye-specific GFP marker. Proc Natl Acad Sci U S A 100:14046-14051.

Goodman CS, Bastiani MJ, Doe CQ, Dulac S (1986) Growth cone guidance and cell recognition in insect embryos. Dev Biol (N Y 1985) 3:283-300.

Gramates LS, Budnik V (1999) Assembly and maturation of the Drosophila larval neuromuscular junction. Int Rev Neurobiol 43:93-117.

Grosshans DR, Clayton DA, Coultrap SJ, Browning MD (2002) LTP leads to rapid surface expression of NMDA but not AMPA receptors in adult rat CA1. Nat Neurosci 5:27-33.

Grossman GL, Rafferty CS, Clayton JR, Stevens TK, Mukabayire O, Benedict MQ (2001) Germline transformation of the malaria vector, Anopheles gambiae, with the piggyBac transposable element. Insect Mol Biol 10:597-604.

Grutzendler J, Kasthuri N, Gan WB (2002) Long-term dendritic spine stability in the adult cortex. Nature 420:812-816.

Guillaud L, Setou M, Hirokawa N (2003) KIF17 dynamics and regulation of NR2B trafficking in hippocampal neurons. J Neurosci 23:131-140.

Gundelfinger ED, tom Dieck S (2000) Molecular organization of excitatory chemical synapses in the mammalian brain. Naturwissenschaften 87:513-523.

Gundelfinger ED, Kessels MM, Qualmann B (2003) Temporal and spatial coordination of exocytosis and endocytosis. Nat Rev Mol Cell Biol 4:127-139.

Gustafsson B, Wigstrom H (1990) Long-term potentiation in the hippocampal CA1 region: its induction and early temporal development. Prog Brain Res 83:223-232.

Handler AM, Harrell RA, 2nd (1999) Germline transformation of Drosophila melanogaster with the piggyBac transposon vector. Insect Mol Biol 8:449-457.

Handler AM, McCombs SD (2000) The piggyBac transposon mediates germ-line transformation in the Oriental fruit fly and closely related elements exist in its genome. Insect Mol Biol 9:605-612.

Handler AM, Harrell RA, 2nd (2001) Transformation of the Caribbean fruit fly, Anastrepha suspensa, with a piggyBac vector marked with polyubiquitin-regulated GFP. Insect Biochem Mol Biol 31:199-205.

Handler AM, McCombs SD, Fraser MJ, Saul SH (1998) The lepidopteran transposon vector, piggyBac, mediates germ-line transformation in the Mediterranean fruit fly. Proc Natl Acad Sci U S A 95:7520-7525.

Harden N, Lee J, Loh HY, Ong YM, Tan I, Leung T, Manser E, Lim L (1996) A Drosophila homolog of the Rac- and Cdc42-activated serine/threonine kinase PAK is a potential focal adhesion and focal complex protein that colocalizes with dynamic actin structures. Mol Cell Biol 16:1896-1908.

Hebb D (1949) The Organization of Behaviour. New York.

Heckmann M, Dudel J (1997) Desensitization and resensitization kinetics of glutamate receptor channels from Drosophila larval muscle. Biophys J 72:2160-2169.

Hediger M, Niessen M, Wimmer EA, Dubendorfer A, Bopp D (2001) Genetic transformation of the housefly Musca domestica with the lepidopteran derived transposon piggyBac. Insect Mol Biol 10:113-119.

Heimbeck G, Bugnon V, Gendre N, Haberlin C, Stocker RF (1999) Smell and taste perception in Drosophila melanogaster larva: toxin expression studies in chemosensory neurons. J Neurosci 19:6599-6609.

Heinrich JC, Li X, Henry RA, Haack N, Stringfellow L, Heath AC, Scott MJ (2002) Germ-line transformation of the Australian sheep blowfly Lucilia cuprina. Insect Mol Biol 11:1-10.

Helmchen F, Denk W (2002) New developments in multiphoton microscopy. Curr Opin Neurobiol 12:593-601.

Helmchen F, Svoboda K, Denk W, Tank DW (1999) In vivo dendritic calcium dynamics in deep-layer cortical pyramidal neurons. Nat Neurosci 2:989-996.

Helmchen F, Fee MS, Tank DW, Denk W (2001) A miniature head-mounted two-photon microscope. high-resolution brain imaging in freely moving animals. Neuron 31:903-912.

Hering H, Sheng M (2001) Dendritic spines: structure, dynamics and regulation. Nat Rev Neurosci 2:880-888.

Hollmann M, Heinemann S (1994) Cloned glutamate receptors. Annu Rev Neurosci 17:31-108.

Holt RA, Subramanian GM, Halpern A, Sutton GG, Charlab R, Nusskern DR, Wincker P, Clark AG, Ribeiro JM, Wides R, Salzberg SL, Loftus B, Yandell M, Majoros WH, Rusch DB, Lai Z, Kraft CL, Abril JF, Anthouard V, Arensburger P, Atkinson PW, Baden H, de Berardinis V, Baldwin D, Benes V, Biedler J, Blass C, Bolanos R, Boscus D, Barnstead M, Cai S, Center A, Chaturverdi K, Christophides GK, Chrystal MA, Clamp M, Cravchik A, Curwen V, Dana A, Delcher A, Dew I, Evans CA, Flanigan M, Grundschober-Freimoser A, Friedli L, Gu Z, Guan P, Guigo R, Hillenmeyer ME, Hladun SL, Hogan JR, Hong YS, Hoover J, Jaillon O, Ke Z, Kodira C, Kokoza E, Koutsos A, Letunic I, Levitsky A, Liang Y, Lin JJ, Lobo NF, Lopez JR, Malek JA, McIntosh TC, Meister S, Miller J, Mobarry C, Mongin E, Murphy SD, O'Brochta DA, Pfannkoch C, Qi R, Regier MA, Remington K, Shao H, Sharakhova MV, Sitter CD, Shetty J, Smith TJ, Strong R, Sun J, Thomasova D, Ton LQ, Topalis P, Tu Z, Unger MF, Walenz B, Wang A, Wang J, Wang M, Wang X, Woodford KJ, Wortman JR, Wu M, Yao A, Zdobnov EM, Zhang H, Zhao Q, et al. (2002) The genome sequence of the malaria mosquito Anopheles gambiae. Science 298:129-149.

Horn C, Wimmer EA (2000) A versatile vector set for animal transgenesis. Dev Genes Evol 210:630-637.

Horn C, Jaunich B, Wimmer EA (2000) Highly sensitive, fluorescent transformation marker for Drosophila transgenesis. Dev Genes Evol 210:623-629.

Horn C, Offen N, Nystedt S, Hacker U, Wimmer EA (2003) piggyBac-based insertional mutagenesis and enhancer detection as a tool for functional insect genomics. Genetics 163:647-661.

Jan LY, Jan YN (1976) Properties of the larval neuromuscular junction in Drosophila melanogaster. J Physiol 262:189-214.

Jontes JD, Smith SJ (2000) Filopodia, spines, and the generation of synaptic diversity. Neuron 27:11-14.

Ju W, Morishita W, Tsui J, Gaietta G, Deerinck TJ, Adams SR, Garner CC, Tsien RY, Ellisman MH, Malenka RC (2004) Activity-dependent regulation of dendritic synthesis and trafficking of AMPA receptors. Nat Neurosci 7:244-253.

Kandel ER, O'Dell TJ (1992) Are adult learning mechanisms also used for development? Science 258:243-245.

Kauvar LM (1982) Defective cyclic adenosine 3':5'-monophosphate phosphodiesterase in the Drosophila memory mutant dunce. J Neurosci 2:1347-1358.

Kawasaki F, Zou B, Xu X, Ordway RW (2004) Active zone localization of presynaptic calcium channels encoded by the cacophony locus of Drosophila. J Neurosci 24:282-285.

Kennedy MB (2000) Signal-processing machines at the postsynaptic density. Science 290:750-754.

Kim JH, Udo H, Li HL, Youn TY, Chen M, Kandel ER, Bailey CH (2003) Presynaptic activation of silent synapses and growth of new synapses contribute to intermediate and long-term facilitation in Aplysia. Neuron 40:151-165.

Kirov SA, Sorra KE, Harris KM (1999) Slices have more synapses than perfusion-fixed hippocampus from both young and mature rats. J Neurosci 19:2876-2886.

Kirov SA, Petrak LJ, Fiala JC, Harris KM (2004) Dendritic spines disappear with chilling but proliferate excessively upon rewarming of mature hippocampus. Neuroscience 127:69-80.

Kuromi H, Kidokoro Y (2002) Selective replenishment of two vesicle pools depends on the source of $Ca2+$ at the Drosophila synapse. Neuron 35:333-343.

Langnaese K, Seidenbecher C, Wex H, Seidel B, Hartung K, Appeltauer U, Garner A, Voss B, Mueller B, Garner CC, Gundelfinger ED (1996) Protein components of a rat brain synaptic junctional protein preparation. Brain Res Mol Brain Res 42:118-122.

Linden DJ, Connor JA (1992) Long-term Depression of Glutamate Currents in Cultured Cerebellar Purkinje Neurons Does Not Require Nitric Oxide Signalling. Eur J Neurosci 4:10-15.

Littleton JT, Bellen HJ, Perin MS (1993) Expression of synaptotagmin in Drosophila reveals transport and localization of synaptic vesicles to the synapse. Development 118:1077-1088.

Liu G, Choi S, Tsien RW (1999) Variability of neurotransmitter concentration and nonsaturation of postsynaptic AMPA receptors at synapses in hippocampal cultures and slices. Neuron 22:395-409.

Livingstone MS (1985) Genetic dissection of Drosophila adenylate cyclase. Proc Natl Acad Sci U S A 82:5992-5996.

Livingstone MS, Sziber PP, Quinn WG (1984) Loss of calcium/calmodulin responsiveness in adenylate cyclase of rutabaga, a Drosophila learning mutant. Cell 37:205-215.

Lobo NF, Hua-Van A, Li X, Nolen BM, Fraser MJ, Jr. (2002) Germ line transformation of the yellow fever mosquito, Aedes aegypti, mediated by transpositional insertion of a piggyBac vector. Insect Mol Biol 11:133-139.

Luo JH, Fu ZY, Losi G, Kim BG, Prybylowski K, Vissel B, Vicini S (2002) Functional expression of distinct NMDA channel subunits tagged with green fluorescent protein in hippocampal neurons in culture. Neuropharmacology 42:306-318.

Luo L, Zong H (2001) Single neuron labeling and genetic manipulation. Nat Neurosci 4 Suppl:1158-1159.

Luscher C, Nicoll RA, Malenka RC, Muller D (2000) Synaptic plasticity and dynamic modulation of the postsynaptic membrane. Nat Neurosci 3:545-550.

Luscher C, Xia H, Beattie EC, Carroll RC, von Zastrow M, Malenka RC, Nicoll RA (1999) Role of AMPA receptor cycling in synaptic transmission and plasticity. Neuron 24:649-658.

Lüscher C, Nicoll RA, Malenka RC, Müller D (2000) Synaptic plasticity and dynamic modulation of the postsynaptic membrane. Nat Neurosci 3:545-550.

Lynch G, Baudry M (1984) The biochemistry of memory: a new and specific hypothesis. Science 224:1057-1063.

Malenka Ma (2002) AMPA receptor trafficking and synaptic plasticity. Annual reviews neuroscience 25:103-126.

Malenka RC, Kauer JA, Zucker RS, Nicoll RA (1988) Postsynaptic calcium is sufficient for potentiation of hippocampal synaptic transmission. Science 242:81-84.

Maletic-Savatic M, Malinow R, Svoboda K (1999) Rapid dendritic morphogenesis in CA1 hippocampal dendrites induced by synaptic activity. Science 283:1923-1927.

Marcus EA, Emptage NJ, Marois R, Carew TJ (1994) A comparison of the mechanistic relationships between development and learning in Aplysia. Prog Brain Res 100:179-188.

Marrs GS, Green SH, Dailey ME (2001) Rapid formation and remodeling of postsynaptic densities in developing dendrites. Nat Neurosci 4:1006-1013.

Marrus SB, Portman SL, Allen MJ, Moffat KG, DiAntonio A (2004) Differential localization of glutamate receptor subunits at the Drosophila neuromuscular junction. J Neurosci 24:1406-1415.

Mathew D, Popescu A, Budnik V (2003) Drosophila amphiphysin functions during synaptic Fasciclin II membrane cycling. J Neurosci 23:10710-10716.

Matsuzaki M, Honkura N, Ellis-Davies GC, Kasai H (2004) Structural basis of long-term potentiation in single dendritic spines. Nature 429:761-766.

McGee AW, Bredt DS (2003) Assembly and plasticity of the glutamatergic postsynaptic specialization. Curr Opin Neurobiol 13:111-118.

Milner B (1966) Amnesia: Clinical, Psychological and Medicolegal Aspects. London: Butterworths.

Morin X, Daneman R, Zavortink M, Chia W (2001) A protein trap strategy to detect GFP-tagged proteins expressed from their endogenous loci in Drosophila. Proc Natl Acad Sci U S A 98:15050-15055.

Mullins MC, Rio DC, Rubin GM (1989) cis-acting DNA sequence requirements for P-element transposition. Genes Dev 3:729-738.

Nicoll RA, Malenka RC (1995) Contrasting properties of two forms of long-term potentiation in the hippocampus. Nature 377:115-118.

Niell CM, Smith SJ (2004) Live optical imaging of nervous system development. Annu Rev Physiol 66:771-798.

Nieto-Sampedro M, Hoff SF, Cotman CW (1982) Perforated postsynaptic densities: probable intermediates in synapse turnover. Proc Natl Acad Sci U S A 79:5718-5722.

Nolan T, Bower TM, Brown AE, Crisanti A, Catteruccia F (2002) piggyBac-mediated germline transformation of the malaria mosquito Anopheles stephensi using the red fluorescent protein dsRED as a selectable marker. J Biol Chem 277:8759-8762.

Nusser Z, Lujan R, Laube G, Roberts JD, Molnar E, Somogyi P (1998) Cell type and pathway dependence of synaptic AMPA receptor number and variability in the hippocampus. Neuron 21:545-559.

Oellig C, Happ B, Muller T, Doerfler W (1987) Overlapping sets of viral RNAs reflect the array of polypeptides in the EcoRI J and N fragments (map positions 81.2 to 85.0) of the Autographa californica nuclear polyhedrosis virus genome. J Virol 61:3048-3057.

Ohtsuka T, Takao-Rikitsu E, Inoue E, Inoue M, Takeuchi M, Matsubara K, Deguchi-Tawarada M, Satoh K, Morimoto K, Nakanishi H, Takai Y (2002) Cast: a novel protein of the cytomatrix at the active zone of synapses that forms a ternary complex with RIM1 and munc13-1. J Cell Biol 158:577-590.

Okabe S, Miwa A, Okado H (2001) Spine formation and correlated assembly of presynaptic and postsynaptic molecules. J Neurosci 21:6105-6114.

Okabe S, Urushido T, Konno D, Okado H, Sobue K (2001) Rapid redistribution of the postsynaptic density protein PSD-Zip45 (Homer 1c) and its differential regulation by NMDA receptors and calcium channels. J Neurosci 21:9561-9571.

Parnas D, Haghighi AP, Fetter RD, Kim SW, Goodman CS (2001) Regulation of postsynaptic structure and protein localization by the Rho-type guanine nucleotide exchange factor dPix. Neuron 32:415-424.

Passafaro M, Nakagawa T, Sala C, Sheng M (2003) Induction of dendritic spines by an extracellular domain of AMPA receptor subunit GluR2. Nature 424:677-681.

Patterson GH, Lippincott-Schwartz J (2002) A photoactivatable GFP for selective photolabeling of proteins and cells. Science 297:1873-1877.

Perera OP, Harrell IR, Handler AM (2002) Germ-line transformation of the South American malaria vector, Anopheles albimanus, with a piggyBac/EGFP transposon vector is routine and highly efficient. Insect Mol Biol 11:291-297.

Peters A, Kaiserman-Abramof IR (1969) The small pyramidal neuron of the rat cerebral cortex. The synapses upon dendritic spines. Z Zellforsch Mikrosk Anat 100:487-506.

Petersen SA, Fetter RD, Noordermeer JN, Goodman CS, DiAntonio A (1997) Genetic analysis of glutamate receptors in Drosophila reveals a retrograde signal regulating presynaptic transmitter release. Neuron 19:1237-1248.

Prange O, Murphy TH (2001) Modular transport of postsynaptic density-95 clusters and association with stable spine precursors during early development of cortical neurons. J Neurosci 21:9325-9333.

Purves D, Lichtman JW (1987) Synaptic sites on reinnervated nerve cells visualized at two different times in living mice. J Neurosci 7:1492-1497.

Reed BH, Wilk R, Schock F, Lipshitz HD (2004) Integrin-dependent apposition of Drosophila extraembryonic membranes promotes morphogenesis and prevents anoikis. Curr Biol 14:372-380.

Roos J, Kelly RB (2000) Preassembly and transport of nerve terminals: a new concept of axonal transport. Nat Neurosci 3:415-417.

Sabo SL, McAllister AK (2003) Mobility and cycling of synaptic protein-containing vesicles in axonal growth cone filopodia. Nat Neurosci 6:1264-1269.

Sambrook JF, E.F and Maniatis (1989) Molecular Cloning: A Laboratory Manual I-III, 2nd. Edition. Cold Spring Harbor, New York, USA: Cold Spring Harbor Press.

Schuster CM, Davis GW, Fetter RD, Goodman CS (1996) Genetic dissection of structural and functional components of synaptic plasticity. I. Fasciclin II controls synaptic stabilization and growth. Neuron 17:641-654.

Schuster CM, Davis GW, Fetter RD, Goodman CS (1996) Genetic dissection of structural and functional components of synaptic plasticity. II. Fasciclin II controls presynaptic structural plasticity. Neuron 17:655-667.

Schuster CM, Ultsch A, Schloss P, Cox JA, Schmitt B, Betz H (1991) Molecular cloning of an invertebrate glutamate receptor subunit expressed in Drosophila muscle. Science 254:112-114.

Seeburg PH (1993) The TiPS/TINS lecture: the molecular biology of mammalian glutamate receptor channels. Trends Pharmacol Sci 14:297-303.

Setou M, Seog DH, Tanaka Y, Kanai Y, Takei Y, Kawagishi M, Hirokawa N (2002) Glutamate-receptor-interacting protein GRIP1 directly steers kinesin to dendrites. Nature 417:83-87.

Shapira M, Zhai RG, Dresbach T, Bresler T, Torres VI, Gundelfinger ED, Ziv NE, Garner CC (2003) Unitary assembly of presynaptic active zones from Piccolo-Bassoon transport vesicles. Neuron 38:237-252.

Shen K (2004) Molecular mechanisms of target specificity during synapse formation. Curr Opin Neurobiol 14:83-88.

Sheng G, Thouvenot E, Schmucker D, Wilson DS, Desplan C (1997) Direct regulation of rhodopsin 1 by Pax-6/eyeless in Drosophila: evidence for a conserved function in photoreceptors. Genes Dev 11:1122-1131.

Sheng M, Lee SH (2001) AMPA receptor trafficking and the control of synaptic transmission. Cell 105:825-828.

Sheng M, Kim MJ (2002) Postsynaptic signaling and plasticity mechanisms. Science 298:776-780.

Sheng M, Hyoung Lee S (2003) AMPA receptor trafficking and synaptic plasticity: major unanswered questions. Neurosci Res 46:127-134.

Sheridan DL, Berlot CH, Robert A, Inglis FM, Jakobsdottir KB, Howe JR, Hughes TE (2002) A new way to rapidly create functional, fluorescent fusion proteins: random insertion of GFP with an in vitro transposition reaction. BMC Neurosci 3:7.

Shi S, Hayashi Y, Esteban JA, Malinow R (2001) Subunit-specific rules governing AMPA receptor trafficking to synapses in hippocampal pyramidal neurons. Cell 105:331-343.

Shi SH, Hayashi Y, Petralia RS, Zaman SH, Wenthold RJ, Svoboda K, Malinow R (1999) Rapid spine delivery and redistribution of AMPA receptors after synaptic NMDA receptor activation. Science 284:1811-1816.

Sigrist SJ, Thiel PR, Reiff DF, Schuster CM (2002) The postsynaptic glutamate receptor subunit DGluR-IIA mediates long-term plasticity in Drosophila. J Neurosci 22:7362-7372.

Sigrist SJ, Reiff DF, Thiel PR, Steinert JR, Schuster CM (2003) Experience-dependent strengthening of Drosophila neuromuscular junctions. J Neurosci 23:6546-6556.

Sigrist SJ, Thiel PR, Reiff DF, Lachance PE, Lasko P, Schuster CM (2000) Postsynaptic translation affects the efficacy and morphology of neuromuscular junctions. Nature 405:1062-1065.

Silva AJ, Paylor R, Wehner JM, Tonegawa S (1992) Impaired spatial learning in alpha-calcium-calmodulin kinase II mutant mice. Science 257:206-211.

Silva AJ, Stevens CF, Tonegawa S, Wang Y (1992) Deficient hippocampal long-term potentiation in alpha-calcium-calmodulin kinase II mutant mice. Science 257:201-206.

Silva AJ, Wang Y, Paylor R, Wehner JM, Stevens CF, Tonegawa S (1992) Alpha calcium/calmodulin kinase II mutant mice: deficient long-term potentiation and impaired spatial learning. Cold Spring Harb Symp Quant Biol 57:527-539.

Sone M, Suzuki E, Hoshino M, Hou D, Kuromi H, Fukata M, Kuroda S, Kaibuchi K, Nabeshima Y, Hama C (2000) Synaptic development is controlled in the periactive zones of Drosophila synapses. Development 127:4157-4168.

Spradling AC, Rubin GM (1982) Transposition of cloned P elements into Drosophila germ line chromosomes. Science 218:341-347.

Spradling AC, Stern D, Beaton A, Rhem EJ, Laverty T, Mozden N, Misra S, Rubin GM (1999) The Berkeley Drosophila Genome Project gene disruption project: Single P-element insertions mutating 25% of vital Drosophila genes. Genetics 153:135-177.

Srivastava S, Ziff EB (1999) ABP: a novel AMPA receptor binding protein. Ann N Y Acad Sci 868:561-564.

Srivastava S, Osten P, Vilim FS, Khatri L, Inman G, States B, Daly C, DeSouza S, Abagyan R, Valtschanoff JG, Weinberg RJ, Ziff EB (1998) Novel anchorage of GluR2/3 to the postsynaptic density by the AMPA receptor-binding protein ABP. Neuron 21:581-591.

Svoboda K, Tank DW, Denk W (1996) Direct measurement of coupling between dendritic spines and shafts. Science 272:716-719.

Svoboda K, Helmchen F, Denk W, Tank DW (1999) Spread of dendritic excitation in layer 2/3 pyramidal neurons in rat barrel cortex in vivo. Nat Neurosci 2:65-73.

Tamura T, Thibert C, Royer C, Kanda T, Abraham E, Kamba M, Komoto N, Thomas JL, Mauchamp B, Chavancy G, Shirk P, Fraser M, Prudhomme JC, Couble P, Toshiki T,

Chantal T, Corinne R, Toshio K, Eappen A, Mari K, Natuo K, Jean-Luc T, Bernard M, Gerard C, Paul S, Malcolm F, Jean-Claude P, Pierre C (2000) Germline transformation of the silkworm Bombyx mori L. using a piggyBac transposon-derived vector. Nat Biotechnol 18:81-84.

Tanzi G (1893) I fatti i le indizioni nell'odierna istologi del sistema nervoso. Riv Sper Freniatr 19:419-472.

Tardin C, Cognet L, Bats C, Lounis B, Choquet D (2003) Direct imaging of lateral movements of AMPA receptors inside synapses. Embo J 22:4656-4665.

The_FlyBase_Consortium_2003 (2003) The FlyBase database of the Drosophila genome projects and community literature. Nucleic Acids Res 31:172-175. http://flybase.org/.

Theer P, Hasan MT, Denk W (2003) Two-photon imaging to a depth of 1000 microm in living brains by use of a Ti:Al2O3 regenerative amplifier. Opt Lett 28:1022-1024.

Thibault ST, Singer MA, Miyazaki WY, Milash B, Dompe NA, Singh CM, Buchholz R, Demsky M, Fawcett R, Francis-Lang HL, Ryner L, Cheung LM, Chong A, Erickson C, Fisher WW, Greer K, Hartouni SR, Howie E, Jakkula L, Joo D, Killpack K, Laufer A, Mazzotta J, Smith RD, Stevens LM, Stuber C, Tan LR, Ventura R, Woo A, Zakrajsek I, Zhao L, Chen F, Swimmer C, Kopczynski C, Duyk G, Winberg ML, Margolis J (2004) A complementary transposon tool kit for Drosophila melanogaster using P and piggyBac. Nat Genet 36:283-287.

tom Dieck S, Sanmarti-Vila L, Langnaese K, Richter K, Kindler S, Soyke A, Wex H, Smalla KH, Kampf U, Franzer JT, Stumm M, Garner CC, Gundelfinger ED (1998) Bassoon, a novel zinc-finger CAG/glutamine-repeat protein selectively localized at the active zone of presynaptic nerve terminals. J Cell Biol 142:499-509.

Tonegawa S, Li Y, Erzurumlu RS, Jhaveri S, Chen C, Goda Y, Paylor R, Silva AJ, Kim JJ, Wehner JM, et al. (1995) The gene knockout technology for the analysis of learning and memory, and neural development. Prog Brain Res 105:3-14.

Toni N, Buchs PA, Nikonenko I, Bron CR, Muller D (1999) LTP promotes formation of multiple spine synapses between a single axon terminal and a dendrite. Nature 402:421-425.

Toni N, Buchs PA, Nikonenko I, Bron CR, Müller D (1999) LTP promotes formation of multiple spine synapses between a single axon terminal and a dendrite. Nature 402:421-425.

Trachtenberg JT, Chen BE, Knott GW, Feng G, Sanes JR, Welker E, Svoboda K (2002) Long-term in vivo imaging of experience-dependent synaptic plasticity in adult cortex. Nature 420:788-794.

Umeda T, Okabe S (2001) Visualizing synapse formation and remodeling: recent advances in real-time imaging of CNS synapses. Neurosci Res 40:291-300.

Wang HH, Fraser MJ, Cary LC (1989) Transposon mutagenesis of baculoviruses: analysis of TFP3 lepidopteran transposon insertions at the FP locus of nuclear polyhedrosis viruses. Gene 81:97-108.

Wang Y, Liu X, Biederer T, Sudhof TC (2002) A family of RIM-binding proteins regulated by alternative splicing: Implications for the genesis of synaptic active zones. Proc Natl Acad Sci U S A 99:14464-14469.

Washbourne P, Bennett JE, McAllister AK (2002) Rapid recruitment of NMDA receptor transport packets to nascent synapses. Nat Neurosci 5:751-759.

Wucherpfennig T, Wilsch-Brauninger M, Gonzalez-Gaitan M (2003) Role of Drosophila Rab5 during endosomal trafficking at the synapse and evoked neurotransmitter release. J Cell Biol 161:609-624.

Yamagata M, Sanes JR, Weiner JA (2003) Synaptic adhesion molecules. Curr Opin Cell Biol 15:621-632.

Yoshimura Y, Yamauchi Y, Shinkawa T, Taoka M, Donai H, Takahashi N, Isobe T, Yamauchi T (2004) Molecular constituents of the postsynaptic density fraction revealed by proteomic analysis using multidimensional liquid chromatography-tandem mass spectrometry. J Neurochem 88:759-768.

Yuste R, Bonhoeffer T (2001) Morphological changes in dendritic spines associated with long-term synaptic plasticity. Annu Rev Neurosci 24:1071-1089.

Zhai RG, Vardinon-Friedman H, Cases-Langhoff C, Becker B, Gundelfinger ED, Ziv NE, Garner CC (2001) Assembling the presynaptic active zone: a characterization of an active one precursor vesicle. Neuron 29:131-143.

Zhang M, Wang W (2003) Organization of signaling complexes by PDZ-domain scaffold proteins. Acc Chem Res 36:530-538.

Zhong Y, Wu CF (2004) Neuronal activity and adenylyl cyclase in environment-dependent plasticity of axonal outgrowth in Drosophila. J Neurosci 24:1439-1445.

Zhong Y, Budnik V, Wu CF (1992) Synaptic plasticity in Drosophila memory and hyperexcitable mutants: role of cAMP cascade. J Neurosci 12:644-651.

Ziff EB (1997) Enlightening the postsynaptic density. Neuron 19:1163-1174.

Zito K, Parnas D, Fetter RD, Isacoff EY, Goodman CS (1999) Watching a synapse grow: noninvasive confocal imaging of synaptic growth in Drosophila. Neuron 22:719-729.

Ziv NE, Garner CC (2001) Principles of glutamatergic synapse formation: seeing the forest for the trees. Curr Opin Neurobiol 11:536-543.

6. 3 Manuscript 1:
Glutamate receptor dynamics during *in vivo* synapse formation

Glutamate receptor dynamics
during *in vivo* synapse formation

One sentence summary: *In vivo* imaging of GFP-labeled receptors reveals the assembly mode of newly forming glutamatergic synapses

Tobias M. Rasse[1], Wernher Fouquet[1], Andreas Schmid[1], Robert J. Kittel[1], Carola B. Sigrist[1], Manuela Schmidt[1], Asja Guzman[1], Carlos Merino[1], Gang Qin[1], Christine Quentin[1], Frank F. Madeo[2], Manfred Heckmann[3]*, and Stephan J. Sigrist[1]*

*corresponding authors (ssigris@gwdg.de, heckmann@physiologie.uni-freiburg.de)

(1) European Neuroscience Institute Göttingen, Max-Planck-Society, Waldweg 33, D-37073 Göttingen (Germany)

(2) Institute for Physiological Chemistry, University of Tübingen, Hoppe-Seyler-Str. 4, D-72076 Tübingen (Germany)

(3) Physiologisches Institut, Hermann-Herder-Str. 7, D-79104 Freiburg (Germany)

Synapse formation is one means the CNS uses to strengthen synaptic transmission during learning and memory. Here the transgenic expression of GFP-labeled glutamate receptors is used to directly observe glutamate receptor dynamics during synapse formation in a strengthening synaptic circuit of intact *Drosophila*. We find that small functional synapses form at sites distant from established synapses to then grow to a mature size. Synapse growth is driven by entry of glutamate receptors from diffuse extrasynaptic pools as shown by *in vivo* photo-labeling. Thus, *de novo* formation and subsequent growth of synapses mediates strengthening of glutamatergic circuits *in vivo*.

Alterations in the strength of existing synapses as well as the formation of new synapses might underlie memory formation. Glutamate receptors, which mediate excitatory transmission in our brains, are recognized as key elements in the context of such synaptic plasticity (*1*). Over the last years, convincing evidence for changes in density and/or function of postsynaptic glutamate receptor has accumulated, using both optical mapping of glutamate sensitivity (*2, 3*) as well as imaging of labeled glutamate receptors (*4, 5*). Both exo- and endocytosis of receptor bearing membrane as well as exchange with diffuse extrasynaptic plasmamembrane pools have been described (*6-8*). For synapse remodeling and new formation during synaptic strengthening, perforation and subsequent splitting of the postsynaptic receptor bearing area (postsynaptic density, PSD) are discussed to be essential intermediates (*9-15*). To gain a deeper understanding it appears necessary to observe the molecular dynamics of glutamate receptor proteins over extended periods during *in vivo* synapse formation and remodeling (*16*). So far, *in vivo* imaging of receptors during synapse formation has been performed only for acetylcholine receptors (*17, 18*).

We here focused on glutamatergic neuromuscular junctions of *Drosophila* larvae whose individual synapses are on the ultrastructural level similar to central mammalian glutamatergic synapses (*19-23*). To label individual synapses in this preparation EGFP was inserted into the *Drosophila* glutamate receptor subunit IIA (GluR-IIA[GFP]) and then expressed at physiological levels from a genomic transgene. We found that GFP-labeled GluR-IIA rescues *GluR-IIA&IIB* deficient animals suggesting that GluR-IIA[GFP] is fully functional. Synaptic currents are indistinguishable comparing GFP-labeled and wild-type GluR-IIA rescued animals (Fig. 1A). GluR-IIA[GFP] expression marks clearly synapses as shown by the co-localization with endogenous GluR-IIA, p21/rac1-activated kinase (PAK), an established PSD marker (*24, 25*), and Nc82 (Fig. 1B), which recognizes the presynaptic site of individual synapses (*26, 27*). Essentially all PSDs visualized by GluR-IIA[GFP] expression are associated with presynaptic activity-dependent vesicle recycling (Fig 1C). Thus GluR-IIA[GFP] is fully functional, labels reliably synapses and is therefore suitable to track the glutamate receptors of individual synapses over time.

GluR-IIA[GFP] expressing larvae were subjected to repeated short periods of confocal live imaging. Between imaging sessions, animals moved freely. As previously

reported (*28*), live imaging showed that the gross morphology of an individual junction is relatively stable. Its size (Fig. 2A) and functional strength, however, increases substantially during larval development (*29-31*). Live imaging allowed us to track individual GluR-IIA[GFP] labeled synapses within this strongly strengthening synaptic system. We found that many synapses were stable over time (white arrow heads in Fig. 2B) while a substantial number of new synapses formed (white arrows). New synapses mostly formed distant from preexisting synapses (Fig. 2B, white arrows) and grew rapidly while large synapses (PSD size >0.4 μm^2) appeared to change little.

To quantify this, data from 5 such experiments were pooled. Starting with 309 synapses we could observe the formation of 165 new synapses within 36h at 16°C. The overall PSD size distribution over all these synapses was rather stable over time (mean PSD size increased from 0.21 μm^2 at 0h to 0.24 μm^2 at 36h; $p < 0.05$; black bars in Fig. 2C). Tracing only a subpopulation of synapses (those detected first at t=12h, white bars in Fig. 2C) showed that new synapses formed small to then grow rapidly reaching a mature PSD size within 24h.

The data presented so far suggest that new synapses form predominantly independent of preexisting synapses implying *de novo* formation of new synapses. However, synapse splitting could happen fast and therefore have escaped detection. We thus tried to trace the origin of the molecular components which accumulate in newly forming synapses using fluorescence recovery after photo-bleaching (FRAP). The synaptic turnover of a label suitable to trace the origin of PSD components must be in a similar time domain as new formation or growth of synapses. To test the suitability of our label we first compared FRAP of PAK, another PSD localizing protein (see also Fig. 1C), with FRAP of GluR-IIA. To label the proteins we used GFP and monomeric red fluorescent protein (*32*), respectively. While FRAP of PAK[GFP] was substantial after 20 minutes, GluR-IIA[mRFP] recovery was slow (Fig. 3A). Visualizing the *in vivo* dynamics of glutamate receptor subunit GluR-IIA might therefore allow to differentiate *de novo* formation from a split-like partitioning mode of synapse formation. Thus, animals co-expressing GluR-IIA[GFP] and GluR-IIA[mRFP] were generated after verifying that bleaching does not affect receptor function (Fig. 3B). This receptor co-labeling allowed to quantify entry of glutamate receptor into bleached synapses (FRAP of GluR-IIA[mRFP]) while the

GluR-IIA^{GFP} signal served as a reference (Fig. 3C). 24h after bleaching GluR-IIA^{mRFP} FRAP indicated that receptor entry was highly variant between synapses. Stable synapses showed very little or no receptor entry regardless of whether they were large (Fig. 3C, white arrow heads) or rather small (Fig. 3C blue arrow head). Preexisting synapses which grew during the time series (Fig. 3C, blue arrow), however, showed considerable glutamate receptor entry (FRAP of GluR-IIA^{mRFP}). Finally new synapses showed even more GluR-IIA^{mRFP} FRAP (Fig. 3C, arrows) in all experiments of this type (n>40). This suggests that new synapses receive "new" receptors from outside the bleached area but not from neighboring synapses. This finding is supported by a quantitative analysis (Fig. 3D), showing the ratio of the GluR-IIA^{mRFP} signal relative to the GluR-IIA^{GFP} signal for stable, growing as well as for new synapses (data normalized to the mean value obtained for new synapses). The red/green ratio is the highest in new synapses, followed by growing and finally stable synapses. This supports a *de novo* mode for synapse formation and growth, and argues against the hypothesis that split-like partitioning events contribute significantly to glutamatergic synapse formation *in vivo*.

To independently test this conclusion, the origin of glutamate receptors for new synapses was determined by directly tracing a photo-labeled receptor population. Photo-activatable GFP (*33*) was inserted into GluR-IIA (GluR-IIA^{GFP-PA}) and subsequently transgenically expressed. GFP was activated at t=0h in parts of a junction with a spot of UV-light and followed. Again no evidence for synapse splitting was obtained. Synapses present at the beginning of an experiment kept their labeled glutamate receptors during time series (Fig. 3E). Receptors integrated into new synapses became visible only when applying a second round of photo-activation at the end of the experiment. Thus, we found again that the glutamate receptors which support the growth of new synapses do not derive from neighboring synapses but from more distant, most likely extrasynaptic pools.

Our data suggest that entry of GluR-IIA is directly correlated with the growth of new synapses (*21*) consistent with the hypothesis that GluR-IIA expression is rate limiting for synapse formation (*34*). Synapses are stable from a certain size on and both GluR-IIA entry and exit are then low (Fig. 3C-E). While we obtained no evidence for internal stores of glutamate receptors it seems that the receptors for new synapses and synapse growth probably derive from diffuse extrasynaptic pools residing within the

plasma membrane. Such pools on the surface of *Drosophila* muscles have already been directly demonstrated in earlier developmental stages using electrophysiology (*30*). Furthermore, in other preparations glutamate receptors were shown to float freely in the plasma membrane diffusing in and out of synapses (*8*). The number of postsynaptic glutamate receptors is also a key parameter for the strength of central glutamatergic synapses (*2-4, 35, 36*). Spines grow while glutamate receptor currents increase during strengthening (*1, 3*). Thus, fundamental mechanisms for strengthening glutamatergic synapses apparently have been conserved during evolution.

Collectively, both our FRAP and photo-activation experiments show that glutamatergic synapses do not split. Instead, new synapses seem to form truly *de novo*. Although new synapses are initially very small having only a few percent of the size of mature synapses they appear nevertheless to function given that they display all properties typical for established synapses (presynaptic vesicle recycling, co-localization with the active zone marker Nc82 and the PSD marker PAK, see Fig. 1). While new synapses are probably already responsive to instructive activity patterns, our data suggest that large synapses are in contrast to small synapses very stable. This is in line with the finding that large synaptic spines are stable for months in the intact mouse cerebral cortex (*37*) and that small spines preferentially grow during synaptic strengthening (*3*). Increases in spine size are mirrored by increases in synapse size (*14, 38*). Thus, small synapses may work as "memory units". During strengthening small synapses can be converted into large synapses, which in turn would be physical traces of memory. Since large synapses have less potential for further growth, they may reliably store information, without interference due to readout of information or strengthening of nearby neighbors (*3*).

We achieved to visualize the assembly of glutamatergic synapses *in vivo*. Elegant live imaging studies of cholinergic mammalian endplates, reviewed in (*39*), have been pivotal for our understanding of synapse formation. Live imaging the dynamic molecular composition of glutamatergic synapses is just at its beginning. Further work will allow to address also the behavior of other glutamate receptor subunits (*23*) and the cellular mechanism which mediate additional synaptic strengthening (*31*). Live imaging of glutamatergic synapses thus has substantial potential for additional progress regarding our understanding of the molecular basis of learning and memory.

References and Notes

1. S. Shi, Y. Hayashi, J. A. Esteban, R. Malinow, *Cell* **105**, 331 (2001).
2. H. Dodt, M. Eder, A. Frick, W. Zieglgänsberger, *Science* **286**, 110 (1999).
3. M. Matsuzaki, N. Honkura, G. C. Ellis-Davies, H. Kasai, *Nature* **429**, 761 (2004).
4. T. Bresler *et al.*, *J Neurosci* **24**, 1507 (2004).
5. M. C. Ashby *et al.*, *J Neurosci* **24**, 5172 (2004).
6. M. Sheng, M. J. Kim, *Science* **298**, 776 (2002).
7. E. D. Gundelfinger, M. M. Kessels, B. Qualmann, *Nat Rev Mol Cell Biol* **4**, 127 (2003).
8. A. J. Borgdorff, D. Choquet, *Nature* **417**, 649 (2002).
9. R. K. Carlin, P. Siekevitz, *Proc Natl Acad Sci U S A* **80**, 3517 (1983).
10. M. Nieto-Sampedro, S. F. Hoff, C. W. Cotman, *Proc Natl Acad Sci U S A* **79**, 5718 (1982).
11. J. M. Wojtowicz, L. Marin, H. L. Atwood, *J Neurosci* **14**, 3688 (1994).
12. N. Toni, P. A. Buchs, I. Nikonenko, C. R. Bron, D. Müller, *Nature* **402**, 421 (1999).
13. C. Lüscher, R. A. Nicoll, R. C. Malenka, D. Müller, *Nat Neurosci* **3**, 545 (2000).
14. R. Yuste, T. Bonhoeffer, *Annu Rev Neurosci* **24**, 1071 (2001).
15. J. C. Fiala, B. Allwardt, K. M. Harris, *Nat Neurosci* **5**, 297 (2002).
16. C. M. Niell, S. J. Smith, *Annu Rev Physiol* **66**, 771 (2004).
17. D. Purves, J. W. Lichtman, *J Neurosci* **7**, 1492 (1987).
18. M. Akaaboune, R. M. Grady, S. Turney, J. R. Sanes, J. W. Lichtman, *Neuron* **34**, 865 (2002).
19. C. M. Schuster *et al.*, *Science* **254**, 112 (1991).
20. S. A. Petersen, R. D. Fetter, J. N. Noordermeer, C. S. Goodman, A. DiAntonio, *Neuron* **19**, 1237 (1997).
21. S. J. Sigrist *et al.*, *Nature* **405**, 1062 (2000).
22. C. Pawlu, A. DiAntonio, M. Heckmann, *Neuron* **42**, 607 (2004).
23. S. B. Marrus, S. L. Portman, M. J. Allen, K. G. Moffat, A. DiAntonio, *J Neurosci* **24**, 1406 (2004).
24. S. D. Albin, G. W. Davis, *J Neurosci* **24**, 6871 (2004).
25. M. Sone *et al.*, *Development* **127**, 4157 (2000).
26. T. Wucherpfennig, M. Wilsch-Brauninger, M. Gonzalez-Gaitan, *J Cell Biol* **161**, 609 (2003).
27. G. Heimbeck, V. Bugnon, N. Gendre, C. Haberlin, R. F. Stocker, *J Neurosci* **19**, 6599 (1999).
28. K. Zito, D. Parnas, R. D. Fetter, E. Y. Isacoff, C. S. Goodman, *Neuron* **22**, 719 (1999).
29. C. M. Schuster, G. W. Davis, R. D. Fetter, C. S. Goodman, *Neuron* **17**, 641 (1996).
30. K. Broadie, M. Bate, *Neuron* **11**, 607 (1993).
31. S. J. Sigrist, D. F. Reiff, P. R. Thiel, J. R. Steinert, C. M. Schuster, *J Neurosci* **23**, 6546 (2003).
32. R. E. Campbell *et al.*, *Proc Natl Acad Sci U S A* **99**, 7877 (2002).

33.	G. H. Patterson, J. Lippincott-Schwartz, *Science* **297**, 1873 (2002).
34.	S. J. Sigrist, P. R. Thiel, D. F. Reiff, C. M. Schuster, *J Neurosci* **22**, 7362 (2002).
35.	M. Sheng, S. H. Lee, *Cell* **105**, 825 (2001).
36.	R. Malinow, R. C. Malenka, *Annu Rev Neurosci* **25**, 103 (2002).
37.	J. T. Trachtenberg *et al.*, *Nature* **420**, 788 (2002).
38.	K. M. Harris, J. C. Fiala, L. Ostroff, *Philos Trans R Soc Lond B Biol Sci* **358**, 745 (2003).
39.	J. W. Lichtman, J. R. Sanes, *J Neurocytol* **32**, 767 (2003).
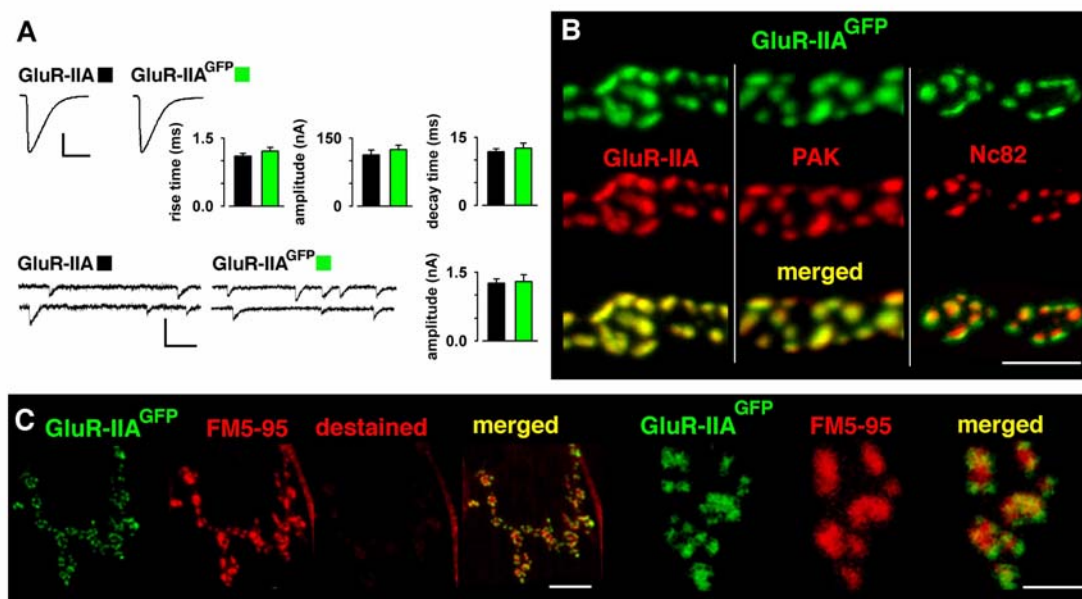
Fig. 1. GluR-IIA[GFP] is fully functional and labels postsynaptic densities **(A)** Spontaneous and nerve evoked synaptic currents from muscle 6 of *GluR-IIA&IIB* deficient animals rescued with untagged GluR-IIA or GluR-IIA[GFP]. Shown are representative traces from two-electrode-voltage-clamp recordings of either nerve evoked EPSCs (scale bars: 20 nA and 50 ms) and bar graphs with standard errors for mean rise time, amplitude, and decay time constant or spontaneous EPSCs (scale bars: 1 nA and 20 ms) with bar graphs for mean amplitude. N = 9 experiments with each genotype (p > 0.05 for all parameters). **(B)** GluR-IIA[GFP] expression visualized by αGFP staining (in green) with either endogenous GluR-IIA, PAK or the presynaptic active zone marker Nc82 (in red) and merged images in the bottom row. Scale bar: 5 µm. (**C**) Confocal images of a GluR-IIA[GFP] expressing junction with presynaptic FM5-95 labelling (in red) after nerve stimulation, higher magnifications on the right (scale bars: 10 and 2 µm, respectively).
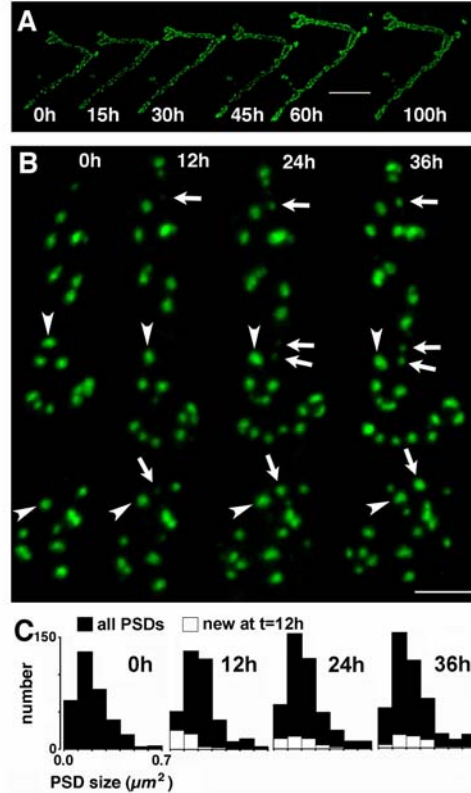
Fig. 2. *In vivo* imaging of glutamatergic synapse formation **(A)** Confocal time series of a GluR-IIA[GFP] expressing junction, scale bar: 15 µm. **(B)** Images from another time series at higher magnification. Examples for new synapses are marked by arrows and examples for synapses which were present from the observation start (t=0h) by arrowheads. Scale bar: 3 µm. **(C)** PSD size distribution for the indicated time points. Black bars show all PSDs, white bars show size distribution only for PSDs which were new at t=12h. Data are pooled from 5 experiments done at 16°C.
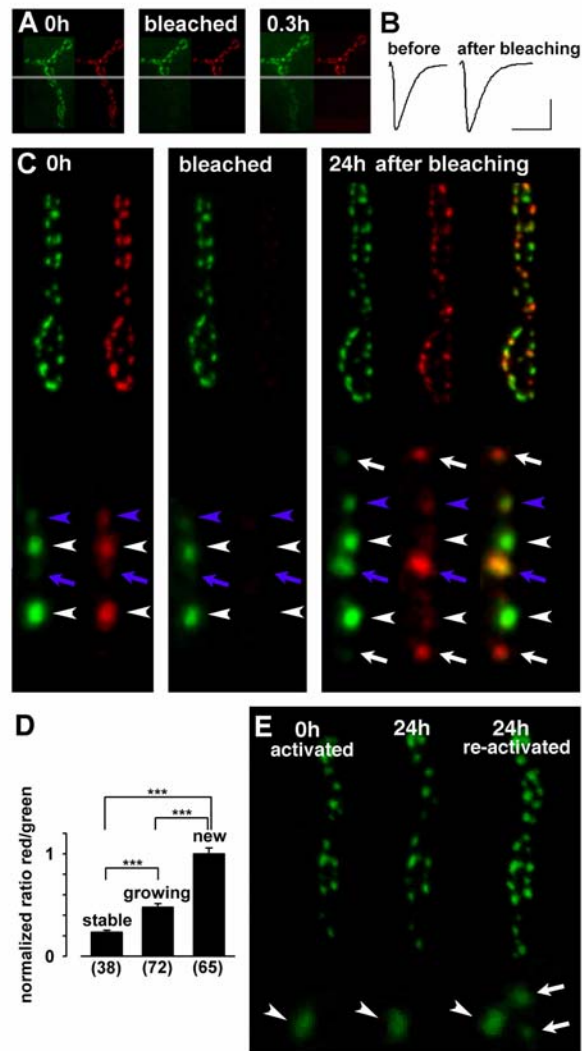
Fig. 3. Photolabeling reveals glutamate receptor dynamics during synapse formation **(A)** *In vivo* FRAP of synaptic protein label: Confocal time series of a GluR-IIA^{mRFP} (red) and PAK^{GFP} (green) expressing synapses. The area below the gray line was bleached. 20 min later recovery of PAK^{GFP} is visible while GluR-IIA^{mRFP} recovery is not visible. **(B)** Nerve evoked synaptic current from muscle 6 of a GluR-IIA^{GFP} rescued larvae, recorded in two-electrode-voltage-clamp mode, prior to and after bleaching GluR-IIA^{GFP}. Scale bar: 20 nA, 50 ms. **(C)** Receptor entry into synapses was visualized using FRAP and animals co-expressing GluR-IIA^{GFP} (green) and GluR-IIA^{mRFP} (red). GluR-IIA^{GFP} and GluR-IIA^{mRFP} were imaged prior to and after bleaching selectively GluR-IIA^{mRFP} at t=0h. The higher

magnifications in the lower half of the panels show that FRAP of GluR-IIA^{mRFP} is essentially restricted to synapses, which are either new (white arrows) or which grew substantially (blue arrows). Synapses, which grew little (white and blue arrow heads) show only very weak GluR-IIA^{mRFP} FRAP. **(D)** The normalized ratio of GluR-IIA^{mRFP} and GluR-IIA^{GFP} signal 24h after bleaching shows that stable or mature synapses and growing synapses (size increase > 1.5 fold) receive less new (unbleached) GluR-IIA^{mRFP} than new synapses (*** indicates $p < 0.0001$, data from 5 experiments). This is not consistent with the hypothesis that new synapses arise by synapse-splitting. **(E)** Confocal time series of a GluR-IIA^{GFP-PA} expressing junction imaged prior to and after a second photo-activation. Higher magnifications are shown in the lower half of the panels. Receptor label does not spread into new synapses which become visible only after a second photo-activation. White arrowhead points at a mature or stable synapse, arrows point at two new synapses nearby.

Supplementary Material:

Molecular Biology and Genetics:

To express fluorescently tagged GluR-IIA, an *Eco*RI/*Xba*I genomic fragment from BACR35L07 entailing 1,2 kb sequence upstream of the start codon was used. The fluorescent tags (GFP, mRFP and photoactivatable GFP) were inserted in the intracellular C-terminus of GluR-IIA after S893. To construct PAK[GFP] the myc-tag in UAS-pak-myc (*1*) was replaced by EGFP. Transgenic PAK[GFP] expression was induced at 16 °C using G14-Gal4 (*2*) as driver. More details concerning the cloning of these constructs are available upon request. All constructs were confirmed by double-strand sequencing and transgenic flies were produced using standard procedures. GluR-IIA[GFP] and GluR-IIA were tested for rescue activity in the *GluR-IIA&IIB* double mutant (*Df(2L)cl*^*h4*/*GluR-IIA&B*^*SP22*) background (*3*). Both constructs rescued in mendelian ratio. For live imaging, all GluR-IIA constructs were expressed in a background heterozygous for *Df(2L)cl*^*h4*.

Electrophysiology and styryl dye labeling

Intracellular recordings were made at 22 °C from muscle fiber 6 of abdominal segments 2 and 3, of late third instar larvae. The larvae were dissected in ice-cold, calcium-free haemolymph-like saline (HL-3) according to (*4*). Composition of the HL-3 solution was (in mM): NaCl 70, KCl 5, $MgCl_2$ 20, $NaHCO_3$ 10, trehalose 5, sucrose 115, HEPES 5, pH adjusted to 7.2. Larval fillets were rinsed with 2ml of HL-3 saline containing 1 mM Ca^{2+}, before being transferred to the recording chamber where two-electrode voltage clamp (TEVC) recordings were performed in 1mM extra cellular Ca^{2+}. The larval junction was visualized with a fixed-stage upright microscope (Olympus, 40x water immersion lens). Whole muscle recordings of both miniature and evoked postsynaptic currents were recorded in TEVC mode (AxoClamp 2B, Axon Instruments) using sharp microelectrodes (borosilicate glass with filament, 1,5mm outer diameter) with resistances of 15-35 MΩ and filled with 3M KCL. All cells selected for analysis had resting potentials between -55 and -70 mV and the input resistance was ≥ 4 MΩ. For stimulation, the cut end of the segmental nerve was pulled into a fire-polished suction electrode and

brief (300 µs) depolarizing pulses were passed at 0.2 Hz (npi stimulus generator and isolation unit). To ensure the stable recruitment of both innervating motoneurons, the amplitude of the pulse was determined by increasing the stimulation strength to 1.5 times the amplitude needed to reach the threshold of double motoneuron recruitment. The clamp was tuned such that it responded to a voltage step from -60 to -70 mV with settling times of 1ms for mEJCs and 500-750µs for eEJCs, this gave voltage errors of maximally 4 mV for eEJCs of approx. -100nA. Both eEJCs (voltage clamp at -60mV) and mEJCs (voltage clamp at -80mV) were low-pass filtered at 1 kHz. For each cell, 20 eEJCs and 90s of mEJCs recordings were used for subsequent analysis (pClamp9, Axon Instruments). In the receptor photo-bleaching experiment, responses to 30 consecutive stimuli, delivered at 1 Hz were averaged. FM5-95 uptake was essentially done as described (*5*). In short: terminals at muscle 4 were labelled by replacing normal saline with normal saline containing 20 µM FM5-95 (T-23360, Molecular Probes, Eugene, USA) followed by stimulating the innervating nerve at 30 Hz for 5 min. After stimulation, preparations were washed three times with Ca^{2+}-free saline. Destaining was done by applying high K^{+} saline for 5 min.

Antibodies:

The rabbit-α-GluRIII antiserum was raised against the two peptide sequences (PRRSLDKSLDRTPKS+C and C+SGSNNAGRGEKEARV), affinity purified and used at a dilution of 1:200. The other antibodies were used at the following concentrations: mouse-α-nc82 (1:100) (gift of E. Buchner, University of Würzburg, Germany), rabbit-α-PAK (1:2000) (gift of N. Harden, The Hospital for Sick Children, Toronto, Canada), mouse-α-FasII (1:50) (ID4, Developmental Studies Hybridoma Bank, University of Iowa, USA), rabbit-α-GFP (1:500) (A-11122, Molecular Probes, Eugene, USA), mouse-α−GluR-IIA (1:100) (concentrated 8B4D2, Developmental Studies Hybridoma Bank, University of Iowa, USA).

Anesthetization of *Drosophila* larvae:

Because non-anesthetized *Drosophila* larvae move strongly, live imaging of individual PSDs demands stable immobilization. The application of 15% (v/v) of Desflurane

(Suprane, Baxter, Unterschleissheim, Germany) for 2 min proved ideal (*6*) because onset and recovery from anesthetization are fast, with anesthetized larvae being immobile and no longer showing internal movements. Second to third instar larvae were mounted between two 0,12 mm microscope coverslips, which were held apart by a plastic slide. A central slit in the centre of the plastic slide allowed placing the larva. Width and length of the slit, as well as the height of the plastic slide were adjusted to the size of the larva to prevent turning of the larva and to allow only minimal movement of the larva in direction of the slit. The lower coverslip was covered with a thin film of Voltalef H10A Oil (Lehmann & Voss, Hamburg, Germany). Air and anaesthetic were applied to the larva via 3 "air-slots" of 200 nm width and 40 nm height, which led from each side of the slit in which the larva was placed towards the edge of the plastic slide. The plastic slide itself was placed in an imaging chamber, which was connected to a custom made 2 channel respiration system. Control experiments using 10 consecutive anesthetizations, separated by 5 min recovery intervals, revealed neither any developmental delay nor increased mortality in anesthetized larvae compared to non-anesthetized but otherwise identically treated sibling larvae.

Image Aquistition:

In vivo imaging was performed on a Leica DM IRE2 microscope equipped with a Leica TCS SP2 AOBS scanhead. FM5-95 labels were scanned on a Leica DM LFSA equipped with a Leica TCS SP2 scanhead, using the TD 488/543/633 as principal beamsplitter for immunostainings and the GFP-channel for FM5-95 labeling and the DD 458/514 to visualize FM5-95. The *in vivo* imaging, as well as all immunostainings were scanned using a Leica HCX PL Apo CS 63x 1.32 NA OIL UV objective, and the FM5-95 labeling was imaged using the Leica HCX APO L 40x 0,8 NA W objective. The other settings were as follows: in-vivo imaging shown in Figure2: Pinhole 1 Airy Unit, Voxelsize: 98nm*98nm*244nm; FRAP experiments shown in Figure 3: Pinhole 1,5 Airy Units, Voxelsize: 98nm*98nm*488nm; all immunostainings Pinhole 1 Airy Unit: Voxelsize 49nm*49nm*145nm; FM-labeling: Pinhole1,5 Airy Units for GFP and 1 Airy Unit for FM5-95 Voxelsize: 98nm*98nm*246nm. The timeseries shown in Figure2 was performed at 16 °C, where development is slowed down, since it allowed to work early in

the morning and at evenings (when the shared microscope was available on a regular basis). All other experiments were performed at 25 °C.

Image Analysis:

The image processing analysis was performed using ImageJ 1.32b (Wayne Rasband, NIH USA, http://rsb.info.nih.gov/ij/download.html). In maximum projected z-stacks individual synapses were segmented by projecting a binary segmentation mask on the z-stack. To do so the sum projected z-stack was defined as Image1 in the *Image Calculator* function *Min.* A binary mask, in which synapses had the value 255 and non-synaptic areas the Value 0 was defined as Image2. The mask itself was obtained by thresholding a median filtered (radius 1 pixel), background corrected, maximum projected z-stack. Individual synapses, which were not separated by this protocol, were manually segmented, by comparing the mask with the original z-stack. In the segmented image synapses were analyzed with the *Analyse Particles* function using the following settings: *Set threshold* of the image to 1 to 255, and *Set Measurements* parameters to *Limit to Threshold, Area, Standard Deviation, Mean Gray Value*. The background was measured in a representative square in the maximum projected z-stack. All synapses were individually background corrected using this value. Further analysis was performed using Microsoft Excel (Microsoft).

Western Blot:

DGluRIIA^{GFP} could be detected as a protein of the predicted 140 kD in extracts of DGluRIIA^{GFP} transgenic embryos (data not shown). For immunoblotting, 12- to 19-h-old wildtype and trangenically GluR-IIA^{GFP} expression *Drosophila* embryos were dechorionated and homogenized in lysis buffer (50 mM HEPES, 60 mM NaCl, 3 mM MgCl$_2$, 1 mM CaCl$_2$, 0.5% Triton X-100, 0.5% Nonidet P-40, 10% glycerol) with protease inhibitor "complete mini" (1836170, Roche Diagnostics, Mannheim, Germany) added. After centrifugation, supernatant was harvested and precleared via AffiPrep proteinA support (1560006, BioRad, Hercules, USA) beads at 4°C. Samples were run on an 8% PAA gel, transferred to nitrocellulose membrane (162 0213, BioRad, Hercules, USA), and probed with the anti-GFP antibody (1 : 1000; ab6556-25, Abcam, Cambridge,

UK) followed by ECL-detection (RPN 2132, Amersham Bioscience, Buckinghamshire, UK).

1. L. H. Ang, J. Kim, V. Stepensky, H. Hing, *Development* **130**, 1307 (2003).
2. H. Aberle *et al.*, *Neuron* **33**, 545 (2002).
3. A. DiAntonio, S. A. Petersen, M. Heckmann, C. S. Goodman, *J Neurosci* **19**, 3023 (1999).
4. B. A. Stewart, H. L. Atwood, J. J. Renger, J. Wang, C. F. Wu, *J Comp Physiol [A]* **175**, 179 (1994).
5. H. Kuromi, Y. Kidokoro, *Neuron* **35**, 333 (2002).
6. D. B. Campbell, H. A. Nash, *Proc Natl Acad Sci U S A* 91, 2135 (1994).

6.4 Manuscript 2:

The monoclonal antibody nc82 identifies the _Drosophila_ CAST/ERC homolog as component of synaptic active zones

The monoclonal antibody nc82 identifies the *Drosophila* CAST/ERC homolog as component of synaptic active zones

Abbreviated title: *Drosophila* homolog of active zone protein CAST/ERC

Dhananjay Wagh[1*], Tobias Rasse[2*], Alois Hofbauer[3], Isabell Schwenkert[1], Heike Dürrbeck[1], Sigrid Buchner[1], Marie-Christine Dabauvalle[4], Qin Gang[2], Stephan J. Sigrist[2], and Erich Buchner[1]

Theodor-Boveri-Institut für Biowissenschaften,
[1]Lehrstuhl für Genetik und Neurobiologie, [4]Lehrstuhl für Zell- und Entwicklungsbiologie
Am Hubland, D-97074 Würzburg, Germany
[2] European Neuroscience Institute Göttingen, Max-Planck-Society, Waldweg 33, D-37073 Göttingen, Germany
[3]Lehrstuhl für Entwicklungsbiologie, Institut für Zoologie,
Universitätsstr. 31, D-93047 Regensburg, Germany

* These authors have contributed equally to the present work

Correspondence: Dr. Erich Buchner
                     Lehrstuhl für Genetik, Am Hubland
                     D-97074 Würzburg, Germany
                     Tel. ..49-931-888-4478   Fax: ..49-931-888-4452
                     email: buchner@biozentrum.uni-wuerzburg.de

Number of Figures: 6
Number of pages: 16

Key words: synapse; active zone protein; cytomatrix; gene structure; *Drosophila*; Anopheles

Abstract

Synaptic vesicles dock, fuse, and release their neurotransmitters at the presynaptic active zone of the plasma membrane. In mammals, few molecular components of the active zone have been defined. For the best studied components of the presynaptic active zone, piccolo and bassoon, no homologs are found in *Drosophila*. The monoclonal antibody (MAB) nc82 is routinely used to specifically stain the neuropil within *Drosophila* brain whole mounts. Here, we show that MAB nc82 recognizes a protein which localizes to the active zones of presumably all synaptic terminals of *Drosophila*. On western blots, MAB nc82 recognizes two protein isoforms of about 180 and 190 kDa. We identified the gene coding for this active zone protein employing 2D-gel electrophoresis and MALDI-TOF mass spectrometry. In the N-terminal half, the encoded protein shows high homology to human CAST/ERC, a protein associated with the cytomatrix at the presynaptic active zone. The C-terminal half of the protein contains a glutamine rich domain that is highly conserved in *Anopheles* but shows no homology to mammalian CAST/ERCs. Rather, it displays similarity to myosin heavy chain and other multifunctional cytoskeletal proteins. The Drosophila *CAST* locus is complex, comprising three genomic regions previously annotated as three independent genes and producing two alternatively spliced transcripts. During embryonic development, CAST transcription coincides with neuronal differentiation. Because of its conserved nature, we speculate that CAST belongs to a molecular core complex generally defining presynaptic active zones. This study opens the way for a functional *in vivo* study of CAST function in particular and active zone function and assembly in general using the efficient genetics of *Drosophila*.

167

Introduction

Synaptic communication between nerve cells takes place at specific sites characterized ultrastructurally by pre- and postsynaptic membrane thickenings and, on the presynaptic side, by synaptic vesicle accumulation and often synaptic ribbons. Considerable efforts have been undertaken in recent years to identify the protein components of the electron dense cytoskeletal matrix associated with the active zone (CAZ) (Landis et al., 1988; Phillips et al., 2001; Rosenmund et al., 2003). This matrix extends from the presynaptic membrane into the presynaptic bouton, where it is associated with synaptic vesicles. Thus, this meshwork of proteins seems to be involved in the docking and priming of vesicles at the active zone (Garner et al., 2000) and may be part of the molecular machinery mediating neurotransmitter release. The fine regulation of this process is believed to be central to nervous system operation including higher functions such as learning, memory and cognition.

In vertebrates, several components of the complex presynaptic CAZ have been identified. In addition to the general cytoskeletal proteins actin and spectrin the large protein bassoon (420 kDa) (tom Diek et al., 1998; Shapira et al., 2003) is specifically found at the CAZ. This protein has been shown to be required for structural active zone formation and/or maintenance. Piccolo (530 kDa) (Fenster et al., 2000) contains several putative protein-protein interaction domains and together with bassoon is assumed to organize components of the active zone, including Rab3-interacting molecule (RIM1), Munc-13, and the CAZ-associated structural protein (CAST/ERC).

Vertebrate CAST/ERC was identified as a major component of the active zone by purifying synaptic densities from rat brain followed by electrophoresis and mass spectroscopy (Ohtsuka et al., 2002) and, independently, in a yeast-two-hybrid screen of a rat-brain cDNA library as a protein interacting with RIM1α PDZ domain (Wang et al., 2002). Several isoforms have been reported to be transcribed from two genes (Wang et al., 2002; Deguchi-Tawarada et al., 2004). Two isoforms (CAST1/ERC2 and CAST2α/ERC1b) are brain-specific and contain four coiled-coil domains as well as a C-terminal IWA motif essential for binding the PDZ domain of RIM1 (Ohtsuka et al., 2002). CASTs form a large oligomeric protein complex with the other known proteins of the CAZ (Munc-13, RIM1, piccolo, bassoon) and are believed to be involved in the molecular organization of presynaptic active zones (Ko et al., 2003) and in the release of neurotransmitter at this site (Takao-Rikitsu et al., 2004).

While most proteins found to be relevant for structure and/or function of the vertebrate nervous system are conserved in invertebrates, no homologs to the genes coding for bassoon

or piccolo have been detected in the *Drosophila* genome. Here, we identify the *Drosophila Cast* gene coding for a protein with homology to CAST/ERC, analyze the structure of this gene, and show that the *Drosophila* CAST proteins localizes at the presynaptic active zone.

Materials and Methods

Antibodies and immunohistochemistry: The mouse monoclonal antibody (MAB) nc82 is an Ig-G produced by a hybridoma clone from a large library generated against *Drosophila* heads (Hofbauer, 1991). The clone was selected because its antibody binds to all neuropil of larvae and adult flies. For immuno-labelling of whole mount preparations (Rein et al., 1999) the nc82 supernatant was used at 1:100 dilution. Rabbit anti-dynamin antiserum was kindly provided by Dr. V. Rodrigues (Tata Institute of Fundamental Research, Mumbai, India) and used at 1:400 dilution. The rabbit-α-DGluRIII antiserum was raised against the two peptide sequences (PRRSLDKSLDRTPKS+C and C+SGSNNAGRGEKEARV), affinity purified and used at a dilution of 1:200. Rabbit-α-PAK was kindly provided by N. Harden (The Hospital for Sick Children, Toronto, Canada) and used at 1:2000 dilution. Secondary antibodies were Alexa-568 labeled anti-mouse Ig and FITC-488 labeled anti-rabbit Ig.

2D-gel electrophoresis: 500 *Drosophila* heads were homogenized in 4 ml 2x Laemmli sample buffer, precipittated overnight at -20 $^{\circ}$C with 9 volumes of chilled acetone, washed 2 times with 90 % acetone, vaccum dried and used for sample preparation. The pellet was dissolved using minimum amounts of lysis buffer 1 (9.5 M Urea, 0.5 % SDS, 5 % 2-mercaptoethanol, 2 % Ampholines pH 2-11 (Serva, Heidelberg, Germany)), followed by lysis buffer 2 (9.5 M urea, 5% NP40 w/w, 5% 2-mercaptoethanol, 2 % Ampholines pH 2-11). Samples prepared in this manner were subjected to the standard NEPHGE followed by SDS PAGE.

Western blots: *Drosophila* heads were homogenized in 5x Laemmli sample buffer (8 heads in 20 µl). After fractionation by SDS PAGE proteins were transferred to a nitrocellulose membrane in prechilled western blot transfer buffer (25 mM Tris, 150 mM Glycin, 10% methanol, pH 8.3) for 2 hours at RT using a semi dry blotter (Peqlab, Erlangen, Germany). The membrane was blocked in 5 % milk-powder in 1x TBST (4 °C overnight). Blots were immunostained with monoclonal antibody nc82 and with horseradish peroxidase conjugated anti-mouse-Ig second antibody (Bio-Rad Laboratories GmbH, Muenchen, Germany) followed by ECL detection (Amersham Buchler GmbH, Braunschweig, Germany).

RT PCR: Total RNA isolated from fly heads (RNAsy midi kit, Qiagen, Hilden, Germany) was directly used or subjected to poly-A^{+} selection (Oligotex mRNA mini kit, Qiagen) and used

for reverse transcription using MMLV H-RT (Fermentas, St. Leon-Rot, Germany) or Superscript II RT (Invitrogen, Karlsruhe, Germany). RT PCR products were subjected to commercial sequencing (MWG, Ebersberg, Germany).

The following primers were used for the RT PCR experiments.

GGA CAA CCA GGT GGA TAT GG

ATC TTG TAG TCG GCC ACC TC

CCA AAC CGA AAC CCG AAA ACA GTC

GGT GCG CTC CAT CTC CTC CTT

CTA TGA ACC CAT ATG CAT AAA ACA CAT AC

AGT CTC GCG CTC CTT CTG C

ACA ACC TTT GGC AGG ACC AC

CGA CTG CAG GTT GTC GTA GT

GGC CGA CTA CAA GAT CAA GC

GGG CTC GAT CCA GTT CCT

CTG TAC CTT GTT CCT TTC AAC CA

CTC GGA GCT GCT GTG GTG

GCA TTA CCA TGC GTG GCA AC

CGC CAT AGA AGC CCA AAT AAA ATG

GTT GCG AAT ACG GGT GAC TTG

ATG GGC AGT CCA TAC TAC CG

TCC CGA ATG GGT ATG AAC TCG

TTG AAC GAG GCA CAC AAG TC

CGG CAG TTT CGG GTA ATC TA

Northern blots: 3 to 8 µg of poly-A$^+$-RNA from fly heads isolated as described above was blotted to nitrocellulose membrane (Amersham HybondNX, Amersham, Little Chalfond, GB) following standard protocols. The blot was probed with γ-^{32}P-ATP randomly labeled DNA (Hexalabel DNA labelling kit, Fermentas Inc, Hanover, MD). The following probes were used: RT PCR product combining CG12933 and CG30336; *Eco*RI digested and gel purified fragment of BDGP cDNA clone AT09405; complete cDNA containing transcribed regions of CG12933, CG30336 and CG30337; PCR product from CG12932; RP49 DNA as a control probe.

Bacterial expression of the partial Cast gene: BDGP cDNA clone AT09405 was amplified by PCR using AAT TGG ATC CAT GCG ACT CAA GGC CAA G and ACA TAA GCT TTC GCA TTG CAT TTA CAT GGT GTC AT, the PCR product was sub-cloned in PCR 4 TOPO

vector (Invitrogen), and the excised *Bam*HI – *Hind*III (recognition sequences underlined) fragment was directionally cloned into pET-28a vector (Novagen, Schwalbach, Germany). Bacterially expressed protein was induced with IPTG at 1 mM fc. Bacterial lysates were fractionated by SDS PAGE, subjected to western blot, and probed with the MAB nc82.

In situ hybridization: The 5' region of the *Cast* transcript was amplified from random primed adult head cDNA using the primers TR674 (5'- ATG GGC AGT CCA TAC TAC CGC GAC ATG-3') and TR687 (5'- CCC GGC ACT CTA GAT CCT TGA T-3') using Takara Taq Polymerase (RP 002 M, Takara Bio Inc., Shiga, Japan). The PCR product which corresponds to the first 700nt of CG12933 was cut and subcloned into precut pCR 2.1 (part in the TA cloning kit (K 2040-01, Invitrogen)). After identifying a clone with the right orientation the vector was cut with *Spe*1 to make the *in situ* probe with T7 (5'- AAT ACG ACT CAC TAT AG -3'). The antisense probe for the 3' region was made with T7 after cutting AT09405 with *Bam*HI. The sense control probe for the 3' region was made with SP6 (5'- GAT TTA GGT GAC ACT ATA G -3') after cutting AT09405 with SmaI. *In situs* were performed following the BDGP standard protocol (www.fruitfly.org).

Results

The MAB nc82 is widely used as a neuropil marker in confocal images of *Drosophila* brain (Fig. 1A), providing a structural framework for the "standard brain" and in conjunction with cell-specific stainings (Laissue et al., 1999; Rein et al., 1999; Jefferis et al., 2004; Wilson et al., 2004). The antibody allows for high transparency in immunofluorescent wholemount stainings, which makes it an ideal tool for 3-D reconstructions and optical sections deep below the brain's surface using confocal microscopy.

Presynaptic active zones are specifically labeled with MAB nc82

We first asked whether synapses and if so, which parts of them would be positive for MAB nc82 binding. In stainings of larval body wall muscles, MAB nc82 selectively labels discrete small spots (Fig. 1, red). These nc82-labeled spots are surrounded by dynamin (Fig 1B, green), a GTPase of the peri-active zone known to be involved in synaptic vesicle endocytosis. MAB nc82 shows a complementary distribution to dynamin. This suggests that MAB nc82 labels active zones. Similar results have been obtained with an antibody to α-adaptin (Wucherpfennig et al., 2003). To further test this, we stained for glutamate receptor subunit DGluRIII (Marrus et al., 2004) and DPAK (Harden et al., 1996) to directly label the

postsynaptic density region (PSDs) at individual synaptic sites (Fig. 1C, D green). The MAB nc82 label always directly oppose the center of the postsynaptic densities from the inside and are aligned with the centre of PSDs (Fig. 1C, D). This strongly suggests that the nc82-labeled spots represent the area of the presynaptic active zone, the region of the presynaptic plasma membrane, where synaptic vesicles dock, fuse and release their neurotransmitters. Having shown that MAB nc82 recognizes an epitope within the area of the presynaptic active zone we wanted to clarify the molecular nature of its antigen.

MAB nc82 identifies a protein of about 200 kDa which is encoded by a large genetic locus

In western blots of homogenized *Drosophila* heads the antibody recognizes two proteins of about 190 and 180 kDa apparent size (Fig. 2A). In order to identify the protein responsible for this reactivity, *Drosophila* head homogenates were subjected to 2-D gel electrophoresis and western blotting. After probing with MAB nc82 two signals of the expected molecular weight were detected. They were found near pH = 5.6 and could be matched in Coomassie stained gels with two spots, which were excised and subjected to MALDI-TOF mass spectroscopy (Toplab GmbH, Martinsried, Germany). Comparison of the peptide fragments with the *Drosophila* protein database reliably identified the two spots as isoforms of a protein which can be conceptually translated from the cDNA clone AT09405, corresponding to the predicted gene locus CG30337 (Berkeley *Drosophila* Genome Project; Flybase Consortium, 2003). We directly tested whether the cDNA AT09405 encoded protein contained the MAB nc82 epitope. In fact, the protein expressed from the cDNA in *E. coli* is recognized by MAB nc82 (data not shown). However, the calculated molecular weight of this protein is only 127.4 kDa while the MAB nc82 identified spots migrate in SDS gels near 190 and 180 kDa. Northern blots of head poly-A$^+$-RNA produced a strong signal at about 11 kb and a weak signal at about 2.3 kb (Fig. 2B, left lane). While the 3' end of the AT09405 cDNA appeared complete, we wanted to extend the 5' end of the mRNA sequence. We systematically performed BLAST homology searches of the computed *Drosophila* proteome with various vertebrate active zone proteins. We noted that the predicted gene CG12933, which is located 22 kb upstream of CG30337, showed significant similarity to CAST/ERC, a protein associated with the cytomatrix at the active zone (Ohtsuka et al., 2002; Wang et al., 2002). This led to the speculation that the two open reading frames CG30337 and CG12933 might actually belong to the same gene. We tested this by RT PCR using mRNA from third instar larvae and from adult flies. Sequencing the specific products in fact verified this, and

demonstrated moreover that the mRNA encoding the MAB nc82 antigen also incorporated the predicted gene CG30336, as well as a short exon between CG30336 and CG30337 (Fig. 3). The cDNA sequences we obtained from larvae and adults are largely identical. In some adult mRNAs the small exon 8 (33 bp) appears to be inserted by alternative splicing, replacing the amino acids VL at position 652-3 (Fig. 4) by 11 amino acids (MQLEEQTTLHK) in the encoded protein. Due to the significant homology of the N-terminus of the encoded protein (Fig. 4) and the specific localization at the active zone we propose that the identified gene codes for the *Drosophila* homolog of the mammalian CAST/ERC (dmCAST). We moreover compared the genomic organization as found in *Drosophila* with that of a highly diverged dipteran insect species, *Anopheles gambiae*. The predicted genes CG30336 and CG30337 correspond to the predicted *Anopheles* protein ENSANGP00000014221, while CG12933 corresponds to the neighboring protein ENSANGP00000002918. Indeed, both these predicted mRNAs can be connected and extended to then closely match the *Drosophila Cast* mRNA over the entire sequence of the encoded protein (Fig. 5). Further comparing the predicted *Anopheles* protein (agCAST), with dmCAST and the genomic region in *Anopheles*, we could predict two more exons, which were missing in the predicted protein ENSANGP00000014221. A fourth predicted gene (CG12932) is located between CG12933 and CG30336 in *Drosophila*, and thus could in principle represent a large alternatively spliced exon of the *Cast* gene (Fig. 3). We find that the *Anopheles* CG12932 homolog lies in a very similar relative genomic position (3R: 52 788 996 : 52 789 985, (Holt et al., 2002) when compared to the genomic organization of *Drosophila melanogaster*. However, we consistently failed to connect CG12932 to the *Cast* gene by RT PCR. Also, when we hybridized the northern blot shown in Fig. 2B (left lane) with a CG12932-specific probe amplified from genomic DNA, only a faint signal at 4.9 kb was detected (Fig. 2B, left lane). Based on these results it seems unlikely that the CG12932 open reading frame might represent or contain alternatively spliced *Cast* exons (cf. Fig. 3).

We constructed a 5560 bp cDNA composed of our RT PCR products and the cDNA AT09405, which now contains a complete open reading frame of the *Drosophila Cast* gene. This sequence has been deposited in the database GENEMBL (accession number pending). MAB nc82 recognizes an epitope, which maps to the C-terminal 1105 amino acids of the 1738 amino acid protein encoded by the composite cDNA. The calculated molecular weight (201.4 kDa) and the isoelectric point (6.28) of the *Drosophila* CAST protein are compatible with presumably the larger spot of the 2-D gel. At present, we cannot tell whether the second slightly smaller signal corresponds to a splice isoform or to a post-translational modification.

***Drosophila* CAST is specifically expressed in postmitotic differentiating neurons**

In order to identify the cells expressing the *Drosophila Cast* gene, *in situ* hybridization on *Drosophila* embryos was performed. For this, *Cast*-specific antisense RNA probes derived from both the C-terminal part (AT09405) as well as from the N-terminal part (CG12933, see Materials and Methods) were used, corresponding sense probes served as specificity controls. A strong specific label indicating *Cast* mRNA expression was detected from stage 12 on. *In-situ* labeling with C-terminal (Fig. 6A-E) and N-terminal probe (Fig. 6F) were identical, with both CNS (Fig. 6B-F) and PNS neurons (Fig. 6E) being strongly positive. The onset of *Cast* expression corresponds to the onset of neuronal differentiation including the formation of the axon (Broadie and Bate, 1993). No expression in non-neuronal tissues (Fig. 6A-F) like e.g. muscle was observed. Thus, the spatio-temporal expression profile of *Cast* mRNA is fully consistent with CAST being a component of the active zones at presumably all presynaptic terminals.

***Drosophila* CAST contains a large C-terminal part not present in mammalian CAST/ERC proteins but highly conserved within dipteran insects**

We finally analyzed the protein sequence of *Drosophila* CAST in more detail. The N-terminal part of the protein reveals high homology with all mammalian CAST proteins and the *Anopheles* homolog. The conservation is highest in regions corresponding to the first 2 coiled-coiled domains of CAST (Fig. 4, for the domain structure of CAST see Ohtsuka et al., 2002). Both, the *Drosophila* as well as the *Anopheles Cast* gene encodes a large C-terminal region (Fig. 5), which is not present in mammalian CASTs and for which no homologous proteins apart from insect CASTs are found. The high level of conservation between *Drosophila* and *Anopheles* within this domain, however, indicates that this part is likely to be functionally important for insect CAST function.

Analysis of the amino acid sequence of *Drosophila* CAST predicts a possible nuclear localization (not supported by immunohistochemistry), numerous possible phosphorylation sites, no transmembrane domains, two leucine zipper domains, and a glutamine-rich C-terminus. However, no PDZ interaction motif for RIM interaction as found in several mammalian CAST forms seems to be present in the insect CAST forms. In addition, significant sequence similarities to myosin heavy chain, plectin, and restin are found, mainly due to coiled-coil regions and leucine zipper domains of the proteins. In the *Drosophila* proteome similarities to LVA (larva lamp), an actin-, spectrin- and microtubule binding

protein, to CLIP-190, MTOR (Megator), ZIP (zipper), and MHC (myosin heavy chain) are detected.

Discussion

Over the last years, some insight into assembly and molecular composition of the cytomatrix found at presynaptic active zones has been gained (Landis et al., 1988; Hirokawa et al., 1989; Garner et al., 2000; Dresbach et al., 2001; Phillips et al., 2001; Rosenmund et al., 2003). Cytoskeletal elements like actin and spectrin, as well as large active zone specific proteins like piccolo and bassoon, seem to form a structural meshwork. Both piccolo and bassoon contain several putative protein-protein interaction domains, which are assumed to help organizing several components of the active zone. The third coiled domain of bassoon contains a motif that is highly homologous to the corresponding region of piccolo and has been shown to bind in competition to piccolo the second coiled coil domain of CAST1/ERC2 (Takao-Rikitsu et al., 2004). This binding of CAST1/ERC2 to bassoon seems to be of functional relevance. When a GST fusion of the bassoon binding site in CAST1/ERC2 is injected into neurons the EPSP amplitude was reduced by 30% within 70 min. This suggests that the binding of CAST/ERC and bassoon is involved in neurotransmitter release (Takao-Rikitsu et al., 2004). CAST1/ERC2 itself has furthermore been shown to bind RIM1 via the C-terminal PDZ motif IWA (Ohtsuka et al., 2002). RIM1 is a target of the RAB3A small G protein, which is implicated in vesicle docking. RIM1 interacts with Munc13-1 implicated in vesicle priming. This complex might control together with vesicular proteins the recruitment of vesicles and their subsequent fusion with the presynaptic membrane. However, so far no coherent picture has emerged of how at active zones Ca^{2+} dependent release is controlled in a spatially restricted manner.

While there is a wealth of information on the ultra-structure of insect synapses (Atwood et al., 1993; Jia et al., 1993; Atwood and Cooper, 1996), the molecular composition of their synaptic active zones is completely unknown. Our work shows that the *Drosophila* homolog of the proteins encoded by the ELKS/Rab6-IP2/CAST (ERC) gene family localizes at the presynaptic active zones presumably of all neuronal terminals. It thereby provides an entry point to study active zone formation and function in *Drosophila*. The open reading frame of the identified cDNA corresponds in size to the protein recognized by MAB nc82. The fact that the prominent northern blot signal is about 5.5 kb larger than the known cDNA indicates that the mRNA contains a large 5' UTR and/or a large 3'UTR. The signal at 2.3 kb cannot be interpreted with present cDNA information. Both signals were identically

reproduced in two independent blots hybridized with probes specific for CG12933 and CG30336, or specific for CG30337, or containing the entire cDNA sequence. No difference was observed with these three probes. When, on the other hand, a probe specific for CG12932, the ORF lying between CG12933 and CG30336, was used, only a faint signal was obtained that did not match the previous signals. It is therefore assumed that CG12932 represents an independent gene nested within the large intron 4 of the *Cast* gene.

In mammals CAST isoforms apparently have both neuronal and non-neuronal roles. *Drosophila* CAST seems to correspond to the neuronal CAST isoforms, while the non-neuronal functions might be vertebrate specific. To our knowledge, besides the protein described here the only published molecule localized specifically at *Drosophila* presynaptic active zones is the Ca^{2+} channel Cacophony, which seems to be responsible for providing the calcium trigger for evoked neurotransmitter release (Kawasaki et al., 2004). Our findings indicate, however, that the molecular structure of the presynaptic active zone might be more conserved between vertebrate and insect synapses than thought previously due to the lack of obvious piccolo and bassoon homologs in insects. We are confident, that in the future studying active zone formation and function in *Drosophila* will be a valuable addition to similar studies in vertebrates, especially considering the powerful genetic tools available for *Drosophila*. In particular, it will be interesting to address the function of the CAST/ERC protein family by genetic knock-out and knock-down experiments and to study the roles of the different domains present in the *Drosophila* CAST isoforms in detail.

References

Atwood HL, Cooper RL: Assessing ultrastructure of crustacean and insect neuromuscular junctions. J Neurosci Methods 1996, 69(1):51-58.

Atwood HL, Govind CK, Wu CF: Differential ultrastructure of synaptic terminals on ventral longitudinal abdominal muscles in *Drosophila* larvae. J Neurobiol 1993, 24(8):1008-1024.

Broadie KS, Bate M: Development of the embryonic neuromuscular synapse of *Drosophila* melanogaster. J Neurosci 1993, 13(1):144-166.

Deguchi-Tawarada M, Inoue E, Takao-Rikitsu E, Inoue M, Ohtsuka T, Takai Y: CAST2: identification and characterization of a protein structurally related to the presynaptic cytomatrix protein CAST. Genes Cells 2004, 9(1):15-23.

Tom Dieck S, Sanmarti-Vila L, Langnaese K, Richter K, Kindler S, Soyke A, Wex H, Smalla KH, Kampf U, Franzer JT et al: Bassoon, a novel zinc-finger CAG/glutamine-repeat

protein selectively localized at the active zone of presynaptic nerve terminals. J Cell Biol 1998, 142(2):499-509.

Dresbach T, Qualmann B, Kessels MM, Garner CC, Gundelfinger ED: The presynaptic cytomatrix of brain synapses. Cell Mol Life Sci 2001, 58(1):94-116.

Fenster SD, Chung WJ, Zhai R, Cases-Langhoff C, Voss B, Garner AM, Kaempf U, Kindler S, Gundelfinger ED, Garner CC: Piccolo, a presynaptic zinc finger protein structurally related to bassoon. Neuron 2000, 25(1):203-214.

Flybase Consortium: The FlyBase database of the *Drosophila* genome projects and community literature. Nucleic Acids Res 2003, 31(1):172-175. http://flybase.org/.

Garner CC, Kindler S, Gundelfinger ED: Molecular determinants of presynaptic active zones. Curr Opin Neurobiol 2000, 10(3):321-327.

Harden N, Lee J, Loh HY, Ong YM, Tan I, Leung T, Manser E, Lim L: A *Drosophila* homolog of the Rac- and Cdc42-activated serine/threonine kinase PAK is a potential focal adhesion and focal complex protein that colocalizes with dynamic actin structures. Mol Cell Biol 1996, 16(5):1896-1908.

Hirokawa N, Sobue K, Kanda K, Harada A, Yorifuji H: The cytoskeletal architecture of the presynaptic terminal and molecular structure of synapsin 1. J Cell Biol 1989, 108(1):111-126.

Hofbauer A: Eine Bibliothek monoklonaler Antikörper gegen das Gehirn von *Drosophila* melanogaster. Habilitation thesis. Würzburg: University of Würzburg; 1991.

Holt RA, Subramanian GM, Halpern A, Sutton GG, Charlab R, Nusskern DR, Wincker P, Clark AG, Ribeiro JM, Wides R et al: The genome sequence of the malaria mosquito Anopheles gambiae. Science 2002, 298(5591):129-149.

Jefferis GS, Vyas RM, Berdnik D, Ramaekers A, Stocker RF, Tanaka NK, Ito K, Luo L: Developmental origin of wiring specificity in the olfactory system of *Drosophila*. Development 2004, 131(1):117-130.

Jia XX, Gorczyca M, Budnik V: Ultrastructure of neuromuscular junctions in *Drosophila*: comparison of wild type and mutants with increased excitability. J Neurobiol 1993, 24(8):1025-1044.

Kawasaki F, Zou B, Xu X, Ordway RW: Active zone localization of presynaptic calcium channels encoded by the cacophony locus of *Drosophila*. J Neurosci 2004, 24(1):282-285.

Ko J, Na M, Kim S, Lee JR, Kim E: Interaction of the ERC family of RIM-binding proteins with the liprin-alpha family of multidomain proteins. J Biol Chem 2003, 278(43):42377-42385.

Laissue PP, Reiter C, Hiesinger PR, Halter S, Fischbach KF, Stocker RF: Three-dimensional reconstruction of the antennal lobe in *Drosophila* melanogaster. J Comp Neurol 1999, 405(4):543-552.

Landis DM, Hall AK, Weinstein LA, Reese TS: The organization of cytoplasm at the presynaptic active zone of a central nervous system synapse. Neuron 1988, 1(3):201-209.

Marrus SB, Portman SL, Allen MJ, Moffat KG, DiAntonio A: Differential localization of glutamate receptor subunits at the *Drosophila* neuromuscular junction. J Neurosci 2004, 24(6):1406-1415.

Ohtsuka T, Takao-Rikitsu E, Inoue E, Inoue M, Takeuchi M, Matsubara K, Deguchi-Tawarada M, Satoh K, Morimoto K, Nakanishi H et al: Cast: a novel protein of the cytomatrix at the active zone of synapses that forms a ternary complex with RIM1 and munc13-1. J Cell Biol 2002, 158(3):577-590.

Phillips GR, Huang JK, Wang Y, Tanaka H, Shapiro L, Zhang W, Shan WS, Arndt K, Frank M, Gordon RE et al: The presynaptic particle web: ultrastructure, composition, dissolution, and reconstitution. Neuron 2001, 32(1):63-77.

Rein K, Zockler M, Heisenberg M: A quantitative three-dimensional model of the *Drosophila* optic lobes. Curr Biol 1999, 9(2):93-96.

Rosenmund C, Rettig J, Brose N: Molecular mechanisms of active zone function. Curr Opin Neurobiol 2003, 13(5):509-519.

Shapira M, Zhai RG, Dresbach T, Bresler T, Torres VI, Gundelfinger ED, Ziv NE, Garner CC: Unitary assembly of presynaptic active zones from Piccolo-Bassoon transport vesicles. Neuron 2003, 38(2):237-252.

Stocker RF, Heimbeck G, Gendre N, de Belle JS: Neuroblast ablation in *Drosophila* P[GAL4] lines reveals origins of olfactory interneurons. J Neurobiol 1997, 32(5):443-456.

Takao-Rikitsu E, Mochida S, Inoue E, Deguchi-Tawarada M, Inoue M, Ohtsuka T, Takai Y: Physical and functional interaction of the active zone proteins, CAST, RIM1, and Bassoon, in neurotransmitter release. J Cell Biol 2004, 164(2):301-311.

Wang Y, Liu X, Biederer T, Sudhof TC: A family of RIM-binding proteins regulated by alternative splicing: Implications for the genesis of synaptic active zones. Proc Natl Acad Sci U S A 2002, 99(22):14464-14469.

Wang Y, Okamoto M, Schmitz F, Hofmann K, Sudhof TC: Rim is a putative Rab3 effector in regulating synaptic-vesicle fusion. Nature 1997, 388(6642):593-598.

Wilson RI, Turner GC, Laurent G: Transformation of olfactory representations in the *Drosophila* antennal lobe. Science 2004, 303(5656):366-370.

Wucherpfennig T, Wilsch-Brauninger M, Gonzalez-Gaitan M: Role of *Drosophila* Rab5 during endosomal trafficking at the synapse and evoked neurotransmitter release. J Cell Biol 2003, 161(3):609-624.

Figure
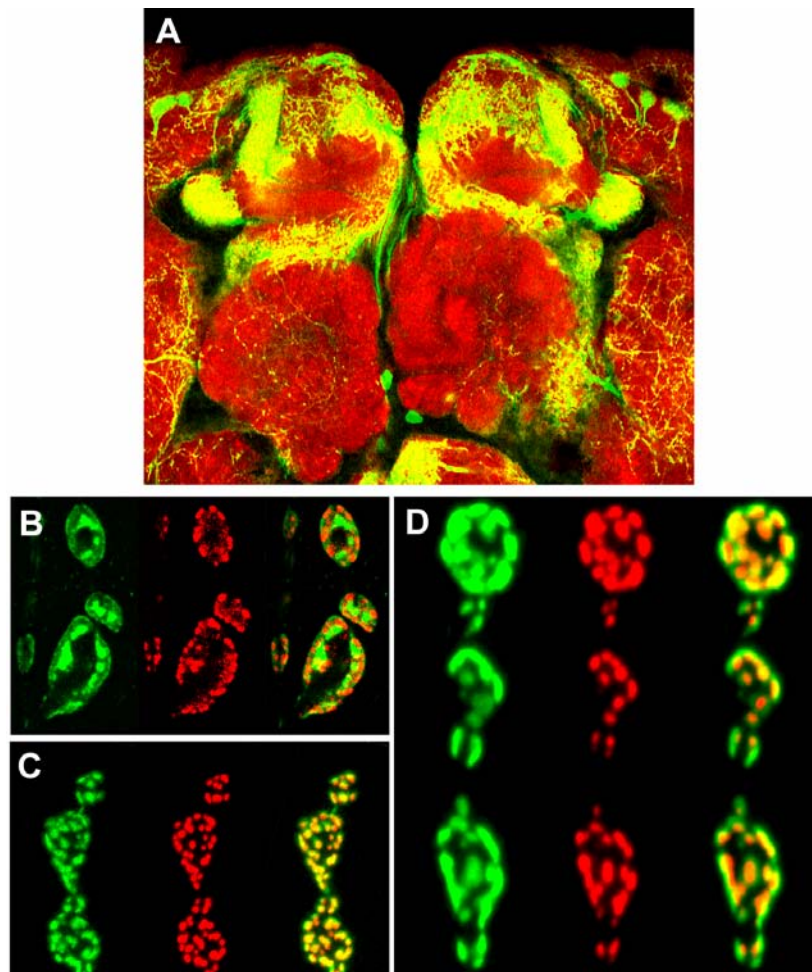
Figure 1

A -Use of the MAB nc82 antibody as neuropil marker in confocal images of *Drosophila* brain

Confocal section showing Gal4-driven expression of cameleon-2.1 (green) on the background of general neuropil staining obtained by the antibody nc82 (red) (Figure kindly provided by Dr. A. Fiala).

B –D- MAB nc82 labels a component of the presynaptic active zone at neuromuscular synapses of *Drosophila*

B-D, Neuromuscular synaptic boutons in wild type *Drosophila* larvae immunostained with MAB nc82 (red) and with antisera against dynamin (green, B), DGluRIII (green, C) or DPAK (green, D). Right panels in B-D: merged images
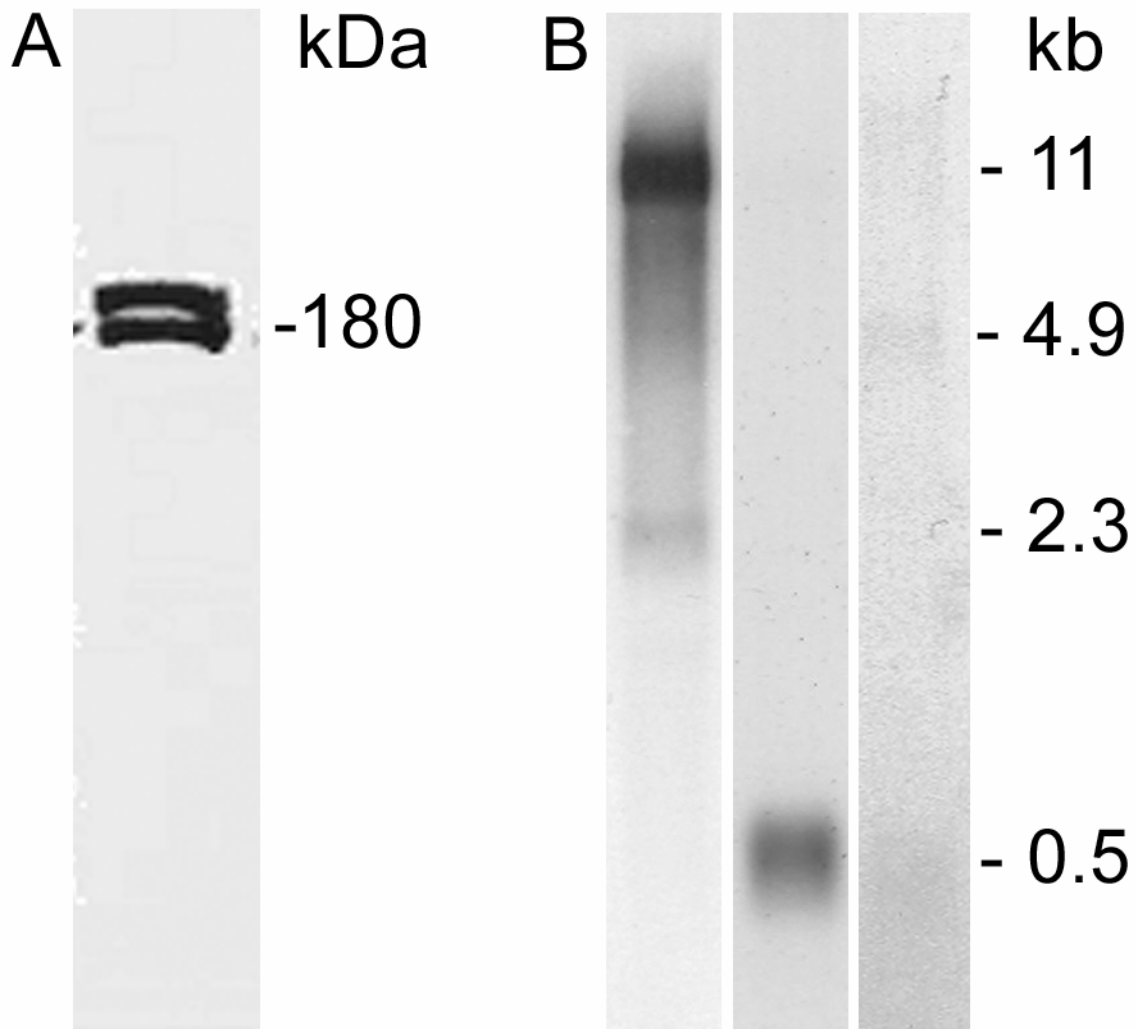
Figure 2

Western blot of homogenized *Drosophila* heads probed with MAB nc82 and Northern blot of poly-A+-RNA from *Drosophila* heads

A, The antibody recognizes two protein isoforms of about 190 and 180 kDa apparent size. B, An 11 kb transcript is recognized by the complete *Cast* cDNA (left lane), a rare transcript is detected by a CG12932-specific probe (right lane), control hybridization with an rp49-specific probe (middle lane)
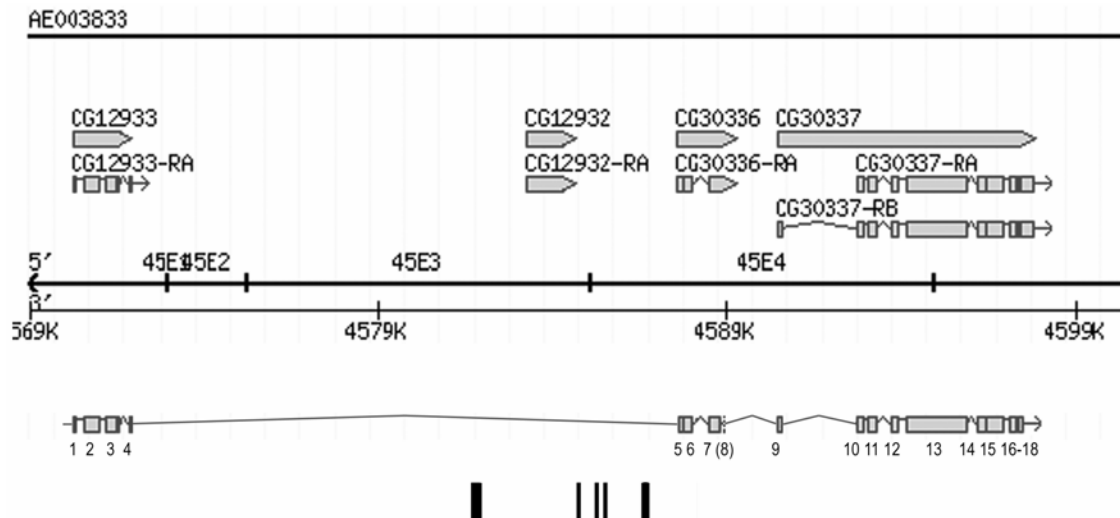
Figure 3

The *Drosophila Cast* gene, modified from flybase

The *Drosophila Cast* gene consists of 18 Exons derived from three loci (CG12933, CG30336 and CG30337), which were previously annotated as independent genes

Figure 4

Alignment of two insect and two vertebrate CASTs

Two vertebrate CASTs, the human KIAA0378 (hsCAST1/ERC2) and the human Rab6-IP-2δ

(hsCAST2β/ERC1a) were aligned with the N-terminal half of two insect CASTs: the

Drosophila melanogaster CAST (dmCAST) and the *Anopheles gambiae* CAST (agCAST)

183
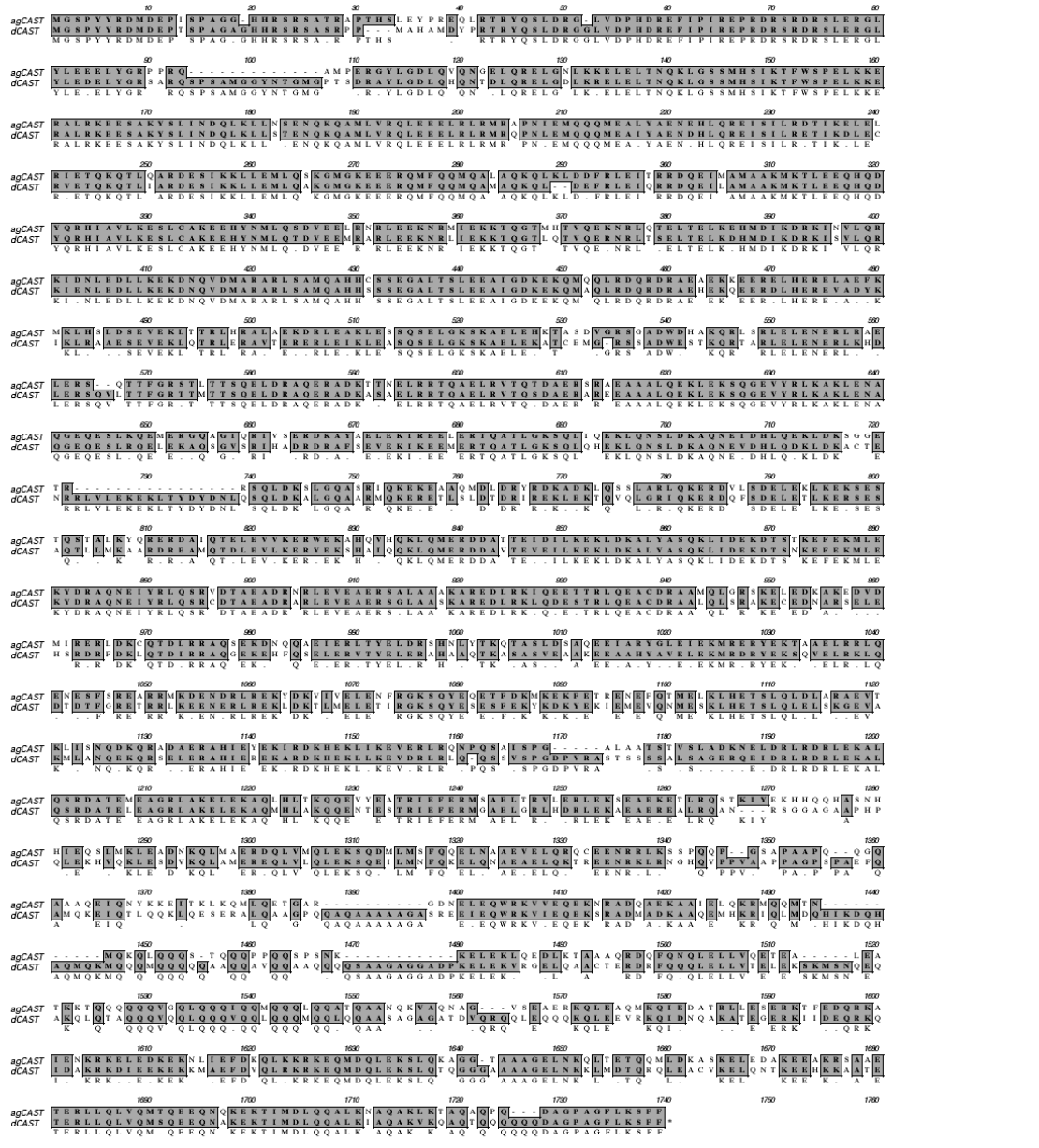
Figure 5

Alignment of dmCAST and agCAST

While the homology between insect and vertebrate CASTs is restricted to the N-terminal half of the CAST protein, there is a high homology between dmCAST and agCAST both in the N-terminal and the C-terminal region of the protein.
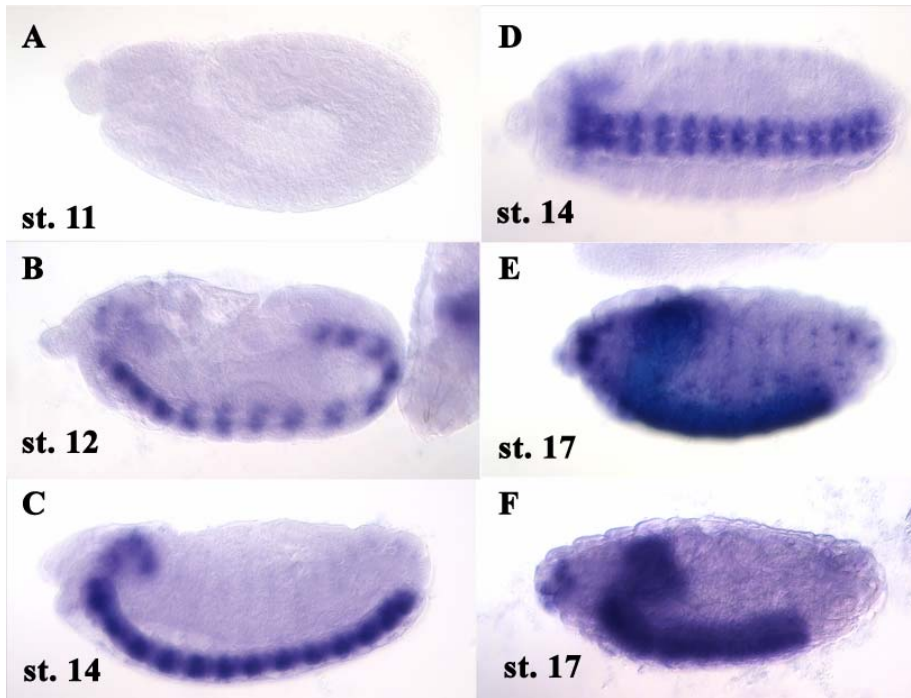
Figure 6

***Drosophila* CAST is specifically expressed in postmitotic / differentiating neurons**

In situ hybridization of *Drosophila* embryos. A-E, the 3' part of the *Cast* cDNA, F, the 5' part of the *Cast* cDNA was used to generate the anti-sense probe.

A strong specific staining indicating *Cast* mRNA expression was detected beginning from stage 12 (compare A and B). Both, CNS and PNS neurons are strongly positive. No expression in non-neuronal tissues like e.g. muscle was observed. The spatio-temporal expression profile of *Cast* mRNA is fully consistent with CAST being a component of the active zones at presumably all presynaptic terminals. The sense probe was negative (not shown).

6.5 Manuscript 3:

Four different subunits are essential for expressing the synaptic glutamate receptor at neuromuscular junctions of *Drosophila*

Four different subunits are essential for expressing the synaptic glutamate receptor at neuromuscular junctions of *Drosophila*

Gang Qin[1], Tobias Schwarz[1], Robert J. Kittel[1], Andreas Schmid[1], Tobias M. Rasse[1], Dennis Kappei[1], Evgeni Ponimaskin[2], Manfred Heckmann[3], and Stephan J. Sigrist[1]°

° corresponding author (**ssigris@gwdg.de**)

(1)European Neuroscience Institute Göttingen, Max-Planck-Society, Waldweg 33, 37073 Göttingen (Germany)

(2) Departments of Neuro and Sensory Physiology, Medical School at the University of Göttingen, Humboldtallee 23, 37073 Göttingen (Germany)

(3) Physiologisches Institut, Hermann-Herder-Str. 7, 79104 Freiburg (Germany)

Three ionotropic glutamate receptor subunits, designated GluR-IIA, GluR-IIB and GluR-III have been identified at neuromuscular junctions of *Drosophila*. While GluR-IIA and GluR-IIB are redundant for viability, it was recently shown that GluR-III is essential for both the synaptic localization of GluR-IIA and GluR-IIB and the viability of *Drosophila*. Here we identify a fourth and a fifth subunit expressed in the neuromuscular system, which we name GluR-IID and GluR-IIE. Both new subunits we show to be necessary for survival. Moreover, both GluR-IID and GluR-IIE are required for the synaptic expression of all other glutamate receptor subunits. All five subunits are interdependent of for receptor function, synaptic receptor expression and viability. This indicates that synaptic glutamate receptors incorporate the GluR-III, GluR-IID and GluR-IIE subunit together with either GluR-IIA or GluR-IIB at the *Drosophila* neuromuscular junction. At this widely used model synapse the assembly of four different subunits to form an individual glutamate receptor channel may thus be obligatory. This study opens the way for a further characterization of *in vivo* glutamate receptor assembly and trafficking using the efficient genetics of *Drosophila*.

Ionotropic glutamate receptors mediate most excitatory synaptic transmission in our nervous system. One subgroup of glutamate receptors, the so called non- *N*-methyl-D-aspartate (NMDA) type glutamate receptor channels, preferentially mediate fast synaptic transmission (Dingledine et al., 1999).

Ionotropic glutamate receptors are supposed to be composed of four subunits in total (Laube et al., 1998; Mano and Teichberg, 1998; Rosenmund et al., 1998). The functional properties of individual non-NMDA receptors, such as single channel conductance, Ca^{2+}-permeability and rectification are subunit dependent and can be controlled by alternative splicing and RNA editing at key positions of individual subunits (Seeburg, 1993; Mayer and Armstrong, 2004). In addition, subunit composition is important for the assembly, trafficking, insertion, synaptic localization, and anchoring of non-NMDA receptors in synapses (Malinow and Malenka, 2002; Bredt and Nicoll, 2003). Many ligand-gated receptor channels such as the glycine receptor and the nicotinic acetylcholine receptor have been shown to have fixed subunit stoichiometries (Colquhoun and Sivilotti, 2004). Nevertheless, initial work implied that non-NMDA glutamate receptors could consist of various subunit combinations. However, assembly of non-NMDA receptors in mammals is assumed to be restricted in that an individual non-NMDA receptor is composed of no more than two different subunits. (Ayalon and Stern-Bach, 2001; Mansour et al., 2001; Sun et al., 2002; Schorge and Colquhoun, 2003). Although elegant work using functional and/or optical subunit labeling has enabled the study of assembly mode, trafficking, insertion and anchoring of individual non-NMDA receptors (reviewed in: Malinow and Malenka, 2002), the subunit composition of entire native receptors still remains difficult to address under physiological conditions at synapses.

Here, we use the glutamatergic neuromuscular junction (NMJ) of *Drosophila* to explore the subunit composition of a synaptic non-NMDA glutamate receptor *in vivo*. This synapse is widely used for functional studies of synaptic transmission (Bellen, 1998; Gramates and Budnik, 1999; Featherstone and Broadie, 2000; Koh et al., 2000) and expresses postsynaptic glutamate receptors which are homologous to vertebrate non-NMDA glutamate receptors (Schuster et al., 1991; DiAntonio et al., 1999; Marrus et al., 2004). Subunit composition has been shown to both regulate biophysical properties of

glutamate receptors and to control synapse formation and function in this model system (DiAntonio et al., 1999; Sigrist et al., 2000; Sigrist et al., 2002b). Our goal was to turn this established experimental preparation into a model system in which the subunit composition of the postsynaptic non-NMDA glutamate receptors can be fully controlled. Therefore, we searched for additional essential non-NMDA receptors at the neuromuscular junction of *Drosophila*. We can identify two additional neuromuscular glutamate receptor subunits, GluR-IID and GluR-IIE, which are essential for viability. GluR-IID can be shown to be expressed within the postsynaptic densities of all NMJs. Knock out and rescue experiments with the 5 subunits in total are performed to address the *in vivo* subunit composition of the synaptic glutamate receptors in this preparation. The data presented below suggest that here individual synaptic glutamate receptor channels may contain not only two but four different subunits.

Material and Methods

Microarray analysis and quantitative real-time PCR

Microarray experiments were performed using Affymetrix *Drosophila* Genechips and standard protocols as described in the Affymetrix genechip user manual (Affymetrix, Inc.). RNA was isolated from whole animal or larval body wall preparations (epidermis with body-wall muscles attached) of mid-stage 3rd instar wild type larvae (CS10) reared at 25°. Biotinylated cRNAs were prepared from double stranded cDNA pools and used to probe Affymetrix high-density oligonucleotide arrays. Hybridization, staining, and washing was done according to the instructions in the user´s manual. Data analysis was performed via Microarray Suite 4.0.

For real-time PCR based mRNA quantification, the same RNA samples as also used for chip analysis were reverse transcribed and PCR amplified by Omniscript RT Kit and QuantiTect SYBY Green PCR Kit (Qiagen). Primers were designed via PrimerExpress v2.0. Primers used were for *tbp-1*: 5´AAGCCCGTGCCCGTATTATG3´ and 5´AAGTCATCCGTGGATCGGGAC3´; *GluR-IIA*: 5´CCCAGATTGGCGAGCAGAT3´ and 5´CCGGTAATCAGAGCCCAGTG3´; *GluR-IIB*: 5´GATGATGGCCAGTTCGACATG3´ and 5´TCAGCACCACGAACAGTCCA3´; *GluR-IIC/III*: 5´CCTCCATCATGACAGCAGGA3´ and 5´GCACCTGTGGACTTCTCGGT3´; *GluR-IID*: 5´ACGTCATCGAACTGCAAACCA3´ and 5´TCGCTGGAACTCGAAGTCCTT3´; *GluR-IIE*: 5´TGGCTGCCTTTTTGACCATC3´and 5´ACCATCCTTGTTATCGGCCAG3´.

Real-time quantitative PCR was performed in GeneAmp 5700 Sequence Detection System (PE Biosystem), data were analyzed with Excel.

Genetics and molecular biology

GluR-IID and *GluR-IIE* genetics. The *GluR-IID* and *GluR-IIE* loci are situated at 92F4. In a recently released pBac transposon insertion collection (Thibault et al., 2004), a *piggyBac* transposon (pBac{RB}e01443, #17952,) was found to be inserted into intron 6 at amino acid position 427 of the *GluR-IID* open reading frame. This allele *GluR-IID^{e01443}* is embryonic lethal both homozygous, over *Df(3R)H-B79* (Bloomington *Drosophila* stock center) which deletes a large genomic region including the *GluR-IID* and *GluR-IIE* locus, and over deficiency *GluR-IID&-IIE^{E3}* (see below). For *GluR-IIE*, imprecise excision screening was performed using the P-element line EP28753 (commercially available with Genexcel), which is inserted ~150bp downstream of the end of the *GluR-IIE* transcript. In brief, P-element EP28753 was remobilized by crossing to the Δ2-3 transposase source, white eye progenies were selected and mated individually, then single fly genomic PCR reactions were performed to map deletions flanking the P-element insertion site. Nearly 1,000 eye color revertants were checked, one line (*GluR-IIE^{E1}*) was found to delete 1.2 kb flanking region in direction of the *GluR-IIE* gene, removing the C-term and transmembrane domain 4 of GluR-IIE. *GluR-IIE^{E1}* is embryonic lethal when homozygous, over *df(3R)H-B79* and over *GluR-IID&-IIE^{E3}*. *GluR-IID&-IIE^{E3}* is a larger deletion also recovered from exision mutagenesis of EP28753, which removes both *GluR-IIE* and *GluRIID* and thus was used in combination with either *GluR-IID^{e01443}* or *GluR-IIE^{E1}* deficiency to study *GluR-IID* and *GluR-IIE* null mutant situations.

Double mutants in *GluR-IIA* and *GluR-IIB* were described previously (Petersen et al., 1997; DiAntonio et al., 1999). In short, *GluR-IIA* and *GluR-IIB* double mutant embryos were recovered by crossing *df(2L)GluR-IIA&B^{SP22}* to *df(2L)cl^{h4}*, mutant embryos were selected using GFP-marked balancer chromosomes. *GluRIIA^{hypo}, GluR-IIB^{null}* larvae have an extremely reduced amount of GluR-IIA and no GluR-IIB expression. For this, a genomic fragment of GluR-IIA encompassing promotor region and the whole open reading frame while missing most part of the 3´-UTR was used. This transgene still produces full length GluR-IIA while in dramatically reduced amount due a loss of message stability (Qin and Sigrist, manuscript in preparation). This

construct was expressed from *pUAST* (using the *GluR-IIA* endogenous promotor). A single transgene copy rescues embryos null for both *GluR-IIA* and *GluR-IIB* (*df(2L)GluR-IIA&B^{SP22}/df(2L)cl^{h4}*) giving *GluRIIA^{hypo}, GluR-IIB^{null}* larvae (see results). The genomic fragment with 3′-UTR deletion was produced as follows: an *EcoR*I/ *Xho*I fragment (5.6 Kb) from BAC clone RPCI-98-35L07 containg the *GluR-IIA* gene including 1.3 kb sequence 5' of the ATG was subcloned into *pSL1180*. Inserting this *EcoR*I/ *Xho*I fragment into pUAST gave a "wild type *GluR-IIA* rescue construct". For the 3′-UTR deleted version, this clone was cut with *Nco*I and *Xho*I, end-blunted and religated, then a *EcoR*I/ *Asp*718 fragment (4.7 Kb) was inserted into pUAST. All constructs were confirmed by double-strand sequencing.

Transgenic rescue constructs. Genomic fragments covering the *GluR-IID* gene and *GluR-IIE* gene were generated by PCR using for IID 5′GGTCTAGAGCGGCCGCGGCCACGAACTGACCCACGGTTTC3′ and 5′GCGGCCCTCGAGCGACGTCAAGGATGTGCCCAC3′ and for IIE 5′GGTCTAGAGCGGCCGCACCTCCCCAAGCTGTCAACTTC3′ and 5′GCGGCCCTCGAGACTGCTCAAAGCTGCTGCCCTG3′. The products were double strand sequenced and cloned into *pUAST*. Several independent lines of transgenic animals were generated. For overexpression studies, *UAS-GluRIID and UAS-GluRIIE* were generated by introducing the full length cDNA into the transformation vector *pUAST*. Full-length cDNAs of *GluR-IID* (RE24732) and *GluR-IIE* (RE07945) were obtained from Berkeley Drosophila Genome Project cDNA libraries.

The construct for inducible RNA interference (RNAi-*GluR-IIE*) was made based on the *pUASTi* plasmid (contains an intron between insertion sites for sense and antisense frgaments; generous gift by Amin Ghabria, Krasnow lab). Selected cDNA fragments coving part of 5'-UTR and coding region were PCR-amplified by using the following primer pairs: 5′GCGCGCCTCGAGCTGTTCGGGAAACTCAAGAAT3′ and 5′GGTCTAGAGCGGCCGCCGTGGTTAGCTCGTTCAAAATG3′ for fragment 1 (sense) and 5′GCTGGTACCTGTTCGGGAAACTCAAGAAT3′ and 5′GCGTCTAGATCGTGGTTAGCTCGTTCAAAATG3′ for fragment 2 (antisense).

The two fragments were inserted into pUASTi plasmid sequentially and verified by sequencing. Several independent lines of transgenic animals carrying *UAS-GluR-IIE* were generated.

To express GluR-IIE-GFP in SF9 cells, a *Hind*III fragment covering the EGFP insertion site (position 880 of GluR-IIE) was cut from full-length *GluR-IIE* cDNA (RE07945) and subcloned into *pSL1180*. On this vector, "circular PCR" with primers 5′GGCAGATGTGTATAAGAGACAGTCGCCAGTCCTCGATGTCAGTAGCTT3′ and 5′CGGGCGCGCCGCCCTTGTACAGCTCGTCCATGCCGAGA3′ was performed and the resulting fragment was blunt end ligated with an EGFP encoding fragment, which was PCR amplified using 5′GGCGCGCCGAGCAAGGGCGAGGAGCTGTTCACCGG3′ and 5′CGGGCGCGCCGCCCTTGTACAGCTCGTCCATGCCGAGA3′ from a EGFP containing vector (Clontech). Correct orientation of EGFP was verified by PCR and sequencing; then the *Hind*III fragment containing EGFP sequence was put back into the full-length cDNA clone and the reading frame was verified by PCR and sequencing; finally the full-length *DGluRIIE* cDNA tagged with EGFP was transferred into *pFastBac* (Invitrogen). Baculovirus expression was performed as described (Swan et al., 2004).

Stainings

In situ hybridization. Whole mount embryonic and larval body wall preps *in situ* hybridizations were performed essentially as described previously (Tautz and Pfeifle, 1989). For preparing antisense RNA probes, both RE24732 (*GluR-IID*) and RE07945 plasmids (*GluR-IIE*) were cut with *Not*I and *in vitro* transcribed using T3 RNA Polymerase.

Immunohistochemistry. Rabbit anti-GluR-IIC/III antibodies were generated against a c-terminal close peptide of GluR-IIC/III (PRRSLDKSLDRTPKS). Rabbit anti-GluR-IID antibodies were

generated against a c-terminal peptide of GluR-IID (ESLKTDSEENMPVED). Both sera were affinity purified and used at 1:500 dilution. Other primary antibodies were used at the following concentrations: mouse monoclonal anti-GluR-IIA antibody (8B4D2, DSHB), 1:100; Goat anti-HRP-Cy5, 1:250; mouse anti-FasII (1D4, DSHB), 1:40; mouse anti-DLG (DSHB), 1:500; Nc82 (generous gift of Erich Buchner, Würzburg), 1:100. Except for samples stained with 8B4D2, which were fixed for 5 min with cold methanol, all of the other stainings were fixed for 10 min with 4% paraformaldehyd.

Dissection and immunostaining. Mid stage 3rd instar larvae were put on a dissection plate, both ends were fixed by fine pins and the specimen was covered by a drop of ice cold HL-3 solution (see below). Dissection scissors were used to make a small hole at the dorsal midline of the larva (near to the posterior end) which was then completely opened along the dorsal midline from the hole to the anterior end. The epidermis was stretched flat and pinned down, then the internal organs and central nervous system were removed carefully with forceps. Late stage embryos (20-22hrs after egg laying) were dissected on sylgard plates, fixed with fine clips and opened using a pair of sharp tungsten needles. The dissected samples were fixed and then incubated with primary antibodies overnight, followed by fluorescence-labelled secondary antibodies (Dianova) and mounted in VectaShield mounting media (Vector Laboratories).

Imaging and analysis. Imaging of embryonic and larval body wall preparations was performed on a Leica DM IRE2 microscope equipped with a Leica TCS SP2 AOBS scanhead, using a Leica HCX PL Apo CS 63x 1.32 NA OIL UV objective. Image processing was performed using ImageJ and Photoshop. Epifluoresence images were taken on a Zeiss Axioscope with Axiocam camera, using a 100x oil objective of NA 1.4.

Electrophysiology

Intracellular recordings were made at 22 °C from muscle fiber 6 of abdominal segments 2 and 3, of late third instar larvae. Larvae were dissected in ice-cold, calcium-free haemolymph-like saline (HL-3) (Stewart et al., 1994). Composition of the HL-3 solution was (in mM): NaCl 70, KCl 5, MgCl$_2$ 20, NaHCO$_3$ 10, trehalose 5, sucrose 115, HEPES 5, pH adjusted to 7.2. Larval fillets were rinsed with 2ml of HL-3 saline containing 1 mM Ca^{2+}, before being transferred to the recording chamber where two-electrode voltage clamp (TEVC) recordings were performed in 1mM extra cellular Ca^{2+}. The larval NMJ was visualized with a fixed-stage upright microscope (Olympus, 40x water immersion lens). Whole muscle recordings of both miniature and evoked postsynaptic currents were recorded in TEVC mode (AxoClamp 2B, Axon Instruments) using sharp microelectrodes (borosilicate glass with filament, 1,5mm outer diameter) with resistances of 15-35 MΩ and filled with 3M KCL. All cells selected for analysis had resting potentials between -60 and -70 mV. For stimulation, the cut end of the segmental nerve was pulled into a fire-polished suction electrode and brief (300 µs) depolarizing pulses were passed at 0.2 Hz (npi stimulus generator and isolation unit). To ensure the stable recruitment of both innervating motoneurons, the amplitude of the pulse was determined by increasing the stimulation strength to 1.5 times the amplitude needed to reach the threshold of double motoneuron recruitment. The clamp was tuned such that it responded to a voltage step from -60 to -70 mV with settling times of 1 ms for mEJCs and 500-750 µs for eEJCs, this gave voltage errors of maximally 4 mV for eEJCs of approx. –100 nA. Both eEJCs (voltage clamp at –60 mV) and mEJCs (voltage clamp at –80 mV) were low-pass filtered at 1 kHz and the holding current never exceeded –10 nA. For each cell, 20 eEJCs and 90 s of mEJCs recordings were used for subsequent analysis (pClamp9, Axon Instruments).

Results

New glutamate receptor subunits expressed within postsynaptic muscle cells of
Drosophila

The *Drosophila* genome encodes about 30 potential glutamate receptor subunits (Littleton and Ganetzky, 2000; Sprengel et al., 2001). We explored how many glutamate receptor subunits might be expressed in total within the postsynaptic muscle cell. To this end, RNA was extracted from larval body wall preparations, which are enriched for somatic muscles but free of CNS tissue and internal organs. Using Affymetrix *Drosophila* gene chips, the abundances of *Drosophila* glutamate receptor subunits were determined in larval body wall RNA. The amount of each subunit was then compared to the abundance in whole larval mRNA. As expected, *GluR-IIA* and *GluR-IIB* (Schuster et al., 1991; Petersen et al., 1997) were found to be enriched in body wall RNA. Also the subunit annotated as *CG4226*, first referred to as *GluR-IIC* (Saitoe et al., 2001; Sprengel et al., 2001) and later as *GluR-III* (Marrus et al., 2004) was found to be enriched. Recent work had shown that *GluR-III* mutant embryos die, most likely due to a defect of glutamatergic transmission. In addition to these already described subunits with NMJ expression, the mRNA of another locus encoding a glutamate receptor subunit (annotated as *CG18039*) was also enriched in body wall preparations.

Next, real time PCR was used to independently quantify the expression of these glutamate receptor subunits. Real time PCR confirmed the body wall enrichments first observed by gene chip analysis (see table I). We further recognized that *CG3201*, the direct neighbor locus of *CG18039,* encodes a glutamate receptor as well. This locus was not represented on the chip used. We also found *CG31201* to be enriched within body wall mRNA (table I). From now on we will refer to the locus encoding subunit *CG18039* as *GluR-IID* and the locus encoding *CG31021* as *GluR-IIE.* These names are meant to reflect muscle expression (see below) along with *Glu-IIA,- IIB* and *–IIC/III.*

To confirm muscle expression of these new subunits, *in situ* hybridization on *Drosophila* embryos and larvae was performed. In fact, the mRNAs of *GluR-IID* (Fig. 1A-D) and *GluR-IIE* (Fig. 1E, F) are specifically expressed in somatic muscles of both the *Drosophila* embryo (Fig. 1A-C, E,F) and larva (Fig.1D). Expression of *GluR-IID* (Fig. 1C-D) and *GluR-IIE* (Fig. 1E) starts in somatic muscles of late stage 12 embryos

(Fig. 1A, E) and extends throughout embryonic and larval development (Fig. 1D, F). Thus, the mRNA expression pattern of the newly identified subunits appears very similar to that of *GluR-IIA, -IIB and -IIC/III* (Petersen et al., 1997; Marrus et al., 2004).

In terms of amino acid sequence, GluR-IID and GluR-IIE define a new type of muscle-expressed glutamate receptor subunit

The muscle-expressed glutamate receptor subunits of *Drosophila* we have identified were further analyzed. We first made sure that these proteins encode all structural features generally conserved in glutamate receptor subunits. Particularly, all putative transmembrane domains were found in positions typical for glutamate receptors (see Figure 2A). As previously noted (Marrus et al., 2004), GluR-IIC/III is closely related to GluR-IIA and IIB. We find that also GluR-IID and GluR-IIE are very closely related to one another (Fig. 2A, B). However, GluR-IID and GluR-IIE are distant from GluR-IIA, IIB and IIC/III. (Figure 2B). In fact, GluR-IID and GluR-IIE are slightly more similar to human kainate receptor GluR-6 than they are to the GluR-IIA, -IIB and -IIC/III group (see dendrogram in Fig. 2B). Thus, GluR-IID and GluR-IIE represent a "new type" of glutamate receptor subunit which is expressed in the *Drosophila* muscle together with the GluR-IIA, -IIB, -IIC/III type. In sequence alignments, several other *Drosophila* non-NMDA glutamate receptors group in between these two clusters represented by GluR-IID, -IIE and GluR-IIA, -IIB, -IIC/III (Littleton and Ganetzky, 2000). GluR-IID and GluR-IIE as well as GluR--IIA, -IIB and -IIC/III all have direct orthologs in other *Drosophila* species (our unpublished observation), indicating that the differentiation of insect muscle-expressed glutamate receptor subunits into two structurally different groups is a conserved trait.

GluR-IID is localized in postsynaptic densities of neuromuscular synapses

To study the expression of muscle-expressed glutamate receptor subunits at the subcellular level, specific antibodies were produced. Our antibody directed against a GluR-IIC/III-specific peptide recognizes a single band of about the predicted 109 kD in *Drosophila* embryo extracts (Fig. 3A, right lane). Moreover, the antibody labels the postsynaptic densities (PSDs) of all neuromuscular synapses (Fig. 3B), as recently shown

with an independently produced antibody (Marrus et al., 2004). So far, GluR-IIE-specific antibodies could not be obtained, mainly due to the fact that there are few immunogenic peptides specific for GluR-IIE which are not also present within the highly related GluR-IID. The specific C-terminal sequence of GluR-IID (boxed in Fig. 2A), however, allowed the production of a specific antiserum. This antiserum recognizes SF9-cell expressed GluR-IID but not the SF9-cell expressed GluR-IIE (Fig. 3A, left lanes). When probing *Drosophila* embryo extracts with this GluR-IID antibody, a single band of about the predicted 102 kD could be detected (Fig. 3A). In immuno-fluorescence stainings, GluR-IID is found at all neuromuscular junctions (NMJs) of larvae (Fig. 3C) and embryos (see below). Furthermore, the expression of GluR-IID is confined to typical punctae (Fig. 3C, arrow heads). These punctae correspond to individual postsynaptic densities (PSDs), because they are surrounded by the HRP-staining known to have perisynaptic expression (Sone et al., 2000). Moreover, these punctae are found directly opposite to the presynaptic Nc82 label. The Nc82 monoclonal antibody labels the presynaptic active zone (Heimbeck et al., 1999; Wucherpfennig et al., 2003). We thus conclude that GluR-IID specifically localizes to the PSD region of individual synaptic sites at the *Drosophila* NMJ.

Null mutants of either *GluR-IID* or *GluR-IIE* is embryonic lethal

To genetically investigate what role GluR-IID and GluR-IIE play in NMJ glutamatergic transmission, we required specific mutants for each of the two genes. We recognized that within a collection of *piggyBac* transposon lines which recently became available (Thibault et al., 2004), a line with an insertion in the *GluR-IID* locus (pBac{RB}^{e01443}) was included . We verified that in this line the transposon has integrated directly into intron 6 of *DGluR-IID* (Fig. 4). This should interfere with productive translation of GluR-IID. In fact, in embryos no GluR-IID protein could be observed at the neuromuscular synapses (see below). We refer to this allele as *GluR-IID*^{e01443}. For *GluR-IIE*, excision mutagenesis screening was performed using transposon line EP28753 whose insertion site is located only 150 bp downstream of the *GluR-IIE* gene (Fig. 4). We could recover a small deficiency (*GluR-IIE*^{E1}) (see Material and Methods) in which the genomic sequence encoding the C-terminal part of GluR-IIE including the last transmembrane

domain is specifically deleted. *GluR-IIE^{E1}* does not extend into neighboring genes. Both *GluR-IID*^{e01443} and *GluR-IIE*^{E1} are embryonic lethal when homozygous. Moreover, they are both embryonic lethal over *GluR-IID&IIE*^{E3} (Fig. 4), a deficiency which deletes *GluR-IID* and *GluR-IIE*. *GluR-IID*^{e01443} is fully viable when crossed over *GluR-IIE*^{E1}. *GluR-IID*^{e01443} is embryonic lethal over independently retrieved null alleles of *GluR-IID* (see accompanying paper by Featherstone et al.), while *GluR-IIE*^{E1} is fully viable over these alleles. Both, *GluR-IID*^{e01443} and *GluR-IIE*^{E1} could be rescued to adult vitality by transgenic addition of a genomic construct encoding *GluR-IID* or *GluR-IIE,* respectively. However, neither the *GluR-IID* mutant nor the *GluR-IIE* mutant could be rescued by the respective other transgene. Thus, we obtained specific null mutants for both *GluR-IID* and *GluR-IIE*. While the neighboring loci *GluR-IID* and *GluR-IIE* encode very similar proteins with largely overlapping expression, both of them are essential for embryonic survival.

Interdependency of all glutamate receptor subunits for receptor function and synaptic receptor expression

GluR-IID or *GluR-IIE* null mutant embryos were subjected to closer inspection. These embryos, while apparently fully developed showed no coordinated movements and did not hatch. This suggests that both subunits are essential for synaptic transmission at the embryonic NMJ. Consistent with a role in synaptic transmission, *GluR-IID* and *GluR-IIE* mRNA expression starts within embryonic muscles well before the onset of neurotransmission (Fig. 1) (Petersen et al., 1997; Marrus et al., 2004). Taken together, both subunits apparently are critically involved in forming postsynaptic glutamate receptors, which in turn are essential for neurotransmission at the developing embryonic NMJ. As mentioned above, GluR-IID consistently localizes to the PSD region of all embryonic NMJ synapses (Fig. 5B, wild type).

In mammals, non-NMDA glutamate receptors are apparently composed of rather closely related subunits (Wenthold et al., 1996; Mulle et al., 2000). Hence, we first investigated whether the closely related GluR-IID and GluR-IIE subunits directly form glutamate receptors. We reasoned that if receptor formation fails, synaptic localization of individual subunits must also be affected. Thus, body wall preparations of late *GluR-IIE*

mutant embryos were investigated in immuno-fluorescence stainings. NMJs still formed in *GluR-IIE* mutant embryos, as shown by staining against HRP and Nc82 epitope (Fig. 5A, blue and green channel). GluR-IID is however absent from *GluR-IIE* mutant embryonic NMJs (Fig. 5B). This finding indicates that GluR-IIE and GluR-IID join into a common glutamate receptor which in turn is essential for synaptic transmission at the embryonic NMJ.

The same phenotype as observed in *GluR-IID* and *GluR-IIE* mutants (a fully developed embryo unable of coordinated movements) is observed within *GluRIIC/III* single or *GluR-IIA&IIB* double null mutant embryos as well. This phenotype was also interpreted as a failure of neuromuscular transmission due to the absence of functional postsynaptic glutamate receptors (Petersen et al., 1997; Marrus et al., 2004). On this basis it was suggested that GluR-IIC/III is an obligatory subunit, which associates with either GluR-IIA or GluR-IIB to form glutamate receptors (Marrus et al., 2004). We tested this idea again by staining *Glu-RIIA&IIB* double mutant embryos. We also note the absence of a GluR-IIC/III label from NMJs of *Glur-IIA&IIB* null mutant embryos (Fig. 5A and B). GluR-IIA together with GluR-IIB can thus be considered a "synthetic essential subunit". In principle, both "groups of subunits" (GluR-IID, -IIE versus –IIA, -IIB, IIC/III) could be essential for embryonic neurotransmission independently of each other. Alternatively, synaptic localization and thus receptor function could be interdependent between both groups. First we addressed whether the synaptic presentation of the GluR-IIC/III glutamate receptor subunit depends on *GluR-IID* or *GluR-IIE*. No synaptic localization of GluR-IIC/III can be found in either *GluR-IID* or *GluR-IIE* null mutant embryos (Fig. 5A and B). *Vice versa*, the synaptic expression of GluR-IID was absent from *GluR-IIA&-IIB* double null mutant embryos (Fig. 5B). Thus, at the embryonic NMJ, the synaptic expression of all essential glutamate receptor subunits is interdependent. The easiest explanation for these data is that at the *Drosophila* NMJ the glutamate receptor is formed by four essential glutamate receptor subunits: GluR-IIC, GluR-IID, and GluR-IIE together with either GluR-IIA or GluR-IIB.

A stoichiometric relationship between all essential subunits for synaptic expression and glutamate receptor function

If the glutamate receptor does in fact form from four different subunits, the expression level of all these subunits must be able to become rate limiting for glutamate receptor formation. Thus, after partially suppressing the level of a single such subunit, glutamate receptor formation and thus synaptic expression of the respective other essential subunits should be lowered accordingly. Using muscle-specific, transgene mediated RNA interference against *GluR-IIE*, we could lower *GluR-IIE* mRNA expression down to about 20% without changing the mRNA expression of all other muscle expressed subunits (real time PCR data). These animals no longer die as embryos (as the *GluR-IIE* null mutants do) but instead develop into mature larvae. At the NMJs of larvae with reduced *GluR-IIE*, both GluR-IID and GluR-IIC/III were clearly reduced (Fig. 6B, D). For a second experiment, we used the fact that already minimal amounts of GluR-IID (produced by the "leaky" expression typically mediated by *UAS-cDNA* transgenes in the absence of a *Gal4*-driver line) can rescue *GluR-IID* null mutant embryos (Fig. 6E-H). At larval NMJs of these *GluR-IID* null mutant larvae rescued by "leaky expression" of GluR-IID, the levels of all other glutamate receptor subunits were very strongly reduced as well (Fig. 6H). Re-expressing GluR-IID to normal levels by using the muscle specific *Gal4*-driver line *Mhc-Gal4* restored the localization of all other glutamate receptor subunits (not shown). We conclude that the levels of GluR-IID and GluR-IIE within the muscles directly control the amount of glutamate receptors able to localize at the NMJ. We next asked, whether reciprocally the amounts of muscle GluR-IIA, -IIB and -IIC/III can control NMJ levels of GluR-IID and -IIE. For this, a genetic situation in which *GluR-IIB* was fully absent and simultaneously *GluR-IIA* was suppressed below 5% of normal mRNA level (*GluRIIA^{hypo}*, *GluR-IIB^{null}*, see Material and Methods) was used. Here, the level of both GluR-IIC/III and GluR-IID were drastically reduced as well (Fig. 7B, D). Collectively, these data suggest that the availability of all essential glutamate receptor subunits controls receptor formation, and as expected that assembling the proper receptor is a precondition for NMJ localization of the subunits. This seems true during both initial formation but also further development of NMJs, where many new synapses get added (Schuster et al., 1996; Gramates and Budnik, 1999). We finally asked whether glutamate receptor function would parallel our findings based on receptor immuno stainings. Between the different genetic situations we use to partially deprive glutamate receptor

subunits in larvae, GluR-IIE interference produced a more moderate donwregulation (Fig. 7 B and D), while the most severe loss of glutamate receptors was observed in *GluRIIA^hypo^, GluR-IIB^null^* larvae (Fig. 7 F and H), with the latter genotype expressing clear signs of paralysis. *GluRIIA^hypo^, GluR-IIB^null^* larvae were thus subjected to two-electrode-voltage-clamp recordings (Fig. 7E, F). In fact, spontaneous miniature currents (mEJCs) were below the detection limit indicating an extreme drop of postsynaptic glutamate receptor function. Accordingly, evoked currents (eEJCs) were also low at these NMJs (*wild type*: 61 nA, n=12, *GluRIIA^hypo^, GluR-IIB^null^*: 21 nA, n=11; p < 0.00005, Mann-Whitney, two-sided non-parametric test*)*. We thus conclude that strongly reducing the expression of a single glutamate receptor subunit is sufficient in severely reducing the level of functional glutamate receptors at the NMJ. In summary, forming functional glutamate receptors at the *Drosophila* NMJ can be controlled by all 5 glutamate receptor subunits so far identified. Consistently, Featherstone et al. (this issue) in fact demonstrate the complete absence of any glutamate receptor function in *GluR-IID* null mutant embryos in patch clamp recordings of embryonic muscle cells.

Discussion

Novel glutamate receptor subunits are essential for glutamatergic transmission at neuromuscular synapses

Glutamatergic neuromuscular synapses of *Drosophila*, in terms of ultrastructure and molecular composition similar to the glutamatergic synapses of our brains, have been intensely used to study synaptic function *in vivo* capitalizing on the efficient genetics and superb experimental accessibility of this model system. At these synapses three non-NMDA type glutamate receptor subunits (GluR-IIA, -IIB, -IIC/III) have been described previously. While only *GluR-IIA&IIB* double mutants but not the respective single mutants lack transmission (Petersen et al., 1997; DiAntonio et al., 1999), lack of GluR-IIC/III alone is fatal with a phenotype suggesting the absence of neurotransmission at neuromuscular synapses (Marrus et al., 2004). Doubts remained about the subunit composition of synaptic receptors at the NMJ. Here we describe two additional non-NMDA glutamate receptor subunits (GluR-IID and GluR-IIE) which, on the basis of *in situ* hybridization (Fig. 1) and antibody staining (Fig. 3), we show to be specifically expressed at the postsynaptic site of all neuromuscular synapses alongside GluR-IIA, -IIB and -IIC/III. While GluR-IID and GluR-IIE are genomic neighbors and very similar to each other, they are not particularly related to GluRIIA-IIC/III. We could retrieve specific null mutations for both *GluR-IID* and *GluR-IIE*. Both *GluR-IID* and *GluR-IIE* null embryos while apparently fully developed, do not hatch and are incapable of any coordinated movement. In the case of *GluR-IIA&IIB* as well as in the *GluR-IIC/III* single mutant this paralyzed phenotype was attributed to a fatal failure of synaptic transmission as well (Petersen et al., 1997). The accompanying manuscript (Featherstone et al., this issue) now directly demonstrates that no postsynaptic sensitivity to glutamate is present at the muscles of *GluR-IID* null mutant embryos. Thus, GluR-IID and GluR-IIE are critically important for mediating glutamate-gated ionic currents at the postsynaptic site of neuromuscular synapses. It appears therefore most likely, that *GluR-IIA&IIB* double mutants as well as *GluR-IIC/III* single mutants also lack any glutamate gated ionic current.

Taken together, lack of either GluR-IIC/III, -IID, -IIE or of both -IIA and –IIB together leads to a fatal lack of glutamate receptor function at the embryonic NMJ. The following arguments indicate that this is directly due to the loss of the respective receptor subunits *within* the embryonic muscles. First, *GluR-IIA*, *-IIB*, *-IIC/III* and *-IIE* expression is seemingly restricted to the somatic muscles (Petersen et al., 1997; DiAntonio et al., 1999). Secondly, the paralysis phenotype of these null mutants could always be fully rescued by a muscle-specific re-expression of the corresponding cDNAs (DiAntonio et al., 1999). Thirdly, muscle-specific down-regulation of *GluR-IIE* (via RNA interference) could effectively down-regulate synaptic expression of GluR-IID and GluR-IIC/III as well. Thus, clearly the lack of the glutamate receptor subunits within the postsynaptic muscle cells is the direct cause of embryonic paralysis due to a loss of all glutamate receptor complexes.

Implications for the stoichiometry of the *Drosophila* glutamate receptor

Recent studies have suggested that AMPA receptors form as a tetramer of subunits (Laube et al., 1998; Mano and Teichberg, 1998; Rosenmund et al., 1998).

We find that the synaptic expression of all glutamate receptor subunits is completely abolished after eliminating either *GluR-IID* or *IIE* alone or *GluR-IIA* and *IIB* together (Fig. 5 this paper, see also Featherstone et al., same issue). Taken together, all data clearly indicate that essential glutamate receptor subunits (GluR-IIC/III, -IID and -IIE) are obligatory part of all postsynaptic glutamate receptors. In addition, either GluR-IIA or GluR-IIB seems obligate for receptor formation as well. One likely scenario therefore is that the glutamate receptor population at the *Drosophila* NMJ is a mix of (IIA)(IIC/III)(IID)(IIE) receptors with (IIB)(IIC/III)(IID)(IIE) receptors. Tetrameric structure of glutamate receptors was suggested solely on the basis of ligand-binding studies and crystal structures of ligand-binding domains. An unequivocal determination of the number of subunits in a functional glutamate receptor thus still awaits physical methods that probe the structure of the receptor itself. Thus, pentameric (or higher) stoichiometry cannot be refuted in the moment and in fact was suggested in the past several times (Premkumar et al., 1997). Therefore, e.g. also stochiometries as $(A)_2(C)(D)(E)$, $(B)_2(C)(D)(E)$ or $(A)(B)(C)(D)(E)$ might still have to be considered.

GluR-IIA- and GluR-IIB-containing receptor complexes differ strongly in their biophysical properties, with GluR-IIA-containing receptors showing slow desensitization and GluR-IIB-containing receptors showing fast desensitization (DiAntonio et al., 1999). Thus, GluR-IIA and GluR-IIB containing complexes are likely to play different roles in synaptic function and development. In fact, increased postsynaptic GluR-IIA protein levels or reduced GluR-IIB gene copy number resulted in an increased strength of NMJ transmission and an addition of junctional boutons harboring increased numbers of synapses. These phenotypes were suppressed by overexpression of GluR-IIB (Sigrist et al., 2002a). Thus, GluR-IIC/III, IID and IIE might establish a "receptor platform" while the incorporation of either the GluR-IIA or the GluR-IIB subunit could determine the specific functions of the respective glutamate receptor.

As discussed above, the interdependency between all essential subunits observed for synaptic localization is easiest explained by assuming the existence of common glutamate receptor. It might, however, be argued that eliminating a certain glutamate receptor subunit could provoke an early defect during the developmental set up of neuromuscular synapses. This in turn might then interfere with the localization of other glutamate receptor complexes. This way, the genetic elimination of a certain subunit could also provoke the loss of synaptic expression (and thus also synaptic function) of another subunit even if these two subunits would not be contained in the same glutamate receptor. At this juncture, such a scenario appears unlikely because of the following arguments. First, partial suppression of any essential glutamate receptor subunit always provokes a corresponding down-regulation of glutamate receptor at larval neuromuscular synapses (Fig. 6 and 7 of this paper; Featherstone et al., this issue Figure 6; Marrus and DiAntonio, 2004; Marrus et al., 2004). This suggests that all essential subunits obey a stoichiometric relationship, where the availability of the least abundant subunit defines the overall amount of glutamate receptors, and that this relation exists throughout development. Secondly, Featherstone et al. convincingly demonstrate a *complete* loss of glutamate mediated currents on GluR-IID mutant embryonic muscles. However, extrasynaptic glutamate receptors have been directly demonstrated on wild type embryonic muscle membranes using the very same experimental set up (Broadie and Bate, 1993; Featherstone et al., this issue). Thus, elimination of GluR-IID abolishes both all the

extrasynaptic as well as the synaptic populations of glutamate receptors on embryonic muscles. Therefore, if interactions between independently forming glutamate receptors are involved, they would have to be absolutely essential already during the intracellular transport and assembly of glutamate receptors. Because we know that at least GluR-IID is clearly expressed in substantial amounts within postsynaptic densities, the existence of subunits evolved only to mediate the intracellular transport or assembly of glutamate receptor complexes appears rather unlikely.

In vivo analysis of glutamate receptor assembly and mobility using a genetically fully accessed set of subunits

Collectively, our *in vivo* analysis clearly favors the idea that forming non-NMDA glutamate receptors can depend on four different subunits. To our knowledge a "strictly hetero-tetrameric stoichiometry" has so far not been described for other ionotropic glutamate receptors. This finding thus potentially indicates that *in vivo* some glutamate receptors can have a rather fixed subunit stochiometry reminiscent of the stochiometry of other types of ligand-gated ion channels as e.g. the nicotinic acetylcholine receptor (Colquhoun and Sivilotti, 2004).

Dissecting the molecular details underlying the functional assembly and cell surface trafficking of various types of glutamate receptors is a focus of current research. It has been suggested that in AMPA receptors the N-terminal domain is largely responsible for subtype recognition among different subunits while the transmembrane-region and the C-terminal part of S2 are critical determinants for the formation of functional channels (Leuschner and Hoch, 1999; Ayalon and Stern-Bach, 2001). In this context it will be interesting to explore which sequences within these the *Drosophila* NMJ subunits confer the essential character of individual subunits, capitalizing on the complete set of mutants for all five relevant glutamate receptor subunits now available. Given the close structural relation between GluR-IID and -IIE, analyzing inter-subunit-chimeras between these subunits in either a GluR-IID or GluR-IIE mutant background might be particularly informative. The accompanying paper by Featherstone et al. reports that GluR-IID is also expressed in the CNS of late embryos / first instar larvae. In this context, we find that *GluR-IID* but not *GluR-IIE* message is expressed within heart

precursor cells (Fig.1A, arrow heads). Thus, between different tissues subunit composition of glutamate receptors can overlap without being identical. It will be interesting to work out whether tissue-specific control mechanisms execute assembly and transport reflecting the glutamate receptor subunit spectrum expressed. Moreover, our lab recently managed to directly visualize glutamate receptor dynamics within living intact larvae during synapse formation (manuscript submitted), applying photo-bleaching and photo-activation procedures *in vivo*. It will be very interesting, whether in fact all essential glutamate receptor subunits show coherent dynamics as to be assumed if they are within one complex.

References

Ayalon G, Stern-Bach Y (2001) Functional assembly of AMPA and kainate receptors is mediated by several discrete protein-protein interactions. Neuron 31:103-113.

Bellen HJ (1998) The fruit fly: a model organism to study the genetics of alcohol abuse and addiction? Cell 93:909-912.

Bredt DS, Nicoll RA (2003) AMPA receptor trafficking at excitatory synapses. Neuron 40:361-379.

Broadie K, Bate M (1993) Activity-dependent development of the neuromuscular synapse during Drosophila embryogenesis. Neuron 11:607-619.

Colquhoun D, Sivilotti LG (2004) Function and structure in glycine receptors and some of their relatives. Trends Neurosci 27:337-344.

DiAntonio A, Petersen SA, Heckmann M, Goodman CS (1999) Glutamate receptor expression regulates quantal size and quantal content at the Drosophila neuromuscular junction. J Neurosci 19:3023-3032.

Dingledine R, Borges K, Bowie D, Traynelis SF (1999) The glutamate receptor ion channels. Pharmacol Rev 51:7-61.

Featherstone DE, Broadie K (2000) Surprises from Drosophila: genetic mechanisms of synaptic development and plasticity. Brain Res Bull 53:501-511.

Gramates LS, Budnik V (1999) Assembly and maturation of the Drosophila larval neuromuscular junction. Int Rev Neurobiol 43:93-117.

Heimbeck G, Bugnon V, Gendre N, Haberlin C, Stocker RF (1999) Smell and taste perception in Drosophila melanogaster larva: toxin expression studies in chemosensory neurons. J Neurosci 19:6599-6609.

Koh YH, Gramates LS, Budnik V (2000) Drosophila larval neuromuscular junction: molecular components and mechanisms underlying synaptic plasticity. Microsc Res Tech 49:14-25.

Laube B, Kuhse J, Betz H (1998) Evidence for a tetrameric structure of recombinant NMDA receptors. J Neurosci 18:2954-2961.

Leuschner WD, Hoch W (1999) Subtype-specific assembly of alpha-amino-3-hydroxy-5-methyl-4-isoxazole propionic acid receptor subunits is mediated by their n-terminal domains. J Biol Chem 274:16907-16916.

Littleton JT, Ganetzky B (2000) Ion channels and synaptic organization: analysis of the Drosophila genome. Neuron 26:35-43.

Malinow R, Malenka RC (2002) AMPA receptor trafficking and synaptic plasticity. Annu Rev Neurosci 25:103-126.

Mano I, Teichberg VI (1998) A tetrameric subunit stoichiometry for a glutamate receptor-channel complex. Neuroreport 9:327-331.

Mansour M, Nagarajan N, Nehring RB, Clements JD, Rosenmund C (2001) Heteromeric AMPA receptors assemble with a preferred subunit stoichiometry and spatial arrangement. Neuron 32:841-853.

Marrus SB, DiAntonio A (2004) Preferential localization of glutamate receptors opposite sites of high presynaptic release. Curr Biol 14:924-931.

Marrus SB, Portman SL, Allen MJ, Moffat KG, DiAntonio A (2004) Differential localization of glutamate receptor subunits at the Drosophila neuromuscular junction. J Neurosci 24:1406-1415.

Mayer ML, Armstrong N (2004) Structure and function of glutamate receptor ion channels. Annu Rev Physiol 66:161-181.

Mulle C, Sailer A, Swanson GT, Brana C, O'Gorman S, Bettler B, Heinemann SF (2000) Subunit composition of kainate receptors in hippocampal interneurons. Neuron 28:475-484.

Petersen SA, Fetter RD, Noordermeer JN, Goodman CS, DiAntonio A (1997) Genetic analysis of glutamate receptors in Drosophila reveals a retrograde signal regulating presynaptic transmitter release. Neuron 19:1237-1248.

Premkumar LS, Qin F, Auerbach A (1997) Subconductance states of a mutant NMDA receptor channel kinetics, calcium, and voltage dependence. J Gen Physiol 109:181-189.

Rosenmund C, Stern-Bach Y, Stevens CF (1998) The tetrameric structure of a glutamate receptor channel. Science 280:1596-1599.

Saitoe M, Schwarz TL, Umbach JA, Gundersen CB, Kidokoro Y (2001) Absence of junctional glutamate receptor clusters in Drosophila mutants lacking spontaneous transmitter release. Science 293:514-517.

Schorge S, Colquhoun D (2003) Studies of NMDA receptor function and stoichiometry with truncated and tandem subunits. J Neurosci 23:1151-1158.

Schuster CM, Davis GW, Fetter RD, Goodman CS (1996) Genetic dissection of structural and functional components of synaptic plasticity. I. Fasciclin II controls synaptic stabilization and growth. Neuron 17:641-654.

Schuster CM, Ultsch A, Schloss P, Cox JA, Schmitt B, Betz H (1991) Molecular cloning of an invertebrate glutamate receptor subunit expressed in Drosophila muscle. Science 254:112-114.

Seeburg PH (1993) The TINS/TiPS Lecture. The molecular biology of mammalian glutamate receptor channels. Trends Neurosci 16:359-365.

Sigrist SJ, Thiel PR, Reiff DF, Schuster CM (2002a) The postsynaptic glutamate receptor subunit DGluR-IIA mediates long-term plasticity in Drosophila. In: J Neurosci, pp 7362-7372.

Sigrist SJ, Thiel PR, Reiff DF, Schuster CM (2002b) The postsynaptic glutamate receptor subunit DGluR-IIA mediates long-term plasticity in Drosophila. J Neurosci 22:7362-7372.

Sigrist SJ, Thiel PR, Reiff DF, Lachance PE, Lasko P, Schuster CM (2000) Postsynaptic translation affects the efficacy and morphology of neuromuscular junctions. Nature 405:1062-1065.

Sone M, Suzuki E, Hoshino M, Hou D, Kuromi H, Fukata M, Kuroda S, Kaibuchi K, Nabeshima Y, Hama C (2000) Synaptic development is controlled in the periactive zones of Drosophila synapses. Development 127:4157-4168.

Sprengel R, Aronoff R, Volkner M, Schmitt B, Mosbach R, Kuner T (2001) Glutamate receptor channel signatures. Trends Pharmacol Sci 22:7-10.

Stewart BA, Atwood HL, Renger JJ, Wang J, Wu CF (1994) Improved stability of Drosophila larval neuromuscular preparations in haemolymph-like physiological solutions. J Comp Physiol [A] 175:179-191.

Sun Y, Olson R, Horning M, Armstrong N, Mayer M, Gouaux E (2002) Mechanism of glutamate receptor desensitization. Nature 417:245-253.

Swan LE, Wichmann C, Prange U, Schmid A, Schmidt M, Schwarz T, Ponimaskin E, Madeo F, Vorbruggen G, Sigrist SJ (2004) A glutamate receptor-interacting protein homolog organizes muscle guidance in Drosophila. Genes Dev 18:223-237.

Tautz D, Pfeifle C (1989) A non-radioactive in situ hybridization method for the localization of specific RNAs in Drosophila embryos reveals translational control of the segmentation gene hunchback. Chromosoma 98:81-85.

Thibault ST, Singer MA, Miyazaki WY, Milash B, Dompe NA, Singh CM, Buchholz R, Demsky M, Fawcett R, Francis-Lang HL, Ryner L, Cheung LM, Chong A, Erickson C, Fisher WW, Greer K, Hartouni SR, Howie E, Jakkula L, Joo D, Killpack K, Laufer A, Mazzotta J, Smith RD, Stevens LM, Stuber C, Tan LR, Ventura R, Woo A, Zakrajsek I, Zhao L, Chen F, Swimmer C, Kopczynski C, Duyk G, Winberg ML, Margolis J (2004) A complementary transposon tool kit for Drosophila melanogaster using P and piggyBac. Nat Genet 36:283-287.

Wenthold RJ, Petralia RS, Blahos J, II, Niedzielski AS (1996) Evidence for multiple AMPA receptor complexes in hippocampal CA1/CA2 neurons. J Neurosci 16:1982-1989.

Wucherpfennig T, Wilsch-Brauninger M, Gonzalez-Gaitan M (2003) Role of Drosophila Rab5 during endosomal trafficking at the synapse and evoked neurotransmitter release. J Cell Biol 161:609-624.

Figure legends

Table I. *GluR-IID* and *GluR-IIE* are enriched in larval body wall mRNA.
Abundances of glutamate receptor subunit transcripts estimated using real time PCR. The control transcript (proteasome subunit *tbp-1*) had the same abundance in body wall preps and whole larvae. The glutamate receptor subunits shown were enriched in body wall RNA when compared to whole larva RNA. The abundances of mRNAs are expressed as C_t values indicating the cycle number with which amplification exceeds detection threshold (Ct difference of one indicates a two-fold difference in abundance). For all reactions, identical amounts of cDNA were used. All data are averages from three independent experiments where each sample was run three times in parallel.

Figure 1. *GluR-IID* and *GluR-IIE*: novel glutamate receptor subunits with muscle specific expression
In situ hybridizations on *Drosophila* embryos (A-C, E,F) and larvae (D) for *GluRIID* (A-D) and *GluRIIE* mRNA (E,F). Both subunits are expressed specifically in presumptive somatic muscle cells (A, B, E, F, arrowheads) but are for example not found in the adjacent epidermis (A, B, F, arrows). Expression of *GluR-IID* and *GluR-IIE* transcript in the presumptive somatic muscles starts in late stage 12 and peaks at around stage 14 (A, E), to then persist during later embryogenesis (B: stage 16; E: stage 17) and larval development (D). *GluR-IID* is also expressed within heart precursor cells (A and B, arrows).

Figure 2. Sequence analysis of GluR-IID and GluR-IIE
A, sequence alignment of predicted amino acid sequences of (from top to bottom) GluRIIC/III, GluR-IID, GluR–IIE and human kainate receptor subunit GluR-6, similar amino acids are indicated by shaded boxes. Putative trans-membrane domains (TM1-4), the channel pore region and the c-terminal peptide of GluR-IID which was used for immunization are indicated as well.
B, dendrogram analysis comparing muscle expressed glutamate receptor subunits of *Drosophila*, together with AMPA receptor subunit GluR1, kainate receptor subunit GluR-6 and NMDA receptor subunit NR-1 (all *homo sapiens*). All muscle expressed glutamate receptor subunits of *Drosophila* fall into the Kainate/AMPA-class of glutamate receptors. However, GluR-IIA, -IIB and IIC/III on one side and GluR-IID and - IIE on the other side are structurally far distant. Dendrogram was generated using MacVector software.

Figure 3. GluR-IID is expressed within postsynaptic densities
A: western blot analysis: the anti-IID peptide antibody recognizes SF9-cell expressed GluR-IID and endogenous GluR-IID from *Drosophila* embryo extract. It does not cross react with the related GluR-IIE protein, which is SF9-cell expressed as a GFP fusion and is recognized using anti-GFP antibody with the predicted size of about 145 kD. GluR-IIC/III is recognized with our peptide antibody in *Drosophila* embryo extract with predicted size as well.
B-C, shown are epifluorescence pictures (upper two panels in B and C) and confocal pictures (lower panels in B and C) of receptor subunits GluR-IIC/III (B, red) and GluR-

IID (C, red) together with the perisynaptic marker HRP (upper panels in B and C, green) or active zone marker Nc82 (lower panels in B and C, green), scale bars: 8 and 4 μm.

Figure 4. Genetic analysis of *GluR-IID* and *GluR-IIE*

GluR-IID and –IIE map to position 92F on chromosome III. Exon-intron structure of both loci is shown, exons are boxed. The null allele *GluR-IID*[e01443] is based on a *piggyBac* transposon insertion within the open reading frame of the *GluR-IID* locus. Null allele *GluR-IIE*[E1] lacks c-terminal sequence of the protein including the last transmembrane domain of the receptor subunit. The genomic stretches used for genomic rescue constructs are shown below.

Figure 5. Interdependence between glutamate receptor subunits for NMJ expression

A, Confocal images of NMJs in wild-type, *GluR-IID* null, *GluR-IIE* null or *GluR-IIA&IIB* double null mutant embryos (20-22 hrs old) stained with antibodies against GluR-IIC/III (red), Nc82 (green) and HRP (blue). Nc82 staining indicates differentiation of presynaptic release sites at the mutant NMJs. Synaptic expression of all glutamate receptor subunits fails at the mutant NMJs. Scale bar: 10 μm
B, Higher magnifications of confocal stainings similar as in A. Stainings of either GluR-IID (left panels) or GluR-IIC/III (right panels) are shown together with Nc82. Scale bar: 5 μm.

Figure 6. A partial reduction of either GluR-IIE or GluR-IID provokes a significant reduction of all glutamate receptor subunits at the NMJ
(A-D) Larval NMJs (muscle 4, abdominal segment 2) stained for GluR-IID (A, B) or GluR-IIC/III (C, D) in control larvae (*G14-gal4/ +*, A and C) or larvae experiencing muscle specific RNA interference against GluR-IIE (*G14-gal/+; UAS-GluR-IIE-RNAi*, B and D). Suppression of *GluR-IIE* leads also to a reduction in the NMJ expression of GluR-IIC/III and GluR-IID. Lower pictures represent higher magnifications.
(E-H) Shown are NMJs (muscle 4, abdominal segment 2) of *GluR-IID* null mutant larvae rescued with a single copy of *UAS-GluR-IID (UAS-GluR-IID/+; GluR-IID*[e01443]*/GluR-IID&IIE*[E3]. Only trace amounts of GluR-IID (F) and GluR-IIC (H) are expressed at the NMJ, HRP stainings (E, G) are added to visualize the NMJ. Non-linear contrasting had to be used to make the trace amounts of GluR-IID (F) and GluR-IIC (H) visible.
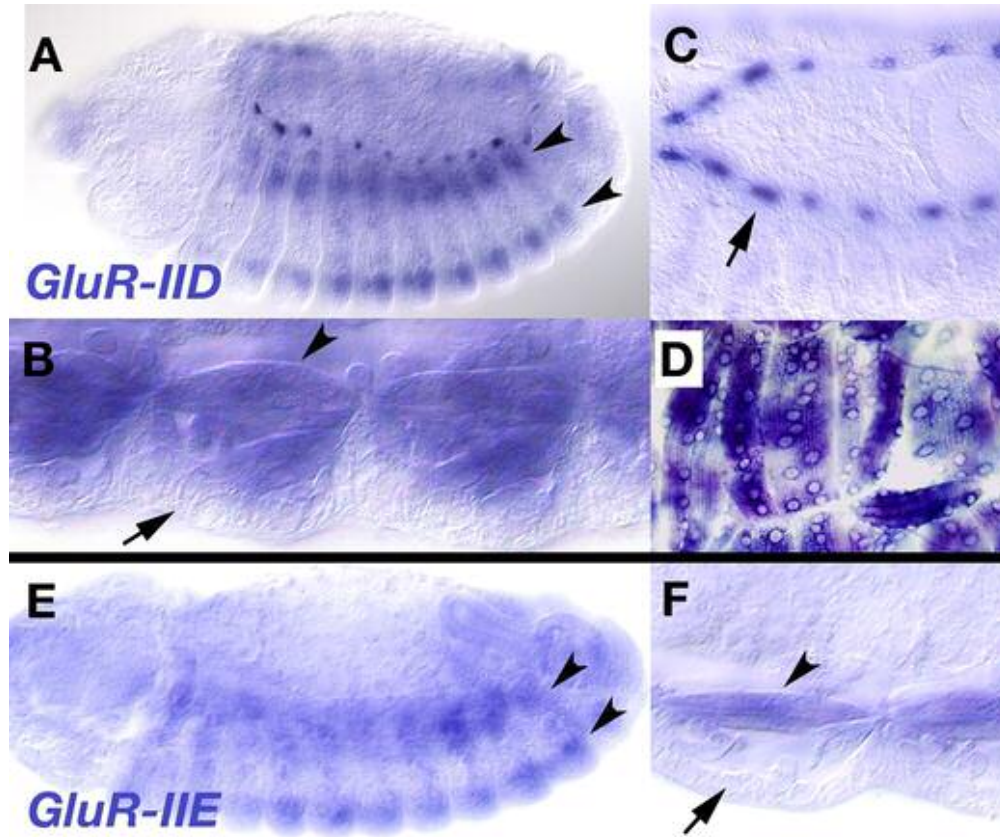Scale bar in upper panel 7,5 μm, in lower panel showing higher magnification 2,5 μm.

Figure 7. Minimal mounts of GluR-IIA and no- IIB: expression of all glutamate receptor subunits and postsynaptic sensitivity are strongly reduced
(A-D) Shown are 3rd instar larval NMJs (muscle 4, abdominal segment 2) stained for GluR-IID (A, B) or GluR-IIC/III (C, D) in wild type controls (A, C) or in animals having only about 5% GluR-IIA and no GluR-IIB (*GluR-IIA*[hypo]*, GluR-IIB*[null,] see Material and Methods). NMJ morphology in HRP labeling is shown in insets to allow NMJ visualization independent of receptor label. In *GluR-IIA*[hypo]*, GluR-IIB*[null] larvae, the synaptic localization of both GluR-IID and GluR-IIC/III is strongly reduced. Apparent differences in between residual GluR-IID and GluR-IIC/III are likely due to slightly different sensitivity of our antibodies.
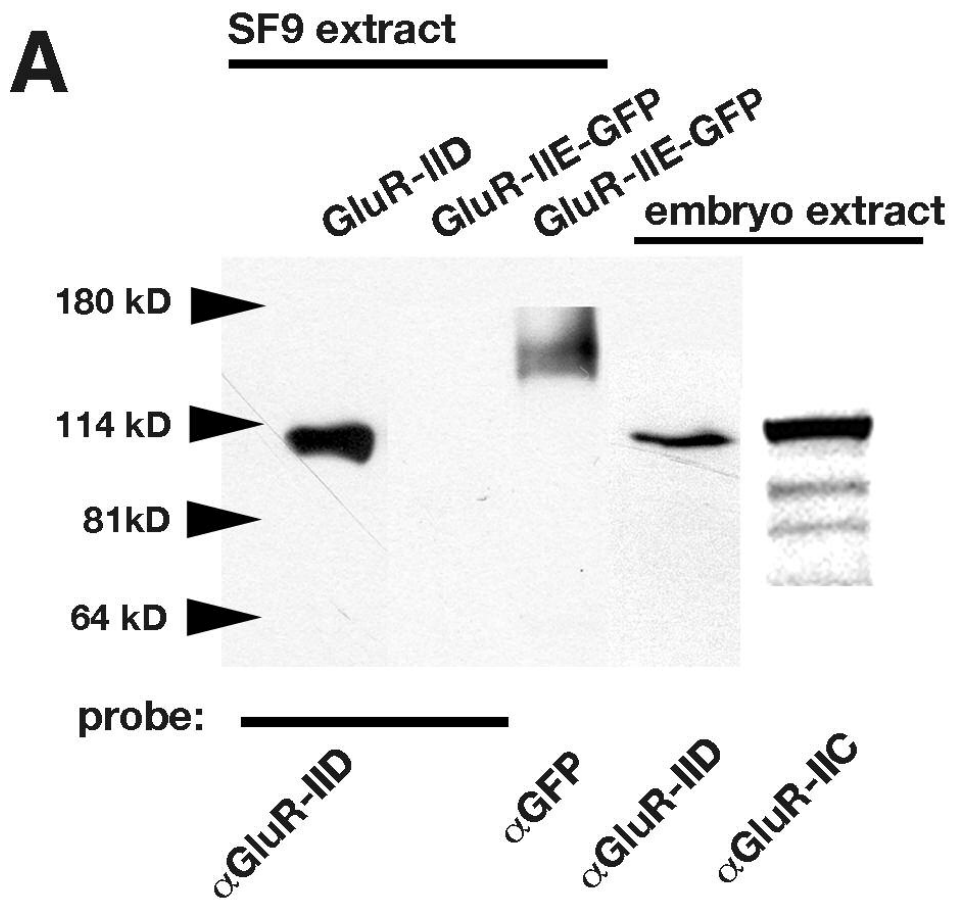
(E, F) Two-electrode-voltage-clamp recordings on 3rd instar larvae (muscle 6, abdominal segment 2), measuring spontaneous (mEJCs) and evoked (eEJCs) junctional currents. The *GluR-IIA^{hypo}, GluR-IIB^{null}* mutant animals (F) are compared to *wild type* controls (E). Postsynaptic glutamate sensitivity is dramatically reduced in *GluR-IIA^{hypo}, GluR-IIB^{null}* mutant larvae, expressed in the lack of any recordable spontaneous currents. In 15 larvae (each recording lasting several minutes), no single spontaneous response could be recorded in *GluR-IIA^{hypo}, GluR-IIB^{null}* mutant larvae using two-electrode-voltage-clamp configuration.
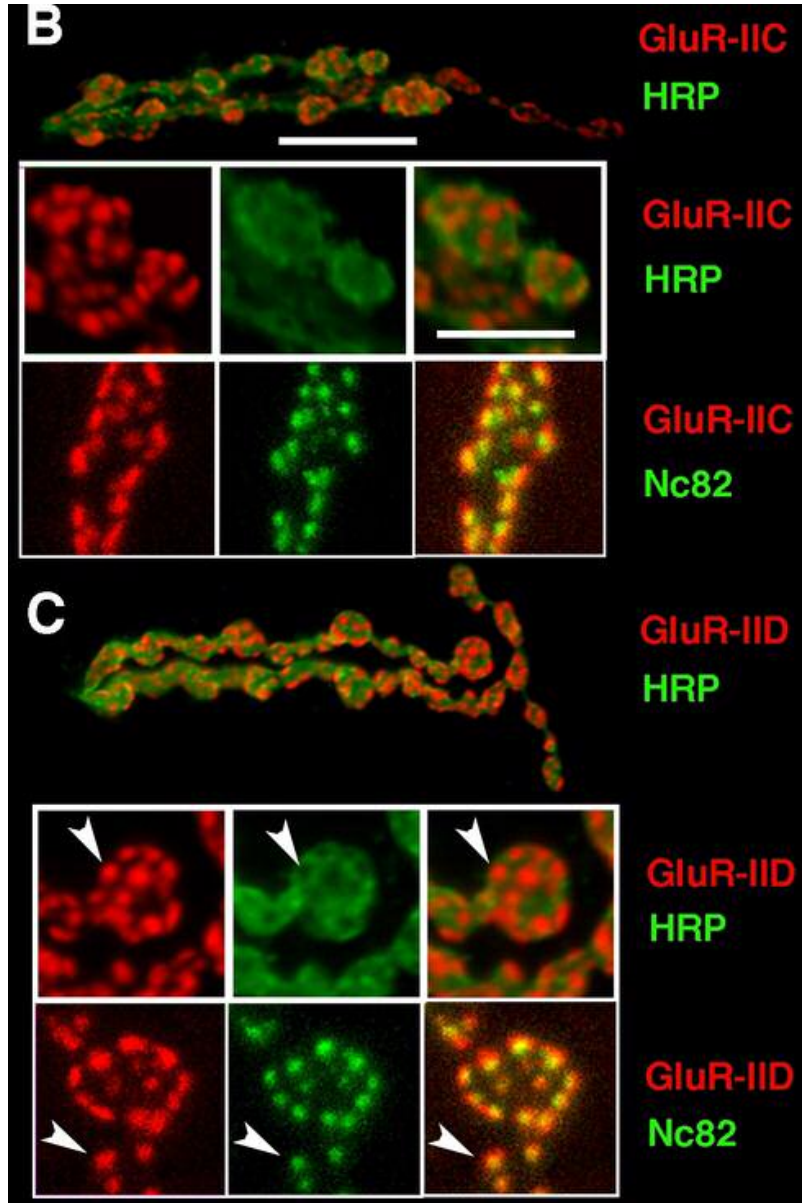
	C_t (body wall)	% control	C_t (total larva)	% control	Body wall /total larva
Glur-IIA (CG6992)	26,7	15,4	28,3	4,4	3,5
Glur-IIB (CG7234)	28,2	5,6	29,5	1,9	3,0
Glur-IIC/III (CG4226)	26,4	18,7	28,9	3,1	6,3
Glur-IID (CG18039)	25,5	35,5	27,0	10,5	3,4
Glur-IIE (CG31201)	24,5	73,7	26,3	17,5	4,2
tbp (control)	23,8	100,0	23,8	100,0	1,0

144x93mm (150 x 150 DPI)

GluR-IID

GluR-IIE

87x73mm (150 x 150 DPI)

127x134mm (150 x 150 DPI)

A

SF9 extract

GluR-IID GluR-IIE-GFP GluR-IIE-GFP embryo extract

180 kD ►

114 kD ►

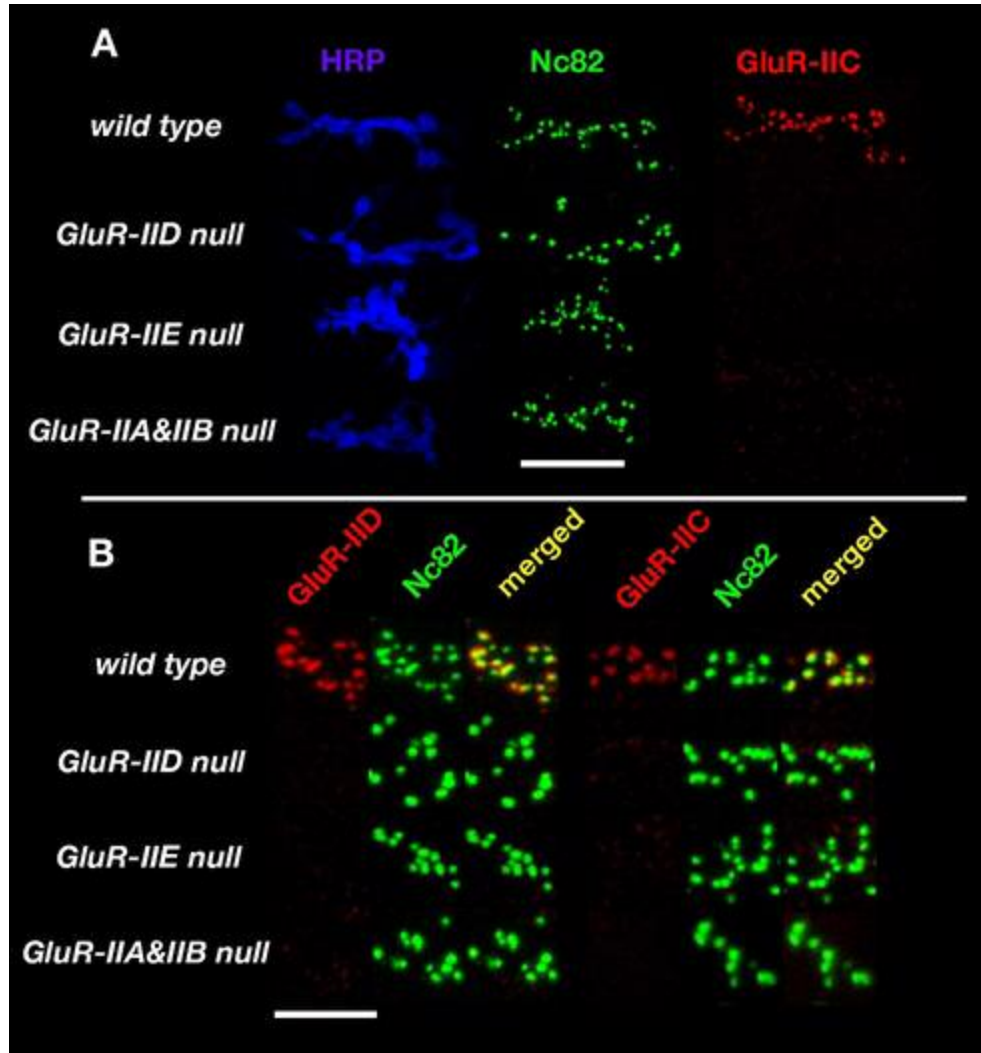81kD ►

64 kD ►

probe:

αGluR-IID   αGFP   αGluR-IID   αGluR-IIC
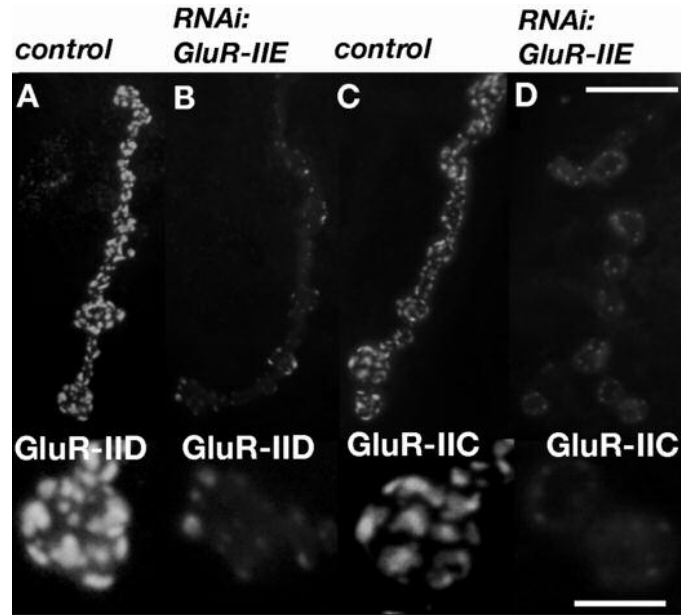
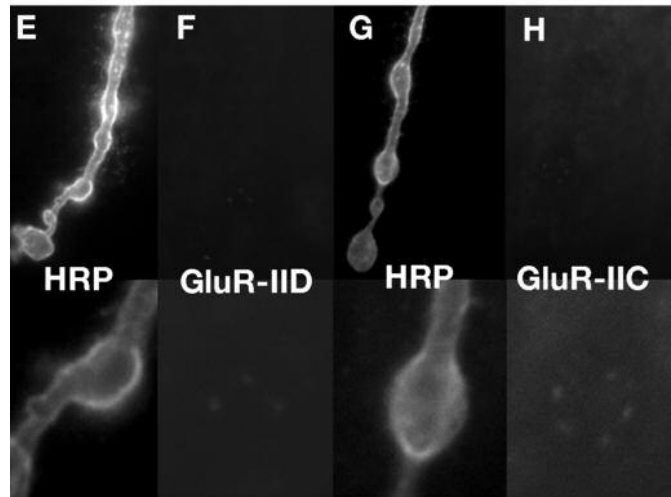82x123mm (150 x 150 DPI)
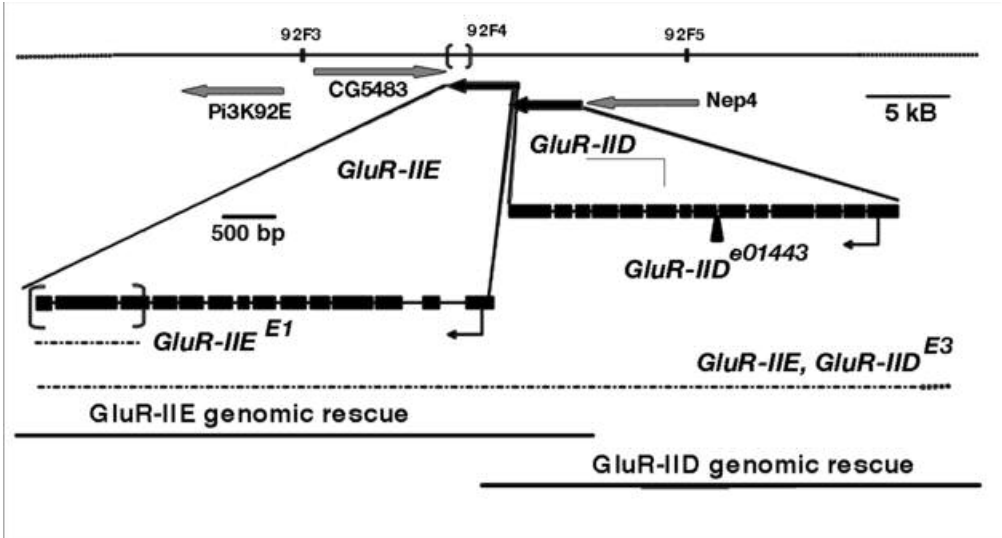
106x57mm (150 x 150 DPI)

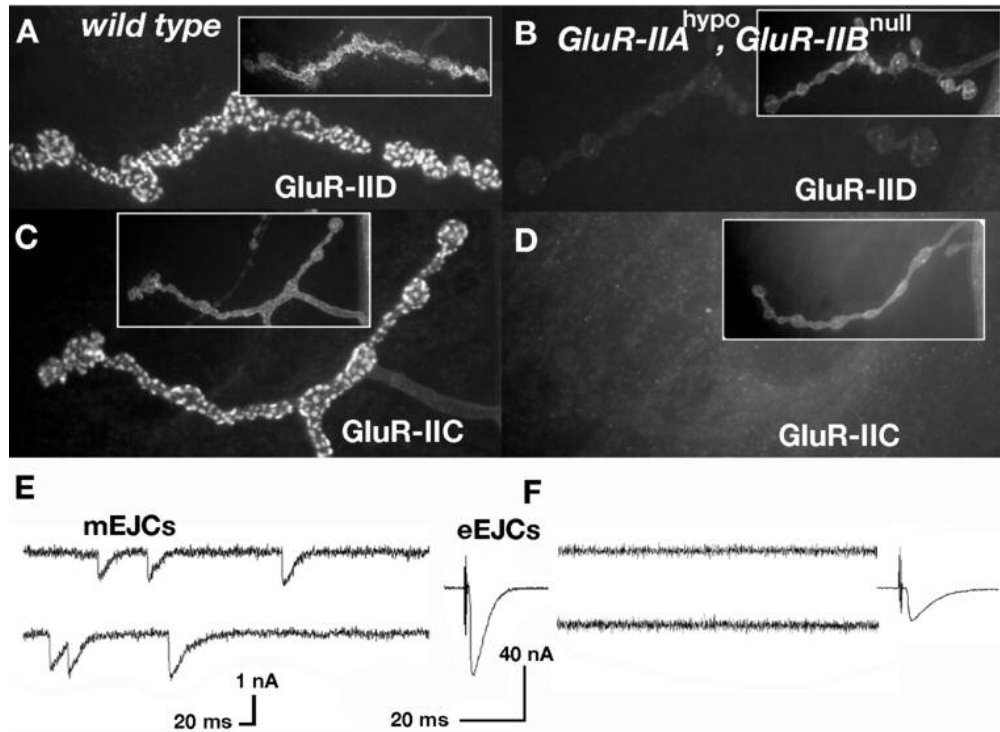82x89mm (150 x 150 DPI)

87x157mm (150 x 150 DPI)

129x94mm (150 x 150 DPI)

6.6 *Curriculum Vitae*

Personal Data: Tobias Manuel Rasse
27.06.77
Ludwigshafen am Rhein, Germany

Education:

1983 - 1987   Primary school Beindersheim, Germany

1987 - 1996   Karolinen-Gymnasium, Frankenthal, Germany
Allgemeine Hochschulreife **(1996)**

1996 - 2001:   FH Mannheim - University of Applied Sciences, Germany

Diplom Ing. (FH) in Biotechnology (**2000**)

Master of Science in Biochemical Engineering **(2001)**

2001-2004   PhD student of the International Max Planck Research School

Neuroscience at the Georg-August University, Göttingen, Germany

Research activity:

1999-2000   Protein Production and Purification in *Thermomyces lanuginosus*,

COPPE, Universidade Federal do Rio de Janeiro, Rio de Janeiro, Brazil

(Diploma Thesis)

2000-2001   Regulation of gene expression: Improvements in the Tet-On and

Tet-Off System, Roche Bioscience, Palo Alto, USA **(Master Thesis)**

2001-2004:   *In-vivo* imaging of long-term changes in the *Drosophila* neuromuscular

system, AG Neuroplasticity, European Neuroscience Institute
Göttingen, Max-Planck Society, Göttingen, Germany **(PhD Thesis)**